



GEOLINKS

INTERNATIONAL CONFERENCE

CONFERENCE PROCEEDINGS

BOOK 1

VOLUME 2

EXTENDED VERSION

AIR POLLUTION AND CLIMATE CHANGE

BIOTECHNOLOGIES

ENVIRONMENTAL GEOLOGY

SOIL SCIENCE

WATER RESOURCES

05-07 OCTOBER 2020 | IMPERIAL HOTEL, PLOVDIV, BULGARIA

DISCLAIMER

This book contains papers which cover the sections: Air Pollution and Climate Change, Biotechnologies, Environmental Geology, Soil Science, Water Resources.

This book contains abstracts, keywords and full papers, which has gone under double blind peer review by the GEOLINKS Review Committee. Authors of the articles are responsible for the content and accuracy.

Opinions expressed might not necessary affect the position of GEOLINKS Committee Members and Scientific Council.

Information in the GEOLINKS 2020 Conference proceedings is subject to change without any prior notice. No parts of this book can be reproduced or transmitted in any form or by any mean without the written confirmation of the Scientific Council of GEOLINKS.

Copyright © GEOLINKS 2020

All right reserved by the International Scientific Conference GEOLINKS.

Published by SAIMA CONSULT LTD, Sofia, 1616, st. Beliya Kladenets, 15, fl. 3

Total print 50

ISSN 2603-5472

ISBN 978-619-7495-07-2

DOI 10.32008/GEOLINKS2020/B1/V2

GEOLINKS CONFERENCE

Secretariat Bureau

e-mail: contact@geolinks.info

URL: <https://www.geolinks.info>

ORGANIZERS AND SCIENTIFIC PARTNERS OF GEOLINKS INTERNATIONAL CONFERENCE

SLOVAK ACADEMY OF SCIENCES
CZECH ACADEMY OF SCIENCES
NATIONAL ACADEMY OF SCIENCES OF UKRAINE
BULGARIAN ACADEMY OF SCIENCES
POLISH ACADEMY OF SCIENCES
ACADEMY OF SCIENCES OF HUNGARY
SERBIAN ACADEMY OF SCIENCES
TURKISH ACADEMY OF SCIENCES
ACADEMY OF SCIENCES OF MOLDOVA
ISLAMIC WORLD ACADEMY OF SCIENCES
LATVIA ACADEMY OF SCIENCES

SCIENTIFIC COMMITTEE OF GEOLINKS INTERNATIONAL CONFERENCE

ASSOC. PROF. JOZEF MARTINKA, SLOVENIA
ASSOC. PROF. ALEKSANDER IVANOV, RUSSIA
ASSOC. PROF. LIGIA MOGA, ROMANIA
ASSOC. PROF. DSC. NITOI DAN, ROMANIA
PROF. DSC. VOLODYMYR POHREBENNYK, UKRAINE AND POLAND
PROF. DSC. IBRAHIM KRASNIQI, KOSOVO
ASSOC. PROF. ZEYNEL FUAT TOPRAK, TURKEY
PROF. RADA JOAN, ROMANIA
ASSOC. PROF. DSC. GIUSEPPE SAPPA, ITALY
PROF. DIMITRIS OSMENI, GREECE
ASSOC. PROF. UWE MACK, GERMANY
ASSIST. PROF. HRISTINA KASTRATI, GREECE
ALEXANDROS TASTH, GREECE
ANDREY ZUMBROICH, FRANCE
TAKACS ILDIKO-CSILLA, ROMANIA
ASSIST. PROF. LAURA GARCIA, SPAIN
ASSIST. PROF. ADONIS LENIS, GREECE
LENNIDAS MOUSAUKU, GREECE

CONTENT

Section AIR POLLUTION AND CLIMATE CHANGE

1. ANALYSES OF GEOMAGNETIC DATA SETS FROM OBSERVATORIES AND CORRELATION BETWEEN THEM *Dr. Laurențiu Asimopolos, Dr. Natalia-Silvia Asimopolos, Asist. Prof. Adrian-Aristide Asimopolos* 13
2. CLIMATE CHANGE AND THE AGRICULTURAL POTENTIAL OF SELECTED LEGUME CROPS IN EAST AFRICA *Mr. Elvis Tangwa, Prof. Vit Voženilek, Dr. Jan Brus, Assoc. Prof. Vilem Pechanec* 23
3. CLIMATE CHANGE IMPACTS ON ULZA DAM LIFESPAN *PhD Student Klodian Zaimi, , Assoc. Prof. Fatos Hoxhaj, Sergio Fattorelli, Francesca Ramazzina* 37
4. NUMERICAL MODELLING OF DUST DISTRIBUTION IN THE ATMOSPHERE OF A CITY WITH COMPLEX RELIEF *DSc. Aleksandre Surmava, DSc. Demuri Demetrashvili, MSc. Vepkhia Kukhalashvili, Dr. Natia Gigauri*..... 47
5. SMOG IN BIALYSTOK IN POLAND. DATA OF PM 2.5 AND PM 10 PARTICULATE MATTER IN OUTDOOR AIR MEASURED IN 2017-2018 BY "THE LABORATORY OF ENERGY-EFFICIENT ARCHITECTURE AND RENEWABLE ENERGIES" AT FACULTY OF ARCHITECTURE OF BIALYSTOK UNIVERSITY OF TECHNOLOGY *Dr arch. Adam Turecki* 55

Section BIOTECHNOLOGIES

6. BIOCONVERSION OF CEREAL SERUM - A SECONDARY PRODUCT FOR PRODUCING PROTEIN CONCENTRATES FROM PEA AND CHICK PEAS *Prof. Dr. Valentina Kolpakova, Ph.D. Student Denis Kulikov, Ph.D. Ruzaliya Ulanova, Dr. Nikolay Lukin, Ph.D. Student Gaivoronskaya Irina*..... 67
7. CONTROL OF PLANTS OF LOTUS CORNICULATUS L. ON AEROBIC AND ANAEROBIC FREE NITROGEN-FIXING BACTERIA *Assoc. Prof. dr. Aurica Breica Borozan, Assoc. Prof. dr. Despina-Maria Bordean, Lecturer dr. Gabriel Bujanca, Lecturer dr. Delia Dumbrava, Prof. dr. Sorina Popescu* 75
8. EFFECTS OF BOILING AND ROASTING ON CRUDE PROTEINS, TOTAL ANTIOXIDANT CAPACITY AND TOTAL POLYPHENOLS CONTENT OF POTATO TUBERS *Assoc. Prof. dr. Despina-Maria Bordean, Assoc. Prof. dr. Aurica Breica Borozan, Lecturer dr. Gabriel Bujanca, Assoc. Prof. dr. Camelia Cioban, Lecturer dr. Delia-Gabriela Dumbrava*..... 83
9. OBTAINING MICROPARTICLES OF CALCIUM CARBONATE LOADED WITH MICROBIAL LIPASE *Valeria K. Scherbakova, Dr. Alla A. Krasnoshtanov*..... 93

Section ENVIRONMENTAL GEOLOGY

10. APPLICATION OF GEOINFORMATION TECHNOLOGIES IN THE STUDY OF CHANGES IN THE STRUCTURE OF LAND USE OF TERRITORIES *Assoc. Prof. Dr. Vasily Nilipovskiy, Graduate student Denis Khabarov, Assoc. Prof. Dr. Irina Khabarova* 105
11. COGNITIVE GEOLOGY OF SUPERIMPOSED SCATTERING OF MOBILE ORE ELEMENTS, PROPER FORMS OF MULTISCALE STRUCTURAL STRESS STABILITY, BIOGENETIC ACCESS CODE OF RESOURCES AND FIELD ARTEFACTS *Dr. Vyacheslav Popkov, Prof. Alexander Sterenberg, Dr. Vladimir Gusev, Dr. Andrey Tyutyayev* 111
12. GEOLOGICAL AND GEOPHYSICAL STUDY FOR ELABORATION OF GEOTHERMAL MODEL IN ORADEA-BAILE FELIX AREA *Dr. Laurențiu Asimopolos, Dr. Natalia-Silvia Asimopolos* 121
13. IDENTIFICATION OF OIL DEPOSIT REFORMATION AND DEEP FEEDING ON EXTRACTED OIL COMPOSITION, *Dr. Yury Turov, Dr. Marina Guznyaeva* 131
14. INDUSTRIAL TYPES OF GOLD DEPOSITS OF THE EAST KAZAKHSTAN *Dr. M. Mizernaya, Prof. B. Dyachkov, Dr. A. Miroshnikova, PhD Student A. Mizerny, Dr. Z. Chernenko, PhD Student S. Aitbaeva* 139
15. MAPPING THE MINERAL RESOURCES DATA OF WEST BALKAN REGION INTO EXISTING EUROPEAN DATA MODEL *Mag. Katarina Hribernik, Jasna Šinigoj, Dr. Duška Rokavec* 149
16. ON THE REGIME OF COVID-19 EPIDEMIC IN RUSSIA AND ITS IMPACT UPON THE FUEL AND ENERGY COMPLEX, INCLUDING IN EDUCATIONAL AND SCIENTIFIC SPHERES *Dr. Svetlana Punanova, Dr. Mikhail Rodkin* 157
17. ORE CONCENTRATIONS OF METALS IN NAPHTHIDES OF HYPERGENESIS ZONE: ASSESSMENT AND ENVIRONMENTAL ASPECT *Dr. Svetlana Punanova* 167
18. POTENTIALLY TOXIC CHEMICAL ELEMENTS OF SHALE PLAYS – ECOLOGICAL THREAT TO THE ENVIRONMENT *Dr. Svetlana Punanova* 177
19. THE CONSOLIDATION OF SOFT CLAY FOUNDATION GROUND USING GEOSYNTHETICS COMBINED WITH THE ELECTRO-OSMOSIS PROCESS *Eng. Florin Sebastian Mustățea, Dr. Eng. Raluca Ioana Nicolae* 187
20. THE VARIATION OF TEMPERATURE OF DIFFERENT OIL RESERVOIR DENSITIES EXPLOITED BY THERMAL METHODS *PhD Student Eng. Ionescu (Goidescu) Nicoleta Mihaela, Prof. Dr. Eng. Vasiliu Viorel Eugen, Prof. Eng. Onutu Ion* 197

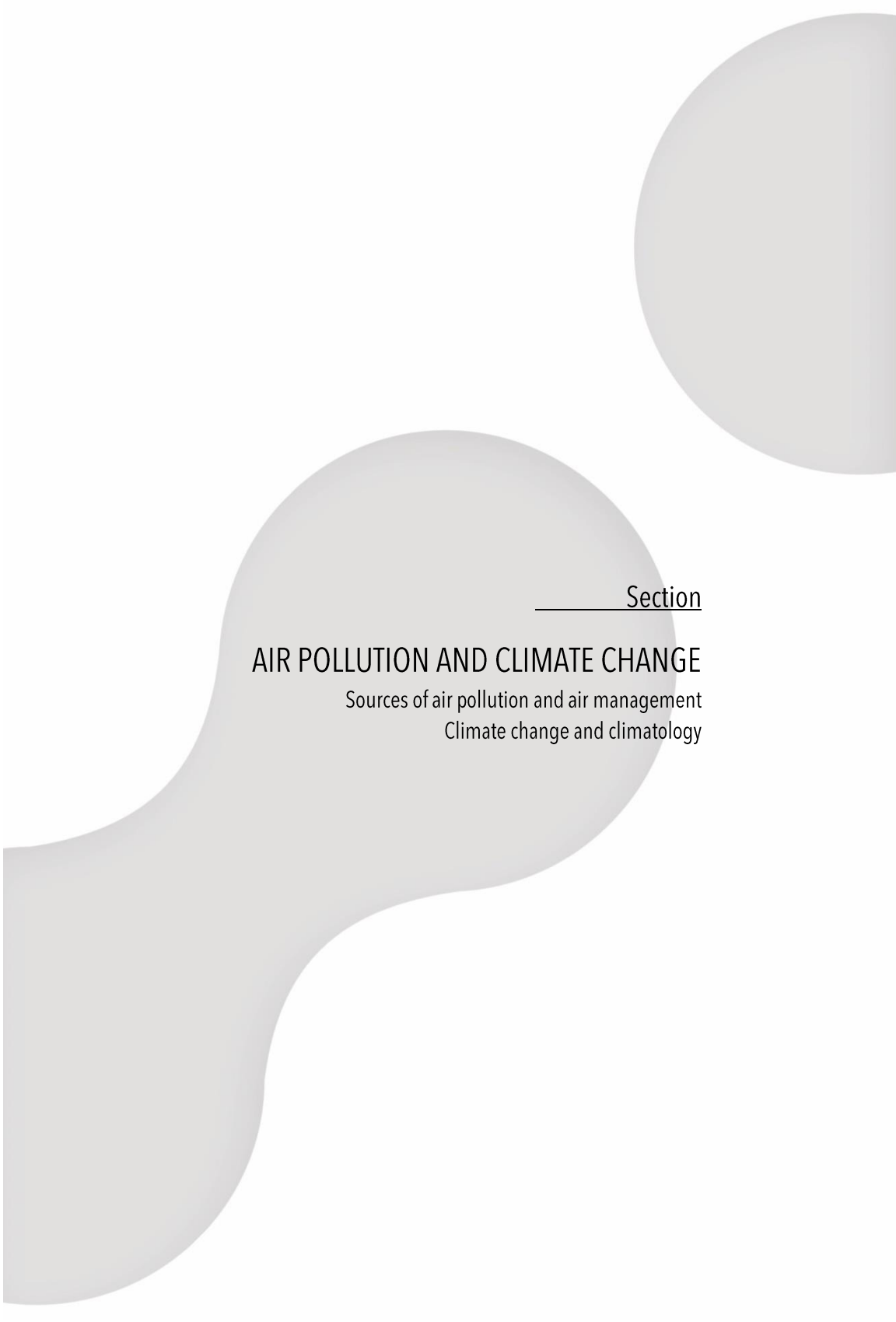
Section SOIL SCIENCE

21. GRAFTED TOMATOES – ECOLOGICAL ALTERNATIVE FOR CHEMICAL DISINFECTION OF SOIL *PhD. Student eng. Dorin Sora, PhD. eng. Mădălina Doltu* 211

22. THE APPLICATION AND VALIDATION OF PHYSICALLY-BASED EROSION AND EMPIRICAL MODEL IN CENTRAL POLAND *Ing. Zuzana Némětová, Ing. Adam Krajewski, PhD., Prof. dr hab. Kazimierz Banasik, PhD., Prof. Ing. Silvia Kohnová, PhD.* 219

Section WATER RESOURCES

23. COMPARING VALIDATION RESULTS OF 1D VERSUS 2D MATHEMATICAL MODEL FOR BUNA RIVER *PhD. Stud. Elona Abazi, Assoc. Prof. Dr. Sotirag Pandazi, Assoc. Prof. Dr. Miriam Ndini* 231
24. FACTOR ANALYSIS OF GEOGRAPHIC COORDINATES AT POINTS OF THE CHANNEL OF A SMALL RIVER ON SPACE IMAGES *Dr. Sc. Prof. Peter Matveevich Mazurkin, Yana Oltgovna Georgieva*..... 241
25. HYDROLOGICAL MODELLING AND ESTIMATION OF THE SEDIMENTS ACCUMULATION IN BOVILLA RESERVOIR *PhD Student Klodian Zaimi, Assoc. Prof. Fatos Hoxhaj*..... 253
26. INTEGRAL ASSESSMENT OF ANTHROPOGENIC PRESSURE ON WATER BODIES IN THE LAKE BAIKAL BASIN *Dr. Irina Ulzetueva, Prof. Bair Gomboev, Dr. Daba Zhamyanov, Dr. Valentin Batomunkuev, Mr. Zorikto Banzaraktsaev*..... 263
27. PROCESSING AND QUALITATIVE VISUALIZATION IN PSEUDO-TRUE COLOURS OF LONG-TERM SERIES OF SATELLITE DATA *Lyudmila Shagarova, Mira Muratova, Aray Yermenbay*..... 271
28. PROSPECTS OF WATER SUPPLY WITH FRESH GROUNDWATER UNDER ANTHROPOGENIC IMPACT CONDITIONS *Aray Yermenbay, PhD Lyudmila Shagarova, Dr. Prof. Malis Absametov, PhD Sergey Osipov* 281
29. WATER TREATMENT RESULTING FROM THE EXPLOITATION OF GAS DEPOSIT - CASE STUDY *Eng. PhD. Student Carmen- Matilda Marinescu (Badica), Eng. PhD. Student Marius-Nicolae Badica, Assoc. Prof. Dr. Silvian Suditu, Assoc. Prof. Dr. Monica Emanuela Stoica* 291
30. WAVELET ANALYSIS OF HEIGHT AT POINTS OF THE CHANNEL OF A SMALL RIVER FROM THE MOUTH ON SPACE IMAGES *Dr. Sc. Prof. Peter Matveevich Mazurkin, Yana Oltgovna Georgieva*..... 301



Section

AIR POLLUTION AND CLIMATE CHANGE

Sources of air pollution and air management

Climate change and climatology

ANALYSES OF GEOMAGNETIC DATA SETS FROM OBSERVATORIES AND CORRELATION BETWEEN THEM

Dr. Laurențiu Asimopolos¹

Dr. Natalia-Silvia Asimopolos²

Asist. Prof. Adrian-Aristide Asimopolos³

^{1, 2} Geological Institute of Romania, Romania

³ University POLITEHNICA of Bucharest, Romania

ABSTRACT

The purpose of this study was to analyze the associated spectrum of geomagnetic field, frequencies intensity and the time of occurrence. We calculated the variation of the correlation coefficients, with mobile windows of various sizes, for the recorded magnetic components at different latitudes and latitudes.

We included in our study the observatories: Surlari (USA), Honolulu (HON), Scott Base (SBA), Kakioka (KAK), Tihany (THY), Uppsala (UPS), Wingst (WNG) and Yellowknife (YKC). We used the data of these observatories from INTERMAGNET for the biggest geomagnetic storm from the last two Solar Cycles.

We have used for this purpose a series of filtering algorithms, spectral analysis and wavelet with different mother functions at different levels.

In the paper, we show the Fourier and wavelet analysis of geomagnetic data recorded at different observatories regarding geomagnetic storms. Fourier analysis highlights predominant frequencies of magnetic field components. Wavelet analysis provides information about the frequency ranges of magnetic fields, which contain long time intervals for medium frequency information and short time intervals for highlight frequencies, details of the analyzed signals. Also, the wavelet analysis allows us to decompose geomagnetic signals in different waves. The analyzes presented are significant for the studied of the geomagnetic storm. The data for the next days after the storm showed a mitigation of the perturbations and a transition to a quiet day of the geomagnetic field.

In both, the Fourier Transformation and the Wavelet Transformation, transformation evaluation involves the calculation of a scalar product between the analyzed signal and a set of signals that form a particular base in the vector space of the finite energy signals. Fourier representation use an orthogonal vectors base, whereas in the case of wavelet there is the possibility to use also bases consisting of independent linear non-orthogonal vectors. Unlike the Fourier transform, which depends only on a single parameter, wavelet transform type depends on two parameters, a and b . As a result, the graphical representation of the spectrum is different, wavelet analysis bringing more information about geomagnetic pattern of each observatory with that own specific conditions.

Keywords: *geomagnetic storm, spectral analysis, Fourier transform, wavelet analysis*

INTRODUCTION

Space weather is a main natural threat to critical infrastructures and their security.

Dynamic conditions on the Sun, in the solar wind, and in the near-Earth space environment can influence the performance of man-made technology, and can also affect human health and activities.

In this paper, we present the results obtained for the geomagnetic data acquired at the Surlari Observatory, located about 30 Km North of Bucharest - Romania. The observatory database contains records from the last seven solar cycles, with different sampling rates.

Also, we used data from other observatories [3], from INTERMAGNET geomagnetic network (www.intermagnet.org), <http://www.noaa.gov> and <https://www.spaceweatherlive.com/en/archive>. The aim of the paper is to analyze the series of geomagnetic data recorded at several observatories during major geomagnetic disturbances. In this study, we analyze the data recorded during the strongest storm in the Solar Cycle, 23 from October, 28-31, 2003.

Geomagnetically induced currents (GICs), a space weather-driven phenomenon, have received the increased international policy, science, industry, and public interest.

GICs flowing on ground-based electrically conducting systems can disrupt the operation of critical infrastructure such as power grids, pipelines, telecommunication cables and railway systems [8], [9], as in figure 1.

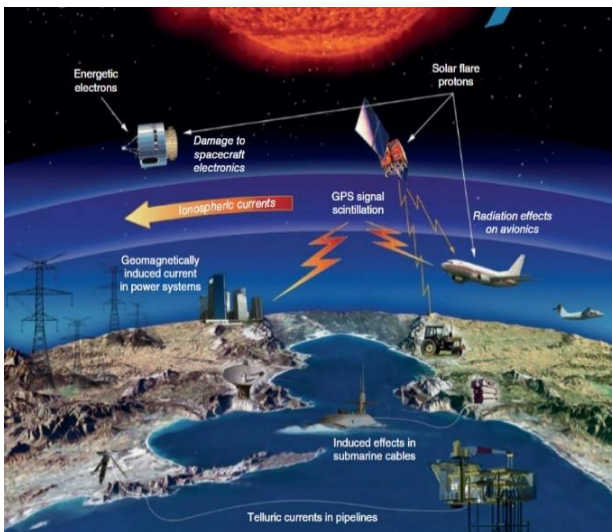


Fig 1 - Technological infrastructure affected by space weather events at the Earth. Source: Courtesy of NASA:

<https://www.nasa.gov>.

A big geomagnetic storm, called the "Halloween Storms of 2003," began after two-three years from solar maximum, when outbreaks 17 major flares (CME), erupted on the Sun. This storm led to a very large

increase in GICs, which caused great damage in the power networks from the countries situated at high northern latitudes.

METHODOLOGY

For the study of correlations between two geomagnetic time series recorded at two observatories during of geomagnetic storm we used correlation coefficient, in mobile windows.

Pearson correlation coefficient $r_{z/w}$ of two parameters (time series) is:

$$r_{z/w} = \frac{n \sum_{i=1}^n z_i w_i - (\sum_{i=1}^n z_i)(\sum_{i=1}^n w_i)}{\sqrt{[n \sum_{i=1}^n z_i^2 - (\sum_{i=1}^n z_i)^2] \cdot [n \sum_{i=1}^n w_i^2 - (\sum_{i=1}^n w_i)^2]}}$$

where: z_i, w_i are time series of two parameters, n is size of time series.

Multiresolution analysis, through wavelets methodology, allow local analysis of magnetic field components through variable frequency windows. Windows that contain longer time intervals allow us to extract low-frequency information, average ranges of different sizes lead to extraction of medium frequency information, and very narrow windows highlight the high frequencies or details of the analyzed signals. The wavelet functions describe the orthogonal bases in the $L_2(\mathbb{R})$ space, with signal approximation properties, while the orthonormal bases in the Fourier analysis are made up of sinusoidal waves. Estimation of geomagnetic field disturbances is similar to the standard problem of estimating a signal disturbed by signal theory. The term noise refers to any modification that changes the periodic or quasi-periodic characteristics of the original signal. The model of the disturbed geomagnetic field is composed of periodic oscillations plus non-periodic oscillations given by the impact of solar wind on the terrestrial magnetosphere [1], [2].

The purpose of wavelet analysis is to build orthonormal bases composed of wavelets that can reconstruct the geomagnetic signals recorded in the observatories.

The wavelet algorithm was originally formulated by Goupillaud, Grossmann and Morlet in 1984 as a constant κ_σ subtracted from a plane wave and then localized by a Gaussian window [6], [14]:

$\Psi_\sigma(t) = C_\sigma \pi^{-\frac{1}{4}} e^{-\frac{1}{2}t^2} (e^{i\sigma t} - k_\sigma)$, where: $k_\sigma = e^{-\frac{1}{2}\sigma^2}$ is defined by the admissibility criterion and the normalization constant C_σ is:

$$C_\sigma = (e^{-\sigma^2} - 2e^{-\frac{3}{4}\sigma^2})^{-\frac{1}{2}} \mathbf{\pi}$$

Multiple resolution analysis is the core of wavelet analysis. This involves the decomposition of a signal in the subscripts at different levels of resolution.

The wavelet analysis is based on the decomposition of an approximate, constant portion, of a function f from the space $L_2(\mathbb{R})$ in a rough approximation and a detail function.

At each level j , approximate f_j of the given function f , can be written as a sum of a coarse approximation f_{j-1} located at the next approximation level and the detail

function g_{j-1} , i.e. $f_j = f_{j-1} + g_{j-1}$. Each detail function can be written as a linear combination of mother wavelet functions:

$\psi_{j,k}(x) = 2^{\frac{j}{2}} \psi(2^j x - k)$, where j is the index of dilatation and k is the index of translation, $j, k \in \mathbb{Z}$. When the index j gets higher, the approximate approximations become finer. For each level of resolution, we have a base function space $(\psi_{j,k})$, $j, k \in \mathbb{Z}$. Therefore, we will work with multiple spaces at different resolutions (multiresolution).

The wavelet function is designed to strike a balance between time domain (finite length) and frequency domain (finite bandwidth). As we dilate and translate the mother wavelet, we can see very low frequency components at large s while very high frequency component can be located precisely at small s .

The transition from STFT to wavelet was done by replacing a fixed-length analysis window, regardless of the frequency of the studied signal, with a set of variable duration analysis windows, so that at low frequencies we use long duration, and at high frequencies we use small durations. To make Wavelet Continue Transform (CWT), a real or complex signal must satisfy the following two conditions:

$$\int_{-\infty}^{\infty} \psi(t) dt = 0 \quad , \quad \int_{-\infty}^{\infty} |\psi(t)|^2 dt < \infty$$

The first property, according to which the signal has a mean null value, suggests a possible oscillating aspect, while the second property, referring to the finite energy value, indicates that the signal concentrates most of the energy within a finite range of time.

The two conditions, together with a so-called admissibility condition (required to define the transformed wavelet inverse) are sufficient for a signal to "qualify" as a wavelet signal. In the literature, numerous such signals have been proposed, some of them with finite (thus compact support) and others with infinite duration, but with concentrated energy within a finite timeframe.

In both, the Fourier Transform and the Wavelet Transformation, transformation evaluation involves the calculation of a scalar product between the analyzed signal and a set of signals that form a particular base in the vector space of the finite energy signals. Fourier representation use a orthogonal vectors basis, whereas in the case of wavelet there is the possibility to use also bases consisting of independent linear non-orthogonal vectors. Unlike the Fourier transform, which depends only on a single parameter, wavelet transform type depends on 2 parameters, a and b .

In the wavelet charts, the frequencies are marked with colors between blue and yellow representing the weight of each frequency in the analyzed signal. According to this, we can find the predominant frequency for each component at each time. The STFT tries to solve the problem in Fourier transform by introducing a sliding window $w(t-u)$. The detailed windows are designed to extract a small portion of the signal $f(t)$ and then take Fourier transform. The transformed coefficient has two independent parameters. The wavelet functions are designed to strike a balance between time domain (finite length) and frequency domain (finite bandwidth). As

we dilate and translate the mother wavelet, we can see very low-frequency components at large scale, while very high-frequency component can be located precisely at a small scale. Another methods used for analyzing of geomagnetic field and prior forecast of geomagnetic storms is Auto-Regressive Integrated Moving Average (ARIMA).

ARIMA models are the most general class of models for forecasting a time series which can be made to be “stationary” by differencing in conjunction with nonlinear transformations. A random time series is stationary if its statistical properties are all constant over time. A stationary series has no trend, its variations around its mean have a constant amplitude, and its short-term random time patterns always look the same in a statistical sense. This condition means that its autocorrelations (correlations with its own prior deviations from the mean) remain constant over time, or equivalently, that its power spectrum remains constant over time [4], [5], [7], [10]. A random variable of this form can be viewed as a combination of signal and noise, and the signal could be a pattern of fast or slow mean reversion, or sinusoidal oscillation, or rapid alternation in sign, and it could also have a seasonal component.

An ARIMA model can be viewed as a “filter” that tries to separate the signal from the noise, and the signal is then extrapolated into the future to obtain forecasts [4], [12].

RESULTS

In figure 2 are shows the North geomagnetic field in October 28, 2003 at Surlari Observatory and spectral analysis. Also, in figure 3, for derived of North geomagnetic field.

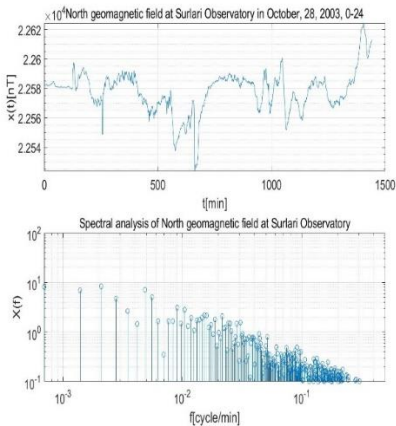


Fig.2-North geomagnetic field on Surlari Observatory, in October 28th, 2003, 0:24, minute mean, and spectral analyses

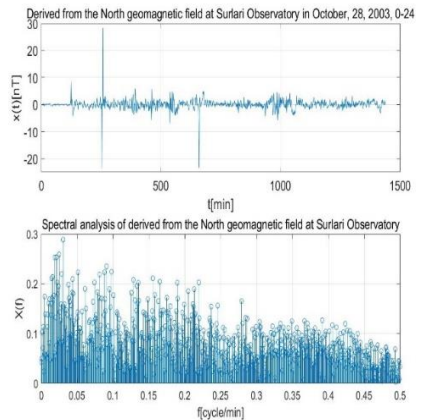


Fig.3-Derived from the North geomagnetic field on Surlari Observatory, in October 28th, 2003 and spectral analyses

Figures 4-9 shows the wavelet power spectra themselves, an important advantage of wavelet analysis over spectral analysis. On the horizontal axis we have the time dimension. The vertical axis gives us the periods. The power is given by the color. The color code indicates ranges of power from blue to yellow.

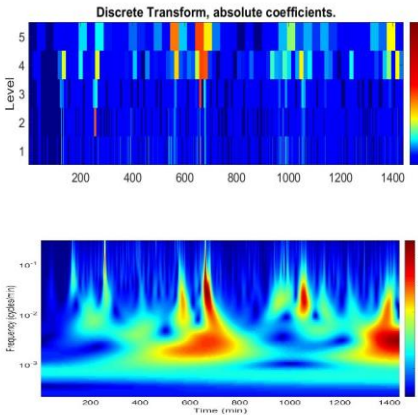


Fig.4 – Absolute coefficients, function db1, level 5 and wavelet image with frequency, time and amplitude, for North geomagnetic field

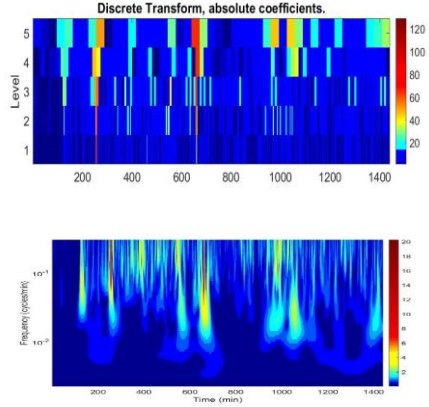


Fig.5 – Absolute coefficients, function db1, level 5 and wavelet image with frequency, time and amplitude for derived of North geomagnetic field.

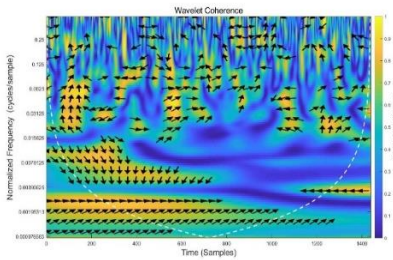


Fig.6 – Wavelet coherences between minute means of North components of the geomagnetic field, October, 28th, 2003, from Surlari Observatory and Honolulu (HON) Observatory.

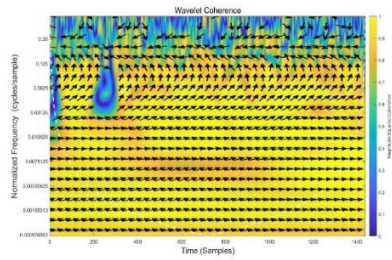


Fig.7 – Wavelet coherences between minute means of North components of the geomagnetic field, October, 28th, 2003, from Surlari Observatory and Tihany Observatory.

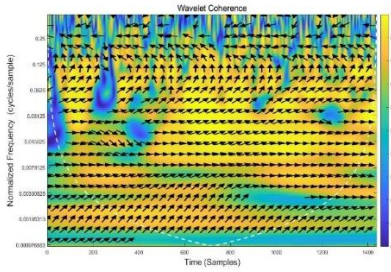


Fig.8 – Wavelet coherences between minute means of North components of the geomagnetic field, October, 28th, 2003, from Surlari Observatory and Wingst (WNG) Observatory.

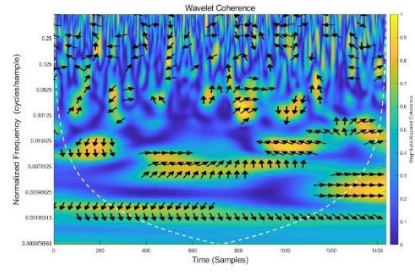


Fig.9 – Wavelet coherences between minute means of North components of the geomagnetic field, October, 28th, 2003, from Surlari Observatory and Yellowknife (YKC) Observatory.

In figures 6-9 are shows the wavelet coherence between geomagnetic field recorded at different observatories during the geomagnetic storm and display the result. The sampling rate was 1 minute and obtained a time-frequency plot of the wavelet coherence, used to indicate the relative lag between coherent components [11], [13], [14]. The arrows are oriented in the direction of the phase difference between the two signals. We calculate for North component of the geomagnetic field, October, 28th, 2003, 0:24, minute means, from Surlari Observatory ARIMA(p,d,q) model, where: p is the number of autoregressive terms, d is the number of non-periodical differences needed for stationarity, and q is the number of lagged forecast errors in the prediction equation (Greene, W. H.. 1997; Box&Jenkins.1994; Hamilton, J. D. 1994)

We obtained the following results:

ARIMA(2,1,0) Model (Gaussian Distribution):

	Value	StandardError	TStatistic	PValue
Constant	0.014229	0.045031	0.31598	0.75201
AR{1}	0.38595	0.0065773	58.679	0
AR{2}	-0.060493	0.016828	-3.5948	0.00032461
Variance	2.823	0.014659	192.57	0

The estimated model is: $0.01\Delta y_{t-1} + 0.39\Delta y_{t-1} - 0.06\Delta y_{t-2} + \epsilon_t$, where ϵ_t is normally distributed with standard deviation 0.01.

The signs of the estimated AR coefficients correspond to the AR coefficients on the right side of the model equation. In lag operator polynomial notation, the fitted model is

$$(1 - 0.39L + 0.06L^2)(1 - L)y_t = \epsilon_t \quad , \quad \text{with the opposite sign on the AR coefficients.}$$

For calculate the difference the data before estimating,

ARIMA(2,0,0) Model (Gaussian Distribution):

	<i>Value</i>	<i>StandardError</i>	<i>TStatistic</i>	<i>PValue</i>
<i>Constant</i>	0.014245	0.045062	0.31611	0.75192
<i>AR{1}</i>	0.38595	0.0065819	58.639	0
<i>AR{2}</i>	-0.060494	0.016839	-3.5924	0.00032768
<i>Variance</i>	2.825	0.01468	192.44	0

The parameter point estimates are very similar to those in EstMdl. The standard errors, however, are larger when the data is differenced before estimation. Forecasts made using the estimated AR model (EstMdlAR) will be on the differenced scale. Forecasts made using the estimated ARIMA model (EstMdl) will be on the same scale as the original data. ARIMA includes moving average (MA), autoregressive (AR), mixed autoregressive and moving average (ARMA), integrated (ARIMA), multiplicative seasonal, and linear time series models that include a regression component (ARIMAX).

CONCLUSION

The use of multi-resolution analysis and different models for the prediction of geomagnetic disturbances, together with the energy and conductivity data of the subsoil, facilitates the calculation of GIC in a variety of situations. A simple but effective way to highlight a geomagnetic storm is calculation gradients of geomagnetic components. sudden geomagnetic variation (SSC, SI, SFE, geomagnetic storms) are relevant through Kp index (only for geomagnetic storms calculated for INTERMAGNET observatories). The Kp indexes = (5-,4,9,8,8-,8-,9-,9-) and Ap=204, from the site <https://www.spaceweatherlive.com/en/archive>, qualify the perturbations from October 28, 2003, in the category of events, as very strong storms. The statistical and spectral analysis of the geomagnetic field variation from geomagnetic observatories provides information on the geomagnetic pattern.

Fourier analysis highlights the predominant frequencies of magnetic field components. Wavelet analysis provides information about the frequency ranges of magnetic fields during the time. Also, the wavelet analysis allows us to decompose geomagnetic signals in different waves. The analyzes presented are significant for the studied of the geomagnetic storm. The data for the next days after the storm showed a mitigation of the perturbations and a transition to a quiet day of the geomagnetic field.

In both, the Fourier Transformation and the Wavelet Transformation, transformation evaluation involves the calculation of a scalar product between the analyzed signal and a set of signals that form a particular base in the vector space of the finite energy signals. Fourier representation use and orthogonal vectors base, whereas in the case of wavelet there is the possibility to use also bases consisting of independent linear non-orthogonal vectors. Unlike the Fourier transform, which depends only on a single parameter, wavelet transform type depends on two parameters, a and b. As a result, the graphical representation of the spectrum is different, wavelet analysis bringing more information about geomagnetic pattern of

each observatory with that own specific conditions. Wavelets, can distinguish between different relationships that occur at the same time but at different frequencies. Also, is useful for all types of time-data comparisons in both the time and frequency domains, as well as in obtaining information on the different phases through which the study variables progress

ACKNOWLEDGEMENT

We gratefully acknowledge the many and significant contributions and comments provided by our colleagues from geomagnetic observatories and INTERMAGNET.

Also, we thank for support by the Ministry of Research for financing of the projects: “The realization of 3D geological / geophysical models for the characterization of some areas of economic and scientific interest in Romania”, with Contract no. 28N / 2019 and project Nr.16PCCDI/2018: „Institutional capacities and services for research, monitoring and forecasting of risks in extra-atmospheric space”, within PNCDIII.

REFERENCES

- [1] Asimopolos, N. S. and Asimopolos, L. 2018. Study on the high-intensity geomagnetic storm from march 2015, based on terrestrial and satellite data, *Micro and Nano Tehnologies & Space Tehnologies & Planetary Science, Issue 6.1, SGEM 2018*, vol.18, pp. 593-600, ISBN 978-619-7408-50-8, ISSN 1314-2704, DOI: 10.5593/sgem2018/6.1
- [2] Asimopolos, L., Niculici, E., Săndulescu, A. M. and Asimopolos, N. S. 2011. Comparisons of geomagnetic data measured in Romania with the data of International Geomagnetic Reference Field 11 (IGRF 11) - *Surveying Geology & Mining Ecology Management*, ISSN 1314-2704, DOI: 10.5593/sgem2011, vol 2, pp. 25-32
- [3] Benoit, S.L. 2012. INTERMAGNET Technical reference manual - Version 4.6, Murchison House West Mains Road Edinburgh EH9 3LA UK, pp.100.
- [4] Box, G. E. P., G. M. Jenkins, and G. C. Reinsel. 1994. *Time Series Analysis: Forecasting and Control* 3rd ed. Englewood Cliffs, NJ: Prentice Hall.
- [5] Chatfield, C. 1989. *The Analysis of Time Series: An Introduction*. 4th Ed. Chapman and Hall, 241 pp.
- [6] Daubechies, I. 1990. The wavelet transforms time-frequency localization and signal analysis. *IEEE Trans. Inform. Theory*, 36, pp. 961–1004.
- [7] Enders, W. 1995. *Applied Econometric Time Series*. Hoboken, NJ: John Wiley & Sons.
- [8] Gannon J. L., Swidinsky A. and Xu Z. 2019. Geomagnetically Induced Currents from the Sun to the Power Grid, *Geophysical Monograph Series*, the

American Geophysical Union, published by John Wiley & Sons, Inc., ISBN: 9781119434344

[9] Gebbins D., Herrero-Bervera, E. 2007. Encyclopedia of Geomagnetism and Paleomagnetism – Springer, pp.311-360/1072.

[10] Greene, W. H. 1997. *Econometric Analysis*. 3rd ed. Upper Saddle River, NJ: Prentice Hall.

[11] Hafner C. M. 2012. Cross-correlating wavelet coefficients with applications to high-frequency financial time series, *Journal of Applied Statistics*, vol. 39, pp. 39–36.

[12] Hamilton, J. D. 1994. *Time Series Analysis*. Princeton, NJ: Princeton University Press.

[13] MATLAB Software. 2011. The Language of Technical Computing, The MathWorks.

[14] Torrence, C., Compo, G.P. 1998. A Practical Guide to Wavelet Analysis, *Bulletin of the American Meteorological Society*, Vol. 79, No. 1, January, pp. 61-78.

CLIMATE CHANGE AND THE AGRICULTURAL POTENTIAL OF SELECTED LEGUME CROPS IN EAST AFRICA

Mr. Elvis Tangwa ¹

Prof. Vit Voženilek ²

Dr. Jan Brus ³

Assoc. Prof. Vilem Pechanec ⁴

^{1, 2, 3, 4} Palacky University, Olomouc, Czech Republic

ABSTRACT

Land expansion to increase agricultural production in East Africa (Burundi, Ethiopia, Kenya, Rwanda, Tanzania and Uganda) will be limited by climate change. In this study, we predict landscape suitability for chickpea (*Cicer arietinum*), common bean (*Phaseolus vulgaris*), lentil (*Lens culinaris*), field pea (*Pisum sativum*) and pigeon pea (*Cajanus cajan*) cultivated across diverse agro-ecological zones (AEZs) in East Africa from 1970 to 2070, under the 4.5 emission scenario. We aimed to understand how suitability shifts among the AEZs might affect the agricultural potential of the selected crops. We use the geolocations of each crop together with response curves from the species distribution software, Maxent to fine-tune the expert-based EcoCrop model to the prevailing climatic conditions in the study region.

Our optimal precipitation and temperature ranges compared reasonably with the FAO base parameters, deviating by ± 200 mm and $\pm 5^\circ\text{C}$, respectively. There is currently a high potential for lentil, pea and common bean in the region. However, under future climates, the suitability of common bean and lentil with a much narrow climate range will shrink considerably while pigeon pea and chickpea will continue to be suitable. Under projected climatic conditions, the agricultural potential of these legumes will be limited by drought or heat stress as landscape suitability will shift optimally toward the cool sub-humid (tcsH), and the cool semi-arid (tcsA) zones. Tanzania, Kenya and Uganda will be the most affected and will lose a large share of suitable arable land.

Different adaptation measures will be needed to increase the agricultural potential and optimized production in vulnerable AEZs. In general, smallholder farmers will have to substitute lentil and common bean for chickpea and pigeon pea or other suitable substitutes to address food security issues. Notwithstanding the limitations of this study, our results highlight the vulnerability of legumes crops as well as their production zones which could be useful in the formulation of adaptation strategies for the East African region.

Keywords: *climate change, EcoCrop, legumes, agro-ecological zone, East Africa.*

INTRODUCTION

Legumes are dominantly produced and consumed in East Africa as dry seed (pulses)[1]. Production is, however, constrained by soil degradation and most importantly, by changing climatic conditions [2], [3], [4]. Climate is important among other factors because more than 90% of agriculture production in the region is rain-fed [5]. Precipitation combined with temperature determines the length of the growing season (LGS) as well as the planting dates[6], [7]. On the other hand, temperature regulates metabolic processes, while the interaction of both factors within their optimal ranges is a prerequisite to optimize growth and yield [5]. While the optimal climate ranges for more than 2500 plant species have been well documented by the United Nations Food and Agricultural Organization (FAO), through its EcoCrop database, the climate ranges for some crops and regions are yet to be validated.

Climate projections show that the East African region will warm between 2 - 6°C on average, while precipitation by the year 2100 will generally increase, for the high (RCP 8.5) emission scenario [8]. However, the intensity of rainfall in the region is still debatable among climate experts because of the complex topography and monsoons of the region which cannot be adequately captured by global climate models (GCM) [3], [9]. Such changing climatic conditions is already having a noticeable impact on the agricultural sector. For example, in West Africa, [6], found that changes in precipitation patterns might delay future planting months of seasonal crops. In the face of changing climatic conditions, crops that can adapt to very narrow climate ranges are usually the most affected [10], [11], [12]. Predictions from crop suitability and crop yield models have consistently reported a spatial shift in landscape suitability of vulnerable crops, mainly from lowland to highlands in the near or distant future [4], [13]. Although the shift in suitability is well recognised, there is also a need to understand how such variations will affect the agricultural potential of these legumes in East Africa because (i) legume cultivation in the region is done across diverse agro-ecological zone (AEZs), with different levels of vulnerability to climate change [7], [13] and (ii) current production is somehow selective with countries such Tanzania and Uganda dominantly focusing on one legume crop type - common bean (FAO). Common bean has been well researched and is known to be a vulnerable crop [11], [12] however, legumes such lentil, field pea and chickpea remained under-researched [10]. Understanding how landscape suitability will change for each of these legumes in the near distant future is probably the first step required to plan adaptation strategies to address food security issues in the region.

OBJECTIVES

This study aimed at analysing the impact of future climate on the agricultural potential of selected legumes cultivated in East Africa. Our objective was to predict possible shifts in agro-ecological zones and their impact on the agricultural potential of the selected crops. We attempt to achieve this goal by adjusting the input parameter for the expert-based EcoCrop model [14], [15] to the prevailing climatic conditions in East Africa using the geolocations of each crop.

Study Region

The study region includes Ethiopia, Tanzania, Kenya, Uganda, Rwanda and Burundi (Fig 1a). The region's landscape is heterogeneous and characterised by rifts valleys lakes and highlands. Annual precipitation in most of the region varies from 800 to 1200mm, with more rainfall in mountainous and lake regions [15]. The rainy season varies from March to May (MAM) for long rains, June to August (JAS) and October to November (ON) for short rains. However, most of the tropical parts experience both the MAM and the ON rainy seasons per year [15].

The legume crops considered in this study include chickpea (*Cicer arietinum*), lentils (*Lens culinaris*), beans (*Phaseolus vulgaris*), dry pea (*Pisum sativum*) and pigeon pea (*Cajanus cajan*). These crops thrive in cool environments and are commonly grown on together with maize, millet, sorghum cassava and groundnuts [3], [16]. Figure 1b show the major AEZs of the study region, which differs in their availability of moisture, temperature and other resources for plant growth [7].

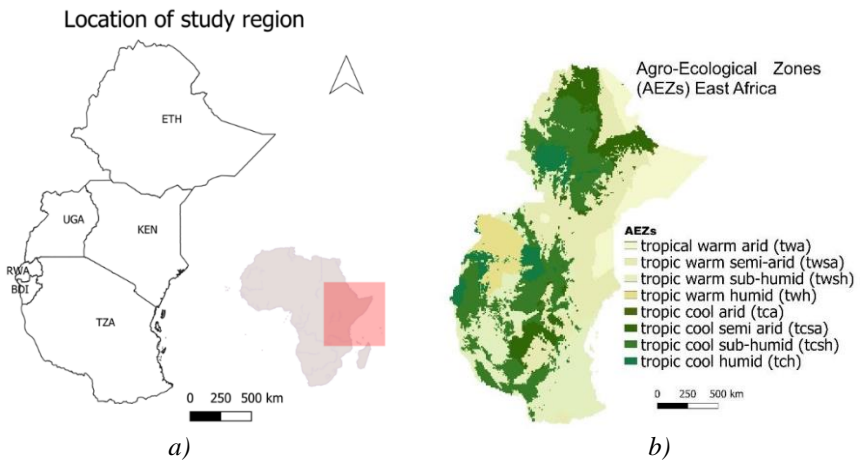


Figure 1: (a) Location of the study region and (b) Agro-ecological zone in the study region (adapted from HarvestChoice 2009)

Precipitation and temperature during the growing season for common bean vary from 200 to 1100mm and from 15 to 25, respectively [3], [16]. Chickpea is generally sown in Late September and depends more on residual moisture to complete its growth cycles [2], [16], [17]. It requires 78 to 380mm 16 to 21°C of moisture and temperature respective during its growing season [1], [2], [16]. Lentils, unlike chickpea, are severely affected at temperatures above 27°C and grow optimally within the temperature range from 18 to 21°C and precipitation from 350 -550mm [17]. Dry pea in Ethiopia is commonly grown from July to December and require 800 to 1000mm and 10 °C to 27°C of rainfall and temperature [17]. Pigeon pea is more drought-tolerant than bean, lentil and chickpea and requires from 250mm to 800mm and 17°C to 35°C of Precipitation and temperature respectively during its growing season [1], [16], [17].

METHODOLOGY AND DATA

We proceed as follows. First, we acquire crop location datasets, climate dataset, agricultural land dataset and agro-ecological zone dataset of the study region. Next, we calibrate and evaluate model parameters and analysed crop distribution and suitability modeling using Maxent [18] and EcoCrop software, respectively. Lastly, we analyse model output, integrate the best model results with agricultural and agro-ecological zone datasets of the region and compare our results with those from existing studies in the region. The methodology we followed is summarized in Fig 2 while Table 1 presents a summary of these datasets

Crop Occurrence

Evidence of pea, chickpea, pigeon pea, beans and lentils occurrence from 1960 to 2017 were obtained from the Plant Genetic Resources for Food and Agriculture (Genesys portal <https://www.genesys-pgr.org>) and from the website of the Global Biodiversity Information Facility (GBIF portal, <https://www.gbif.org>). We use evidence data for this time range to get enough geolocations because legume data for most of the region is rare [1]. These datasets were processed, by checking and removing duplicate points to reduce sampling bias, removing missing or completely absent coordinate as well as misrepresented coordinates. Thus, the processed sample size for bean = 685, chickpea = 694, lentil= 249, pea=394 and pigeon pea =315. Figure 2 shows the locations of production sites of legume crops in the study region.

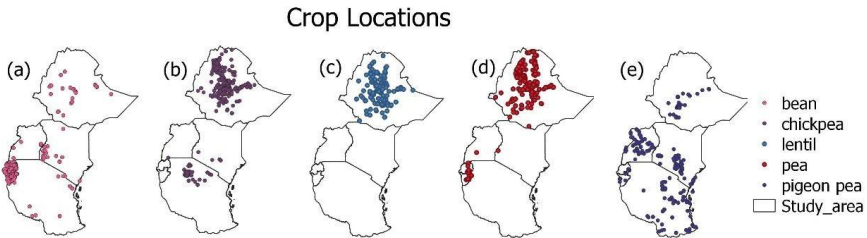


Figure 2: Crop locations (a) common bean, (b) chickpea, (c) lentil, (d) pea (e) pigeon pea

Climate Dataset

We obtained long-term averages of historical climate datasets at 30-second arc resolution (~1km at the equator) from 1970 to 2000 (also referred to as “current climate”) and future climate data for the year 2070 from www.worldclim.org [19]. The future climate datasets are calibrated outputs from Global Climate Models (GCMs) of phase 5 of the Coupled Model Inter-comparison Project (CMIP5) on which the 5th assessment report of the intergovernmental panel on climate change (IPCC5) is based. In this study, we used the mean ensemble (on a pixel basis) of 4 GCMs for RCP 4.5. The 4 GCMs included: ACCESS 1-0, CCSM4, HadGEM-ES and NorESM1-M.

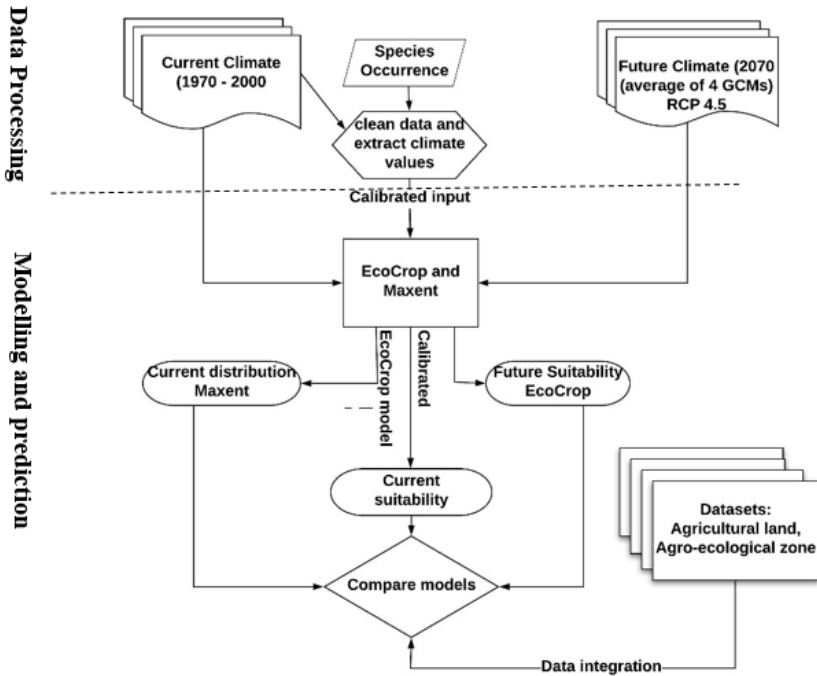


Figure 2: Methodology and conceptualisation of workflow

Table 1: Summary of data sources

Data	Source(s)	Resolution
Climate	WorldClim.org	30 sec arc
Crop locations	Genesys, https://www.genesys-pgr.org/ GBIF, https://www.gbif.org/	
Agro-Ecological Zones (AEZs)	HarvestChoice/International Food Policy Research Institute (IFPRI) https://harvestchoice.org/data/aez8_clas	5 min arc
Agricultural land	SEDAC, http://sedac.ciesin.columbia.edu/es/aglands.html	5 min arc

Spatial Modelling

Before spatial modelling, we respectively use 70%, and 30% of each crop together with the default background sample size to train and validate the spatial distribution of each crop in Maxent software. We use two or more of following bioclimatic variables (predictors) directly related to plant growth as predictors: Bio10 (Mean Temperature of Warmest Quarter), Bio11 (Mean Temperature of

Coldest Quarter), Bio12 Annual Precipitation), Bio16 (Precipitation of Wettest Quarter) and Bio17(Precipitation of Driest Quarter).

We modelled the suitability of each crop for the current and future climate using EcoCrop [14], [15]. EcoCrop predicts suitability on a pixel basis by comparing the specific temperatures and precipitation ranges of a crop with prevailing condition elsewhere. The model scores suitability on a scale of ‘0’ (for unsuitable areas) to ‘1’ (for excellently suitable areas) depending on the climate range of the crop. The implementation of EcoCrop in GIS softwares is always supported by the EcoCrop database documenting the base biophysical parameter of more than 2500 plant species. These biophysical parameters may be too generic depending on or crop type or the scale of the study.

Model Calibration and Evaluation

To calibrated and evaluated model parameters; we use the geometric mean of the growing season. From the growing season, we created two fictitious growing seasons for mean temperature and total precipitation from (equation 1 & 2) respectively. Each of the false growing seasons had 12 consecutive sequences of four months for chickpea, lentil, common beans and six months for pigeon pea. For field pea with a growing season of 3 months, we use the quarterly bioclimatic variable (BIO10, BIO11, BIO16 and BIO12) from worldclim.org and extracted their values from each point.

$$T_{GS} = \frac{1}{4} \left(\sum_{i=1}^{i=4} t_{avg_i}, \sum_{i=2}^{i=5} t_{avg_i}, \dots, \sum_{i=12}^{i=3} t_{avg_i} \right) \quad (1)$$

$$R_{GS} = \left(\sum_{i=1}^{i=4} r_{sum_i}, \sum_{i=2}^{i=5} r_{sum_i}, \dots, \sum_{i=12}^{i=3} r_{sum_i} \right) \quad (2)$$

Where i represents the month(s), the mean temperature(t_{avg_i}) for 12 consecutive growing seasons (T_{GS}), has four consecutive months per season. The total rainfall (r_{sum_i}) for 12 consecutive growing seasons (R_{GS}) has four consecutive months per growing season

From the 12 potential growing seasons, we choose the sequence with the lowest and highest mean temperature to calibrate temperature inputs. For precipitation, we selected the sequence with the highest sum of rainfall to ensure enough moisture during the growing season. For each crop locations, we then extracted the current temperature, and precipitation values from these sequences and adapted the approach of [14] to determine EcoCrop model input. To further fine-tune model inputs, we compare the optimum temperature and precipitation values with those from existing field studies as well as with the results of response curves of the main predictors in Maxent. Thus, we use the precipitation range of pea as a proxy for bean because both crops have nearly the same precipitation but slight different temperature requirement [17], (FAO). Moreover, the range equally compares with field values for the study region [16]. For pigeon pea, we used annual precipitation

to derive its optimal and marginal precipitation inputs because annual rainfall was a significant predictor in Maxent. Secondly, pigeon pea has a very long growing season. Table 1 summarizes the input parameters used to drive EcoCrop

RESULTS

We present and evaluate the calibrated temperature, and precipitation ranges for each crop as well as changes in suitability across agro-ecological zones.

Crop climate niche

Figure 4a and 4b show the variation in annual precipitation against the mean annual temperature of the selected crops.

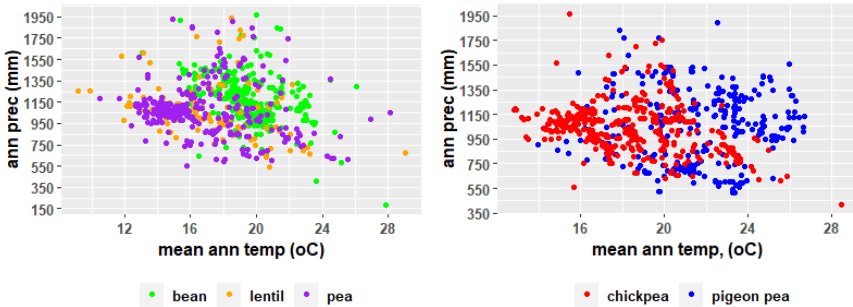


Figure 3: Annual temperature and precipitation range of the chosen crops (a) bean, lentil and pea (b) chickpea and pigeon pea

Generally, rainfall and temperature at production sites vary from 550 to 1550mm and from 8°C to 29°C respectively and roughly reflects each crop's climate niche. In Fig 4a most pea, bean and lentil-growing areas receive almost the same amount of precipitation per year. However, the mean annual temperature for lentil and pea production sites range from 13 °C to about 19 °C while in bean growing areas, it varies from 16°C to 22 °C. In Fig 4b, the mean annual temperature range for chickpea and pigeon pea locations are almost the same. However, the temperature range for most chickpea locations varies from 12°C to 25°C compared to 20°C to 27°C for pigeon pea. These differences in temperature precipitation range broadly show some differences in adaptation to climatic conditions

Model calibration and evaluation

Table 2 shows the calibrated model parameters used to drive EcoCrop. These parameters are presented together with the FAO base parameter for comparison. Generally, the calibrated temperature inputs for all crops except for pea were 3 to 5 degrees lower than the based parameter. All calibrated optimum minimum precipitation (RopMn) were ~50 to 100mm less than base except for pea. While the optimum max precipitation for all crops except for common bean was 150 to 200mm higher than the FAO base input.

Table 2: Comparison of calibrated inputs with FAO base parameter

	LGS (days)	Tkil l (°C)	Tm n (°C)	TopM n (°C)	TopM x (°C)	Tm x (°C)	Rmn (mm)	RopM n (mm)	RopM x (mm)	Rmx (mm)
Bean	90	0	10	15	20	27	151	452	1054	1355
FAO base	160	0	7	16	25	32	300	500	2000	4300
Chickpea	120	0.85	3.4	10.2	24	31	182	547	1274	1638
FAO base	135	-9	7	15	29	35	300	600	1000	1800
Lentil	120	0.75	3	9	21	27	167	506	1180	1517
FAO base	155	0	5	15	29	32	250	600	1000	2500
Pea	90	0.82	3.3	9.9	23.1	29.7	151	452	1054	1355
FAO base	100	-2	4	10	24	30	350	800	1200	2500
Pigeon pea	180	1.1	5	14.1	33	42.3	220	658	1537	1976
FAO base	228	0	10	18	38	45	400	600	1500	4000

Where: Rmx= maximum rainfall, RopMx= optimum maximum rainfall, RopMn= optimum minimum rainfall, Rmn= minimum rainfall, Tmx= maximum temperature, TopMx=maximum optimum temperature, TopMn= optimum minimum temperature, Tmn= minimum temperature, Tkill= temperature that will kill the crop and LGS = length of the growing season

Table 2 also shows that Field pea has the lowest moisture requirement (Rmn) while pigeon pea and chickpea have the highest maximum temperature (Tmx). Compare to the base input, Table 2, equally shows that the FAO based maximum precipitation have largely been overestimated at least for the study region. Notwithstanding, the calibrated model inputs are reasonably within the ranges for each crop.

Table 3 shows the proportion of crop locations which fall within the EcoCrop suitability threshold of $\geq 41\%$ or a higher threshold of $\geq 60\%$. Table 3 shows that increasing threshold reduces prediction rate by 5% for bean, pea and pigeon pea except for lentil and chickpea. Based on the area under the receiver operating curve (AUC), Table 3 also shows that Maxent model performance for each crop was within the acceptable range [18] although its thresholds and statistical approach is different from Ecocrop.

Table 3: Model prediction rate in Maxent and EcoCrop

	EcoCrop		Maxent		
	Threshold	Threshold	Threshold	AUC Value	
Bean	0.41	0.68	0.60	0.53	0.90
Chickpea	0.41	0.97	0.60	0.96	0.86
Lentil	0.41	0.89	0.60	0.88	0.89
Pea	0.41	0.83	0.60	0.77	0.91
Pigeon pea	0.41	0.71	0.60	0.64	0.75

Crop Suitability.

Figure 5a – 5e shows the current suitability pattern for each crop. The figure shows that that suitability of chickpea (Fig 5d) and pigeon pea (Fig 5e) is homogeneous compared to a heterogeneous pattern for common bean, lentil and pea and reflect the vulnerability of the later. Generally, there is currently a high potential for all the selected legumes in the study region.

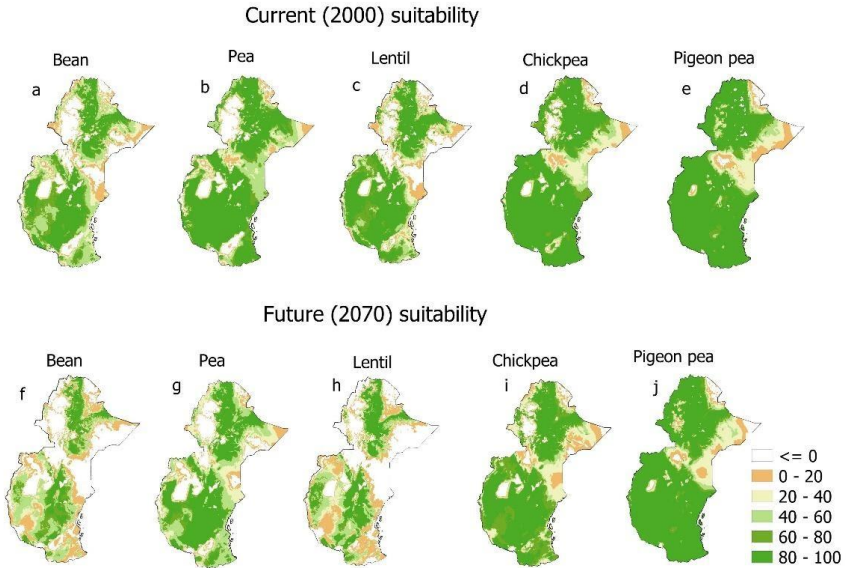


Figure 4: Suitability of legume crops, (a - e) current suitability, (f - j) future suitability

Under future climatic conditions (Fig 5f to 5j), there will be more variability in the suitability of common bean (Fig 5f,) and lentil (Fig 5h) compared to pea, chickpea and pigeon pea. There will also be a significant contraction in the share of suitable areas for common bean and lentil compared to chickpea and pigeon pea which will remain unchanged, thus reflecting the broad climate range and adaptability of the later.

At the country level, Figure 6a shows the estimated share of suitable agricultural land that could be lost (total lost minus total gained) for each country. Approximately 61,000 and 33,000 km² share of suitable arable land for common bean, lentil will be lost in Tanzania and Uganda, respectively. Most of the suitable agricultural land in Ethiopia will remain suitable, although the share of suitable land for pea cultivation will reduce. There will be little or no loss of suitable land in Rwanda.

Across AEZs, Figure 6b shows that under future climatic conditions, the most optimal zones for legume cultivation will be the cool humid (tch) the cool semi-arid (tcsa) and the cool sub-humid (tcsh) zones. Suitability within these zones will

increase by 10% and 15% respectively and will be most favourable field pea cultivation. Within the warm AEZs, the warm sub-humid (twsh) and the warm semi-arid (twsa) zones will be the most impacted, decreasing suitability at all production sites. Generally, land suitability for, pea will be most reduced in the warm semi-arid (twsa) and the warm (twa) arid zone compared to other crops. The suitability of lentil, chickpea and pigeon pea will be more reduced in the warm humid (twh) zone compared to common bean and pea. The cool humid (tch) zones and cool arid (tca) zones will be negligibly affected.

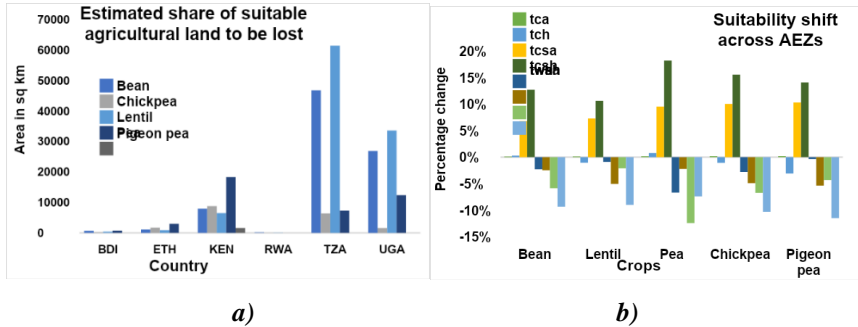


Figure 5. (a) estimated share of suitable arable land that could be lost (b) suitability shift across AEZs. The share of suitable land in each country is based on an overlay with agricultural land, which is cropland + pastureland. In Fig 3b, tca = tropic cool arid, tch= tropic cool humid, tcsa= tropical cool semi-arid, twsh=tropic cool sub-humid, twa= tropic warm arid, twsh= tropic warm humid, twsa= tropic warm semi-arid, twsh=tropic warm sub-humid.

DISCUSSION

Climate data and crop suitability

Under baseline conditions, we observe an overlap in the climate range of selected legumes (Fig 4a and 4b) which implies that they can easily substitute each other. Lentil and pea have the same climate niche but differ from common bean, which has a slightly higher temperature requirement in agreement with [17]. The fact that our optimal temperature and precipitation range compared reasonably with the FAO base input (Table 2), although deviating by $\pm 200\text{mm}$ and $\pm 5^\circ\text{C}$, respectively, suggest that the approach could be promising for other crops. We also observe some deviations in optimal precipitation from field studies which could be attributed to the fact field studies tend to be very localized and not representative of the entire region. Thus low prediction rate of $\sim 68\%$ for common bean even after calibration may have been due to sampling not being adequate to represent its full climate range. However, our results show that beside Ethiopia and to a lesser extent Kenya, there is currently a high potential for lentil and field pea production in Burundi, Rwanda, Uganda and Tanzania which appear to be neglected. Smallholder farmers in these countries could take advantage to diversify crops while climatic conditions are still favourable.

Under future climates, we observe (not presented) that there will be more precipitation in most parts of the study region by 2070. The average temperature will increase by $\sim 2.7^{\circ}\text{C}$ in agreement with existing studies, [8]. These legumes will adapt differently to changing climatic conditions. Pigeon pea and chickpea with broadest climate range will be the most adaptable crop (Fig 5j and 5i) while common bean and lentil will be the least. While these results are similar to existing studies [2], [4], we equally acknowledge the uncertainty of these predictions due to the inherent uncertain in our climate datasets and notably in the rainfall patterns of East Africa [9].

Climate impact on land suitability

By integrating both the agro-ecological zone and agricultural land dataset to the output from EcoCrop model, we had a better assessment of the impact of climate change. The shift in suitability among the agro-ecological zones also reflects the dominant stress factor limiting crop suitability in each zone. Generally, heat will be the dominant stress factor reducing crop suitability in the future, as reported by [4]. The impact of heat stress is based on the fact that suitability either increase or nearly remain constant in the cool agro-ecological zones as opposed to the warm AEZs. In addition to heat stress drought will equally be a limiting factor, especially in the warm semi-arid zones (twsa) and will significantly reduce the agricultural potential of field pea. Excessive moisture, in addition to heat stress in the warm humid zones (twh), will be the limiting factor affecting lentil, chickpea and pigeon production [17].

The impact of climatic change, on landscape suitability for each of these countries, will also largely depend on which AZE dominates. The share of suitable land for common bean and lentil cultivation in Uganda, Kenya and Tanzania will shrink considerably because a large share of the arable land in these countries are within the warm sub-humid (twsh) and the warm semi-arid (twsa) zones. Most of the agricultural land in Burundi, Rwanda and Ethiopia with a more stable cool sub-humid and cool semi-arid conditions will continue to be suitable. Although suitability will generally decrease for all crops and each of these countries, chickpea and pigeon pea being the most resistant to drought [2], [16], (Fig 6d and 6e) or climatic variation will continue to be suitable in the warmer AEZs.

The decreasing suitability of the warm AEZs will also imply that different adaption measures will be needed to increase the agricultural potential of the region optimize legume production in future. For example, shortening crop cycles by delaying planting dates or months [6] will be ideal for the warm sub-humid zones while switching to more drought-tolerant legume variety could be a workable solution for the warm semi-arid zones [2]. Generally, Chickpea and pigeon pea together with other suitable substitutes [12] will be future crops for the region.

It is worth noting that our assessment of the possible impact of climate change on the agricultural potential of the region is based on a much coarser dataset at 5 minutes' degree for the agro-ecological zone and the agricultural land. Hence, we may have missed spatial variability at the country level. Secondly, we must stress that the climate dataset used in this study is based on long term averages of GCMs which may not have adequately capture precipitation pattern in East Africa [3], [8],

[9]. Moreover, we did not analyse seasonal or inter-annual variability, which could equally be helpful for detail assessment especial of the fragile AEZs. These considerations will be necessary to improve these results.

CONCLUSION

In this study, we have attempted to predict and quantify the impact of climate change by 2070 on five commonly grown legumes (field pea, chickpea, lentil, common bean and pigeon pea) in East Africa (Burundi, Ethiopia, Kenya, Rwanda, Tanzania and Uganda). The approach we follow builds on the work of [14] who successfully validated the generic EcoCrop model input parameter for sorghum. We use the geolocations of crops together with response curves from the species distribution software, Maxent to fine-tune the crop suitability model, EcoCrop model to the prevailing climatic conditions in the study region. We found that our calibrated optimal temperature and precipitation ranges compared reasonably with the FAO base parameters, deviating by $\pm 200\text{mm}$ and $\pm 5^\circ\text{C}$, respectively. Our prediction rate based on suitability range of EcoCrop varied from ~70 to 90% and implied that the approach could be useful for other crops. There is, however, a need to improve the calibrated parameters, especially of common bean using more representative datasets.

Notwithstanding, there is currently a high potential for lentil and field pea production in Tanzania, Rwanda and Kenya, which appears to be neglected. Farmers from these countries can take advantage of this opportunity to diversify production while climatic conditions in the region are still favourable. As most of the region warm-ups and also receive much precipitation by 2070, suitability across agro-ecological zones will shift towards the cool zones. The most optimal of which will be cool sub-humid (tcsH) and cool semi-arid (tcsA) zones, highlighting the fact that heat stress will be a major factor limiting legume suitability in the future. Drought and waterlogging may equally be limit factors, especially in semi-arid and sub-mid agro-ecological zones. Different adaption measured will be needed to optimize the agricultural potential of the most vulnerable AEZs. Generally, smallholder farmers will have to substitute bean, lentil and pea with pigeon pea and chickpea or with other drought-resistant crops.

The impact of climate change will be different among the six countries considered. Generally, Tanzania, Kenya and Uganda with a considerable share of warm sub-humid or warm semi-arid arable land will be the most affected. Ethiopia and Rwanda with a large share of cold subhumid and cool-semi arid arable land will be the least affected.

Some of the limitations of this study include the fact that we used data from global climate models which do not adequately capture monsoonal processes and precipitation patterns in East Africa. Hence these uncertainties will equally be propagated into model input and outputs. We did not explore extreme or seasonal climatic variation, which should be helpful for better assessment of the agricultural potential and adaptation, especially in fragile agro-ecological zones. Our result could further be improved with finer or regional agricultural and agro-ecological zones dataset of the study region. Nonetheless, our results highlight the

vulnerability of legumes crops as well as their production zones which could be the first step in the formulation of adaptation strategies for the study region.

ACKNOWLEDGEMENTS

This paper was supported by the Internal Grant Agency of Palacky University Olomouc as part of the project "Innovation and application of geoinformatics methods for solving spatial challenges in the real world." (IGA_PrF_2020_027).

REFERENCES

- [1] Snapp S, Rahmanian M, Batello C. Pulse Crops for Sustainable Farms in Sub-Saharan Africa. *Pulse Crops for Sustainable Farms in Sub-Saharan Africa*. 2018.
- [2] Singh P, Nedumaran S, Boote KJ, Gaur PM, Srinivas K, Bantilan MCS. Climate change impacts and potential benefits of drought and heat tolerance in chickpea in South Asia and East Africa. *Eur J Agron* [Internet]. 2014;52:123–37. <http://dx.doi.org/10.1016/j.eja.2013.09.018>
- [3] Ramirez-Villegas J, Challinor A. Assessing relevant climate data for agricultural applications. *Agric For Meteorol* [Internet]. 2012;161:26–45. <http://dx.doi.org/10.1016/j.agrformet.2012.03.015>
- [4] Thornton PK, Jones PG, Alagarswamy G, Andresen J, Herrero M. Adapting to climate change: Agricultural system and household impacts in East Africa. *Agric Syst* [Internet]. 2010;103(2):73–82. <http://dx.doi.org/10.1016/j.agry.2009.09.003>
- [5] FAO. Handbook on climate information for farming communities-What farmers need and what is available [Internet]. 2019. 184 p. <http://www.wipo.int/amc/en/mediation/rules>
- [6] Egbeyi TS, Lennard C, Crespo O, Mukwenha P, Lawal S, Quagraine K. Assessing future spatio-temporal changes in crop suitability and planting season over West Africa: Using the concept of crop-climate departure. *Climate*. 2019;7(9).
- [7] Fischer G, Nachtergaele F, Prieler S, Velthuizen HT van, Verelst L, Wiberg D. Global Agro-ecological Zones :Model documentation. Food Agric Organ United Nations. 2008;179.
- [8] Niang I, Ruppel OC, Abdrabo MA, Essel A, Lennard C, Padgham J, et al. Africa. *Clim Chang 2014 Impacts, Adapt Vulnerability Part B Reg Asp Work Gr II Contrib to Fifth Assess Rep Intergov Panel Clim Chang*. 2015;1199–266.
- [9] Nicholson SE. Climate and climatic variability of rainfall over eastern Africa. *Rev Geophys*. 2017;55(3):590–635.
- [10] Manners R, van Etten J. Are agricultural researchers working on the right crops to enable food and nutrition security under future climates? *Glob Environ Chang* [Internet]. 2018;53(September):182–94. <http://doi.org/10.1016/j.gloenvcha.2018.09.010>

[11] Ramirez-Cabral NYZ, Kumar L, Taylor S. Crop niche modeling projects major shifts in common bean growing areas. *Agric For Meteorol* [Internet]. 2016;218–219:102–13. <http://dx.doi.org/10.1016/j.agrformet.2015.12.002>

[12] Rippke U, Ramirez-Villegas J, Jarvis A, Vermeulen SJ, Parker L, Mer F, et al. Timescales of transformational climate change adaptation in sub-Saharan African agriculture. *Nat Clim Chang*. 2016;6(6):605–9.

[13] Seo N, Mendelsohn R, Kurukulasuriya P, Dinar a, Hassan R. Differential adaptation strategies to climate change in African cropland by agro-ecological zones [Internet]. Policy Research Working Paper - World Bank. 2008. 42- p. Available from: [cabi:20083213527](http://dx.doi.org/10.1016/j.agrformet.2011.09.005)

[14] Ramirez-Villegas J, Jarvis A, Läderach P. Empirical approaches for assessing impacts of climate change on agriculture: The EcoCrop model and a case study with grain sorghum. *Agric For Meteorol* [Internet]. 2013;170:67–78. Available from: <http://dx.doi.org/10.1016/j.agrformet.2011.09.005>

[15] Hijmans RJ, Guarino L, Cruz M, Rojas E. Computer tools for spatial analysis of plant genetic resources data : 1 . DIVA-GIS. *Plant Genet Resour Newsl*. 2001;127:15–9.

[16] van Loon MP, Deng N, Grassini P, Rattalino Edreira JI, Wolde-meskel E, Bajjukya F, et al. Prospect for increasing grain legume crop production in East Africa. *Eur J Agron* [Internet]. 2018;101(September):140–8. <https://doi.org/10.1016/j.eja.2018.09.004>

[17] Telaye A, Bejiga G, Saxena MC, Solh MB. Cool-season Food Legumes of Ethiopia. Proceedings of the First National Cool-season Food Legumes Review Conference, 16-20 December 1993, Addis Abeba, Ethiopia. ICARDA/Institute. 1994. vii + 440 pp.

[18] Phillips S. “A Brief Tutorial on Maxent” in Species Distribution Modeling for Educators and Practitioners. *Lessons Conserv* [Internet]. 2010;3:107–35. <http://ncep.amnh.org/linc>

[19] Hijmans RJ, Cameron SE, Parra JL, Jones PG, Jarvis A. Very high resolution interpolated climate surfaces for global land areas. *Int J Climatol*. 2005;25(15):1965–78.

CLIMATE CHANGE IMPACTS ON ULZA DAM LIFESPAN

PhD Student Klodian Zaimi ¹

Assoc. Prof. Fatos Hoxhaj ²

Sergio Fattorelli ³

Francesca Ramazzina ⁴

^{1,2} Institute of GeoSciences, Energy, Water and Environment, Albania

^{3,4} BETA Studio srl, Italy

ABSTRACT

Ulza Dam is one of the oldest hydropower infrastructures in Albania. The water capacity of the reservoir has been reduced because of the accumulation of the sediments coming from Mat River. The bathymetric measurements and river sediment transport are used for quantifying the water storage change up to nowadays. Analyzing the future climate change impact in the sediment transport from the river is very important for understanding the Ulza Dam lifespan. In order to analyze the sediment regime in the future, the climate change projection from the EURO-CORDEX has been downscaled for Mat River catchment and used as input for the HEC-HMS hydrological model considering also the erosion and sediment module. The hydrological model was also calibrated with the MUSLE parameters, and it reproduces the average value of the total sediment transport. The analysis of climate change impact on erosion and sediment transported at the reservoirs was done considering the mean annual load for the different 30-year simulated periods related to values from the historical period 1981-2010. Considering the impacts of climate change, the mean annual sediment siltation could increase for RCP4.5 and RCP8.5 scenarios. Over this hypothesis, the remaining lifespan can be reduced drastically in both scenarios. Different land-use scenarios were analyzed to evaluate the impact of erosion and, because the current land use scenario doesn't produce any impact on the hydrological process, but only effects at a small scale, two hypothetical scenarios were defined at large scale and applied for Mat River catchment. Extensive management of land use and reforestation produce a positive effect on the hydrological process and reducing the erosion rate. The change of land use significantly counteracts the negative effects of climate change by 15% and a 24% reduction in the case of these land-use scenarios.

Keywords: *climate change, hydrological model, sediments, land-use, catchment*

INTRODUCTION

Ulza dam was built between 1952 and 1958 in the Mat river. The dam and the hydro-power plant are situated next to the village Ulza and are in the vicinity of the town of Burrel in Albania. The dam is of concrete-gravitational type with a height of 64.2 m and length of the crown of 260 m. The total volume of the reservoir (in the period when it was built) was 240×10^6 m³, and the volume of the body of the dam is 260 000 m³. The average annual inflow of water in the reservoir is 1170×10^6

m³. The altitude of the crown of the dam is 131.7 m a.s.l. The maximal water level of the reservoir is 129.5 m and the maximal operative level is one meter lower, 128.5 m. The minimal operational water level is 117 m. The weir is on the altitude of 109.0 m a.s.l. with a maximal discharge capacity of 2160 m³/s. The maximal discharge of Mat river for the Ulza dam cross-section is 1200 m³/s [1]. The reservoir “Ulza” has a primarily energetic function, but also it has several secondary functions like fishing, tourism, local-climatic and other functions. Because of this, the reservoir “Ulza” is of grave importance not only for the region but also for the whole country. Ulza catchment is a sub-basin of the Mati river basin about 70 km from Tirana, covering almost the entire Mat district of the Diber region. The total area of the Ulza catchment is 1224 km². The surrounding mountains forming the watershed are over 2000 m a.s.l., with the highest peak of 2245 m a.s.l. The length of the main tributary, the Mat River, is about 68 km. The average slope of the river is around 0.3% in the valley from Klos to Ulza and around 4% in the mountain area. The following Figure 1 shows the hypsometric curve of the Ulza catchment. It can be observed that the catchment can be considered in his late maturity stage according to Scheidegger's definition [2].

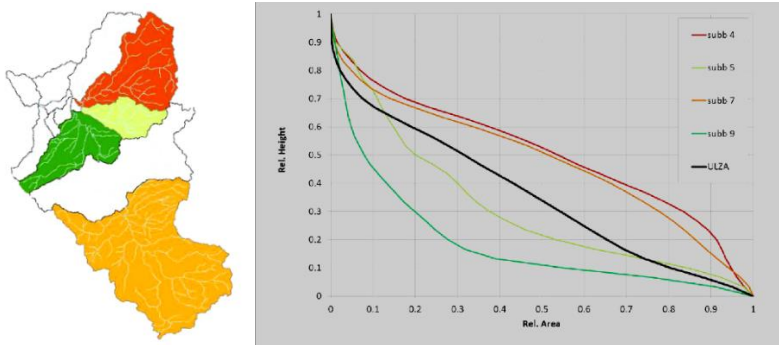


Figure 1 – Hypsometric curves of some sub-basins: sub-basins n.5 and 9 (green) are in the old age, sub-basins 4 and 7 (red, orange) are in the maturity age.

The geologic formations in the Ulza catchment belong mainly to highly consolidated magmatic (effusive, ultrabasic, etc.) rocks, that bordering the basin in the upper and the central part. The lower part of the Mat River is composed of brown soils rich in humus. The soils are characterized by low reaction and limited fertility. Erosion and land degradation are some of the main problems in the watershed, leading to downstream problems on landslides and flooding. About 70% of the Ulza basin is covered by forest (both broad-leaved and coniferous) and less than 3% of the area is bare or only barely wooded. Grasslands and pastures cover about 14% of the area, while 12% are dedicated to agriculture. The analysis of the available CORINE Land Cover maps from 2000, 2006 and 2012 and of the data collected for this study shows that there’s not been an evident evolution in land use during the last years. It can be observed that from 2000 to the present days there are no significant changes in land cover (less than 0.1% for some land use classes). This situation doesn’t affect the hydrological cycle at the basin scale and as a consequence, there is no significant change in sediment transport. The water level data from Shoshaj hydrological station have been converted to discharges data, for

the HEC-HMS hydrological model calibration, together with the calculated (from Ulza dam operator) inflow to the Ulza reservoir.

MATERIALS AND METHODS

For the simulations, the dataset (temperature and precipitation) used is the 30 years weather data originated from bias-corrected EURO-CORDEX, the European branch of the international CORDEX initiative, which is a program sponsored by the World Climate Research Program. This dataset represents also the basis of what was used in the climate change analysis, whose aim is to provide high-resolution climate projection data for impact analysis on the Ulza catchment area with the use of bias-corrected climate data for the 3 periods:

- a. on the period 1981-2010 (historical data);
- b. on the period 2011-2100 under IPCC RCP4.5 scenario;
- c. on the period 2011-2100 under IPCC RCP8.5 scenario.

Assessment of the models' bias and application of the bias correction techniques require, as a fundamental preliminary step, the availability of good-quality long time series of observations for the simulated meteorological variables to be corrected. Daily precipitation and daily maximum and minimum temperature for the period 2002-2011 (stations Macukull, Kurbnesh, Bulqize, Shengjergj, Fshat-Klos, and Burrel). Based on this concept, the observed data was validated through a basic integrity test and a test for the identification of anomalous values. On the basis of these tests, the initial dataset was reduced. The "best" model was selected on the basis of a comparison between the available observed precipitation and temperature data and all the currently available EURO-CORDEX simulations over the area of interest. A preliminary evaluation based on the HEC-HMS hydrological model was conducted for the period 2002-2011. The model was calibrated based on the water level data at Ulza dam, elaborated to obtain the flow data, based on the storage capacity. Shoshaj hydrological station discharge data was used for the calculation of the total sediment transport, equal to 1254 t/year/km². The HEC-HMS hydrological model has also been calibrated with the MUSLE parameters, and it reproduces the average value of the total sediment transport. Total sediment transport simulated at Ulza reservoir shown in Figure 2, is calculated to be 1266 t/year/km². The model works transporting the sediment that reaches the reservoirs during main hydrological events. With this method, the calibration was achieved, and the model can be used for future analysis. The model runs also for the 30 years period 1981 – 2010, whose meteorological data were obtained from the bias-corrected EURO-CORDEX model. During the 30 years period, the average precipitation trend is characterized by higher rainfall amounts, that produce a greater value of sediment at the reservoirs, equal to 1472 t/year/km² for Ulza dam. These numbers are used in the comparison of different scenarios. As anticipated, the land-use scenario with a simple projection of the current trend doesn't present any significant changes with reference to soil conservation and water balance. In order to verify a significant impact, different assumptions must be done as important land-use changes have been considered in order to analyze the impacted run-off and

erosion. Different scenarios can be introduced in order to define any action plans for reducing erosion in the dam reservoir.

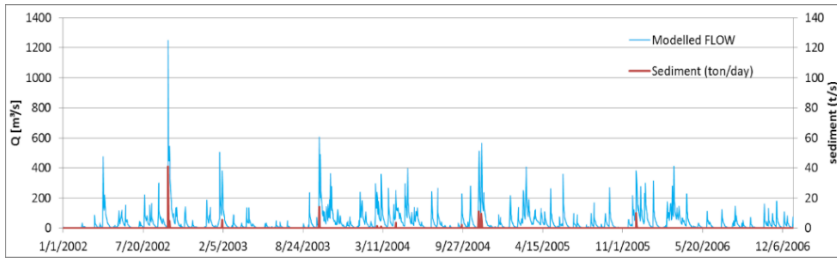


Figure 2 – Model results for Ulza reservoir, simulated water flow, and sediment load.

RESULTS AND DISCUSSION

In general, from the results obtained, the climate change signal is well preserved when the calibration contains more data. Given the objective of the present hydrological study, it is important to note that the total annual precipitation presents a fairly constant trend, lightly decreasing in the case of the IPCC RCP85 scenario for the annual precipitation trend for Fshat-Klos meteorological station. The maximum daily precipitation in the simulated period presents an increasing trend (+20%) both in RCP45 and RCP85 shown in Figure 3 for Fshat-Klos meteorological station. Considering the calibration period 2002-2011, under RCP4.5 the trend is properly preserved by bias-corrected model for temperature variables, while for precipitation slight differences in trend values are recorded for Burrel station. Under RCP8.5 trend is generally well preserved for each variable and for each case.

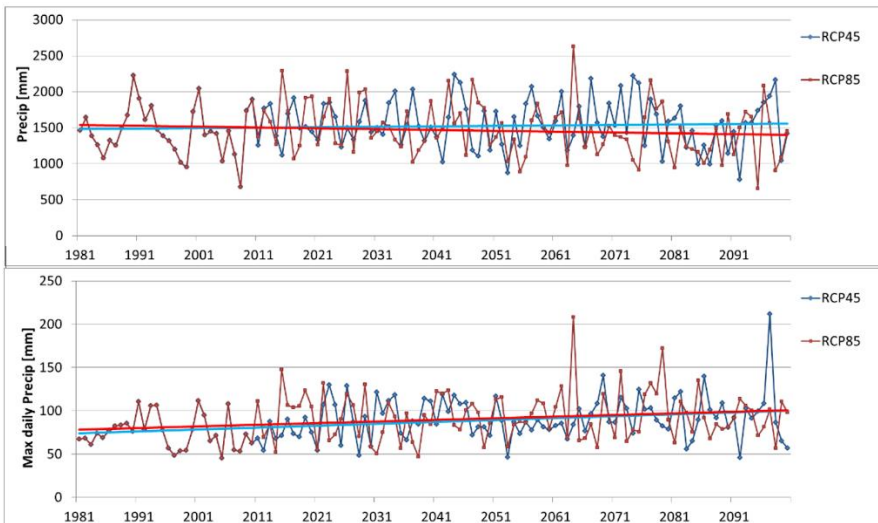


Figure 3 – Annual and Maximum daily Precipitation at Fshat-Klos meteorological station in the IPCC RCP4.5 scenario (blue line) and IPCC RCP8.5 scenario (red line).

The first results of the high-resolution (EUR-11) future climate simulations from EURO-CORDEX were presented in the literature in 2013. The analysis carried out was directed towards regional climatic changes in Europe, addressing the differences between mean changes in annual mean temperature and total precipitation for the IPCC RCP4.5 and RCP8.5 scenarios [3]. In HEC-HMS the physical watershed is represented in the basin model. Hydrologic elements are added and connected to one another to model the real-world flow of water in a natural watershed. The model components used to simulate the hydrological process are including precipitation and temperature data [4]. The Modified USLE method (Williams, 1975) was adapted from the original Universal Soil Loss Equation, based on precipitation intensity [5]. The MUSLE equation changed the formulation to calculate erosion from surface runoff instead of precipitation. Ulza basin was divided into many sub-basins in order to better calculate the inflow at the reservoir. MUSLE parameters were attributed based on the analysis carried out in GIS environment, to identify the critical areas. The following Figure 4 shows the analysis of the hydrological model results for Ulza catchment in terms of simulated maximum annual flow (daily values) using rainfall and temperature dataset of RCP4.5 and RCP8.5 scenarios.

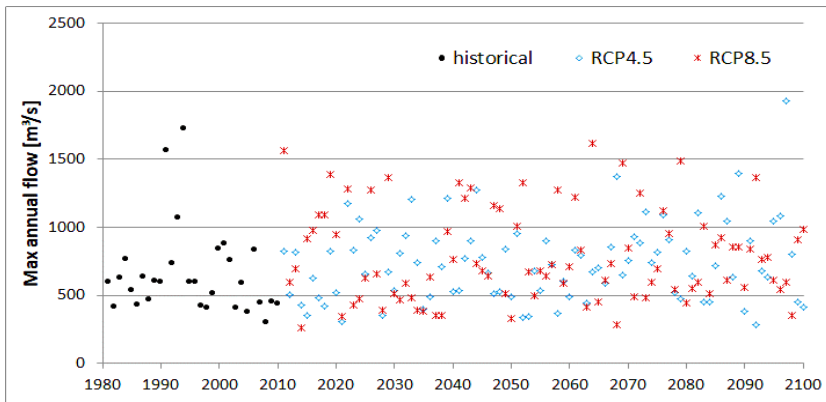


Figure 4 – Hydrological model results for Ulza basin: simulated maximum annual flow using rainfall and temperature dataset of RCP4.5 and RCP8.5 scenarios.

It can be observed that there is a slight variation of the highest flow peaks caused by extreme events (i.e. 100 years return period) and the simulated maximum annual flow series present a slightly increasing trend both for RCP4.5 and RCP8.5 scenarios. The probability density distribution (Gaussian) of simulated maximum annual flow (Figure 5) shows a small different behaviour of the two CC scenarios in terms of flow peaks mean value. The RCP8.5 scenario results show more flow peaks in the range from 1200 to 1800 m^3/s than RCP4.5 scenario results. The distribution of medium-high flow peaks is more frequent in the CC scenarios for the range 400-600 m^3/s in comparison with the historical period. The flows with a peak in the range of 600-800 m^3/s become also more frequent. From the CC scenarios, a 19% increase of the annual mean flow is calculated, as compared to the historical period results. The mean flow grows from 40.4 m^3/s (historical) to 48.0 m^3/s and 48.1 m^3/s , respectively for RCP4.5 and RCO8.5 scenarios. The climate

change scenarios lead to more rainy winter and more droughts in summer. Considering rainfall events, the more significant variations are expected in November and December, with a 50% increase in monthly mean flow. Considering the dry period, the more significant variations are expected from June to August, with a 37% and 30% decrease of monthly mean flow respectively in RCP8.5 and RCP4.5 mean flow. The mean daily flow data were used to evaluate the changes in the retention basin in terms of volume and water balance. To define the mean daily water demand taken for multi-purpose use from the reservoir, with the same procedure above description for inflow data, has been analyzed the daily average discharge from Ulza reservoir from 1981 to nowadays. From the complete list of data has been removed the contribution from the spillway.

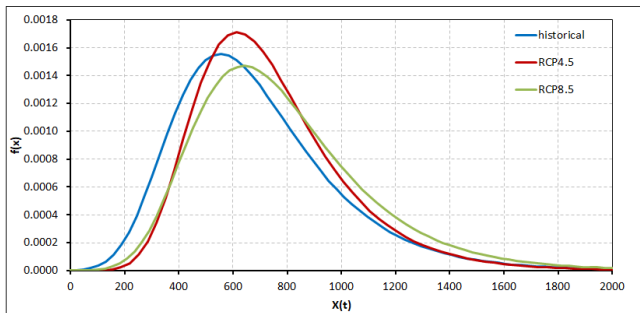


Figure 5 – Hydrological model results for Ulza basin: probability density distribution (Gaussian) of simulated maximum annual flow using rainfall and temperature dataset of RCP4.5 and RCP8.5 scenarios.

The analysis of climate change impact on erosion and sediment transported at the reservoirs was done considering the mean annual load for the different 30-year simulated periods. Figure 6 shows the relative value of the sediment load at the reservoir in relation to the first 30-year simulated period (1981-2010), the sediment load is closely related to the rainfall-runoff events and their distribution. RCP4.5 scenario would lead up to 1.25 the current sediment load while the RCP8.5 scenario would lead up to 1.30 the current sediment load in the last 30-year simulated period.

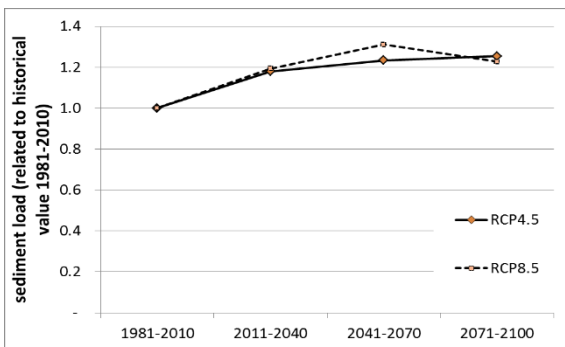


Figure 6 – Model results for Ulza basin: simulated sediment load at the reservoir for RCP4.5 and RCP8.5 scenarios (values are related to historical value 1981-2010)

The current total specific average annual sediment inflow has been evaluated to be about 1214 t/y, km². Considering an average bulk density of bottom sediment

of 1,20 t/m³ and trapping efficiency of the reservoir of 83%, the current mean annual sediment siltation in the reservoir could be evaluated in 1052000 m³/y. The current reservoir total storage volume has been evaluated to be 177 Million m³. The remaining lifespan, until complete filling of the reservoir, in the same hypothesis, could be evaluated in about 168 years from nowadays. Considering climate change scenarios, the mean annual sediment siltation could increase to 1315000 m³/y for the RCP4.5 scenario and to 1370000 m³/y for the RCP8.5 scenario. Over this hypothesis, the remaining lifespan would reduce to 134 or 119 years respectively. The present paragraph describes the combined effects of climate change and hypothetical land-use scenarios for 2071-2100. As described above, many different land-use scenarios were analyzed in order to evaluate the impact in terms of erosion and, because the projected current land-use scenario produces only impact at a small scale on the hydrological process. The two hypothetical scenarios were defined on a large scale. In order to verify the combined effect of climate change and land-use scenarios, the simulations listed in Table 1 were modeled.

Table 1 – Simulations modeled to analyze the combined effect of climate change and land-use scenarios for 2071-2100.

CC scenario	Land-use scenario
RCP4.5	S2: all land not currently under forest is reforested, with the exclusion of urban areas
RCP4.5	S3: all land classified as US3 (tree crops), US4 (agricultural land), US5 (bare soil) are converted to US2 Land use Index
RCP4.5	S4: all land classified as US4 (agricultural land), US5 (bare soil) are converted to US3 Land use Index
RCP4.5	S5: deterioration of the current situation, with a 20% decrease of currently forested areas
RCP8.5	S2: all land not currently under forest is reforested, with the exclusion of urban areas
RCP8.5	S3: all land classified as US3 (tree crops), US4 (agricultural land), US5 (bare soil) are converted to US2 Land use Index
RCP8.5	S4: all land classified as US4 (agricultural land), US5 (bare soil) are converted to US3 Land use Index
RCP8.5	S5: deterioration of the current situation, with a 20% decrease of currently forested areas

Extensive management of land use and reforestation produce a positive effect on the hydrological process and reducing the erosion rate. The change of land use in Scenario S2 significantly counteracts the negative effects of climate change (15% and 25% reduction for Ulza dam). In particular, the positive effect would balance the climate change impact (Figure 7), controlling the erosion phenomena and extending the lifespan of the Ulza reservoir.

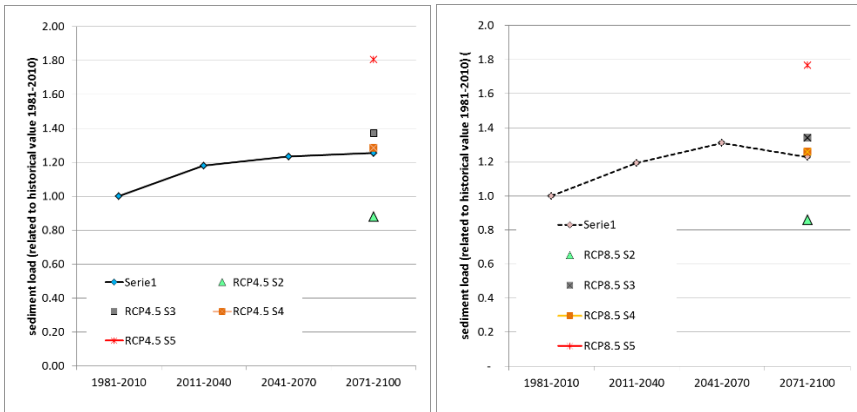


Figure 7 – Model results for Ulza reservoir for the period 2071-2100: simulated sediment load for RCP4.5 (left) and RCP8.5 (right) scenarios with different land-use scenarios (current, S2, S3, S4, S5).

CONCLUSION

Ulza dam is one of the most important hydropower plants in Albania. The capacity of the reservoir is reduced from the time of construction in the middle of the past century. The Climate Change scenario was selected on the base of a comparison between the available observed precipitation and temperature data and the available EURO-CORDEX simulations over the area of interest. The effect of climate change in water regime has increased the siltation of the total sediments in the Ulza reservoir. The climate changes current land-use scenario produces only impact at a small scale on the hydrological process. For this reason, two hypothetical scenarios were defined on a large scale together with climate change. The current reservoir total storage volume has been evaluated to be 177 Million m³. The remaining lifespan, until complete filling of the reservoir with the present trend, is about 168 years from nowadays. Considering the two climate change scenarios, the remaining lifespan would reduce to 134 or 119 years respectively. The study shows that land-use is very important in the future of the Ulza reservoir. The change of land-use in Scenario S2 significantly counteracts the negative effects of climate change (15% and 25% reduction for Ulza dam). The negative impacts of climate change in the reservoir capacity can be reduced drastically with the application of the best practices of the land-use in this catchment.

REFERENCES

- [1] Blinkov I., Study and Analysis of Innovative Financing for Sustainable Forest Management in the Southwest Balkan, WB –PROFOR, October 2014.
- [2] Scheidegger A.E., Systematic geomorphology, Wien and New York Springer, 1987.

[3] Jacob D., EURO-CORDEX: new high-resolution climate change projections for European impact research, *Reg Environ Change*, 2013, 14(2), 563–578.

[4] USACE 2000, HEC-HMS hydrologic modeling system user's manual, Hydrologic Engineering Center, Davis, CA, USA, 2000.

[5] Williams J.R., Sediment-Yield Prediction with Universal Equation Using Runoff Energy Factor. In: *Present and Prospective Technology for Predicting Sediment Yield and Sources*, US Department of Agriculture, Agriculture Research Service, Washington DC, 1975, pp 244-252.

NUMERICAL MODELLING OF DUST DISTRIBUTION IN THE ATMOSPHERE OF A CITY WITH COMPLEX RELIEF

DSc. Aleksandre Surmava ¹

DSc. Demuri Demetrasvili ²

MSc. Vepkhia Kukhalashvili ³

Dr. Natia Gigauri ⁴

^{1, 2, 4} Institute of Hydrometeorology at the Georgian Technical University,
Georgia

^{1, 2, 3} M. Nodia Institute of Geophysics at the Iv. Javakishvili Tbilisi State
University, Georgia

ABSTRACT

Microscale processes of dust distribution in the city of Tbilisi with very complex topography are modeled using a 3D regional model of atmospheric processes and numerical integration of the transport-diffusion equation of the impurity. The Terrain-following coordinate system is used to take into account the influence of a very complex relief on the process of atmospheric pollution. Modeling is carried out using horizontal grid steps of 300 m and 400 m along latitude and longitude, respectively. The cases of the stationary background of eastern and western weak winds are considered. In the model, motor transport is considered as a nonstationary source of pollution from which dust is emitted into the atmosphere.

Modelling of dust micro-scale diffusion process showed that the city air pollution depends on spatial distribution of the main sources of city pollution, i.e. on vehicle traffic intensity, as well as on spatial distribution of highways, and micro-orography of city and surrounding territories. It is shown that the dust pollution level in the surface layer of the atmosphere is minimal at 6 a.m. Ground-level concentration rapidly grows with increase of vehicle traffic intensity and by 12 a.m. reaches maximum allowable concentration ($MAC = 0.5 \text{ mg/m}^3$) in the vicinity of central city mains. From 12 a.m. to 9 p.m. maximum dust concentration values are within the limits of 0.9-1.2 MAC. In the mentioned time interval formation of the highly dusty zones, and slow growth of their areas and value of ground-level concentrations take place. These zones are located in both central and peripheral parts of the city. Their disposition and area sizes depend on spatial distribution of local wind generated under action of complex terrain, as well as on the processes of turbulent and advective dust transfer. From 9 to 12 p.m. reduction of dust pollution and ground-level concentration takes place. After the midnight city dust pollution process continues quasi-periodically.

As a result of the analysis of the vertical distribution of dust concentration is obtained that a basic dust mass emitted into the atmosphere is located in the 100 m surface layer. The concentration value in the upper part of this layer reaches 0.8 MAC and rapidly decreases with altitude increase.

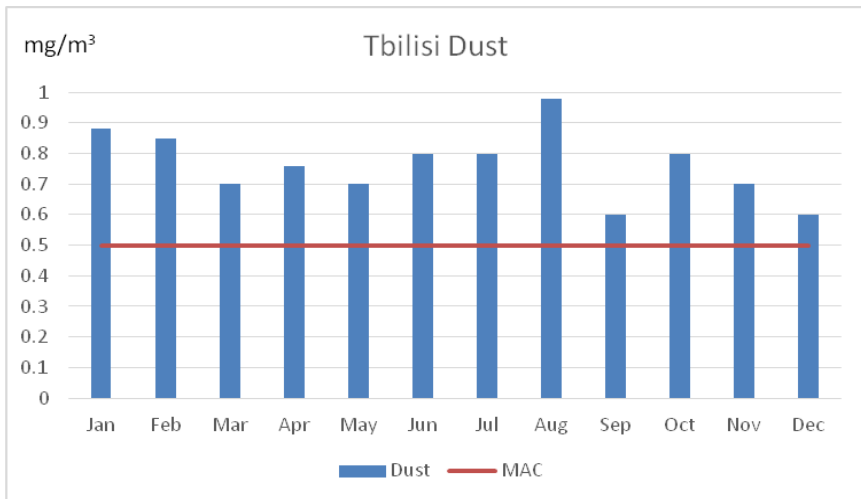
Keywords: Numerical modeling, pollution source, diffusion, dust distribution, atmospheric wind.

INTRODUCTION

Human health heavily depends on the level of atmospheric air purity [1], [2]. According to World Health Organization data, 7.6% of population mortality in 2016 has been caused by atmospheric air pollution [3]. Therefore, the study of environmental facilities pollution and its mitigation is a very important problem from both ecological and human health protection standpoints.

Tbilisi is located in the South Caucasus and represents a main junction point of the Great Silk Road that connects Europe and Asia. Many thousands of light and heavy vehicles pass through a city every day, and hundreds of a thousand cars drive about narrow and complex-shape city streets. Microparticles emitted from cars and dust picked up from the underlying surface are the main sources of city pollution. According to data of National Environmental Agency at the Ministry of Environmental Protection and Agriculture of Georgia, dust concentration frequently exceeds maximum allowable concentrations [4] (Fig. 1).

Fig.1. Monthly average dust concentrations in Tbilisi air, in 2015.



Currently, atmospheric air pollution studies using the regular measurements [5], [6], mathematical diagnostic and forecast models [7], [8], [9] are carried out in many cities worldwide.

In the presented article, for the first time for the city of Tbilisi, the kinematics of dust propagation emitted during motion of motor transport – the main polluting source of the atmosphere, will be studied via numerical modelling. The numerical model of atmospheric processes on the Caucasus and polluting ingredients propagation elaborated in the M. Nodia Institute of Geophysics at I. Javakhishvili Tbilisi State University will be used for modelling [10], [11].

STATEMENT OF THE PROBLEM

For modelling of the dust distribution process in the Tbilisi city the area with sizes $30.6 \times 24 \text{ km}^2$ is considered. Tbilisi city is placed in the center of this area. Its relief is very difficult: from the east, west, north and from south-west Tbilisi is surrounded by mountain ridges, on south-east of city a lowland territory is located. Within the city of Tbilisi there are the several small mountains and gorges. A relief altitude varies from 350 m to 1.5 km from the sea level. In Fig. 2 Tbilisi orography is shown. Actual geographic coordinates are placed on the axes.

For proper description of the spatial-temporary evolution of meteorological and pollution processes over a territory with difficult relief the relief-following coordinate system $(x, y, \zeta = (z - \delta)/h)$ is used. Here x and y and z are the orthogonal coordinate axes directed to the east, north and vertically upward, respectively; ζ is no-dimensional vertical axis; δ is altitude of relief; $h = H - \delta$; $H(t, x, y)$ is height of the tropopause; t is a time.

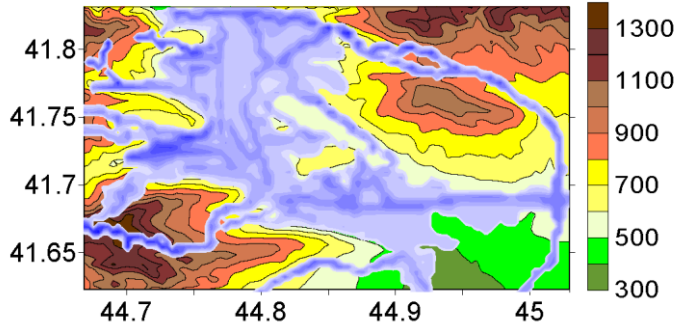


Fig.2. Tbilisi relief (in m) and the pollution sources (blue zone and lines).

Equation for dust atmospheric propagation in the taken coordinate system is written in the following form

$$\frac{\partial C}{\partial t} + u \frac{\partial C}{\partial x} + v \frac{\partial C}{\partial y} + (\tilde{w} - \frac{w_0}{h}) \frac{\partial C}{\partial \zeta} = \mu \left(\frac{\partial^2 C}{\partial x^2} + \frac{\partial^2 C}{\partial y^2} \right) + \frac{1}{h^2} \frac{\partial}{\partial \zeta} v \frac{\partial C}{\partial \zeta}, \quad (1)$$

where, C is dust concentration in atmosphere; u , v , w and \tilde{w} are the components of wind velocity along x , y , z and ζ axes; w_0 is rate of dust particle sedimentation determined according to Stoke's formula; μ and v – kinematic coefficients of horizontal and vertical turbulence.

Initial and boundary conditions used in the model allow to modelling the dust distribution in Tbilisi in case of stationary background eastern light air. The background wind speed grows linearly from 1m/s at $z = 2 \text{ m}$ to 20 m/s at $z = 9 \text{ km}$. Relative atmospheric moisture is 45%.

The wind speed components and kinematic coefficients of turbulences in the surface layer of atmosphere and in free atmosphere on the any moment of the time

are defined by means of the Regional Model of Atmospheric Processes in the Caucasus [10], [11].

The initial concentrations of the dust at 2 m height in the populated area are taken as 0.1 mg/m^3 , in the unpopulated area – 0. Using analysis of the observation and experimental measurement data there was found that in Tbilisi in the vicinity of central motorways there is almost a linear dependence of dust concentration on car traffic intensity. It was also found that near the central motorways and streets, where intensity of car motion is about 8000 cars per hour, the dust concentration is approximately equal to 0.8-1.3 MAC. Therefore, the initial and boundary concentrations in the vicinity of main city streets are taken in accordance to motor traffic intensity (Fig.2).

Equation (1) is solved numerically using the Crank-Nicolson scheme and splitting method [12]. The grid steps are equal to 300 and 400 m along axes x and y , respectively. The vertical step in the free atmosphere is equal to $1/31$ in the relief-following system, in the surface layer it varies from 2 to 15 m. Calculations were made for the period 72 h with time step equal to 1 s.

RESULTS OF MODELLING

In Fig. 3 a spatial distributions of dust concentration and wind velocity obtained through calculations at 2, 100 and 600 m heights for $t = 0, 3$ and 6 hours are shown. It is seen from Fig. 3 that at 2 m height from underlying surface the dust pollution gradually decreases from the midnight and becomes minimal at 6 a.m. At this time, concentration value in the city and surrounding territories varies within the range of 0.001-0.2 MAC. Concentration equal to 0.1 MAC is obtained in the most part of the city, in both urbanistic and recreation zones and in unpopulated areas. At 100 and 600 m height the concentration is less changeable. Its value in the 600 m thick atmospheric layer varies within 0.1-0.3 MAC.

After 6 a.m., along with rapid growth of motor car traffic intensity, the increase of the quantity of dust entering the atmosphere and pollution of the city atmosphere are begins. At 9 a.m. at 2 m height dust concentration is increased alongside the highways and in their vicinity (Fig. 4). Advective, convective and diffusive dust transfer occurs influenced by local wind. Dust transfer direction is different and depends on the direction of local ground wind.

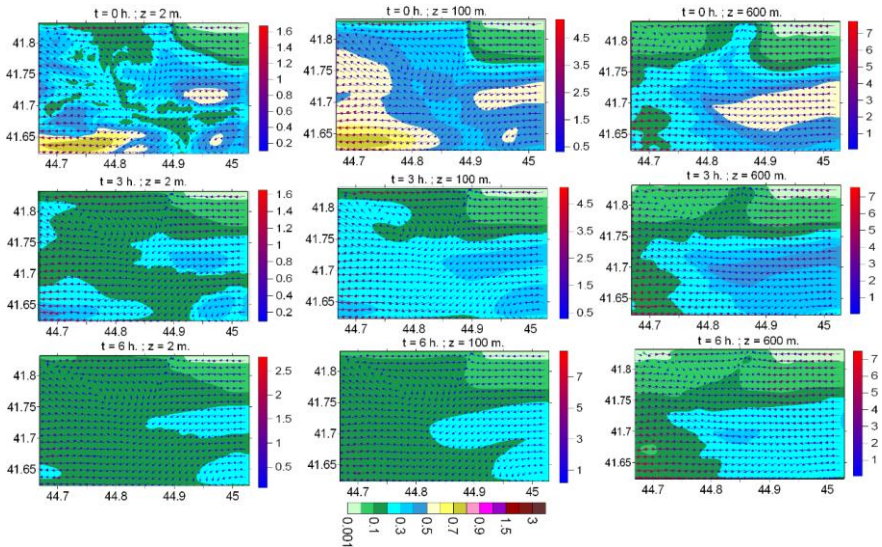


Fig.3. Wind velocity (in m/s) and dust concentration (in MAC) distribution at $t = 0, 3$ and 6 h at $2, 100$ and 600 m heights from earth surface.

From 9 a.m. formation of heavily polluted zones begins. Among these zones are the city center and some territories located in the northern and southern parts of city. In these territories are some motorways or they directly adjoin highways. Concentration values in the vicinity of highways are 0.9-1.2 MAC, and in remoted urban parts they are within the limits of 0.5-0.9 MAC. In recreation and unpopulated areas, where we have

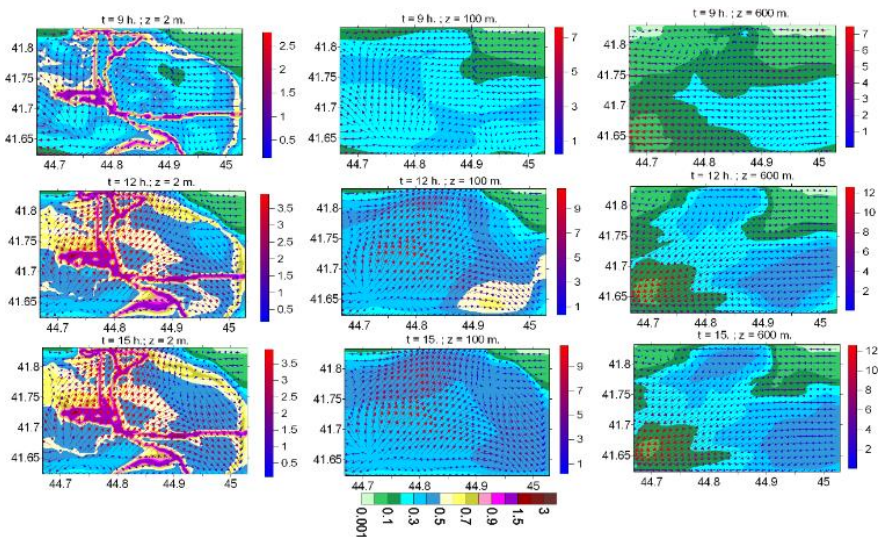


Fig.4. Wind velocity (in m/s) and dust concentration (in MAC) distribution, at $t = 9, 12$ and 15 h at $2, 100$ and 600 m heights from earth surface.

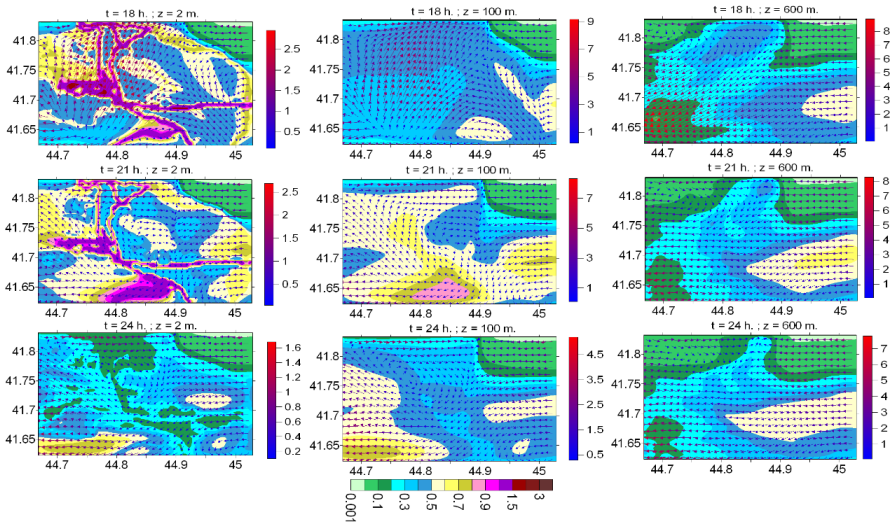


Fig.5. Wind velocity (in m/s) and dust concentration (in MAC) distribution, at $t = 18, 21$ and 24 h at $2, 100$ and 600 m height from earth surface.

no pollution sources, pollution mainly occur according to advective and diffusion transfer mechanisms. As a result, the concentration near to earth surface there is relatively small and varies in the range of 0.3-0.5 MAC. Dust available in the ground layer propagates upward and at noon dust concentration at 100 m height reaches 0.7 MAC, while at 600 m height – 0.5 MAC.

Starting with 3 p.m. and up to 9 p.m. the dust concentration spatial pattern doesn't experience any significant qualitative changes (Fig. 4, 5). Instead, we have quantitative changes: at 2 m height the area of high pollution zones in the central parts of the city is getting smaller, while in southern suburban parts it increases. Concentration increases in the surroundings of Tbilisi by-pass road and Tbilisi Sea, as well. Bands with the same concentration value experience deformation in time. Deformation has a complicated shape and is caused by time and space variation of local wind formed under influence of city terrain.

Maximum pollution level at 100 m height from earth surface is obtained when $t = 21$ h and it covers a significant part of modeling area. Its formation depends on mountain-and-valley circulation processes caused by daily temperature variation in the domain with complex relief, resulting from which an intense ascension of warmed air masses and vertical transfer of significant part of the dust take place during the day. By this moment, concentration values obtained via calculation are within the limits of 0.5-0.7 MAC at 100 m height from earth surface.

After 9 p.m. traffic intensity reduces and related dust dispersion in the atmosphere and atmospheric pollution level are getting smaller. When $t = 24$ h we obtain such spatial distribution of dust concentration, which is close to distribution obtained at $t = 0$ h. It shows, so the dust accumulated in the city atmosphere is taken out from this territory and city atmosphere self-purification occurs. Further

calculations showed that in case of stationary background wind a quasiperiodic change of dust concentration in the city atmosphere takes place.

CONCLUSION

Nonstationary process of dust propagation formed by motor transport in Tbilisi is surveyed. Space and time variation pattern of dust concentration in the city with complex terrain is studied. By analysis of wind velocity and concentration fields there is established that a spatial distribution of heavily polluted areas depends on many factors, namely: on highways disposition, traffic intensity, and on local circulation processes formed as a result of relief and background wind interaction under of the underlying surface thermal action.

It is obtained via calculations that Tbilisi atmosphere at 2 m height from earth surface is minimally polluted at 6 a.m. By this time concentration value doesn't exceed 0.2 MAC. From 6 a.m. to noon a rapid growth of dust surface concentration and formation of high pollution zones in the central and some suburban parts of the city occur. Concentration values in the high pollution zones are within the limits of 0.9-1.2 MAC. From noon to 9 p.m. dust concentration increases relatively slowly. In parallel, concentration spatial distribution change and accumulation zone formation take place. Dust concentration in the accumulation zone is high and roughly equals to 1.5 MAC. Vertical dust transfer becomes especially intense between 3 p.m. and 9 p.m. In this period of time concentration value at 100 m height above dust accumulation zone reaches 0.8-0.9 MAC.

ACKNOWLEDGMENT

This work was supported by Shota Rustaveli National Science Foundation of Georgia (SRNSFG) [FR-18 -3667].

REFERENCES

- [1] Ji S., Cherry C.R., Zhou W., Sawhney R., at al., Environmental justice aspects of exposure to PM_{2.5} emissions from electric vehicle use in China, *Environ. Sci. Technol.*, vol. 49, pp 13912-13920, 2015.
- [2] Ikenna C.E., Hemkens L.G., Bucher H.C., Hoffmann B. at al., *Environ Health Perspective*, vol. 123(5), pp 381–389, 2015.
- [3] Mortality and burden of disease from ambient air pollution-WHO. https://www.who.int/gho/phe/outdoor_air_pollution/burden/en/
- [4] Environmental pollution, <http://nea.gov.ge/ge/service/garemosdabindzureba/7/biuleteni/>.
- [5] Amato F., Pandolfi M., Moreno T., Furger M., at al., Sources and variability of inhalable road dust particles in three European cities. *Atmos. Environ*, vol. 45, pp 6777–6787, 2011. DOI: 10.1016/j.atmosenv.2011.06.003.

[6] Kutenev V.F., Stepanov V.V., Azarov, V.K., About real Particulate Emissions from Road Transport, Ecology, Russia, vol. 4 (81), pp 45-47, 2013. (in Russian).

[7] List of atmospheric dispersion models. https://en.wikipedia.org/wiki/List_of_atmospheric_dispersion_models.

[8] Long J., Cheng S., Li J., Chen D., Zhou Y. et al., A Monitoring and Modeling Study to Investigate Regional Transport and Characteristic of PM_{2.5} Pollution. Aerosol and Air Quality Research, vol. 13, pp 943-956, 2013. DOI: 10.4209/aaqr.2012.09.0242

[9] Shlichkov, V.A., Malbakhov, V.M., Leghenin, A.A., Numerical Modeling of Atmospheric Circulation and Transfer of Contaminating Impurities in Norilsk Valley, Atmospheric and Oceanic Optics, USSR, vol. 18, pp 490-496, 2013. (in Russian).

[10] Gigauri N.G., Surmava A.A., Spatial Distribution of the Local Meteorological Fields and Dust Concentration in Kakheti Atmosphere in Case of the Northern Background Wind. J. Georgian Geophysics Soc., Issue B, Physics of Atmosphere, Ocean and Space Plasma, Georgia, vol. 20 B, pp 11-23, 2017.

[11] Gigauri N.G., Gverdtsiteli L.V., Surmava A.A., Intskirveli L.N., Numerical Simulation of Industrial Dust Distribution in the Territory of Zestafoni, Georgia, WIT Transactions on Ecology and the Environment, Georgia, vol. 230, pp 119-128, 2018. DOI:10.2495/AIR180111.

[12] Marchuk G.I., Mathematical modelling in the environmental problem, USSR, p 319, 1982 (in Russian).

**SMOG IN BIALYSTOK IN POLAND. DATA OF PM 2.5 AND
PM 10 PARTICULATE MATTER IN OUTDOOR AIR
MEASURED IN 2017-2018 BY "THE LABORATORY OF
ENERGY-EFFICIENT ARCHITECTURE AND
RENEWABLE ENERGIES" AT FACULTY OF
ARCHITECTURE OF BIALYSTOK UNIVERSITY OF
TECHNOLOGY**

Dr arch. Adam Turecki

Bialystok University of Technology, Poland

ABSTRACT

The differences between what in the winter 2017 was presented by the government measurement station of air quality, belonging to the Chief Inspectorate of Environmental Protection (CIEP) in Bialystok in Poland, and what the citizens could see and smell, were the reason for installing the monitoring system of PM10 and PM2.5 particulate matter, in the "Laboratory of Energy-efficient Architecture and Renewable Energies" (LEARE) at the Faculty of Architecture of Bialystok University of Technology. The measurements were compared with done by CIEP and the information of "The World Air Quality Index" (WAQI). This project started in 2007. It is proving transparent Air Quality information for more than 70 countries, covering more than 9000 stations in 600 major cities. Since 16 Nov 2017, data was also downloaded from the new European Air Quality Index (EAQI) website, created by the European Environment Agency (EEA). From the beginning of 2018, data from the public-private service AIRLY was added to the study. They installed four online dust meters in Bialystok. The density of the dust measurement network was still insufficient, so the mobile measurements were started. Recently, the use of a drone equipped with a dust meter for tests at various heights has begun.

Measurements deny EAQI presentation of so good air quality in Bialystok. The levels of PM2.5 and PM10 are often much higher than those presented by EAQI and CIEP. Government measuring station, located in the center of Bialystok, poorly reflects air pollution in peripheral districts.

Keywords: smog, PM2.5 PM10, LEARE, Bialystok, monitoring

INTRODUCTION

Thirty-three cities from Poland are included in the World Health Organization (WHO) Report 2016 listing fifty cities in the European Union with the most polluted air. In the report of the European Environment Agency (EEA) 2017 mentioning the concentration of PM2.5 in the air in European cities among the ten most polluted as many as seven cities are in Poland. 16 Nov 2017 European Environment Agency

(EEA) and the European Commission introduced a new European Air Quality Index (EAQI) that allows checking the current air quality across Europe's cities and regions. The new EEA online service is based on measurements from more than 2000 air quality-monitoring stations across Europe. The Index consists of an interactive map presenting the local air quality situation at station level, based on five key pollutants that harm people's health and the environment: particulate matter (PM2.5 and PM10), ground-level ozone (O3), nitrogen dioxide (NO2) and sulphur dioxide (SO2). The worst rating for any of the five pollutants measured by the station are shown by a coloured dot on the map, corresponding to the pollution level (turquoise - good, green - fair, yellow - medium, orange - poor, red - very poor).

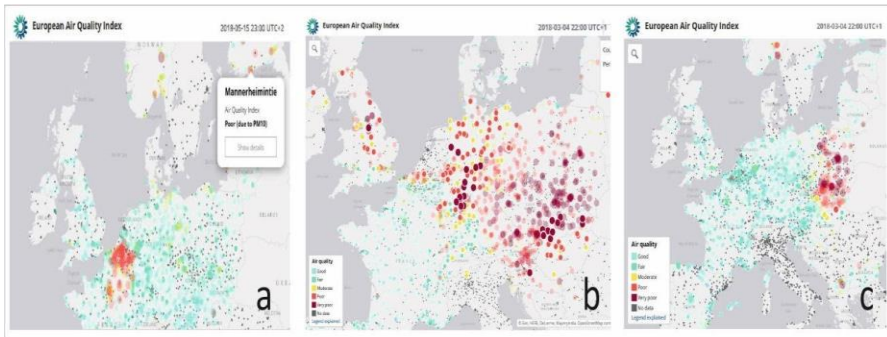


Fig.1 Air quality in Europe according to EAQI: a- rare, b- sometimes, c- often; (gray points mean non-functioning or disconnected measuring stations), a. A. Turecki

BIALYSTOK

The population of the city was 300.000, it's area ~102 km². Therefore, the population density is low - less than 3 thousand persons per 1 km². The city looks green. Especially in terms of greenery. It has many gardens, squares, parks, a very large XVIII c. garden composition, even meadows and forests. Within the city limits, there are as much as 1847 ha, almost 19 km² of forests, much more in the neighborhood -1175km². The city is surrounded by them. Currently, after the fall of factories from the 19th and 20th centuries in the city, we have almost no industry that pollutes the environment. In statistics, everything looks "very eco". Some time ago, a slogan promoting the region - the "Green Lungs of Poland" - was created. And so it is, until winter comes. Then it gets a little redder and sometimes brown [Fig.1]. But not as badly as in cities in the south of Poland. Usually, on the governmental air quality maps Bialystok has a green indicator. But even ordinary "observations" reveal a slightly different picture. Especially in peripheral districts of one family houses.

There are several reasons - historical, technical, economic, social and wrong location of government measurement station.

- During the Second World War 80% of the city center was destroyed. New buildings are connected to the heating network of the city.

Thermal power plants, located in the periphery, have high chimneys, so “high emission” of exhaust fumes due to the effective filtration required by law is limited and usually blown out into suburban areas.

- Districts around the city center that survived WWII were inhabited usually by poor residents. Their homes were made in a very economical way with low insulation and tightness of the: walls, roofs and windows. Currently, many of them are almost one hundred years old and have not been renovated. The traditional heat sources of these houses are ovens and furnaces that use solid fuels. Their characteristic feature is a bad combustion process and heavy smoking during the ignition.
- The economic situation of some owners is bad, many of them are elderly. They cannot afford to improve technical condition of their houses, good quality fuel, sometimes any, so they burn waste. We define this as "energy poverty". Only municipal help can solve this problem.
- Poorly conceived economy and avarice forcing to not wasting anything that burnt can heat the house, as well as saving on the costs of waste disposal by burning. One can see the smoke in districts inhabited by wealthy owners [Fig.2].



Fig.2 Morning heating in one family houses district - S-E part of Białystok,

Source: A. Turecki

- The main municipal air quality measurement station is located in the middle of downtown Białystok [1] where buildings are connected to the heating network. What's worse, it was placed in the middle of large complex of 11-story buildings [Fig.3]. They form a high ring that stops the flow of air from neighboring areas and major urban roads,

so the air quality in this place is usually better than in other parts of the city.

That was the reason for installing the monitoring system of PM10 and PM2.5 particulate matter, in the "Laboratory of Energy-efficient Architecture and Renewable Energies" at the Faculty of Architecture of Bialystok University of Technology [2].



Fig.3 A – Hypsometry of Bialystok: 1- LEARE, 2- CIEP main station of air quality measurement, 3 – districts not connected to city heating net. B – photo of central district where main measurement station is located: 2- main station,
Source: A. Turecki

MONITORING SYSTEM

The basis of the system are two SDS011 dust meters analyzing the scattering of laser light on dust particles (Mie Theory). They are managed by a PIC microcontroller, with an Ethernet interface for transmission over the Internet. Current data is visible on two displays. SDS011 enables measurement of particles in the range of 0-999 $\mu\text{g}/\text{m}^3$. The meter has a built-in fan that forces the flow of sampled air through the laser sensor chamber. The system enables continuous readings and recording of data that it sends to the server. This allows you to generate charts and transmit current and historical data. At outdoor air humidity above 65% dust meter readings are overstated by fog droplets. Preheating the tested air can eliminate that problem, but LEARE monitoring hasn't such equipment yet.

The study of parallel measurements of dust meters with and without air preheating was presented by J. Bartyzel “at average air humidity of 65%, the differences of readings between the dustmeters with and without preheating differ by 10-15%”[3]. Such differences can be considered as acceptable at the values several times higher than recommended in the EU.

The meter analyzes the outside air stream in the ventilation unit with the intake at height 4m above the ground. Ventilation works in 24/7 mode. Measurements were taken and recorded every 30 seconds, what allows testing the short-term changes of dust.

However this meter isn't "golden standard", but in periods of good, average and poor air quality, without winds, it repeatedly shows similar values of PM2.5 and PM10 as the CIEP main measurement station. Due to the insufficient number of measurement stations, low-cost meters may be useful in assessing the distribution of air pollution in cities. Measurements of air dustiness around the burning waste warehouse in Warsaw were possible thanks to the dense network of such meters [4]. In December 2016, the National Advisory Council for Environmental Policy and Technology provided US-EPA recommendations for how to maximize the benefits of citizen science and ... integrate it into the full range of EPA's work [5].

The place where the laboratory was built has high variability directions of wind at low speeds, with an annually average lower than 3.5 m/s. In addition to measurements of air pollution, other data provided by weather station Davis, located on the roof of the laboratory, were used. It can monitor and record many parameters: external temperature, humidity, wind speed and direction, solar radiation, UV index, atmospheric pressure, precipitation. Five of them were used: external temperature, humidity, wind speed, wind direction and solar radiation.



Source: A.Turecki

MEASUREMENTS

The laboratory building is located on the border of two different types of districts. The city center connected to the heating network of Bialystok on the east side. From the west and south, the laboratory building parcel is adjacent to the district of old, two-story buildings, usually heated by burning poor quality fuel. They are both residential and commercial, so the behavior of their users and the duration of their operation vary. In residential buildings that are permanently inhabited, the use of cooking stoves and hearths is used for heating and preparing

meals. Small houses have single central oven, integrating heating and cooking. Heating usually takes place twice a day - in the morning and more intensively in the evening. Cooking three times - also in the afternoon. Commercial buildings, used during the day, are intensively heated once in the morning - at night they cool down.

The effect of heating these buildings on air dust around the laboratory building was tested. The dependence was visible during the windless days or when the winds were blowing from their side. Then the dust levels of PM_{2.5} and PM₁₀ were significantly increased. At that time photographs were taken to see the smoke from the chimneys. Long exposure times - from 10-30s allowed showing it also at night. The weather station Davis indicated outdoor air humidity above 65%.

When the wind blew from the side of neighboring buildings the system recorded “thermal activity” of their inhabitants. It showed not only heating in the early morning and evening hours, but also short-term lower increases during the day - probably associated with cooking.

At the end of 2017, only two CIEP stations and the LEARE measurement point were operating in Białystok. Only three measuring points is less than one on 33km² area, and all located in the city center. To test air pollution in the rest of the city, a portable dust meter was additionally used [Fig.5].

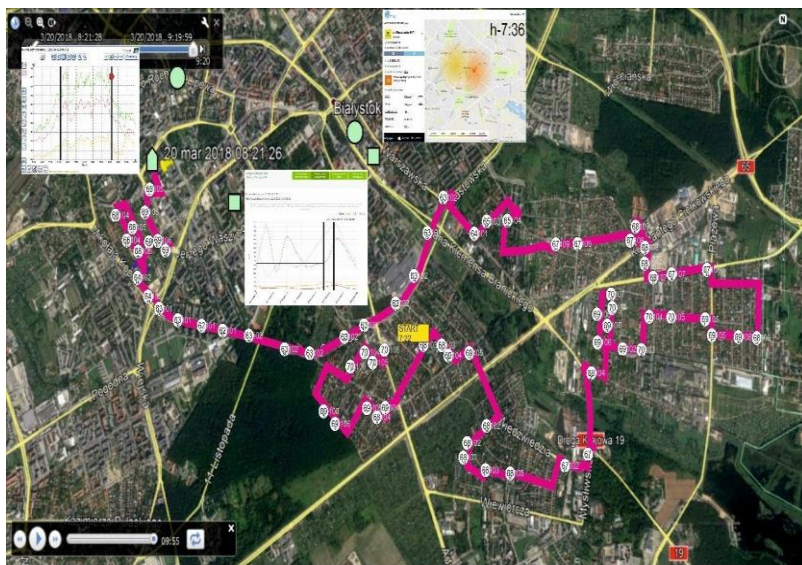


Fig.5 Graph of mobile measurement in S-E part of Białystok. The value of PM_{2,5}= ~62-70μg/m³, PM₁₀= ~101-106μg/m³; (20.03.2018, h. 7:22-8:21; dust meter SDS011 [without air preheating], mounted on the car, speed 30-40km/h, recorded every 30s; GPS positioning; GoogleEarth map; charts from CIEP, AIRLY and LEARE), Source: A. Turecki

At the end of April 2018 LEARE began the study of the vertical smog distribution using a drone to lift the dustmeter into the air at a height of 100m. The photos taken in winter 2017, from a height of about 30m showed a smog layer

approximately 50m [Fig.6]. These measurements will be continued in the next winter.



Fig.6 Smog visible on the long exposure photo (15s), N-E part of Bialystok, (31.03.2017 h.22:05

Source: A. Turecki

CONCLUSION

The LEARE monitoring system operate steadily for many months. During the periods of good, average and poor air quality, without winds, despite the use of low-cost meter it repeatedly shows similar values of PM2.5 and PM10 as the CIEP main measurement station. Local maximum concentrations of PM2,5 and PM10 often far exceeded the maximum values shown by the city station. The 30 second measurement period allows to show even short-term high particles concentrations, invisible in one and eight hours averages.

LEARE location on the border of district of old, two-story buildings, heated individually allows to study the impact of such districts on the level of air pollution. They determine the formation of smog in Bialystok - the city center is heated by a central network powered by municipal heat plants which have good filtration and thanks to their high chimneys, emissions are transferred to rural areas. In single family homes districts, there are characteristic hours of dust growth: 6-8, 13-15, 17-19 and 21-23. They are poorly presented in data measured by station located in the city centre.

Not only “energy poverty” and poor technical condition of old houses is the cause of smog formation in Bialystok - one can see the smoke in districts inhabited by wealthy owners.

Due to the insufficient number of measurement stations, low-cost meters may be useful in assessing the distribution of air pollution in cities. Such data, although not fully precise, allow to create maps of smog distributions in the city, helpful in future activities improving air quality, directing resources where they will be most effective

In cities with central districts connected to heating net and neighbourhoods of homes heated individually with bed solid fuel, measurements should be made by a many stations - central and peripheral in accordance with local wind directions.

Measurements carried out behind the ventilation unit with recuperation show improvement in air purity due to the efficient operation of its filters. This improves the health conditions in the buildings and reduces the risk of many diseases.

ACKNOWLEDGEMENTS

The author would like to thank the company "Bartosz Sp.j." from Białystok for help in constructing the monitoring system of PM2.5/PM10 and friendly support.

Partially funded as part of S/WA/1/2017 funded by MSWiN

REFERENCES

[1] PWIOS, Informacja Podlaskiego Wojewódzkiego Inspektora Ochrony Środowiska o stanie środowiska na terenie powiatu miasta Białystok, Raport WIOS, Poland, p 19, 2016.

[2] Turecki A., Budynek „Laboratorium Architektury Energooszczędnej i Energii Odnawialnych” Wydziału Architektury Politechniki Białostockiej, Architecturae at Artibus 4/20, Poland, pp 57-59, 2016.

[3] Bartyzel J., Calibration and validation of measurements using TSI DustTrackII dustmeters, in REPORT. Mobile measurements of suspended dust concentrations in the area of Kraków, Podhale and Upper Silesia, AGH, Poland, , pp 73-74, 2016.

[4] Turecki A., O jakości powietrza w warszawskich dzielnicach mieszkaniowych sąsiadujących z płonąca sortownią, SMOGLAB, Poland, 2018 <https://smoglab.pl/tag/adam-turecki/>

[5] Woodall G.M., Hoover M.D., Williams R., Benedict K., Harper M., Soo J., Jarabek A.M., Stewart M.J., Brown J.S., Hulla J.E., Caudill M., Clements A.L., Kaufman A., Parker A.J., Keating M., Balshaw D., Garrahan K., Burton L., Batka S., Limaye V.S., Hakkinen P.J., Thompson B., Interpreting Mobile and Handheld Air Sensor Readings in Relation to Air Quality Standards and Health Effect Reference Values: Tackling the Challenges, Atmosphere 2017 8,182, Switzerland, p 6, 2017.



Section

BIOTECHNOLOGIES

Genetic engineering and molecular diagnostic

Bio-energy production and environmental bioremediation

Bio-safety, systems biology and bioethics

BIOCONVERSION OF CEREAL SERUM - A SECONDARY PRODUCT FOR PRODUCING PROTEIN CONCENTRATES FROM PEA AND CHICK PEAS

Prof. Dr. Valentina Kolpakova ¹

Ph.D. Student Denis Kulikov ²

Ph.D. Ruzaliya Ulanova ³

Dr. Nikolay Lukin ⁴

Ph.D. Student Gaivoronskaya Irina ⁵

^{1, 2, 4, 5} All-Russian Research Institute for Starch Products – Branch of V.M. Gorbatov Federal Research Center for Food Systems of Russian Academy of Sciences, Russia

³ S.N Vinogradsky Institute of Microbiology, Federal Research Center "Fundamental Foundations of Biotechnology", of Russian Academy of Sciences, Moscow, Russia

ABSTRACT

Studies on the bioconversion of whey water formed from chickpea and pea grains in the preparation of protein concentrates have been performed. The serum remaining after precipitation of the main part of the protein was subjected to a symbiotic transformation of *Saccharomyces cerevisiae* 121 and *Geotrichum candidum* 977 yeast cultures with the formation of protein-containing products with a mass fraction of protein (52.27-57.90% of DS) and a complementary amino acid composition. A microbial-plant concentrate was used as an additive in the feeding of Wistar laboratory rats. After 25 days of feeding, there was no negative effect on the physiological parameters and behavior of animals, which indicates the high quality of the protein product and the prospects of its inclusion in the composition of animal feed and diets.

Keywords: *pea flour, chickpea flour, extracts, bioconversion, biomass, concentrates, amino acid composition*

INTRODUCTION

For modern agriculture, new technologies are being developed and sources of fodder and food products are being sought. One of these areas is the involvement of bioconversion of secondary products into food and feed additives in resource-saving flour processing schemes. Microorganisms on certain compositions of nutrient media have a high growth rate and the ability to synthesize a wide range of nutrient compounds: proteins, lipids, carbohydrates, carotenoids, etc. [1]. The biomass of microorganisms is intended for the diets of farm animals and poultry in order to increase their productivity. The basis for the cultivation of feed biomass of microorganisms is often the secondary products of the food industry and agriculture. Thus, a preparation obtained during the fermentation of corn stalks with saccharomycetes or a consortium of saccharomycetes, *L. plantarum* and *L. casei* had a positive and safe effect on the animal organism and the environment [2], [3].

The yeast introduced into the feed of broiler chickens in an amount of 0.8% also increased the efficiency of their use [4]. A study of the microbiota of fecal samples on days 21 and 42, carried out using the polymerase reaction (PR), revealed a positive effect of the additive on the microflora of broiler chickens, and the introduction of *S. cerevisiae* yeast in ruminant feed increased fiber digestibility and increased the population of cellulolytic bacteria *R. flavefaciens* scar [5].

It was also proved that the addition of *S. cerevisiae* and / or *A. oryzae* to the diet of cattle increased milk yield and fat content of milk [6], [7]. Feed additives from coffee sludge [8], from distillery stillage with wheat bran, obtained by cultivation with *S. diastaticus* yeast and carotene-forming yeast *Rh. species* to increase the content of essential amino acids in feed [9]. With yeast *Rh. glutinis*, *Rh. mucilaginosa* and *Rh. Gracilis* synthesized a feed additive with carotenoids and lipids from a deproteinized wastewater generated during the processing of potatoes and glycerol wastes [10]. Mushroom biomass with *A. Niger* with a yield of 35 g / dm³ [11] was also obtained from the distillery's waste, and a feed microbial-plant concentrate (FMPC) synthesized with *S. cerevisiae* yeast was extracted from the extract remaining in the production of triticale starch with a mass fraction of protein of $25.2 \pm 2.1\%$, fat - $22.1 \pm 3.2\%$, carbohydrates - $40.8 \pm 1.6\%$ [12]. Potassium and calcium prevailed among macroelements, cobalt, iron, zinc, molybdenum, nickel, which are necessary for maintaining the normal development of a living organism, prevailed among microelements.

With secondary products formed during the extraction of pea protein, a food mycoprotein concentrate was obtained to replace meat. The studies were performed with 5 strains of fungi (*A. oryzae*, *F. venenatum*, *M. purpureus*, *N. Intermedia*, *R. oryzae*), which were grown at 35 ± 2 °C for 48 h with a protein content in biomass of 43.13-59.74% of DS. The process can provide about 680 kg of mushroom biomass with 38% additional protein for every 1 ton of by-product [13]. It is important to note that the processing of secondary products of leguminous crops by bioconversion for other technological schemes has been little studied, so today such studies in this direction are quite relevant.

This work aims to develop a bioconversion process for liquid grain whey, which is formed as a secondary product of the processing of flour from pea and chickpea grains into protein concentrates, by the symbiosis of *S. cerevisiae* yeast and a new strain of *G. candidum* 977.

MATERIALS AND METHODS

As objects, pea serum was used from flour obtained from the grain of the Yamal variety with 11.6 % moisture and mass fraction, % of DS: protein (Nx6.25) – 25.7; ashes – 2.67; fat – 1.46; starch – 51.50; carbohydrates – 18.76 and chickpea whey from flour, ground from Volzhanin grains with 9.1% moisture and mass fraction, % of DS: protein (Nx6.25) – 23.40; ashes – 2.91; fat – 4.89; starch – 43.82; carbohydrates – 24.98. Peas were grown in the Altai Territory in 2017, chickpeas – in 2018 in the Volgograd Region with a yield of 18-20 kg/ha.

To isolate protein concentrates and a by-product of cereal whey from flour, enzyme preparations from Novozymes A / S (Denmark) were used: Shearzym 500

L, Viscoferm L, Fungamyl 800 L, AMG 300 L 2500 and Distizym Protacid from Erbslon. To obtain FMPC, we used cultures of the fungus *Geotrichum candidum* 977 and yeast *Saccharomyces cerevisiae* 121 from the collection of S.N Vinogradsky Institute of Microbiology. The phylogenetic position of the new strain *G. candidum* 977 was determined in conjunction with the Federal State Budget Scientific Research Institute of Genetics (Russia).

RESULTS AND DISCUSSION

Proteins were extracted from a suspension of pea and chickpea flour separately by a biotechnological method with the stepwise addition of hydrolytic enzyme preparations (EP) of various actions (cellulases, xylanases, amylases, proteases). The scheme and parameters of protein extraction for each stage are presented in [14]: hydromodule 1:15, EP concentration 1.5% / g protein, fermentation time 4 hours, reaction temperature 55 ± 1 °C, stirring speed 200 min⁻¹. After protein precipitation and centrifugation of the suspension, formed whey, which was subjected to bioconversion for processing flour into food and feed protein preparations. The use of liquid whey without any processing in the composition of the feed is difficult, due to the impossibility of long-term storage and the complexity of transportation, so we further selected the conditions for the preparation of the nutrient medium and microorganisms to assimilate its components and obtain dry feed additives. Whey contained digestible nitrogenous substances, mono- and oligosaccharides (Table 1).

Table 1 – The average chemical composition of pea and chickpea serum

DS, %	Nitrogen Substances, % of DS (Nx6,25)	Serum carbohydrates, mg / 100 g of product				
		Fructose	Glucose	Maltose	Maltotriosis	HMWC*
1.85±0.35	13.94±5.32	144.3±0.2	185.7±1.2	270.6±23	51.1±1.2	398.2±0.43

* Note: HMWC – high molecular weight compounds

For this substrate, microorganisms were selected from yeast of the genera *Pichia*, *Rhodotorula*, *Hansenula*, *Saccharomyces* and micromycetes used in cheese making (*Geotrichum*, *Penicillium*). Representatives of the genera *Pichia* and *Saccharomyces* grew with the highest speed and activity on both types of serum, while *Rhodotorula* and *Hansenula* developed poorly. For further studies, *S. cerevisiae* yeast and *G. candidum* 977 micromycete, which we deposited at the Federal State Budget Scientific Research Institute of Genetics (registration number VKPM Y-300), were selected. The *G. candidum* 977 culture was able to grow in a wide pH range of the nutrient medium and regulate the acidity of the medium with alkalization of the substrate to alkaline values *G. candidum* 977 was used in our experiments in a consortium with *S. cerevisiae* at a ratio of 1:1. Pea and chickpea whey had a positive effect on the morphology of cells, both of individual monocultures, and their consortium (Figure 1). To determine the growth conditions of microorganisms, we studied the effect of substrate pH, temperature, and the amount of seed on biomass formation for 2 days.



Figure 1 – Cells of monocultures and their consortium: 1 – *S. cerevisiae*; 2 – *G. candidum* 977;

3 – *S. cerevisiae* + *G. candidum* 977

The most effective for the synthesis of biomass was a pH value of 6.0-6.5. At lower pH values (4.5-5.0) and higher (7.5-8.0), the growth of microorganisms slowed down (Figure 2). An effective amount of seed was a dose of 3 % (Figure 3), a growth temperature of 26-28 °C.

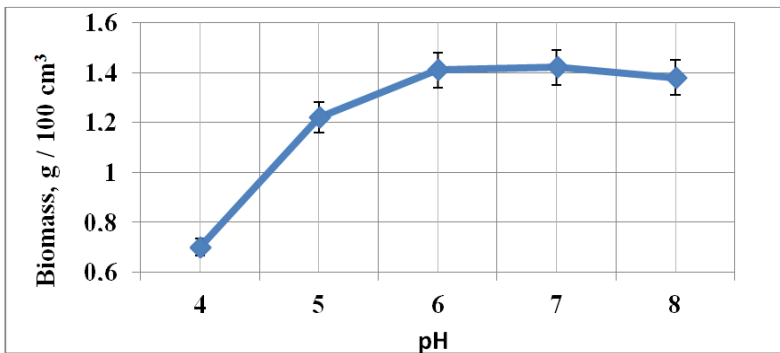


Figure 2 – Effect of pH on the amount of biomass *G. candidum* 977 + *S. Cerevisiae* 121

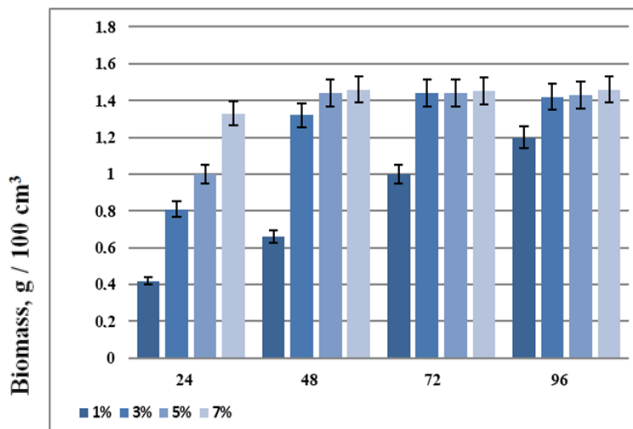


Figure 3 – Effect of seed dose on the amount of biomass (pH 6-7)

Co-cultivation of yeast and micromycete positively influenced the accumulation of biomass and the formation of protein, the mass fraction of which was 57.90 ± 0.1 % of DS for pea whey and 52.27 ± 0.72 % of DS for chickpea whey, while in some cultures the amount of protein reached only 16.39...50.23 % of DS. The least amount of protein was contained in biomass with *G. candidum* 977 fungus (Table 2).

Table 2 – Mass fraction of protein in biomass with microorganisms, %

Biomass with culture	Dry substance (DS), %	Mass fraction of protein, % of DS (Nx6,25)
<i>G. candidum</i> 977	17.49±0.21	16.39±0.31
<i>S. cerevisiae</i>	19.21±0.34	50.23±0.42
<i>G. candidum</i> 977 + <i>S. cerevisiae</i>	18.89±0.41	57.90±0.51

The culture fluid and biomass were dried and FMPC-2 was obtained, and after centrifugation of the total suspension, washing the precipitate with water and drying it, the FMPC-1 biomass preparation was obtained. According to the organoleptic characteristics, the concentrates were crumbly powders: FMPC-1 light cream color, FMPC-2 cream color, odorless. A typical chemical and amino acid composition of FMPC-2 obtained from pea whey biomass with *S. cerevisiae* 121 and *G. candidum* 977 is shown in table 3.

Table 3 – Chemical and amino acid composition of FMPC-2 from biomass crops

Moisture, %	Mass fraction, % of DS							
	Protein (Nx6.25)	Ash	Lipids	Carbohydrates				
26.8±0.5	61.68±0.47	8.60±0.03	8.31±0.36	21.41±0.55				
Amino acid composition, mg / g of product								
Val	His	Ile	Leu	Lys	Met+Cys	Thr	Trp	Phe+Tyr
10.98	11.45	8.79	17.44	22.40	12.23	18.46	2.59	23.07

The safe properties of dry pea concentrate FMPC-2, obtained from a microbial suspension of pea whey with a consortium of cultures of *G. candidum* 977 and *S. cerevisiae* 121, were studied when feeding rats. The introduction of FMPC-2 in the feed did not change the color, smell and its uniformity. The effect of the concentrate on the appetite, tolerance and growth of animals, studied over 25 days, showed that the degree of eating, estimated by the remainder of the feed, is the same in both the control and experimental groups. There was no difference between the experimental and control rats for appetite, no digestive disorders, inhibition of behavior, increase or decrease in motor activity. The response to external stimuli (transfer of animals from the cells, fixation of the animal during weighing) was also the same (Table 4).

Table 4 – The effect of additives with FMPC-2 on the characteristics of behavior and microbiological parameters of experimental and control rats

Indicators	Control group	Experienced group
Animal condition (motility, appetite)	Animals are mobile, appetite is good	Animals are mobile, appetite is good
Degree of Eating and Tolerance	Animals actively ate food, normal manifestation of thirst	Animals did not refuse food, actively ate food

Behavior (motor activity, reaction to external irritations)	Disorders of behavior and oppression were not observed	Disorders of behavior and oppression were not observed
The condition of the skin of the coat and eyes	The condition of the skin of the coat and eyes	The condition of the skin of the coat and eyes
Feces characterization	Spindle-shaped with a dark gray tint, about 10 mm long, characteristic for this group of animals	Spindle-shaped, with a dark gray tint, about 10 mm long, the first 2 days are more humid and shiny than in the control
Microflora, CFU / g (on day 25)		
General bacterial contamination	1,5 x 10 ⁸	1,6 x 10 ⁸
Escherichia coli bacteria	1,3 x 10 ⁶	1,1 x 10 ⁶
Lactic acid bacteria	1,1 x 10 ⁵	1,2 x 10 ⁵

Studies of the microflora of fecal samples, performed at the beginning and at the end of feeding the rats for 25 days, showed no changes in the number and composition of the microbiocenosis of the experimental and control animals (Table 4). The total bacterial contamination, the number of bacteria of the group of Escherichia coli (Escherichia, Citrobacter, Enterobacter, Serratia) and lactic acid bacteria in the feces of both groups of animals was identical. The conclusion is made about the benignness of FMPC-2 and the prospects of its inclusion in the composition of animal feed and diets. On the base of the data obtained, was developed a concept for the processing of whey obtained from the isolation of protein concentrates from pea and chickpea flour with the formation of FMPC (Figure 4), which requires further testing under experimental conditions.

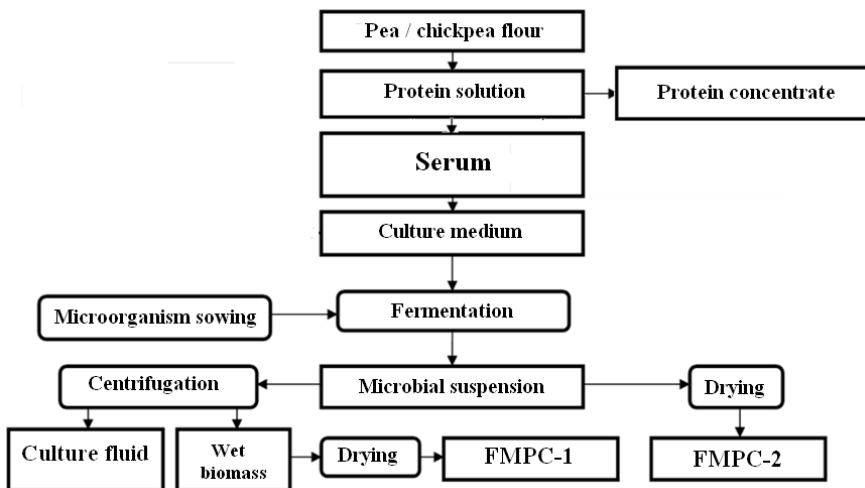


Figure 4 – Scheme for the production of FMPC by microbial transformation of serum

CONCLUSION

The possibility of processing the whey formed during the isolation of protein from a suspension of pea and chickpea flour by bioconversion with a symbiosis of cultures of the fungus *G. candidum* 977 and the yeast *S. cerevisiae* 121 into FMPC was established. A composition from cultures of microorganisms is proposed for the synthesis of FMPC from grain serum of peas and chickpeas. FMPC obtained from pea whey had a protein mass fraction of 57.90% of DS, from chickpea whey – 52.27% of DS. The resulting protein concentrate did not adversely affect the behavior and performance of experimental rats, which indicated its safety and prospects for animal diets. Therefore, for whey obtained as a secondary product in the processing of one triticale grain [12], and in the processing of triticale serum together with pea flour into starch and protein concentrates [15], the symbiosis of these types of microorganisms is also effective for the bioconversion of one pea or chickpea whey with a sufficiently high mass fraction of protein in the FMPC.

REFERENCES

- [1] Sarris D., Sampani Z., Rapti A., Papanikolaou S. Valorization of Crude Glycerol, Residue Deriving from Biodiesel- Production Process, with the Use of Wild-type New Isolated *Yarrowialipolytica* Strains: Production of Metabolites with Pharmaceutical and Biotechnological Interest // Current pharmaceutical biotechnology, Vol. 20, Iss. 10, P. 881-894.
- [2] Zhou X.L., Ouyang Z., Zhang X.L., Wei Y.Q., Tang S.X., Ma Z.Y., Tan Z.L., Zhu N., Teklebrhan T., Han X.F. Sweet Corn Stalk Treated with *Saccharomyces Cerevisiae* Alone or in Combination with *Lactobacillus Plantarum*: Nutritional Composition, Fermentation Traits and Aerobic Stability, *Animals*, Vol. 9, Iss. 9, Article Number: 598, 2019.
- [3] Sun Z, Wang T, Aschalew N.D, Zhao W, Chen X, Zhang X.F, Zhen Y.G, Qin G.X. Effects of yeast cultures with different fermentation times on the growth performance, caecal microbial community and metabolite profile of broilers, *Journal of animal physiology and animal nutrition*, No 15, 2019.
- [4] Zhen Y.G., Zhao W., Chen X., Li L.J., Lee H.G., Zhang X.F., Wang T. Effects of yeast culture on broiler growth performance, nutrient digestibility and caecal microbiota, *South African Journal of Animal Science*, Vol 49, No 1, P. 99-108, 2019.
- [5] Sousa D.O., Oliveira C.A., Velasquez A.V., Souza J.M., Chevaux E. Mari L.J., Silva L.F.P. Live yeast supplementation in pastures throughout the year, *Animal feed science and technology*, Vol. 236, P. 149-158, 2018.
- [6] Shakira G., Qubtia M., Ahmed I., Hasan F., Anjum M.I., Imran M. Effect of indigenously isolated *Saccharomyces cerevisiae* probiotics on milk production, nutrient digestibility, blood chemistry and fecal microbiota in lactating dairy cows, *Journal of animal and plant sciences*, Vol. 28, Iss. 2, P. 407-420, 2018.
- [7] Sallam S.M.A., Abdelmalek M.L.R., Kholif A.E., Zahran S.M., Ahmed M.H., Zeweil H.S., Attia M.F.A., Matloup O.H., Olafadehan O.A., The effect of

Saccharomyces cerevisiae live cells and *Aspergillus oryzae* fermentation extract on the lactational performance of dairy cows, *Animal Biotechnology*, Jun 17, P. 1-7, 2019.

[8] Bashashkina E.V., Pashinina E.A., Pashinin A.E., Suyasov N. Coffee sludge as a raw material for obtaining a feed additive, *Advances in chemistry and chemical technology*, V. 22, № 13, P. 38-40, 2008 [In Russian].

[9] Serba E.M., Sokolova E.N., Fursova N.A., Volkova G.S., Borscheva U.A. Obtaining biologically active additives based on enriched yeast biomass, Storage and processing of agricultural raw materials, № 2, P. 74-79, 2018 [In Russian].

[10] Kot A.M., Błażejczak S., Kieliszek M., Gientka I., Bryś J., Reczek L., Pobiega K. Effect of exogenous stress factors on the biosynthesis of carotenoids and lipids by *Rhodotorula* yeast strains in media containing agro-industrial waste, *World Journal of Microbiology and Biotechnology*, № 35, P. 157-160, 2019.

[11] Chuppa-Tostain G., Hoarau J., Watson M., Adelard L., Alain Shum Cheong Sing A.S.Ch., Caro Y., Grondin I., Bourven I., Francois J-M., Girbal-Neuhausser E., Petit T. Production of *Aspergillus niger* biomass on sugarcane distillery wastewater: physiological aspects and potential for biodiesel production *Bioremediation, Biodiesel, Lipids, Fungal Biology and Biotechnology*, № 5, P. 1-6, 2018.

[12] Andreev N.R., Kolpakova V.V., Goldstein V.G., Kravchenko I.K., Ulanova R.V., Gulakova V.A., Shevyakova L.V., Makarenko M.A., Lukin N.D. Utilization of secondary triticale processing products with production of fodder microbial-vegetative concentrate for pond fish. South of Russia: ecology, development, V. 12, no. 4, P. 90-104, 2017. DOI: 10.18470/1992-1098-2017-4-90-104 [In Russian]

[13] Pedro F., Souza Filho, Ramkumar B. Nair, Dan Andersson, Patrik R. Lennartsson, Mohammad J. Taherzadeh. Vegan-mycoprotein concentrate from pea-processing industry byproduct using edible filamentous fungi, *Fungal Biology and Biotechnology*, № 5, P. 5-8, 2018.

[14] Kolpakova V., Kulikov D., Ulanova R., Kravchenko I. Obtaining protein concentrates from triticale extract and pea flour with application of enzymes, *GEOLINKS International Conference on geosciences. Conference proceedings*, 26-29 march, Novotel, Athens, Greece, Book 2, V. 1, P. 17-24, 2019.

[15] Kolpakova V.V., Ulanova R.V., Kulikov D.S. and al. Grain composites with complementary amino acid composition for food and feed purposes, *Food Engineering and Technology*, V. 2 (49), P. 301-311, 2019. DOI: 10.21603/2074-9414-2019-2-301-311 [In Russian]

CONTROL OF PLANTS OF *LOTUS CORNICULATUS* L. ON AEROBIC AND ANAEROBIC FREE NITROGEN-FIXING BACTERIA

Assoc. Prof. dr. Aurica Breica Borozan ¹

Assoc. Prof. dr. Despina-Maria Bordean ²

Lecturer dr. Gabriel Bujanca ³

Lecturer dr. Delia Dumbrava ⁴

Prof. dr. Sorina Popescu ⁵

^{1, 2, 3, 4, 5} Banat's University of Agricultural Sciences and Veterinary Medicine
King Mihai I of Romania, Timisoara, Romania

ABSTRACT

The free nitrogen fixing bacteria can mobilize important soil nutrients, transforming through biological processes the unusable molecular nitrogen into an active form

and to improve soil fertility, influence many aspects of plant health and ensure their growth, showing interest for the scientific world and farmers.

But, on the other hand, this bacterial segment may be influenced by the edaphic factors and the interconnection with the plants, the growth phase, the physiological state and the root system of the plant, by the root exudates, which demonstrates the importance of the bacterial community monitoring from the area of plants influence throughout the growing periods

The aim of this study was to evaluate the influence of the age of the plants used as biofertilizer and soil moisture on the free nitrogen fixing bacterial communities (the genera *Azotobacter* and *Clostridium*) associated with the roots of the perennial plants of *Lotus corniculatus* L. There were two zones of interest, namely the area of influence of the roots of the plants (rhizosphere) but also the more distant area (edaphosphere). For the study of aerobic and anaerobic free nitrogen fixing bacteria soil samples were taken together with adjacent plants of *Lotus corniculatus* L.

The experimental variants were located in the western part of Romania, the plants being cultivated on the same soil type, but on different plots, that were in the I-IV years of culture. The influence of *Lotus corniculatus* L. plants on the free nitrogen fixing bacteria has been reported in control experimental variants. Isolation and study of this bacterial group from the 8 experimental variants was performed on a specific mineral medium, favorable for the growth of the two bacterial genera.

The results were evaluated after 5 and 10 days of incubation. Between the two assessments, there were no noticeable differences in the nitrogen fixing bacterial community, except for the stimulatory effect observed in the control variant and rhizosphere of the first year culture.

The plants` influence on aerobic and anaerobic free nitrogen fixing bacteria was obvious in the II and IV years of the *Lotus corniculatus* L. culture, compared

to the control variants and varies substantially depending on the age of the plant. In most analyzed soil samples, both bacterial genera, *Azotobacter* and *Clostridium* were present, confirming the known ecological relation of unilateral advantage or passive stimulation of the aerobic bacteria compared to the anaerobic clostridia. Exceptions were the samples from the cultures of the first year (rhizosphere and control), but also the rhizosphere from the culture of the year II, where only anaerobic nitrogen fixing bacteria were detected. Our results suggested that plant-soil interactions exert control over the bacteria being studied.

Keywords: *Soil, Lotus corniculatus L., Free nitrogen-fixing bacteria, Azotobacter genus, Clostridium genus*

INTRODUCTION

In nature, plants control the microorganisms` populations through root exudates and create their own rhizosphere microbiome. Besides, the studies carried out by Lei and collaborators (2019), [5] emphasized that approximately 44,85% from rizosphere bacterial communities could be attributed to plant species.

Other authors considered that the crop management mode, the stage of plant development [8], the soil type and properties [2], are factors that influence the diversity and functions of the microbial community.

On the other side some authors have shown that the rhizosphere microbiome contributes to productivity, protection and improvement of host plant health, increases soil fertility and promotes plant growth [9], through the contribution of phytohormones and nutrients, in particular the biologically fixed nitrogen. Microorganisms associated with plants play an important role in global biogeochemical cycles. Of the chemical elements, nitrogen is among the key elements that ensure plant growth and productivity in aquatic and terrestrial ecosystems.

It is known that by symbiosis, established in particular between bacteria and leguminous plants, the highest amount of nitrogen is fixed. However, some research has shown, that free nitrogen-fixing bacteria can also fix significant amounts of nitrogen in different ecosystems (between 0-60 kg N/ha/year), [3].

The composition of free nitrogen-fixing micro-organisms and the activity of nitrogenase are influenced by the species, the genotype and plant rhizosphere, soil content in nutrients, soil pollution, soil moisture and temperature [4].

Among the free diazotrophe bacteria which have unique characteristics we can mention the genus *Azotobacter* and *Clostridium*, whose evolution is also of interest in this work, known as the mutual relationship between *Lotus corniculatus L.* and symbiotic nitrogen fixing bacteria.

The objectives of this research were (1) the study of the community of aerobic and anaerobic nitrogen-fixing bacteria in the rizosphere of *Lotus corniculatus L* plants in different crop years (I-IV), placed on the same soil type and (2) the evolution of the two nitrogen fixing bacteria genus, namely *Azotobacter as an*

aerobic and *Clostridium* as an anaerobic one, under the influence of the plant and soil moisture.

MATERIALS AND METHODS

The study was conducted within the boundaries of Arad county (46°22'N 21°48'E), located in the west Romania (fig. 1) characterized by a temperate continental climate with oceanic influences, with an annual average temperature of 10°C, average annual precipitation s between 565-600 mm in the plain area [14] and the variability of telluric-edaphic factors [15].



Fig. 1 Arad county - the place from which the soil samples were taken (Source 12,13: processed image)

The soil samples were taken from the control plots (uncultivated) and the plots covered with *Lotus corniculatus* L.), in the flowering phase, years I-IV of the culture, from the depth of 0-20 cm, in the summer season (June - July). The community of aerobic and anaerobic free nitrogen fixing bacteria was studied during the same calendar year, from the rhizosphere of plants and from the soil (control variants) not influenced by the plant roots.

The processing and evaluation of this group of free soil bacteria was carried out in the laboratory of Microbiology, University of Agricultural Sciences and Veterinary Medicine of the Banat "King Michael I of Romania" from Timisoara.

Isolation of free nitrogen fixing bacteria from the control soil samples and from the rhizosphere was performed on Ashby liquid mineral medium [10]. The optimum growth temperature of the aerobic and anaerobic free nitrogen fixing bacteria was 28°C, and the incubation time was 5-10 days. Bacterial growth was followed by reading and interpreting the results based on McCrady tables [10].

Soil samples moisture was determined by the thermo-gravimetric method, aided by a Sartorius scale MA-50 at 105°C, as described by Bordean et al. 2011 [1].

RESULTS AND DISCUSSION

The community of free aerobic and anaerobic bacteria in the rhizosphere of *Lotus corniculatus* L. plants (I-IV crops) was evaluated in comparison with the control plots (not influenced by legumes). The tests were performed after the isolated bacteria were incubated 5, respectively 10 days on nutrient medium. The results showed: (1) an increase in the probable number of free nitrogen fixing bacteria in the root of the cultures in the years I to IV compared to control variants; (2) keeping a constant number of free nitrogen fixing bacteria in most cases included 10 incubation days, with the exception of the control and variants of the rhizosphere from the first culture year, where there was a slight increase of the bacteria, with 0.35-0.51%. In figures 2-4 the results obtained after 5 days of incubation are presented.

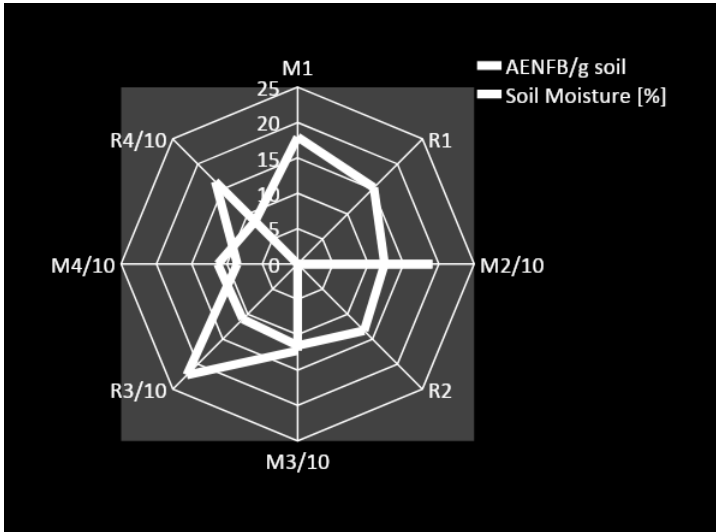


Fig. 2 Development of Aerobic Nitrogen Fixing Bacteria from *Lotus corniculatus* L. culture (AENFB)

Legend: M1- control, the first year M2/10- control, the second year M3/10- control, the third year; M4/10- control, the fourth year; R1- rhizosphere, the first year; R2- rhizosphere, the second year; R3/10- rhizosphere, the third year; R4/10- rhizosphere, the fourth year

$$R3 > M2 > R4 > M4$$

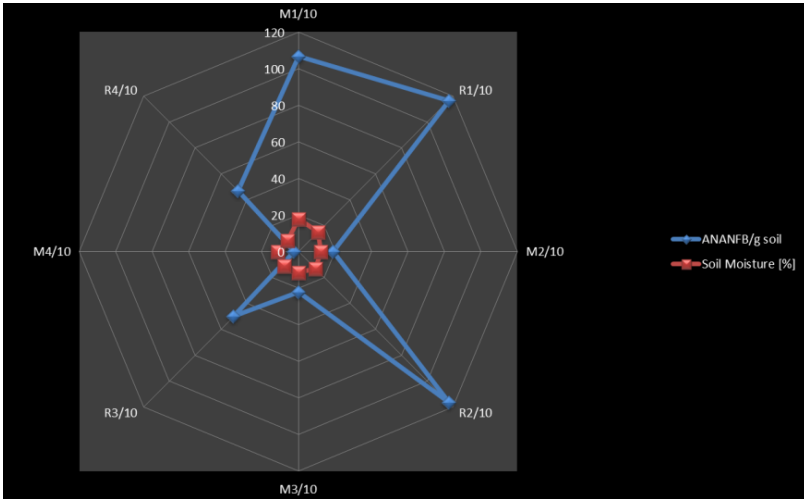
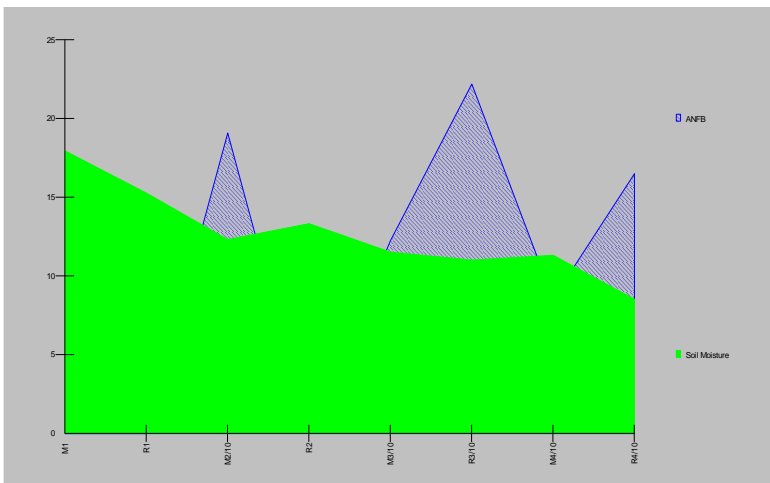


Fig. 3 Development of Anaerobic Nitrogen Fixing Bacteria (ANANFB) from *Lotus corniculatus L.* culture (AENFB)

Legend: M1- control, the first year M2/10- control, the second year M3/10- control, the third year; M4/10- control, the fourth year; R1- rhisophere, the first year; R2- rhisophere, the second year; R3/10- rhisophere, the third year; R4/10- rhisophere, the fourth year

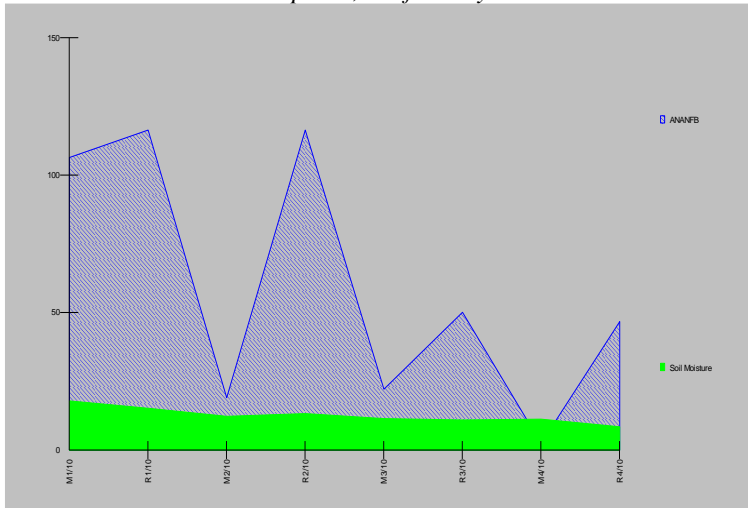
$$R2 > R1 > M1 > R3 > R4 > M3 > M2 > M4$$

From figures 2 and 3 it was observed: (a) the increase of the number of anaerobic free nitrogen fixing bacteria compared to the aerobic ones, which were absent in variants M1, R1 and R2, (b) the decrease in the number of nitrogen fixing bacteria concomitant with the culture year, (c) and the reduction of the number of fixing bacteria from the low humidity variants, especially from the M4 variant.



a. ANFB – Aerobic free nitrogen fixing bacteria from *Lotus corniculatus* L. culture

Legend: M1- control, the first year M2/10- control, the second year M3/10- control, the third year; M4/10- control, the fourth year; R1- rhisophere, the first year; R2- rhisophere, the second year; R3/10- rhisophere, the third year; R4/10- rhisophere, the fourth year



b. ANANFB – Anaerobic free nitrogen fixing bacteria from *Lotus corniculatus* L. culture

Legend: M1- control, the first year M2/10- control, the second year M3/10- control, the third year; M4/10- control, the fourth year; R1- rhisophere, the first year; R2- rhisophere, the second year; R3/10- rhisophere, the third year; R4/10- rhisophere, the fourth year

Fig. 4 The influence of humidity on the evolution of free nitrogen fixing bacteria

According to the literature data the nitrogen fixing microorganisms are sensitive to the changes that occur in their living environment, which is also observed in the case of samples from the variants with lower humidity; even though they are adapted to various environmental conditions and play an important role in the biogeochemical cycle of nitrogen, they rarely dominate in terrestrial ecosystems [11].

Even if we did not report the results to other crop plants, the fact that the probably number is larger in the rhizosphere, both in the case of aerobic and anaerobic fixing bacteria, enable us to consider that there is an obvious effect of the cultivated plants on this bacterial segment. In support of these results we also add the studies of Mirza and colleagues (2014), [7] who argue that the response of diazotrophs is a direct consequence of changes in plant communities.

CONCLUSION

In agreement with our studies, the same authors pointed out that the microbial communities involved in nitrogen fixation are influenced by the rhizosphere, the plant species, their life span, but also the physico-chemical properties of the soil.

The growth coefficient of aerobic free nitrogen fixing bacteria varies and does not show a constant line depending on soil moisture, whereas anaerobic free nitrogen fixing bacteria are correlated with soil moisture value (Fig. 4). Merlo et al. (2014), [6] argue that soil moisture is one of the major abiotic factors that control the abundance of nitrogen-fixing bacteria.

From this study it can be concluded that the plant, through the root exudates, had somewhat the control over the free nitrogen fixing bacteria in the rhizosphere, in all 4 years of culture, compared to the control variant, even if the summer season, which was quite dry, also influenced these bacteria. In particular, we noticed that the anaerobic bacteria have an ascending tendency, compared to the aerobic ones, especially in the variants in which the moisture content was higher (R1, M1, R2).

REFERENCES

- [1] Bordean D.M., Bărăscu M., Borozan A.B., Alda L., Filimon N., Popescu R., et al., Studies regarding speciation and chemical fingerprinting as fruit products quality markers, *Journal of Horticulture, Forestry and Biotechnology*, 15(4), pp 101-105, 2011.
- [2] Bulgarelli D., Rott M., Schlaeppi K., van Themaat E.V.L., Ahmadinejad N., Assenza F., Schulze-Lefert P., Revealing structure and assembly cues for *Arabidopsis* root-inhabiting bacterial microbiota, *Nature*, 488(7409), pp 91–95, 2012.
- [3] Burgmann H., Widmer F., Von Sigler W., Zeyer J., New molecular screening tools for analysis of free-living diazotrophs in soil, *Appl. Environ. Microbiol*, 70, pp 240–247, 2004.
- [4] Deslippe J. R., Egger K. N., Henry G. H., Impacts of warming and fertilization on nitrogen-fixing microbial communities in the Canadian High Arctic, *FEMS microbiology ecology*, 53(1), pp 41-50, 2005.
- [5] Lei S., Xu X., Cheng Z., Xiong J., Ma R., Zhang L., Tian B., Analysis of the community composition and bacterial diversity of the rhizosphere microbiome across different plant taxa, *Microbiology Open*, 8(6), 2019.
- [6] Merlo C., Reyna L., Abril A., Amé M.V., Genti-Raimondi S., Environmental factors associated with heterotrophic nitrogen-fixing bacteria in water, sediment, and riparian soil of Suquía River, *Limnologica*, Volume 48, pp 71-79, 2014.
- [7] Mirza B.S., Potisap C., Nüsslein K., Bohannan B.J., Rodrigues J.L., Response of free-living nitrogen-fixing microorganisms to land use change in the Amazon rainforest, *Applied and environmental microbiology*, 80(1), 281–288, 2014.

[8] Pii Y., Borruso L., Brusetti L., Crecchio C., Cesco S., Mimmo T., The interaction between iron nutrition, plant species and soil type shapes the rhizosphere microbiome, *Plant Physiology and Biochemistry*, 99, 39–48, 2016.

[9] Pii Y., Mimmo T., Tomasi N., Terzano R., Cesco S., Crecchio C., Microbial interactions in the rhizosphere: Beneficial influences of plant growth-promoting rhizobacteria on nutrient acquisition process: A review, *Biology and Fertility of Soils*, 5(4), pp 403–415, 2015.

[10] Stefanic Gh., Metode de analiză a solului (biologică, enzimatică și chimică), ediția a II-a, ICDA Fundulea, XXVIII, 2006.

[11] Wartianen I, Eriksson T, Zhang W, Rasmussen U., Variation in the active diazotrophic community in rice paddy – nifH PCR-DGGE analysis of rhizosphere and bulk soil, *Appl Soil Ecol*, 39, pp 65–75, 2008.

[12] https://all-free-download.com/free-vector/download/romania-map-bw_55087.html

[13]https://ro.m.wikipedia.org/wiki/Fi%C8%99ier:Judetul_Arad_3D_map.jpg

[14] [https://www.bnr.ro/Monografie_ARAD%20\(1\).pdf](https://www.bnr.ro/Monografie_ARAD%20(1).pdf).

[15]<https://www.ospaarad.ro/cadrul-natural-al-jud-arad>

EFFECTS OF BOILING AND ROASTING ON CRUDE PROTEINS, TOTAL ANTIOXIDANT CAPACITY AND TOTAL POLYPHENOLS CONTENT OF POTATO TUBERS

Assoc. Prof. dr. Despina-Maria Bordean ¹

Assoc. Prof. dr. Aurica Breica Borozan ²

Lecturer dr. Gabriel Bujanca ³

Assoc. Prof. dr. Camelia Cioban ⁴

Lecturer dr. Delia-Gabriela Dumbrava ⁵

^{1, 2, 3, 4, 5} Banat's University of Agricultural Sciences and Veterinary Medicine King Mihai I of Romania, Timisoara, Romania

ABSTRACT

Compared with other sources, potato can bring multiple nutritional benefits because it's naturally low energy food (0.7 kcal), having high water, fiber and starch content. Even if the consumption of potatoes is in decline, it is still considered a source of valuable nutrition. Depending on the method of preparation, potatoes contains a significant levels of proteins and antioxidants and can offer considerable protection against cardiovascular diseases and cancer. Natural antioxidants are present under different forms in all plants, being the base source of these compounds for humans.

The objective of this study was to determine the moisture content, crude protein, total antioxidant capacity and phenolic content of three assortments of potatoes (*Solanum tuberosum*) available on the Romanian local market (Timis County).

The study was carried out on raw, unpeeled, boiled and roasted potatoes. The moisture content was determinate thermogravimetrically using Sartorius thermo balance, crude protein quantified by using a rapid colorimetric method, total antioxidant capacity determinate using CUPRAC method and total polyphenols content using Folin-Ciocalteu assay.

The experimental results show that blue roasted potatoes present the highest content of crude protein, total antioxidant capacity and total polyphenols content and the lowest water content. The obtained data are used to create a graphical fingerprint of raw and processed potatoes in order to identify the best options to mix different potatoes assortments and to create innovative nutritious food products.

Keywords: *potato, CUPRAC method, antioxidants, polyphenols, graphical fingerprint*

INTRODUCTION

The potato (*Solanum tuberosum*) is a nutritious vegetable, mainly when cooked in its skin. The potato is a high-yielding carbohydrate-rich crop, described by a high-quality protein and a significant level of vitamin C (Woolfe 1987), carotenoids

and phenolics. The potato tubers are important in human medicine where they are used both, internally and externally. Antioxidant-rich diets containing Vitamin C, flavonoids and carotenoids [4], [5] have been associated with a lower incidence of cardiovascular diseases [8], [9], some forms of cancers, cataracts and macular degeneration [10], [15]. For internal use, the potato is recommended as an adjuvant in kidney, digestive tract and liver diseases, being consumed as such, in light culinary preparations.

The fresh, raw juice extracted from the potato tubers is recommended for hepatitis and gallstones, and healing of the digestive mucosa. Potato juice is used to treat gastric cancer, hepatopathy, constipation, hemorrhoids, glycosuria, scurvy, insomnia, chronic pain etc. Potato starch shows anti-inflammatory effect in gastrointestinal diseases and in poisoning with toxic substances [14].

Natural antioxidants are present under different forms in all plants, being the base source of these compounds for humans. The richest sources of antioxidants are fruits, vegetables, legumes, cereals, herbs and spices, coffee, cocoa and tea, wine and beer [13]. Plant polyphenols act as free radical terminators, reducing agents, singlet oxygen quenchers and metal chelators [1], [11], [12].

MATERIALS AND METHODS

Sampling and preparation of materials:

To perform this study, three assortments of potatoes (yellow, blue and white) purchased from the local market (Timis County Romania), raw, roasted and boiled in skin, were analyzed; all samples were weighed before the chemical analyses on an analytical balance to the nearest 0.0001 mg.

Conditioning of plant material:

The potatoes were washed twice (tap water and distilled water) and gently drying with blotting paper. The analyses were performed on raw, roasted in an oven and boiled (both unpeeled).

Chemical analysis of samples:

The analyses were carried out in the laboratory of Food Analysis of the Faculty of Food Engineering, Banat's University of Agricultural Sciences and Veterinary Medicine "King Michael I of Romania" from Timisoara. For each analyzed sample (raw and thermal processed), the analyses were performed in triplicate. All needed chemicals were analytical-reagent grade and the water used for solubilization was double distilled. The plant material was dried in a circulating-air oven (37 ± 2 °C), powdered and extracted in 1:1 ethanol:water (v/v) 4 hours at 20°C. Absorbance measurements, done at 450 nm and 750 nm to determine the antioxidant activity by CUPRAC method, respectively the quantitative analyze of the total phenolic content by Folin-Ciocalteu assay and crude protein, were recorded using a Analytik Jena SPECORD 205 UV-VIS spectrophotometer.

Thermogravimetric analysis of moisture content were performed as described by Bordean et al, 2011 and Bordean et al, 2014 [2], [3].

Evaluation of total antioxidant capacity (TAC) by CUPRAC method: the neocuproine complex can be monitored at 450 nm. The extraction of the active compounds from the vegetal material was performed with ethanol 50%, for 4 hours at 20°C. For blank it was used ethanol 50%. The absorption was read after 30 minutes at 450 nm. TAC in raw, roasted and boiled potatoes were expressed as $\mu\text{mol Trolox/mL}$ ethanolic extract.

Total polyphenols content – TPC (based on the method described by Folin-Ciocalteu): The Folin–Ciocalteu reaction is an antioxidant assay based on electron transfer, and gives quantified information about the reductive capacity of an antioxidant. The method is mostly used to determine TPC of plant and plant-derived food samples by using 2.0 M Folin-Ciocalteu phenol reagent, gallic acid and anhydrous carbonate. The absorption was read after approximately 2 hours at 20°C, at 750 nm and gallic acid was used as a standard.

Crude protein (CP) was determined using the method described by Cioccia et al, 1995 [6].

Statistical analysis of experimental data was made using PAST 2.14 [7] and MVSP 3.22 programs.

RESULTS AND DISCUSSION

For all analysis, the extracts prepared according to the analysis protocols were evaluated in comparison with the control samples. The results are presented in table 1. Table 1

Crude protein, total antioxidant capacity and total polyphenols content

Crt. No.	Samples	M[%]	CP[g/100g]	TAC[mg/mL]	TPC[$\mu\text{mol/mL}$]
1	YRAP	79.73	1.9	0.43	1.31
2	YROP	7.60	3.57	3.15	5.49
3	YBOP	70.59	1.77	0.53	1.30
4	BRAP	76.01	4.27	1.78	3.96
5	BROP	10.60	9.56	5.02	7.64
6	BBOP	65.95	3.85	3.11	6.85
7	WRAP	74.97	3.16	0.40	1.96
8	WROP	8.98	6.75	2.76	4.98
9	WBOP	67.21	2.79	0.48	2.23

Legend: M[%]= moisture content, CP[g/100g] = crude protein content, TAC[mg/mL] = Total Antioxidant Capacity; TPC[$\mu\text{mol/mL}$] = Total polyphenol content, YRAP= yellow raw potatoes; YROP = yellow roasted potatoes; YBOP= yellow boiled potatoes; BRAP= blue raw potatoes; BROP = blue roasted potatoes; BBOP= blue boiled potatoes; WRAP = white raw potatoes; WROP = white roasted potatoes; WBOP= white boiled potatoes;

As we can observe, the highest content of crude protein (9.56 g/100g), total antioxidant capacity (5.02 mg/ml) and total polyphenols content (7.64 $\mu\text{mol/ml}$) are

present in the roasted blue potatoes (BPROP), followed by white roasted potatoes (WRPOP), for crude protein and blue boiled potatoes (BBOP) for the other analyzed samples. Because of these observations, we can affirm that roasted potatoes in skin present higher nutritional value than boiled. Also blue potatoes present higher TAC and TPC compared to white and yellow potatoes.

The lowest values of crude protein (1.77 g/100 g potatoes) and total polyphenols content (1.30 $\mu\text{mol/ml}$) are registered for yellow boiled potatoes (YBOP) and the lowest total antioxidant capacity (0.40 mg/ml) is discovered in white raw potatoes (WRAP).

The spider representations in figure. [1] present the profiles of the experimental data, bi-dimensionally, being more effective when comparing profiles of samples.

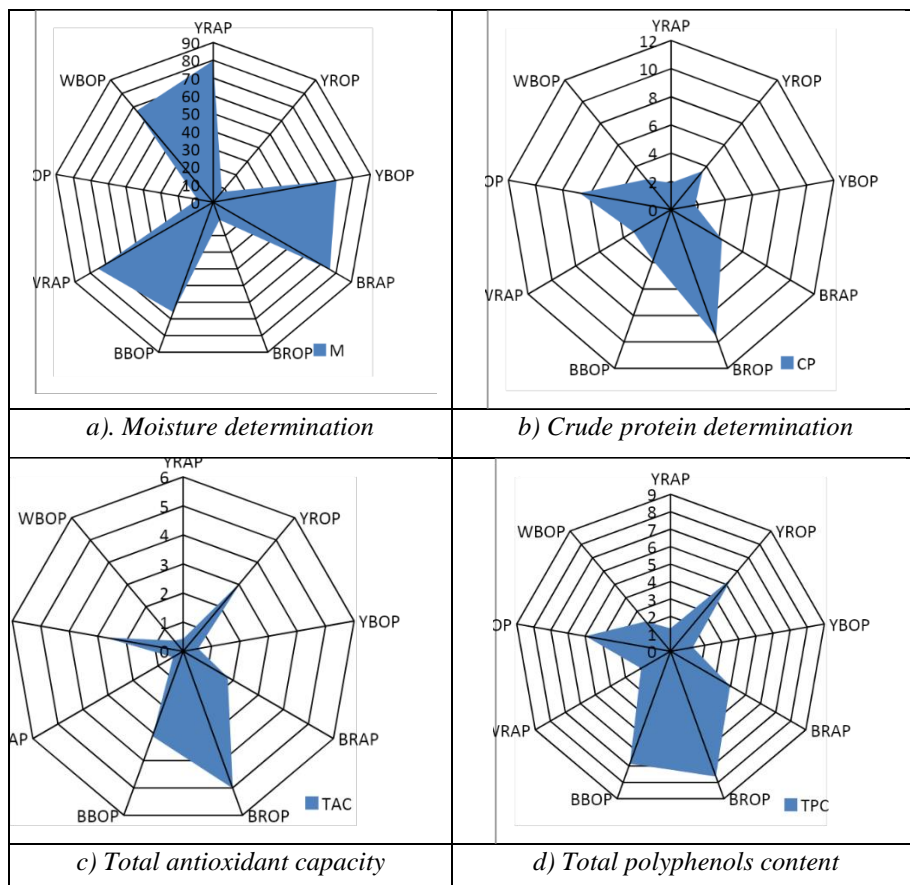


Figure 1 . Effect of thermic processes (roasted and boiled in peels) on different assortments of potatoes

Legend: M[%]= moisture content, CP[g/100g] = crude protein content, TAC[mg/mL] = Total Antioxidant Capacity; TPC[μ mol/mL] = Total polyphenol content, YRAP= yellow raw potatoes; YROP = yellow roasted potatoes; YBOP= yellow boiled potatoes; BRAP= blue raw potatoes; BROP = blue roasted potatoes; BBOP= blue boiled potatoes; WRAP = white raw potatoes; WROP = white roasted potatoes; WBOP= white boiled potatoes;

Pearson's correlation coefficient has the role to evaluate the strength of a linear relationship between experimental data. Based on the fact that positive values indicate positive linear correlation; negative values represent negative linear correlation; a value of **0** denotes the absence of linear correlation, in our case (table 2), the correlation coefficient **r** shows a strong linear positive relationship between CP and TAC (0.84766) and TPC (0.77725). CP, TAC and TPC present medium negative strong correlation between moisture content (%) CP (-0.72128), TAC - 0.78088) and TPC (-0.68049).

Table 2

Pearson correlation "r" of the analyzed data

Analized data	M[%]	CP[g/100g]	TAC[mg/mL]	TPC[μ mol/mL]
M[%]	0	0.028295	0.01299	0.043657
CP[g/100g]	-0.72128	0	0.003902	0.013706
TAC[mg/mL]	-0.78088	0.84766	0	1.90E-05
TPC[μ mol/mL]	-0.68049	0.77725	0.96785	0

Legend: M[%]= moisture content, CP[g/100g] = crude protein content, TAC[mg/mL] = Total Antioxidant Capacity; TPC[μ mol/mL] = Total polyphenol content, YRAP= yellow raw potatoes; YROP = yellow roasted potatoes; YBOP= yellow boiled potatoes; BRAP= blue raw potatoes; BROP = blue roasted potatoes; BBOP= blue boiled potatoes; WRAP = white raw potatoes; WROP = white roasted potatoes; WBOP= white boiled potatoes;

Principal component analysis (PCA) helps to increase interpretability, reducing the information loss, by creating new uncorrelated variables that successively maximize variance. In this case, the principal component PC1 shows 84.869% variance, PC2 - 8.8515% variance and PC3: 5.854% variance.

Graphical fingerprint (figure 3) offers the possibility to be used as an interactive map and simplify the selection of the preferred vegetables assortments in order to create optimized or innovative food products.

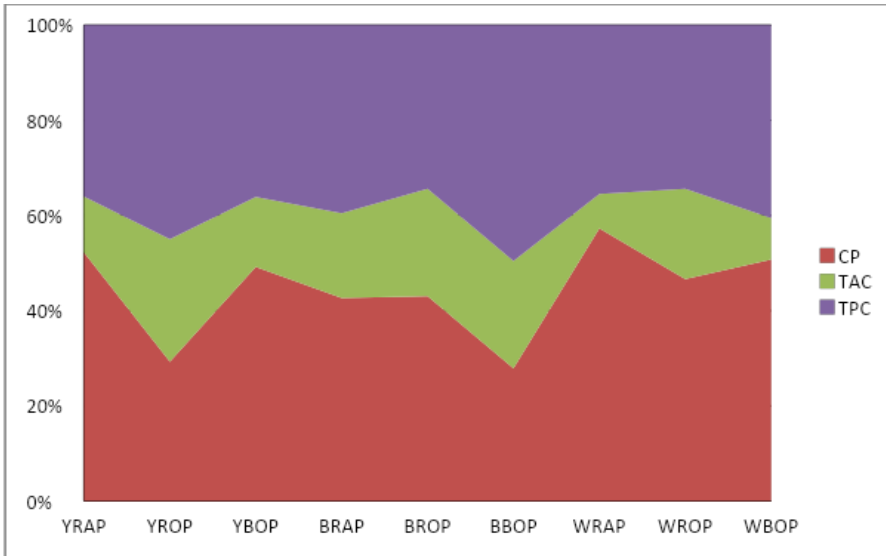


Figure 3. Raw and processed potatoes fingerprint

Legend: M[%]= moisture content, CP[g/100g] = crude protein content, TAC[mg/mL] = Total Antioxidant Capacity; TPC[μ mol/mL] = Total polyphenol content, YRAP= yellow raw potatoes; YROP = yellow roasted potatoes; YBOP= yellow boiled potatoes; BRAP= blue raw potatoes; BROP = blue roasted potatoes; BBOP= blue boiled potatoes; WRAP = white raw potatoes; WROP = white roasted potatoes; WBOP= white boiled potatoes

CONCLUSION

Potatoes (*Solanum tuberosum*) are a valuable nutrient source, because they contain a variety of phytonutrients, vitamins and minerals, with high antioxidant activity like: carotenoids, flavonoids, caffeic acid, proteins such as patatin, which shows evidence of activity against free radicals.

Blue color potatoes present a higher content of crude protein, total antioxidant capacity and total polyphenols content compared to white and yellow potatoes. When comparing boiled and baked or roasted potatoes, the experiment shows that the potatoes roasted in skin present higher content of crude protein, total antioxidant activity and total polyphenols, compared to boiled potatoes, which recommends them as the best choice for consumers.

The processing form of the blue potatoes is not influenced negatively the antioxidant capacity of the blue potatoes, even after processing they still present the highest content of crude protein, antioxidant activity compared to white and yellow potatoes regardless of their variety: raw or processed. Total polyphenols content shows highest content for blue potatoes in roasted and boiled form.

The graphical fingerprint of data can help potatoes manufacturers and processors to identify combination of different potatoes assortment in order to create innovative healthy food products with high nutritional value.

ACKNOWLEDGEMENTS

All authors have contributed equally to this paper. The present work was funded by the project “Study of synergic bioactivity of some antioxidant mixes fortification with the role to fortify patients with Parkinson's disease”, No 47/12.11.2015, financed by Antiparkinson Association Romania.

REFERENCES

[1] Akbarirad H., Kazemeini S.M., Mousavi Khaneghah A., Ardabili A.G., Some important sources of natural antioxidants, https://www.academia.edu/12561390/Some_Important_Sources_of_Natural_Antioxidants

[2] Bordean D.M., Bărăscu M., Borozan A.B., Alda L., Filimon N., Popescu R., Pîrvulescu L., Gergen I., Alda S., Studies regarding speciation and chemical fingerprinting as fruit products quality markers, *Journal of Horticulture, Forestry and Biotechnology*, 2011, Volume 15(4), p. 101- 105;

[3] Bordean D.M., Gergen I., Catargiu A., Borozan A.B., Draghici G.A., Pîrvulescu L., Ciobanu C., Alda L., Gogoasa I., 2014, Chemical Fingerprint of some mint teas available on the Romanian market, *Proceedings of the 20th International Symposium on Analytical and Environmental Problems*, 22 September 2014, Szeged, HUNGARY, 2014, p.155-158;

[4] Cao G, B Shukitt-Hale, PC Bickford, JA Joseph, J McEwen, and RL Prior. Hyperoxia-induced changes in antioxidant capacity and the effect of dietary antioxidants. *J. Appl. Physiology*, 1999, 186, p.1817-1822;

[5] Cao G., Booth S.L., Sadowski J.S., Prior R.L., Increase in human plasma antioxidant capacity after consumption of controlled diets high in fruit and vegetables, *Am J. Clin. Nutr.* 1998, 68, p.1081-1087;

[6] Cioccia A. M., Gonzalez E., Perez M., Mora J.A., Romer H., Molina E., Heval P., Application of a colorimetric method to the content of commercial foods, mixed human infantile diarrhea determination of the protein diets and nitrogen losses, *International Journal of Food Sciences and Nutrition*, 1995, 46, p.21-29;

[7] Hammer, O., Harper, D.A.T. & Ryan, P.D., Past: Paleontological statistics software package for education and data analysis, *Palaeontologia Electronica*, 2001, 4, p.1-9;

[8] Hertog M.G.L., Feskens E., Hollman P., Katan M., Kromhout D., Dietary antioxidant flavonoids and risk of coronary heart disease: The Zutphen elderly study, *Lancet* 1993, 342, p.1007-1011.

[9] Knekt P., Jarvinen R., Reunanen A., Maatela J., Flavonoid intake and coronary mortality in Finland: a cohort study, *British Med. J.*, 1996, 312, p.478481;

[10] Kruezer H., Incorporating lutein into foods and beverages,. Suppl Food Prod Design 2001, 11(4), p. 5;

[11] Mathew, S., Abraham, E.T., Studies on the antioxidant activities of cinnamon (*Cinnamomum verum*) bark extracts, through various in vitro models, Food Chemistry, 2006, 94, p. 520-528;

[12] Mousavi Khaneghah, A., An overview on some of important sources of natural antioxidants. International food research journal, 2016, 23(3), p.928-933;

[13] Sikora, E., Cieslik, E., Topolska, K., The source of natural antioxidants, Acta Sci. Pol., Technol. Aliment. 2008, 7(1), p.5-17;

[14] Umadevi, M., Sampath, P., Bhowmik, D., Duraivel, S., Health benefits and cons of *Solanum tuberosum*, Journal of Medicinal Plant Studies, 2013, 1(1), http://www.plantsjournal.com/vol1Issue1/Issue_jan_2013/3.pdf;

[15] Wang H., Nair M.G., Strasburg G.M., Chang Y.C., Booren A.M., Gray J.I., DeWitt D.L., Antioxidant and anti-inflammatory activities of anthocyanins and their aglycon, cyanidin, from tartcherries, J. Nat. Prod., 1999, 62, p.294-296.

OBTAINING MICROPARTICLES OF CALCIUM CARBONATE LOADED WITH MICROBIAL LIPASE

Valeria K. Scherbakova¹

Dr. Alla A. Krasnoshtanov²

^{1,2}Russian Chemical and Technological University named after D.I. Mendeleev, Russia

ABSTRACT

At present, lipases of animal and microbial origin are increasingly used in human practice, namely in cheese production, milk chocolate production, confectionery industry, dry egg powder, production of flour, leather industry (for degreasing wool, bristles, leather), silk production, washing agents, as well as biodiesel. However, the practical use of lipase is limited by its low stability, reduced storage activity, and inability to reuse. One way to overcome these disadvantages is to microencapsulate the enzyme into various carriers. One promising carrier is calcium carbonate, characterized by ease of production and low cost. Therefore, the purpose of this work was to select the conditions for including lipase in the calcium carbonate microparticles. As the subject of the investigation, lipase of bacteria *p. Pseudomonas fluorescens* with the activity of 27 u/mg was used in the work. This paper compares two methods of including protein molecules in carbonate microparticles: adsorption in pores (previously prepared carrier microparticles are added to the protein solution) and microencapsulation (formation of microparticles occurs simultaneously with inclusion of protein molecules). For both ways the capacity of microparticles of a carbonate of calcium by a bacterial lipase was determined and it was established that the maximum capacity equal was 0.2 mg/mg was reached when using a method of adsorption in pores. The specific activity of lipase, in this case, is 5.21 units/mg. The dynamics of bacterial lipase release from carbonate microparticles have been investigated. It has been found that within 90 minutes the degree of lipase release from microparticles does not exceed 28%, and the decrease in its specific activity does not exceed 10%. This fact suggests a higher prolongation of the action of lipase included in calcium carbonate microparticles compared to native. The operational stability of the bacterial lipase included in the calcium carbonate microparticles was evaluated as compared to native lipase. It was found that the temperature optimum did not occur, it remained at 37 ° C, but the operating stability increased in the lower temperature area. The optimum pH shifted from the slightly alkaline (pH 8.0) towards the neutral (pH 7.0), wherein in the region of alkaline pH values the operational stability of the microencapsulated lipase significantly increases. Microencapsulation of bacterial lipase into carbonate microparticles has been shown to increase storage stability by a factor of twice that of native.

Keywords: *uacterial lipase, microencapsulation, calcium carbonate microparticles*

INTRODUCTION

Lipases are used in food, pharmacological, agrochemical and leather industries, in the production of detergents, surface and optically active compounds, flavoring and aromatic components, for analytical purposes in medicine [1], [2]. Lipases can be used as a biocatalyst in the production of biodegradable polyesters and lubricants [1], [3], [4], as well as for the decomposition of oils and fats in wastewater produced by the dairy industry and slaughterhouses [5]. Free fatty acids generated by the action of lipases on milk fat provide many dairy products, especially soft cheeses, with their specific taste characteristics [6].

Another area of application for lipases is the cost-effective production of biodiesel. This area has a perspective due to the environmental safety of the process and the need for energy and resource conservation in the chemical industry. Lipase catalysis in the production of biodiesel is designed to rid it of a fundamental drawback - a large amount of alkaline waste, to reduce the specific costs of water and energy [7], [8], [9]. Lipases are also used in the textile industry to remove stains of lubricants or adhesives, in order to give the fabric greater absorbency to improve the uniformity of dyeing [10].

However, the widest use of lipases is constrained by difficulties in creating an optimal reaction system, contamination of most enzyme preparations, low thermal stability, low reaction rates, and other factors. The solution to most of the above problems lies in the way of using immobilized enzymes. Immobilization of lipases promotes the separation of the enzyme from reaction products, saves the enzyme, increases the thermal stability and activity of lipases.

In this regard, various methods of lipase immobilization are currently being intensively studied: physical sorption on hydrophilic adsorbents, inclusion in hydrophobic gels or in hydrophobic concentrates, treatment of the enzyme with synthetic lipid-like reagents. Various immobilization methods make it possible to obtain catalysts with widely varying properties and change the direction of their application.

The authors of [11] compared various types of materials (PVC, chitosan, chitin, agarose, sepharose, and trisacryl) for lipase binding efficiency. It was found that chitosan has the highest lipase capacity, but the immobilized enzyme in this case showed low hydrolytic activity, the lipase immobilized on PVC showed lower specific activity, but better thermal and operational stability, and trisacryl had a low enzyme loading efficiency. but the lipase associated with this carrier had a high specific activity.

In the article [12], pork pancreatic lipase was immobilized by adsorption on chitin and chitosan, then crosslinked with glutaraldehyde, and in the work [13] on other polymer carriers. The highest catalytic activity was achieved by covalent binding of the enzyme to a polyacrylamide ball polymer. Researchers [14] selected various carriers for immobilization of porcine pancreatic lipase. As the studied carriers, we selected: polypropylene, activated alumina, kaolin, montmorillonite, ion-exchange resins, and zeolites.

Among a large number of inorganic compounds that have found wide practical application in various industries and medicine, calcium carbonate occupies an important place. Due to their good mechanical properties, physical stability, high biocompatibility, adsorption ability and mild dissolution conditions, particles can be successfully used as the basis for creating microcontainers for a prolonged and controlled release of pharmacological substances. It was proposed to use colloidal microparticles of calcium carbonate in the modification of vaterite as a system for the delivery of drug compounds to the central nervous system during their intranasal administration. This method of drug administration has already been used for intranasal delivery of insulin [15].

This work aims to obtain and evaluate the effectiveness of a biocatalyst obtained on the basis of microencapsulation of bacterial lipase in carbonate microparticles.

MATERIALS AND METHODS

Lipase of *p. Pseudomonas fluorescens* with 27 units/mg activity were used as the subject of the study.

The catalytic activity of lipase was determined by the amount of ioliolysis formed by the oliolein (olive oil) oleic acid, which was measured by the titrimetric method. The protein content was determined by Lowry's colorimetric method.

For the preparation of calcium carbonate microparticles, the water 0.33 M solution of sodium carbonate (15 ml) was added with rapid mixing (400-900 rpm) to 15 ml 0.33 M of water solution of calcium chloride. After mixing for 60 with suspension formed spherical microparticles were left for 5-7 minutes until the full crystallization of calcium carbonate. Then the sediment was washed three times with distilled water and separated by filtering, then washed with acetone, then dried for 1.5 hours at 50-60 degrees Celsius. The resulting microparticles of calcium carbonate were stored in an airtight seal at room temperature. The size of the microparticles measured on the Nanotrak ULTRA 253 nanotrack (Microtrac, USA) ranged from 3 to 5 microns. To obtain microparticles of calcium carbonate, loaded with bacterial lipase, by the method of adsorption in the pores received calcium carbonate particle powder weighing 50 mg was suspended in 1 ml of water enzyme solution with a given activity. After incubation on the IKA-VIBRAX-VXR shaker (1200 min⁻¹) for 2 hours, the microparticles were separated by filtering. Then the particles were washed twice with water and dried at room temperature. To obtain calcium carbonate microparticles loaded with bacterial lipase, by the microcapsulation method mixed the water 0.33 M solution of sodium carbonate (15 ml), containing lipase with a given activity, and 15 ml 0.33 M of water solution of calcium chloride. The mixture was stirred at a rate of 400-900 rpm for 60 s. Then the suspension of the formed spherical microparticles was left for 5-7 minutes until the calcium carbonate was completely crystallized. Then the sediment was washed three times with distilled water and separated by filtering, then washed with acetone, and then dried at 30°C. The resulting calcium carbonate microparticles, loaded with lipase, were stored in an airtight seal at a temperature of 4-6°C.

To determine the degree of inclusion of lipase in microparticles, we measured the protein concentration by the Lowry method, as well as the residual activity of lipase.

RESULTS AND DISCUSSION

According to literary data, the inclusion of protein molecules in carbonate microparticles can be carried out in two ways: by absorbing in the pores (when pre-acquired microparticles of the carrier are added to the protein solution) or by the method of microcapsulation (when microparticle formation occurs simultaneously with the inclusion of protein molecules). Therefore, the first phase of the study was comparing the effectiveness of these two methods of obtaining calcium carbonate microparticles loaded with bacterial lipase. As a criterion of effectiveness, the specific capacity of the received microparticles on lipase was chosen, which was evaluated both by the mass of the protein included and by a specific activity.

The results are presented in Fig. 1 and 2.

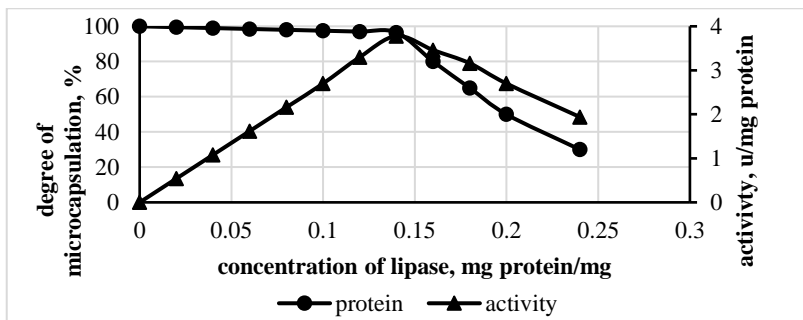


Fig.1. Determining the capacity of carbonate microparticles by bacterial lipase when it is included by microcapsulation.

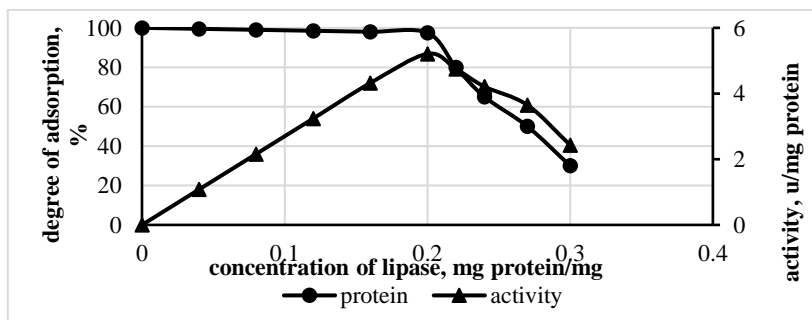


Fig.2. Determining the capacity of carbonate microparticles by bacterial lipase when it is included by the absorption method of adsorption in the pores.

From the presented data it follows that both methods allow to obtain carbonate microparticles loaded with bacterial lipase. However, in the case of microcapsulation, the maximum capacity of calcium carbonate particles for lipase

is 0.14 mg/mg and the activity of the resulting biocatalyst is 3.78 units/mg of protein.

In the case of the method of adsorption in the pores, the above parameters are 0.2 mg/mg and 5.21 units/mg of protein, respectively. The observed fact may be related to the fact that in the second case the inclusion of protein occurs in already formed spherical microparticles, which increases the movement of the process.

Thus, based on the data obtained to produce carbonate microparticles loaded with bacterial lipase was chosen method of adsorption in the pores.

The molecules of the enzyme at the center of the particles of the immobilized biocatalyst are exposed to a lower concentration of the substrate than in the volume of the solution due to the gradients of the concentration of substrate, which leads to a decrease in the reaction rate. The more mass transfer limitations are, the larger the size of the biocatalyst particles and the greater the reaction rate. However, the inclusion of enzyme molecules in microparticles usually ensures the prolongation of the action by reducing the rate of inactivation. Therefore, the next stage of the work was studied the release of lipase from microparticles. To do this, the carbonate microparticles, loaded with bacterial lipase, in the amount of 10 mg were suspended in 1 ml of acetate buffer with pH 8.0 at 50°C, which corresponds to the optimal conditions of the enzyme. During incubation at certain points of time samples of reaction suspension were taken, microparticles were precipitated by centrifuge (1600 g, 5 min). In the supernatant the concentration of protein by Lowry method and the activity of lipase were determined.

The results are shown in Fig. 3.

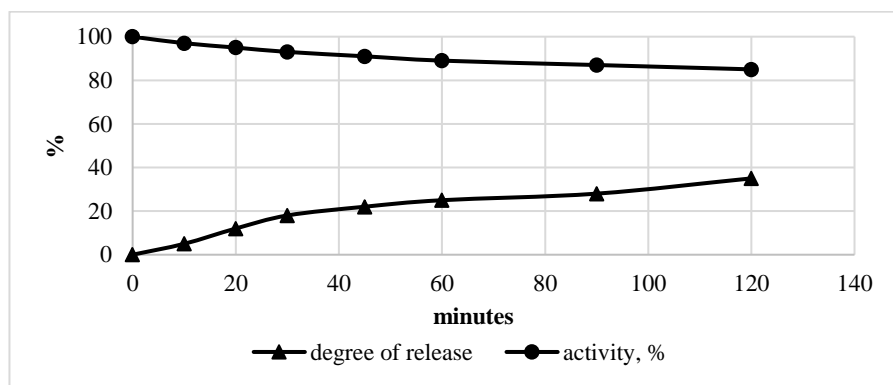


Fig. 3. Dynamics of the release of bacterial lipase from carbonate microparticles.

The results show that during 90 minutes the degree of release of lipase from microparticles does not exceed 28%, while the decrease in its specific activity does not exceed 10%. This fact suggests a higher prolongation of the lipase, included in the microparticles of calcium carbonate in comparison with the native.

An important parameter that characterizes the enzyme drug is also its stability in storage, that is, the ability to maintain enzymatic activity for a long time. To assess it, the effect of storage time on the change in the enzymatic activity of the

solution of the native lipase in the phosphate buffer with the optimal pH (8.0) and at the optimum temperature (37°C) was investigated. The results are shown in Fig. 4. For comparison, the same figure shows the dynamics of maintaining the activity of the native bacterial lipase. When processing the results of the experiment for 100% took the activity of a freshly prepared enzyme solution.

The drawings show that when stored for 2 weeks (336 hours), the residual activity of the native lipase is 32.5%, and when the immobilized lipase is stored for 4 weeks (720 hours), the residual activity of the immobilized lipase is 67%. One of the most important characteristics of enzymes is their operational stability, which is understood to be the ability to maintain enzyme activity over an extended range of operating temperatures and pH.

Therefore, the next stage of the work was to study the effect of the temperature and pH of the environment on the operational stability of the received microcapsulated form of lipase, which was evaluated by hydrolysis of olive oil at the values of temperature and pH of the environment, excellent optimal.

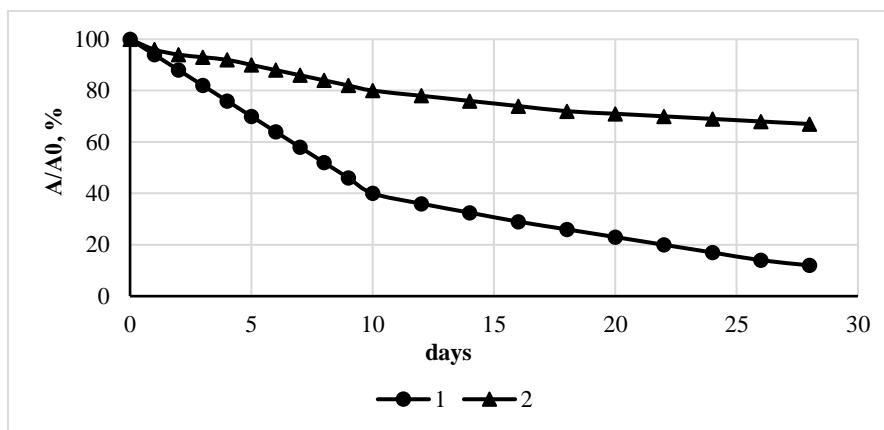


Fig. 4. Changes in enzymatic activity in the storage of the drug native lipase (1) and lipase included in carbonate microparticles (2)

The experiment was carried out under the following conditions: the concentration of the enzyme drug - 10.7 units/ml, the concentration of the substrate - 20 % (mass.), the incubation time - 60 minutes. Temperatures ranged from 25-75 degrees Celsius to an optimal pH value of 8.0 (phosphate buffer). The effect of the pH of the environment on the specific activity of lipase was investigated in the range of values 5.0-11.0 at an optimal temperature of 37 degrees Celsius. The results of the change in specific activity of microcapsulated and native lipase are given in Fig. 5.

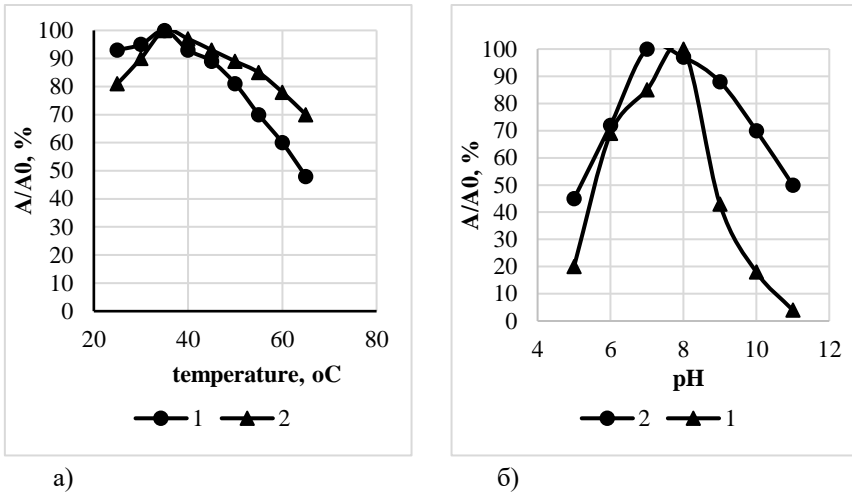


Fig. 5. Definition of temperature (a) and pH (b) optimums of bacterial lipase: 1 - microcapsulated, 2 - native

Analyzing experimental data, we can conclude that the operational thermostability of immobilized lipase in comparison with the native lower in the interval of temperatures above the optimal. It is evident that the temperature optimum for both native and microcapsulated lipase is 37 degrees Celsius. It should be noted that the activity of the immobilized lipase is slightly higher in the area of temperatures below the optimal, i.e. operational stability has increased in the area of lower temperatures. There was no temperature optimization, it remained at 37 degrees Celsius.

The data obtained indicate that the pH of the optimum immobilized lipase is 7.0, which indicates that pH optimum has shifted from low-alkaline (pH 8.0) towards neutral. Analyzing the results of the experiment, it can be concluded that in a wide range of pH the operating pH stability of the immobilized lipase increases very significantly, especially in the alkaline area: residual activity in the reaction in the environment with pH 11.0 is 51%.

Thus, as a result of studies, it was found that microcapsulation of bacterial lipase into carbonate microparticles leads to an increase in the effectiveness of the enzyme drug by increasing its operating stability, as well as stability in storage. All this makes promising the use of this form of microbial lipase for hydrolysis of fat-containing substrates.

CONCLUSION

In this work, a comparison was made of two methods of incorporating protein molecules into carbonate microparticles: adsorption in the pores (pre-received microparticles of the carrier are added to the protein solution) and microcapsulation (microparticle formation occurs at the same time as the inclusion of protein molecules). For both methods, the capacity of calcium carbonate microparticles on

bacterial lipase is determined and the maximum capacity equal to 0.2 mg/mg is achieved by using the method of adsorption in the pores. The specific activity of lipase in this case is 5.21 units/mg. The dynamics of the release of bacterial lipase from carbonate microparticles have been investigated. It has been established that during 90 minutes the degree of release of lipase from microparticles does not exceed 28%, while the decrease in its specific activity does not exceed 10%. This fact suggests a higher prolongation of the lipase, included in the microparticles of calcium carbonate in comparison with the native. The operational stability of bacterial lipase, included in calcium carbonate microparticles, was assessed in comparison with the native one. It was established that there was no temperature optimization, it remained at 37°C, but operational stability increased in the area of lower temperatures. PH optimum has shifted from low-alkaline (pH 8.0) towards neutral (pH 7.0), with the operational stability of microcapsule in the alkaline pH values significantly increasing. It has been shown that microcapsulation of bacterial lipase into carbonate microparticles leads to an increase in stability in storage twice as compared to native.

REFERENCES

- [1] Bezborodov A. M., Zagustina N. A., *Enzymatic Reactions in Chemical Synthesis of Drugs (review), Applied Biochemistry and Microbiology*, Vol. 52, issue 3, pp. 257-271, 2016.
- [2] Samoilova Yu.V. et al., *The use of bacterial thermostable lipolytic enzymes in modern biotechnology processes: review, Catalysis in industry*, Vol. 18, issue 6, pp. 61-73, 2019.
- [3] Godoy, C.A., Klett, J., Di Geronimo, B., Guisan, J.M., Carrasco-Lopez, C. *Disulfide engineered lipase to enhance the catalytic activity: A structure-based approach on btl2, International Journal of Molecular Sciences*, Vol. 20(21), pp. 524-532, 2019.
- [4] Abdullah, A., Abd Gani, S.S., Yun Hin, T.Y., Kassim, M.A., Effendi Halmi, M.I., *Lipase-catalyzed synthesis of red pitaya (Hylocereus polyrhizus) seed oil esters for cosmeceutical applications: process optimization using response surface methodology, RSC Advances*, Vol. 9(10), pp. 5599-5609, 2019.
- [5] Kravtsova M. V., Pisklova O. P., Belova I. V., *Analysis of the effectiveness of the use of biological products for wastewater treatment in the food industry, Engineering - from theory to practice*, Vol. 3 (40), pp. 97-110, 2015.
- [6] Vistovskaya V.P., *Hydrolytic enzymes in cheese biotechnology, News of Altai State University*, vol. 2, no. 3, p. 9-12, 2012
- [7] Garabadzhiu A. V. et al., *Basic aspects of the use of lipases for biodiesel production (review), Bulletin of the St. Petersburg State Technological Institute (Technical University)*, no. 7, pp. 63-67, 2010.
- [8] Xie, W., Huang, M. *Enzymatic production of biodiesel using immobilized lipase on core-shell structured Fe₃O₄@MIL-100(Fe) composites, Catalysts*, Vol. 9(10), pp. 850-878, 2019.

[9] Miao, C., Li, H., Zhuang, X., Lv, P., Luo, W., Synthesis and properties of porous CLEAs lipase by the calcium carbonate template method and its application in biodiesel production, *RSC Advances*, Vol. 9(51), pp. 29665-29675, 2019.

[10] Tolkacheva A.A. et al. Industrial Enzymes — an Overview of the Market of Enzyme Preparations and Prospects for Its Development, *Bulletin of the Voronezh State University of Engineering Technologies*, vol. 79, issue 4 (74), pp. 197-203, 2017

[11] Savina A.A. et al., Effect of polymers, nano-and microparticles on the catalytic activity of pancreatic porcine lipase, *Chemical thermodynamics and kinetics*, Collection of reports of the Seventh International Scientific Conference, pp. 252-253, 2017.

[12] Kılınc, A., Teke, M., Onal, S., Telefoncu, A., Immobilization of pancreatic lipase on chitin and chitosan, *Preparative biochemistry and biotechnology*, Vol. 36(2), pp.153–163, 2006.

[13] Bagi, K., Simon, L. M., Szajani, B., Immobilization and characterization of porcine pancreas lipase, *Enzyme and microbial technology*, Vol. 20(7), pp. 531–535, 2007.

[14] Scherer R.,OliveiraV., Pergher S., de Oliveira D., Screening of supports for immobilization of commercial porcine pancreatic lipase, *Materials Research*, Vol. 14(4), pp. 483-492, 2011.

[15] Haruta S., Hanafusa T., Fukase H., Miyajima H., Oki T., An effective absorption behavior of insulin for diabetic treatment following intranasal delivery using porous spherical calcium carbonate in monkeys and healthy human volunteers, *Diabetes Technol Ther.*, Vol. 5, issue 1 pp. 1-9, 2003.

Section

ENVIRONMENTAL GEOLOGY

Protectional and Conservation of the Geological Heritage

Regional and structural geology

Petrology and hydrogeology

Sedimentology

APPLICATION OF GEOINFORMATION TECHNOLOGIES IN THE STUDY OF CHANGES IN THE STRUCTURE OF LAND USE OF TERRITORIES

Assoc. Prof. Dr. Vasily Nilipovskiy ¹

Graduate student Denis Khabarov ²

Assoc. Prof. Dr. Irina Khabarova ³

^{1, 2, 3} State University of Land Use Planning, Russia

ABSTRACT

The purpose of this paper is to develop the flow charts of the processes of implementation of the main and alternate geo-information methods, when studying the changes in the land use structure of territories based on the materials of multi-zone space imaging. The research methods are geo-information method and comparative analysis. The paper provides a review of scientific publications on the research topic, proposes the key indicators, which are used as a basis for accomplished comparative analysis of the proposed geo-information methods implementation.

The proposed methods of determination of changes in the land use structure of territories, on the basis of materials provided by the multi-zone space imaging and data from national reports on the status and use of lands in the Russian Federation, enable estimation of dynamics of urbanization of certain territories, as well as the forecast of changes in the land use structure.

Keywords: *geoinformation system, land use structure, space imaging, comparative analysis, efficient management of natural resources*

INTRODUCTION

Data of the Earth's remote sensing (ERS) became vital for mapping of peculiarities of the Earth's landscapes and infrastructures, management of natural resources and study of the environment. Thanks to the creation of the higher-end technologies of capturing and automated thematic interpretation of ERS data, the materials of space imaging in high definition became one of the most prompt, reliable and efficient information sources for monitoring of status and historical changes in the land use.

The changes in land use are an important component of global changes in the environment. Analysis and forecasting of the changes related to the use of the land resources are of great importance for regional development and land use management for the purposes of sustainable development. Further on, following the Order of the Government dated November 08, 2018 "Action Plan for Improving of the Legal Regulation of the Land Relations", the development of methods of application and implementation of remote sensing data, including for the purposes of efficient use of natural resources, is particularly one of the priorities [1].

MAIN TERMS AND DEFINITIONS

Land category means a part of the land reserves, identified by its intended use and having a specific legal regime applicable to use and protection of the same. The lands on the Russian Federation are subdivided by their intended uses into the following categories: agricultural lands, residential lands, industrial and other special lands, lands of specially protected territories and objects, forest reserve lands, water reserve lands, reserve lands [2].

Conversion (change) of the land uses may be defined by the mutually exclusive land use conditions, covering the full range of changes in the land use [3].

REVIEW OF SCIENTIFIC PUBLICATIONS ON THE TOPIC

This research topic has been regarded in various Russian papers by V. A. Malinnikov, A. P. Sizov, P. V. Klyushin, D. A. Shapovalov, V. A. Shirokova and some others.

Thus V. A. Malinnikov and V. N. Nguen recommend in their paper to use the Markov chains to forecast the conversion of the land uses [3].

The paper by A. P. Sizova and D. A. Khabarov proposes to estimate the process of land withdrawal and land return by creation of all sorts of change options in the land status (man-induced impact) at various options of land conversion from one category to the other. The matrix developed by the authors enables more efficient analysis of historical changes in biosphere and environmental properties of territories development of the Russian Federation to the authorities possessing a reliable information on the quantity of land, which have been converted from one category to some other during a number of years [4].

P. V. Klyushin, P. A. Lepekhin, V. M. Stolyarov and some others addressed in their papers the contemporary problems of efficient land use. The authors establish that the system of efficient land use should be of preserving and resource-saving nature and provide for soil conservation, limiting impacts on flora and fauna, geological rocks and other components of the environment. Recommendations on the organization of efficient environmental management in the selected research area were also given [5], [6], [7], [8].

The Model Law on Strategic Forecasting and Planning of Social and Economic Development adopted by the International Assembly of the member states of the Commonwealth of Independent States (No. 41-10 dd. 28.11.2014) also touches upon the topic of the selected research. In particular, this law states that the biosphere and environmental indicators and criteria are zonal in nature and determined by physical and geographical conditions, which are specific to various regions of the planet and states [9].

METHODS AND METHODOLOGY

MAIN PART

In this paper, the successive stages of QGIS application for assessment of a level of change in the land use structure of territories based on materials of multi-zone space imaging are used as the main geo-information method. Fig. (1) shows the flow chart of processes of implementation of the main geo-information method. Fig. (2) shows the flow chart of processes of implementation of the alternate geo-information method.

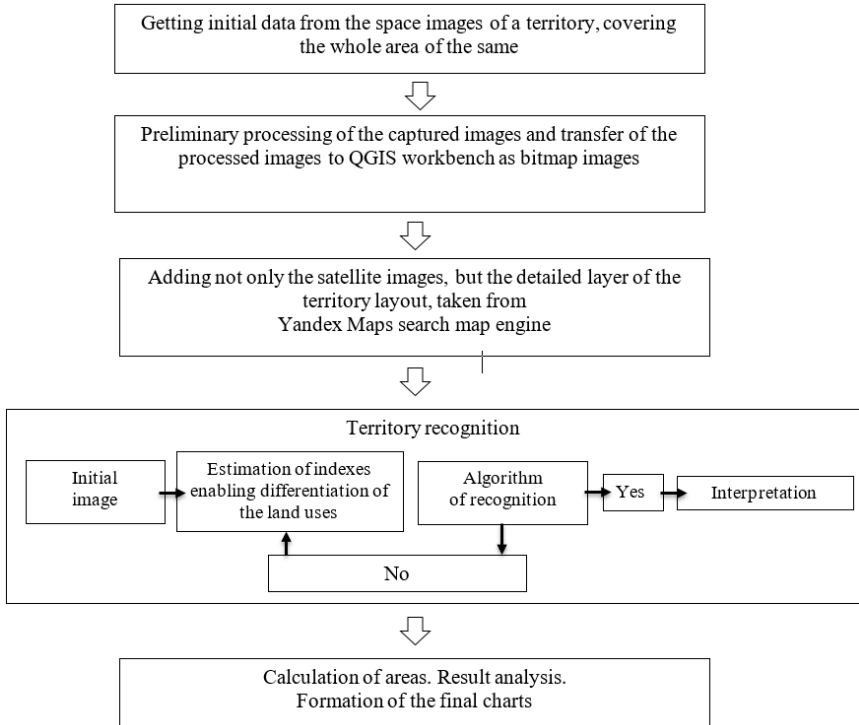


Fig. 1. Flow chart of processes of implementation of the main geo-information method

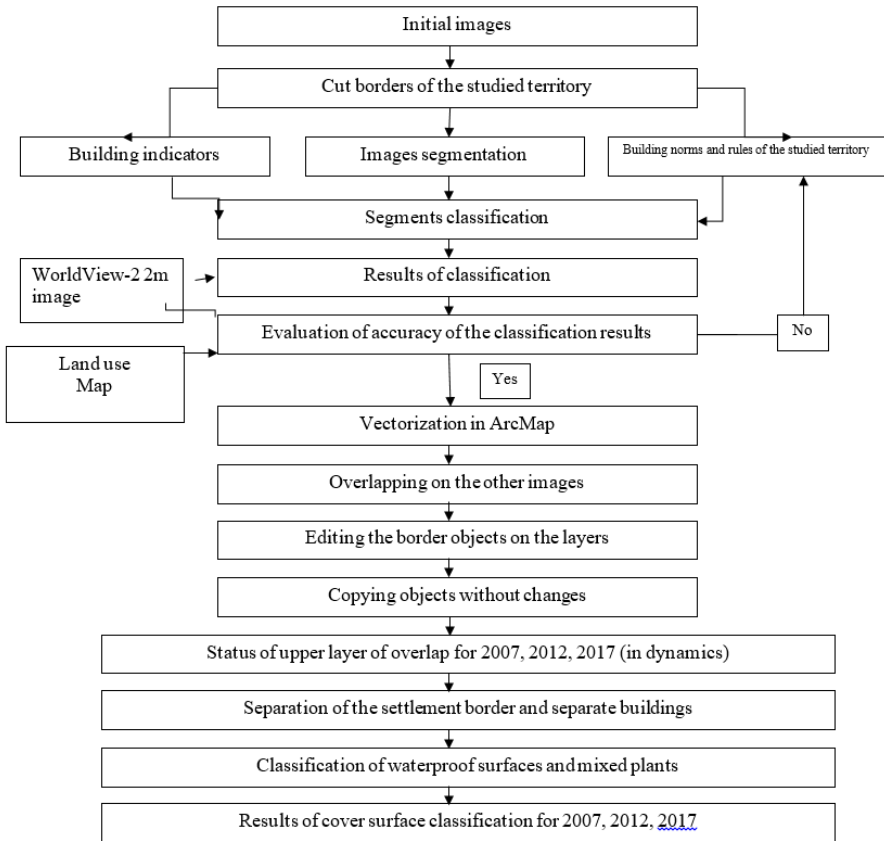


Fig. 2 Flow chart of processes of implementation of the alternate geo-information method

The result may be obtained even without GIS application, i.e. on the basis annual

National Reports "Status and Use of Lands in the Russian Federation", stating the changes in the country's land reserve structure with breakdown by 7 categories of lands (stating from/to which category the lands we converted). A. P. Sizov and D. A. Khabarov established that the process of lands withdrawal and return can be estimated by building all sort of options of the land status changes (man-induced impact) at various options of lands converted from one category to the other. Such built matrix and obtained historical changes in the land use structure also enable assessment of territories urbanization [4].

COMPARISON BETWEEN THE MAIN AND ALTERNATE METHODS

The following key indicators are proposed to compare between the main and alternate methods: GIS used during method implementation, software obtaining type, image processing method, reliability of interpretation results. They were used to carry out the comparative analysis of implementation of the main and alternate methods, when studying the changes in land use structure of territories according to materials of multi-zone space imaging, as shown in Table below.

Table 2. Comparative analysis of implementation of the main and alternate methods, when studying the changes in land use structure of territories according to materials of multi-zone space imaging

Key indicator	Main method	Alternate method
used, when implementing GIS method	QGIS	ArcMap, eCognition, IDRISI Selva
software obtaining type	free of charge	paid
processing method	spectral	spectral+texture
reliability of interpretation results	80–85 %	85–90 %

Various GIS, such as QGIS, ENVI, ERDAS Imagine and some others may be used for the study of changes of the land uses of territories with the materials of multi-zone space imaging. The proposed methods of achievement of the set aim have the same final result, further on, it is possible to forecast the changes in the land use structure by building the Markov chains with IDRISI Selva® software.

CONCLUSION

This paper addressed main terms and definitions, reviewed scientific publications on the research topic, developed flow charts of processes of implementation of the main and alternate geo-information methods, proposed the key indicators used as basis for comparative analysis of implementation of the main and alternate methods, when studying the changes in the land use structure of territories on the basis of materials of multi-zone space imaging. Using GIS incorporates high analytic opportunities, which are required during the data processing. This proves the timeliness of GIS use for the purposes of land planning and natural resources use.

ACKNOWLEDGEMENTS

We thank the GEOLINKS Conference team and especially Ms. Paolina Watt for their methodological assistance in organizing the research work.

REFERENCES

[1] “On approval of the action plan for improving the legal regulation of land relations” [Electronic resource] Decree of the Government of the Russian Federation of 08.11.2018 N 2413-р - accessed with computer-assisted legal research system Consultant Plus.

[2] The Land Code of the Russian Federation: Federal Law dated 25.10.2001 N 136-FZ (in wording dated 02.08.2019). - accessed with computer-assisted legal research system Consultant Plus.

[3] Malinnikov V. A., Nguen V. N. The use of Markov chains and Earth remote sensing data for predicting the conversion of land uses in large urban agglomerations // *Izvestiia vysshikh uchebnykh zavedenii. Geodeziia i aerofotosiemka = Izvestiya Vuzov. Geodesy and aerophotography*. 2017. No. 5. Pp. 99-105.

[4] Khabarov D.A., Sizov A. P. Using the dynamics of the land reserve of the Russian Federation to analyze its environment-forming properties // *Izvestiia vysshikh uchebnykh zavedenii. Geodeziia i aerofotosiemka = Izvestiya Vuzov. Geodesy and aerophotography*. 2017. No.3. Pp. 57-61.

[5] Efficient land use in the North Caucasus Federal Orkug / P.V. Klyushin, P.A. Lepkhin, G.V. Lomakin, S.V. Savinova, V.M. Stolyarov, Musaev M.R. // a collection of materials of the All-Russian Scientific and Practical Conference dedicated to the 45th anniversary of the FSBEI HE DSTU. 2018. - Published in Dagestan State University (Makhachkala), 2018. - Pp. 52-57.

[6] Zharnikov V.B. Rational land use and basic condition of its realization // *Vestnik SGUGiT= Vestnik of SSUGT*. 2017. V.22. No.3. Pp. 171-179.

[7] Musaev M.R., Shapovalov D.A., Klyushin P.V., Savinova S.V. Ecology of land use of agricultural land in the North Caucasus Federal District // *Iug Rossii: ekologiya, razvitiye= South of Russia: ecology, development*. 2016. V.11, N2. Pp. 132-142.

[8] Vershinin, V.V., Murasheva A.A., Shirokova V.A., Khutorova A.O., Shapovalov D.A., Tarbaev V.A. The solutions of the agricultural land use monitoring problems // *International Journal of Environmental and Science Education*. 2016. V. 11. No.12. Pp. 5058-5069.

[9] Model Law on Strategic Forecasting and Planning for Socio-Economic Development, adopted by the International Assembly of Member States to the Commonwealth of Independent States [Electronic resource]. - accessed with computer-assisted legal research system Consultant Plus.

**COGNITIVE GEOLOGY OF SUPERIMPOSED
SCATTERING OF MOBILE ORE ELEMENTS, PROPER
FORMS OF MULTISCALE STRUCTURAL STRESS
STABILITY, BIOGENETIC ACCESS CODE OF
RESOURCES AND FIELD ARTEFACTS**

Dr. Vyacheslav Popkov ¹

Prof. Alexander Sterenberg ²

Dr. Vladimir Gusev ³

Dr. Andrey Tyutyaev ⁴

^{1, 2, 3, 4} Samara State Technical University, Russia

ABSTRACT

The authors present the theory is numerical/analytical method of multi-scaled 4D geomechanics – geo-dynamics of energy integration in geo-physical rhythms of Eigen-solution of Navier-Stokes equations for multi-level geological time-space of evolution in structural compacted mass transfer at the basis of Newton’s Differential Law $\int^T \rho dS \cdot \partial^2 \xi / \partial t^2$ following the integration formula of A. Einstein $E(u,t) = \rho VC^2 + \int^T \rho \langle uv \rangle dt dx$. Create the theory (Restoration) and Maintenance of Water Eco-System with Given Parameters. They establish the geophysical seismic rhythms of geological cycles in deep structural formations of the Volga-Urals and Siberia and Kamchatka at dissipative emission, adsorption and nuclear magnetic resonance. The authors propose the systematic velocity model of convective diffusion drift of $\rho \langle uv \rangle$ in deep phase components of heterogenic structures with complexly structured geology in off-shore and global aeration of Middle Ridges from the Urals to the Rocky Mountains. They have also considered the energy time-space of more than 4,5 billion years to find the organic markers of quantum photo-synthesis and multiple circulating energy waves in physical and chemical reactions of compacted formation genesis in fissile and relict shales, including the facies with symmetrical absolutely-saturated porosity of classical fields. They establish the geophysical seismic rhythms of geological cycles in deep structural formations of the Volga-Urals and Siberia and Kamchatka at dissipative emission, adsorption and nuclear magnetic resonance. The authors propose the systematic velocity model of convective diffusion drift of $\rho \langle uv \rangle$ in deep phase components of heterogenic structures with complexly structured geology in off-shore and global aeration of Middle Ridges from the Urals to the Rocky Mountains. They have also considered the energy time-space of more than 4.5 billion years to find the organic markers of quantum photo-synthesis and multiple circulating energy waves in physical and chemical reactions of compacted formation genesis in fissile and relict shales, including the facies with symmetrical absolutely-saturated porosity of classical fields’ cognitive geology, artefacts.

Keywords: *evolution, phase knobs, conductivity, relaxation, basin*

INTRODUCTION

Currently, the energy production companies are facing the problem of deteriorating quality of the bottom-hole, ore reservoirs and well production rates [1], [2], [7]. To maintain and increase production levels, it is necessary to locate complex bottom-hole and multi-segment wells in challenging geological conditions, compacted ultra-low-permeable formation rocks and uncompacted unconsolidated zones of reservoirs with a high content of shale and compacted shale rock. This entails high risk uncertainty in well construction, drilling and equipment stability, as well as a long-term forecast of quality in development and in business. Geo-information models are required for assessing the geological risks while developing marine, Arctic and deep-sea off-shore areas and mountain regions. We need conjugate models of adjacent structures of the continental slope and foothills of the mountains, shale reservoirs (compacted and low-amplitude) with high-resistance and low-permeability, geological reserves that are considered low-profitable but having the reserves much larger in their size than traditional ones.

Scientific interest is given to the method of decomposition with additive integrated solutions in 4D geomechanics structural polarization of space-time continuum with continuous quality development of substances, evaluation of geological risk with anthropogenic factors of geophysical fields synergy not in the two-level [13], Fig. 1. The evolution of substance structure development is not taking place in macro-scale of the averaged space of classical linear 3D models, but is in the micro level of physical and chemical processes of 4G+ molecular mobility. The energy of substance development is continuously distributed at the phase levels of atoms and electrons in ionized fields [15]. Molecular mobility starts with energetic ion and quantum processes of phase mobility, matrix stress stability and nuclear magnetic resonance. Stress stability and resistance present the initial state of space and time with substance. This criterion meets the model of a single multiscale energy distribution potential and the structure of space and time. We consider the model with a like-foam structure from gas to condensate, liquid to solid and back to dust, followed by its reverse repeated dissolution of the reversed destruction and deposition. These models of noosphere by V.I. Vernadskiy [14], the reflection of neurons by I.P. Pavlov, and the evolution of the Earth by O.Yu. Schmidt, type of progressive waves of substance phase development by L.D. Landau.

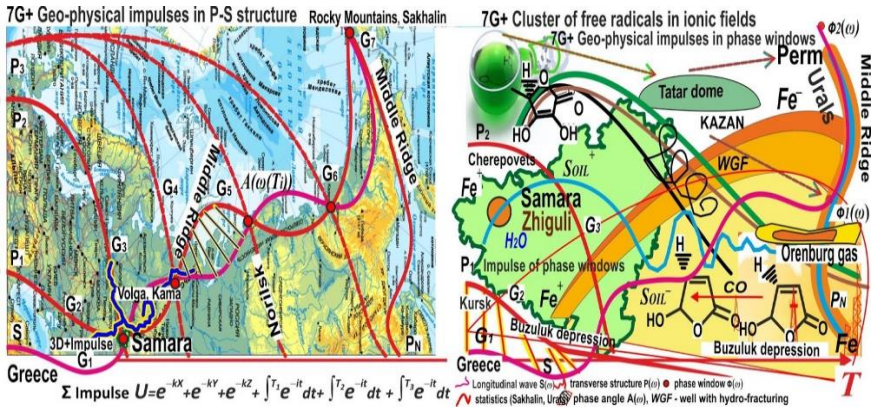


Fig.1. Decomposition of dissipation halos in mobile elements $A(\tau, t)$ of evolution in proper forms of reservoir development and phase windows of cognitive geology and artefacts

To start effectively the new information 4D+ models (Fig.1) cognitive technologies of business processes [8], [9], [10] are actively introduced into production activity. These technologies allow us to reduce the time of field start-up into operation and increase the efficiency of decisions taken by data integration that was not used earlier in the analysis, which in its turn gives a new vector in development. Based on the results of the analysis several companies identified the following priority areas for the introduction of cognitive technologies:

- Digital processing of 4D seismic data massifs;
- Geological and hydrodynamic modeling of 4D geomechanics;
- Complex analysis of multi-scale research results;
- On-line processing of hydrodynamic studies of operations;
- On-line detection and prediction of challenges;
- Automation of data pick-up processes and machine processing of 4G+ data massifs.

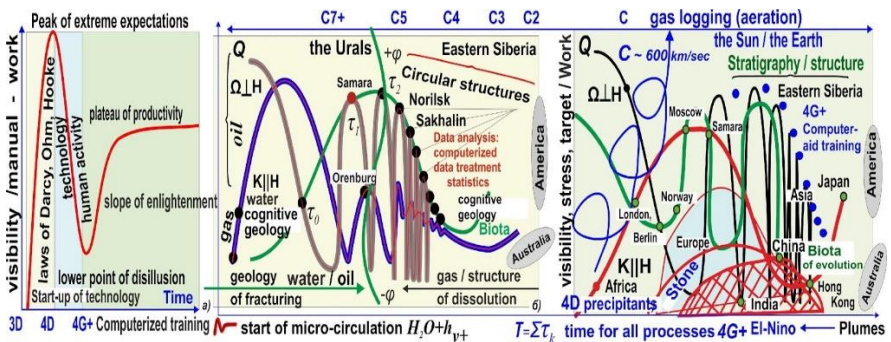


Fig. 2. Global cycles (Gardner) in cognitive geology of longitudinal and transversal geo-navigation ($K||H, \Lambda \infty H$), indices of reservoir development

The dilemma of time uncertainty with additive robotic technologies is clearly presented in Gardner-type geological cycles (Fig. 2). Uncertainties with expectations of geo-exploration procedures, drilling and development occur both at the beginning and at the end of further cycles of historical and man-made development of deposits, when it would seem that everything is known about the fields like Mukhanovskoye, Romashkinskoye and Samotlorskoye. Unsolved problems with modeling from the view-point discrete statistics and tectonics are resolved quite successfully in a continuous space of time, when viscosity of fluids, according to interfacial relaxation, passes into viscoelastic plastic structures of repeatedly reversed energy processes of destruction, dissolution and deposition. We are speaking in this case about the global sustainability of multi-scale reservoirs of the Atlantic area of development from the Mediterranean Sea up to the Bering Strait of the Pacific Ocean, Sakhalin and Kamchatka. Plastic substances are washed out continuously up to the ore rock skeleton, shale oil, forming compacted borders, impermeable for the new stage of 4D+ development. Therefore, in the course of operation, the field evolves either in the non-reservoir areas, lens-type or vertically uniaxial, fractured deposits, which are actually traps and what is observed on all layers on the entire planet during the complete time of their development. In the global timeline of today the oil from a single continuous space does not flow where it flowed yesterday or will flow tomorrow. This solves the problem with multi-scale flow around the Earth along the 4G+ spiral of the shady ion structure by gas flows of hydrogen and carbon dioxide from Antarctica to Africa, the North Pole, the Bering Strait and the Rocky Mountains. There is a hydrodynamic kinematic reversal of the jet streams processes in numerous faults, depressions of the Pacific Ocean such as the Mariana, towards America, China, and the Ring of Fire – the El Nino current to Australia, India, and the Mediterranean Sea. There is a continuous process of the Earth core compaction and a cyclical shift of the Earth's magnetic pole from Greenland to Taimyr.

Geologists identify the roofs of the fields, but any roof rests on wedging areas, areas of relict shale and higher phases of C+7 oil catagenesis. However, this is also the oil of a single time development in organic deposition of the global aeration with the Middle Ural Range, Kamchatka and the Rocky Mountains. Therefore, we need to solve the problem of the swelling surface of the Earth and the deposited rocks from Gondwana to the present days. In this case the differential laws of Newton and Darcy do not have members that transmit information in time, such as the similarity of deformation moments and the amount of movement. We need the information that the same substance had come to point "b". It is necessary to determine the oil at the control points of the system (*Backup*). So, just yesterday shale oil was not included in the concept of oil, and today due to its presence oil reserves in America have increased in many times. The laws used today take into account the movement of parallel similarity of ballistic paraboloids of the Bernoulli type, and exist only in local sections of global spiral trajectories. It is necessary to involve higher-order derivatives of multiscale correlation in velocity pulsations. These are small velocities but with ultra-small angles of deformation moments in excess of large double-sided fractal areas, polar density pulsations and shady structure velocities. Electromagnetic induction fields can melt the iron in fractions of seconds, having second-order boundary conditions such as zero gradients. On

what kind of thermodynamics can we speak at the edges and corners of the pyramid, if the sides are made of iron, carbon and gas having various densities? Electric induction currents occur. Moreover, it should be noted that we are not speaking about the processes with open systems, but with the closed ones, quite terrestrial, the latest kitchen technologies. According to the law of equilibrium with communicating vessels, the ions, penetrating into the system, (e.g. organics) near Moscow (see Fig.1), "instantly" exit on the opposite contact under the Samara, without flowing through the conductor.

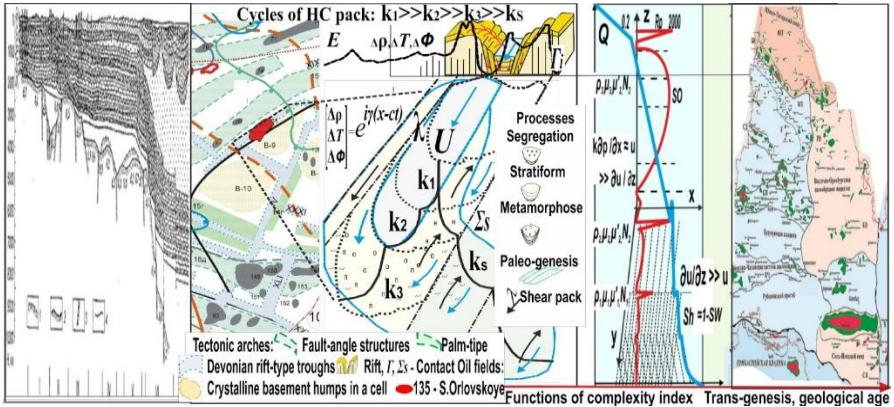


Fig. 3. Seismic geological profile of geo-navigation indices for the graben-type depressions and uplifted blocks of reservoirs in Buzuluk depression of the Volga-Urals region.

The concept of multi-scale similarity for system models of complex reservoirs fully fits into the theory of 4D facies geomechanics and compacted formations from the Mediterranean Sea to Sakhalin, which includes gas pipes as well as Taimyr. If the formation intersects the well at an angle of $+\varphi$, then on the other hand it is already $-\varphi$, then what should we take for the angle of indexing and geo-navigation? It should be noted that no pressure gradient of complex mining equipment can turn back the speed of the opposite migration towards the direction of the bottom hole or the well, unless forced to carry away the differential "piece". The fracture must at least have the same type of complexity as the matrix, only with a negative phase sign. Thus, the Volga-Ural formations have many sub-indices with strokes, either double and triple. Fig.3(a) compiled in the 50s by Yu.N. Godin et al. corresponds to the cognitive geology of the proposed 4D model of the regional reservoir up to Sakhalin and Kamchatka. Fig.3(b), where *I* - the South-Eastern slope of the Tatar arch; *II* - the Sernovodsk-Abdulinskaya depression; *III* - the Kinel arch; *IV* - the Buzuluk hump; *V* - the Chagansky-Kamelikskiy bar; *VI* - the Northern side of the Caspian depression; 1 - the surface of possibly Proterozoic formations; 2 - the surface of the Pre-Cambrian Foundation; 3 - fault zones; 4 - dislocations in the sedimentary rock column.

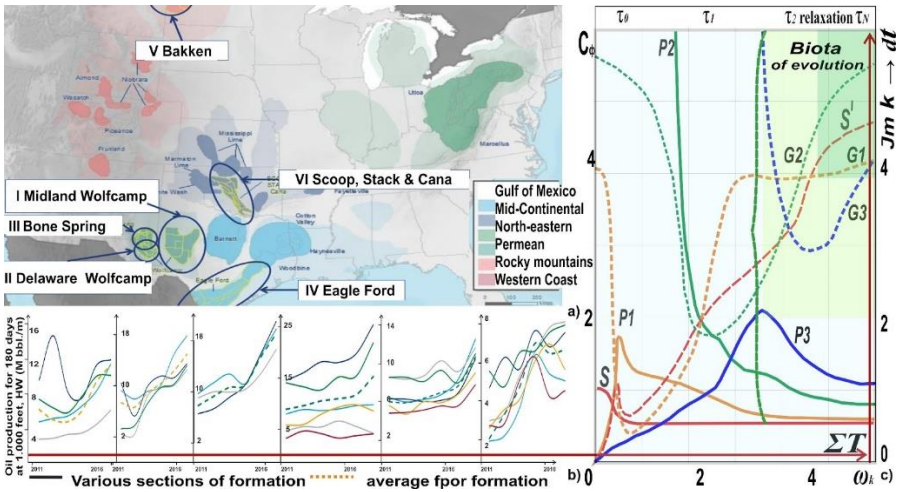


Fig 4. Regional formation quality for the formation of shale oil in Rocky Mountains (a,b) scales of phase velocity and attenuation of dissipative structure development (c)

Geophysical generation and accumulation of rock formations and facies phase boundaries of the deep-water shield are characterized by the following General features:

- Complex organization of multi-scale space, weakly expressed structural control, fluctuations in production and inflow profiles;
- Limitation of deposits by faults, lithological re-placement of reservoirs, low permeable drain compacted segments, lack of production, phase inflow, stagnant capillary-jammed zones of counter-flow impregnation, convective-diffusion shear deformations of tangential stresses;
- Changing in time grid of lines and planes of multiscale sliding and free surfaces, fractures and mass and volume deficits.

Non-equal temperature, viscosity and difficulty in inversion of saturation, pressure, undefined phase concentrations of 4G+ momentum transfer moments, scope of motions, foam structure of nuclear magnetic resonances, compacted scales of deformation moments, and the near-zero arm of ultra-large high-amplitude polar impulses of the anti-phase shady structure.

Main observations, facies, formations, and geological uncertainties

Figure 4 presents the 6 main formations of hard-to-recover US oil reserves and the quality of their production rates, which account for >90% of production of unconventional fluid reserves. These are compacted formations of shale oil: 1. Midland Wolf-camp; 2. Delaware Wolf-camp; 3. Bone Spring; 4. Eagle Ford; 5. Bakken; 6. Scoop, Stack & Cana. Shale is an oil-saturated carbonate and shale formation. It consists of four intervals A, B, C, or D. The largest number of wells is drilled in the Wolf-camp interval “B”. Wolf-camp continues to be one of the most

stable unconventional oil formations due to the developed infrastructure and constantly growing productivity of wells that provided break-even development of the main zones of the formation. In the Permian deposits, which have a long history of oil and gas production, there is a developed structure of oil gathering, processing and transportation compared to other less mature formations of hard-to-recover oil. Operators and companies engaged in oil processing, storage and transportation continue are actively planning to build additional capacity to accommodate the growing production in the region. Initial production rates in each formation zone are still increasing, but this increase in ultimate recoverable reserves is more modest. Operators are trying to optimize the balance between initial production rates and volumes of the ultimate recoverable reserves.

METHOD AND THEORY

New technologies to provide the influence upon the reservoirs, the development of technical control and monitoring means over the production processes as well as simulation of the fields with hard-to-recover reserves often do not have any adequate reflection in the cognitive science of solutions such as in road maps widely used at the scale of industry. This is due to the fact that very often for complex cases there are no sufficient specialized physical and mathematical algorithms and techniques [3], [4], [5], that allow improving the control over the development processes. Scientific support of the problem is related to the integral method in resolving fundamental theoretical and applied problems of non-linear functions with distributed time parameters [6]:

- Thermodynamics of vector contact of two-level space in a porous medium (horizontal well), which is the basic problem of large-scale averaging of volume mass transfer and wave transmission of momentum of the number of the motion;
- Geo-physical interpretation using conceptually new information on the structure of productive layer (skin factor of dynamic anisotropic roof-bottom stratification, etc.);
- Development of a theoretical adapted understanding of specific models and methods to calculate stresses and deformations in rock masses, the movement of concentration and dispersion halos of the resources during field development.

The result of the work is the development of new ideas on the complex geological environment, the system organization of multi-scale phase movements, the principles of synergy and self-organization. The multi-scale "anomalous" behavior of "rock – fluid" tandem with definition of main filtration flows is a geo-physical generalization of the Pollard-Pearson double pore space. Dynamically non-equalized shear layer of tangential stresses has a maximum level of dissipative energy accumulation, structural 4G+, and higher pumping phases [10]. The stressed deformed state of the deep medium forms the asymmetric deformations of the polarized mass transfer with matrix conductivity and permeability. The neo-tectonics of fractures increases the regional hydrodynamic structural relationship by orders of magnitude. If a fracture is formed once, it will never disappear forever and

will develop from the tangential structure of the "viscous" vacuum to the compacted elasticity of the substance in the geological body.

Geo-physical Rhythms of Structural Compaction and Proper Forms of Space Geological Polarization

Equation recorded in cylindrical system of coordinates has the shape of Bessel's differential pressure [2]. The solution is recorded as the shape of longitudinal and transversal waves [11], [12] with complex wave number k for the equations of the fourth order:

$$\varphi(z_\varphi) = a_1 J_0(z_\varphi) + a_2 Y_0(z_\varphi); \quad \psi(z_\psi) = a_3 J_1(z_\psi) + a_4 Y_1(z_\psi),$$

where, $J_0(z_\varphi)$, $Y_0(z_\varphi)$ - Bessel's function, $z_s = k_s r$, $s = \varphi, \psi$. Satisfying the boundary conditions we get a system of equations of the fourth order. This result in characteristic equation for the proper frequencies in sheared layer $\det \{A\} = 0$, where, $\{A\}$ - is the characteristic matrix. Fig.3 (a) presents the phase velocities $c_\varphi = c/c_0$ and attenuation factors $Im(k)$ of permeable membrane depending on the frequency $\omega_k = \omega h/c_0$, where, $c_0 = (\mu(3\lambda + 2\mu)/(\lambda + \mu)\rho)^{1/2}$. In case with no shear stress the diffusion is equalized by dissipation velocity

$$\Phi = \omega/4 \int_1^i \{ [\lambda^*(\omega) - \lambda(\omega)] \varepsilon_{ij} \varepsilon_{ij}^* + [\mu^*(\omega) - \mu(\omega)] \varepsilon_{ij} \varepsilon_{ij}^* \} dx,$$

where, ε_{ij} - deformation. In this case the normal stresses are attenuated, the tangential stresses are increasing and pressure gradients are restructured into tangent stresses. Symmetrical pressure is split-down into asymmetric stresses, radial velocities - into molecule-diffusive pulsing impulses. Shear stresses coinciding in their direction with the averaged velocity increase diffusion $\langle pv \rangle$ and imbibition velocity $\langle uv \rangle$. In reverse case they drop it down, thus the displacement front becomes a selective one, re-distributing, heterogenic-phase type in its density. Almost at zero frequency a bending wave appears, defined by the Young's modulus. As the frequency increases the phase velocity tends to the speed of the transverse wave. At high frequencies the phase velocities merge on a large scale and become self-similar.

With natural frequencies there are sharp declines in the attenuation coefficients. With the natural frequency of $\omega_k \sim 1$ the amplitude becomes several tens of times greater than the thickness of the shear layer thus forming powerful transverse surges of the trapped density. The anisotropy coefficient becomes less than 1, increasing the deformation of the inclined sliding surfaces of hydrogen, carbon dioxide, methane hydrocarbons, gas-oil and water-oil contacts, carbon-mica and shale strata, and breakouts of displacing agents during development. While the normal stresses are attenuating the tangents increase with the natural reformation of radial pressure gradients in the shear and membrane stresses. The symmetric pressure is split into asymmetric stresses, and the radial velocities of the averaged filtration are split into diffusion pulsations. The permeability anisotropy coefficient becomes less than 1. Shear stresses that coincide in the direction with the wave velocity, i.e. if the torque coincides with the direction of the filtration flow, increase the diffusion of "pv" and the impregnation rate of "uv". In the opposite case they reduce them, thus the displacement front becomes redistributive. In the absence of shear stresses at the boundary, diffusion is balanced by the rate of dissipation. With natural frequencies

the diffusion attenuation coefficients and the ion energy transfer are reduced. The amplitudes become significantly larger than the thickness of the shear layer by several tens of times. As a result of resonant-wave decompression of the rock, the declining-vertical zones of secondary porosity are formed and they that do not coincide with the geometry of the initial sedimentation.

The presence of a closed, hydrophobic porous medium radically changes the thermo-dynamics of hydrocarbon mixtures in pore space and the hydrophilic aeration phase of the Mid-Ocean Ridges. The existence of surface layers with an internal compacted structure has been proved experimentally and theoretically. The most convincing is the statement on block formation movements in structural elements of sedimentary cover traps and it "works" when modeling the areas with ancient foundations. Due to planetary stresses the dynamic structures of tension and compression are formed here, as well as diagonal structures of shears and sliding planes. The same time deposits of different timing structure are formed:

- Structures associated with the erosion foundation of step-like sinking structures.
- Lateral distribution of the stretching tension forces of con-dimensional processes in small structures of sedimentation.
- Compression stresses are clearly presented in the formation of neo-tectonic structures of mass deficit pulses and volumes of initial development in fractures with negative curvature of borders, potentials and gradients.

CONCLUSION

Convective-diffusion fields of cognitive geology as a function of reservoir quality integration form a new type of dynamic stability, such as stable stress stability in blocks of the wells, regional exploration programs and forecast of the stationary part with the inflow stages.

Shear structural surfaces with abnormal complex evolution of inorganic and organic reservoir systems are able to accumulate energy and arrange mass transfer along the certain trajectories of nuclear magnetic resonance phase interactions in sliding surfaces.

The block structure of heterogeneous stability in the compacted-decompressed space and resonant-wave phase relaxation of natural and technogenic pulses opens up new possibilities for searching, exploring and simulation of potentials' quality, in diagnostics and regulation of inflow and optimization taking into accounts the risks of cognitive geology and the evolution of the substance.

REFERENCES

[1] An L.Y., Paleochannel sands as conduits for hydrocarbon leakage across faults: an example from the Wilmington oil field. California. AAPG Bulletin. Amer. Assoc. of Petroleum Geologists. 2009;

[2] Astafiev V.I., Kakhidze M.G., Popkov V.I., Popkova A.V., Multi-scale Stress-deformed Status of Porous Geo-sphere and Filtration Well Outflow. Bulletin of SamSU. V.110. Is.9/2, 2013, pp. 154-171;

[3] Bykova M.I., Verveyko N.D., Sumets P.P., Shakshina S.A., Techeniye i Deformirovaniye Materialov Odnorodnoy Microstructurey. Voronezh. 2010;

[4] Volokitin A.I., Dubas E.V., Singularities in radiative heat generation and interaction forces for two rotating nanoparticles caused by the anomalous Doppler Effect. JETP Letters, vol.105. Is. 11. 2017, pp. 733-738;

[5] Goldshtik M.A., Shtern V.N., Yavorskiy N.I., Viazkiye Techeniya s Paradoksalnymi Svoistvami. Novosibirsk. Nauka. 1989;

[6] Kumar N. Karthik, Joshi Sameer, Banerjee Raj, Sundaram K.M., A New Method for Gas Well Deliverability Potential Estimation Using MiniDST and Single Well Modeling: Theory and Examples Engineers Source. SPE 113650. 2008;

[7] Shashel A.G., Shipovskiy A.P., Khludnev V.F., Alexandrov A.A., Danielyan B.Z., Geodinamika Kamelik Chaganskoy Strukturnoy Zony v Devonskoye Vremya v Svyazi s Poiskami Zalezhey Nefti i Gaza. Geologia Nefti i Gaza, vol.10, 1997, pp. 26-33;

[8] Popkov V.I., Shterenberg A.M., Gusev V.V., Unified Complexly Structured Potential of Compacted Formations and Geological Evolution of Hydro-Carbon as per A. Einstein's Formula. Neft. Gaz. Novacii. V.2. 2019, pp. 28-36;

[9] Melkikh A.V., Khrennikov A., Yampolskiy R.V., Quantum Metalanguage and the New Cognitive Synthesis. NeuroQuantology, vol.17/issue01, 2019, pp. 72-96;

[10] Popkov V.I., Shterenberg A.M., Stepanova L.V., 4D Geomexanics of Integration of Energy of Evolution, Collectors and Oil Structures According to A.Einstein Formula. Geolinks International Conference on Geosciences, Novotel, Athens. Greece, 2019, pp. 114-122;

[11] Voropaev G.A., Popkov V.I., Energy and kinematic characteristics of wave propagation in a viscoelastic layered hollow cylinder. International Applied Mechanics, vol.24, is.7. 1988, pp. 669-673;

[12] Khromov A.I. Patlina O.V., Ductile Flows in the Area of Rounded Angle Slots. Bulletin of ChGPU named after I.Ya. Yakovlev. Mechanics of Extreme Status, vol.2, is.8, 2010, pp. 521-529;

[13] Krivistkiy S.V., Ostroumov S.A., Eco-Bio Engineering: Creation (Restoration) and Maintenance of Water Eco-System with Given Parameters. Bulletin of St. Petersburg University, vol.8, is.4, 2018, pp. 693-714;

[14] Vladimir Vernadskiy. Biosphere and Neo-sphere. Edited by N. Kostisashkin, E. Goncharova. Airispress. 2004;

[15] Pavlov A.N., Geophizika. Obschiy Kurs o Prirode Zemli. SPb RGGMU. 2011.

GEOLOGICAL AND GEOPHYSICAL STUDY FOR ELABORATION OF GEOTHERMAL MODEL IN ORADEA- BAILE FELIX AREA

Dr. Laurențiu Asimopolos ¹

Dr. Natalia-Silvia Asimopolos ²

^{1,2} Geological Institute of Romania, Romania

ABSTRACT

Thermal methods consist of measuring thermal gradient and satellite data, which can be used to determine the Earth's surface temperature and thermal inertia of surficial materials, of thermal infrared radiation emitted at the Earth's surface.

Thermal gradient measuring, with a knowledge of the thermal conductivity provides a measure of heat flow. Conditions that may increase or decrease and heat flow are influenced by hydrologic, topographic factors and anomalous thermal conductivity.

Also, oxidation of sulphide bodies in-place or on waste deposits, if sufficiently rapid, can generate thermal anomalies, which can provide a measure of the amount of metal being released to the environment.

The geothermal gradient on the territory of Romania, the increase of the temperature with the depth, has an average value of 2.5°-3°C/100m, which corresponds to a temperature of 100° C at 3000 m deep. There are many areas where the value of the geothermal gradient differs considerably from this average.

For example, in areas where the rock plate suffered rapid dips and the basin was filled with sediment "very young" from a geological point of view, the geothermal gradient may be less than 1° C/100m. On the other hand, in other geothermal areas the gradient exceeds much this average.

These areas are true underground thermal reservoirs of potentially high geothermal energy which under certain favourable conditions can be exploited to serve heating installations and domestic hot water systems.

The geothermal prospecting for the entire territory of Romania, carried out by temperature measurements allowed the development of geothermal maps, highlighting the temperature distribution at different depths.

Geophysical data obtained through various methods and geophysical modelling provide generalized and non-unique solutions to the geometry of underground geological relations as well as to the physical characteristics of different formations.

The non-uniqueness of these models (solutions to the direct problem) arises from the impossibility of knowing the boundary conditions between different strata, which together with the propagation equations of the different fields (depending on the geophysical method used for the investigation of the basement) form the systems that offer the solutions of the model.

The Oradea geothermal reservoir is located in the Triassic limestones and dolomites at depths of 2,200-3,200 m, on an area of about 75 km², and it is exploited by 14 wells with a total maximum flow rate of 140 l/s geothermal water with well head temperatures of 70-105°C. There are no dissolved gases, the mineralisation is 0.9-1.2 g/l, the water being of calcium-sulphate-bicarbonate type.

The Oradea Triassic aquifer is hydrodynamically connected to the Felix Spa Cretaceous aquifer, and together are part of the active natural flow of water. The water is about 20,000 years old and the recharge area is in the northern edge of the Padurea Craiului Mountains and the Borod Basin.

***Keywords:** geological and geophysical model, geothermal water, thermal conductivity, flow rate*

INTRODUCTION

Geothermal energy is an unconventional renewable energy source with enormous potential for exploitation, of which only a very small part is currently used today.

Worldwide, countries with a high geothermal potential are Iceland, New Zealand and in Europe are Hungary, Romania, Serbia. In these countries, as well as in many others, there are geological conditions that allow geothermal phenomena to manifest on the surface of the Earth. The limited exploitation of this energy resource is still limited by existing technologies and by the high cost of deep-water equipment.

For the future, geothermal energy is considered to be Earth's most important energy resource, given the estimate that the temperature in the centre of the Earth is equal to the temperature at the surface of the Sun. The problem lies in finding the most suitable technologies for exploitation both in areas with geothermal phenomena on surface and in areas with these manifestations in underground [12].

The main geothermal systems discovered on the Romanian territory are found in porous permeable formations such as sandstones interbedded with clay and shales or carbonate formations of Triassic age in the basement of the Pannonian Basin and Aptian age in the Moesian Platform.

Geothermal reservoir Oradea is located in the Triassic limestone and dolomites at the depths between 2200m to 3200m on an area of about 75Km² with a total flow rate of 140 l/s geothermal water with temperatures at the head of 70-105 degrees Celsius. Recharge area is in the Northern edge of the Padurea Craiului Mountains and the Borod Basin. Although there is a significant recharge of the geothermal system, the exploitation with a total flow rate of 300 l/s generates pressure draw down in the system [4].

The Bors geothermal reservoir is a tectonic closed aquifer with a surface area of 12km², situated at about 6 km North-West to Oradea with geological framework is completely different from the Oradea geothermal reservoir although the reservoirs are in the same fissured carbonate formations.

In relation to geothermal resources and, especially, to their exploitation for geothermal energy utilization, sustainability means the ability of the production system applied to sustain the production level over long times. Sustainable production of geothermal energy therefore secures the longevity of the resource, at a lower production level [9].

GEOLOGICAL AND GEOPHYSICAL FEATURES, MAPS WITH GEOPHYSICAL PARAMETERS AND RESULTS.

In the North-West part of Romania, we can see as major units the Transylvanian basin with its Neozoic sediments covers a former Cretaceous mountain chain that closed the branch of Tethys, joining the Tisa and Dacia continental blocks, that represent fragments of the European Plate that were detached from it with the opening of Tethys. Their likeness to the European Plate took place during the Alpine orogenesis, especially the tectonic phases in the Middle and Upper Cretaceous.

The Dacia unit, located south and east, consisted of metamorphic rocks with lower Palaeozoic sedimentary affected by an early metamorphism. The non-metamorphosed sediments consist of discontinuous Carboniferous-Permian-Mesozoic sediments.

The Tisza Bloc, of which the Apuseni Mountains also belong, consist of a succession of nappes placed in the middle Cretacic, consisting of a meso- and epicrostalline foundation and a Permian Mesozoic blanket.

The sedimentary succession, subdivided into 7 layers have with a total thickness of up to 22 km. It is composed of the Carpathian nappe pile and the post-collisional (post-Early Cretaceous) Paleo to Neogene Transylvanian Basin, which covers the local Late Cretaceous to Paleogene Tarnava Basin [4].

Different crustal blocks characterized by clearly distinct geometries and velocity structures were identified: the Tisza-Dacia crustal block, which underlies the Transylvanian Basin and most of the Eastern Carpathian Orogen.

The sedimentary sequence is composed of the East Carpathian flysch nappes and the Neogene infill of the Transylvanian Basin.

A regional geological interpretation for the elucidation of deep structures must be made on the maps of the anomalies mediated to eliminate the effects of surface geological structures. In this way we must to combine the results of filtering methods with previous knowledge.

For a good image of the geothermal potential in the West part of Romania, we present, the geophysical maps with main zones of geothermal potential. These maps we made with the Surfer program, based on the data presented on geophysical portal on the WEB page of the Geological Institute of Romania [1], [2], [5], [7], [8].

These maps indicate temperature of 3000m depth (fig.1), geothermal flow (fig.2), Bouguer anomaly, after filtering and smoothing of gravity data (fig.3) and

Free Air anomaly (fig.4), after filtering of gravity data with Fourier analyses 2D, on the Romanian territory.

By overlaying this geophysical information, corroborated with other geological, geophysical, geodetic, laboratory and drilling data, conclusions can be drawn regarding the geothermal systems on the territory of Romania.

Gravity measurements define anomalous density within the Earth. Ground-based gravimeters are used to precisely measure variations in the gravity field at different points. Gravity anomalies are computed by subtracting a regional field from the measured field, which result in gravitational anomalies that correlate with source body density variations. Positive gravity anomalies are associated with shallow high-density bodies, whereas gravity lows are associated with shallow low-density bodies.

Physical parameter measured in gravity method is total attraction of Earth's gravity field (the vertical attraction of anomalous masses) for calculating the rock density contrast. In gravity are important other parameter such as gradient of gravity, analytical continuation of gravity field, filtering's and smoothing of gravity data.

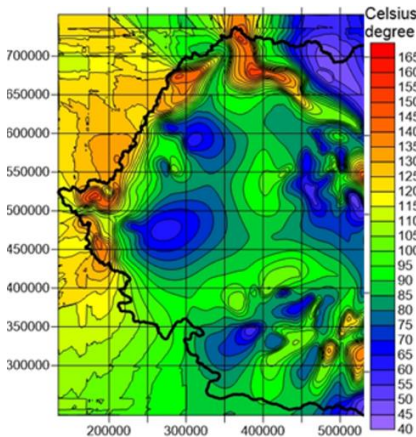


Fig.1 – Temperature of 3000m depth on the West part of Romanian territory, after data from the geophysical portal of Geological Institute of Romania.

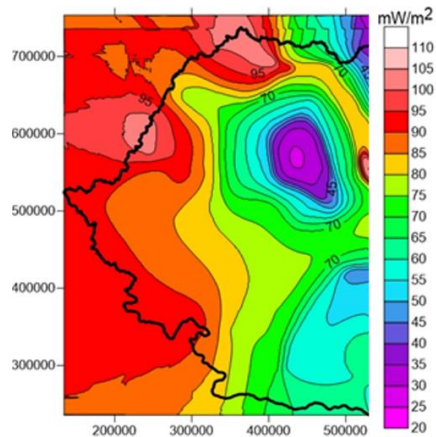


Fig.2 - Geothermal flow on the West part of Romanian territory, after data from the geophysical portal of Geological Institute of Romania.

In fig. 3 is residual map of the Bouguer anomaly, after the trend surface of order 6 has been extracted:

$Z=A+BX+CX^2+DX^3+EY+FXY+GX^2Y+HX^3Y+IY^2+JXY^2+KX^2Y^2+LX^3Y^2+MY^3+NXY^3+OX^2Y^3+PX^3Y^3$, where coefficients A,...,P are:

A= -896 5115703326 , B= 5 3598654924 , C= -0.0044335874 , D= -0.0000008798 , E= 6.9021045916
 F= -0.0437772562 , G= 0.0000483387 , H= -0.0000000063 , I= -0.0154970146 , J= 0.0001026575
 K= -0.0000001351 , L= 0.0000000000 , M= 0.0000107958 , N= -0.0000000738 , O= 0.0000000001
 P= 0.0000000001

X is longitude, Y is latitude and Z is trend surface of order 6 (mgal).

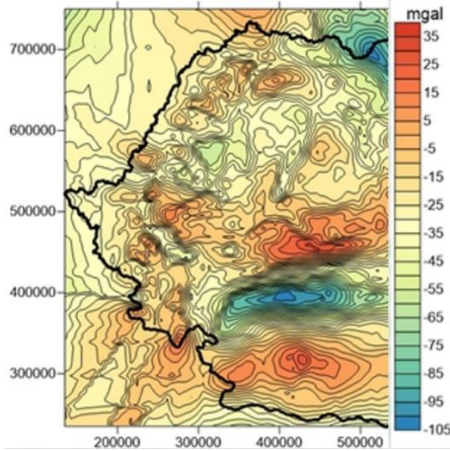


Fig.3 – Bouguer anomaly, after filtering and smoothing of gravity data, on the West part of Romanian territory (data from the geophysical portal of Geological Institute of Romania and [13]).

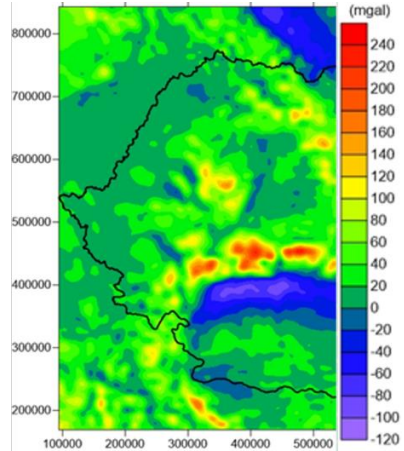


Fig.4 – Free Air anomaly, after filtering of gravity data with Fourier analyses 2D, on the West part of Romanian territory (data from the geophysical portal of Geological Institute of Romania and [13]).



Fig.5 – Geothermal map, on the West part of Romanian territory (after Geological Institute of Romania, 2006)

In fig. 4 is the map with Free Air anomaly, after filtering of gravity data with Fourier analyses 2D, on the West part of Romanian territory, with [14] and [15].

The map from fig.5 indicate (with blue color) that geothermal resources concentrate the 60 to 120 °C (for the exploitation of geothermal water for the production of thermal energy) and possible areas for exploiting geothermal energy in order to generate electric power (with yellow color).

Applying the theoretical results to the geodetic and gravity data at the level of the Romanian territory over which we superimposed the neotectonics structural elements, we obtained the results presented in the images from figures 6 and 7.

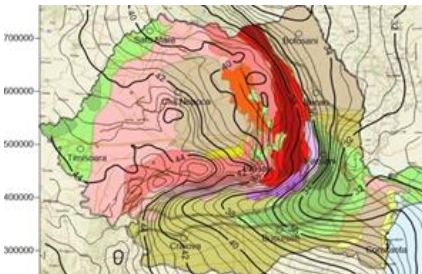


Fig.6 – Geoid of Romania

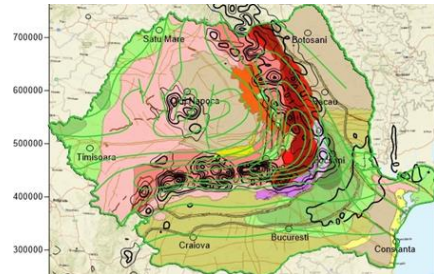


Fig. 7 – Differences between geoid and quasigeoid

Due to the fact that in determining the geoid the actual gravity is taken into account at each point, and in determining the quasi-geoid we use normal gravity, the quasigeoid-geoid separation is a particularly eloquent indicator for determining the difficulty or excess mass in the basement [3], [6], [10], [11].

Although this separation is only of the order of centimetres or at most of tens of centimetres on the territory of our country, it still follows rigorously, even bringing new details of the isobaths to Moho, determined by seismic methods. Thus, the quasi-geoid is located above the geoid in the sinking area of the Moho surface.

CONCLUSION

By overlapping the information obtained from the processing, corroborated with geological and geophysical data of knowledge, we can conclude that the complex image of Bouguer anomalies and outdoor anomaly, indicates the juxtaposition of effects produced by density contrasts (mass) located at different depths.

This is due to the deep structures of the subsurface platforms. By the presence of major lithospheric fracture systems, areas of inhomogeneity are created at their intersection that are manifested in the response functions of the subsoil through a multitude of geophysical parameters (density, seismic wave velocity differences, electrical resistivity differences) and large gradients. of them.

Assuming that the observed gravity anomalies were accurately estimated, there are still other sources of error related to the accuracy of the digital terrain model, the error in estimating topographic effects and the effect of terrain correction errors on geoid height determinations.

There are also differences between the methods for determining terrain corrections. Especially in mountainous regions, these corrections can have a significant impact on gravity anomalies.

All the knowledges about geological-geophysical-structural data, rock's and hydrogeological features are essential to characterize the geothermal resources.

The main geothermal resources in the country are found in porous and permeable sandstones and siltstones (such as in the western plains), or in the fractured carbonate formations (such as at Oradea and Bors in the western part of the country).

On the territory of Romania, more than 200 drillings for hydrocarbons met at depths between 800 and 3500 m of geothermal resources. The use of extracted geothermal energy is used in the proportion of 37% for heating, 30% for agriculture (greenhouses), 23% for industrial processes, 7% for other purposes.

Geothermal waters represent an inexhaustible and non-polluting energy resource, of great importance, which will have to be used in the future and for the production of electricity.

ACKNOWLEDGEMENT

We gratefully acknowledge for support by the Ministry of Research for financing of the project:

“The realization of 3D geological / geophysical models for the characterization of some areas of economic and scientific interest in Romania”, with Contract no. 28N / 2019 and project Nr.16PCCDI/2018:

„Institutional capacities and services for research, monitoring and forecasting of risks in extra-atmospheric space”, within PNCDIII.

REFERENCES

- [1] Asimopolos N.S., Asimopolos L. – 2018 - Highlighting the deep tectonic elements of the eastern carpathians by analyzing the morphology of geoid, Conference Proceedings, Vol.18, Geology, Issue Issue 2.2, pp. 821-828
- [2] Asimopolos L., Asimopolos N.S., Cociuba I. – 2019 - Systematization and processing of geological and geophysical data in the part of North-West of Transylvanian Basin, Conference proceedings Volume 19, Science and technologies in geology, exploration and mining, Issue 1.1, Geology, pp 561-568, ISBN 978-619-7408-76-8, ISSN 1314-2704, DOI: 10.539/sgem2019/1.1
- [3] Barthelmes F. & Kohler W. - 2016. Journal of Geodesy. The Geodesists Handbook, International Association of Geodesy. 90(10): 907-1205.
- [4] Cohut I. – 1998 – Utilisations of Geothermal resources in Romania – Romanian Journal of Geophysics
- [5] Ioane D., Ion D. 2005-A 3D crustal gravity modelling of the Romanian territory: Journal of Balkan Geophysical Society, Vol.8, No 4, November 2005, p.189-198
- [6] Martinec, Z., P. Vaniček, A. Mainville, M. Veronneau, 1996, The evaluation of topographical effects in precise geoid computation from densely sampled heights, Journal of Geodesy, 70, , 746-754.
- [7] Polonic, G., 1998 - The structure and morphology of the crystalline basement in Romania. CERGOP —South CarpathiansI monograph, vol. 7 (37), pp. 127–131. Warszawa.
- [8] Rădulescu Fl., 1988. Seismic models of the crustal structure in Romania, Rev.Roum.Geol.Geophys.Geogr.Ser.Geophys., 32, 13–17
- [9] Rybach, L. – 2003 - Geothermal energy: sustainability and the environment Geothermics 32, 463–470
- [10] Sjöberg, L.E., 1995, On the cvasigeoid to geoid separation, Manuscripta geodaetica, Vol. 20, No. 3, pp. 182-192
- [11] Tenzer R., Chen W., and Jin S., 2015, Effect of Upper Mantle Density Structure on Moho Geometry, Pure Appl. Geophys. 172, 1563–1583
- [12] Veliciu S. – 1998 - Dezvoltari recente in exploatarea geofizica a resurselor geotermale in Romania - Romanian Journal of Geophysics
- [13] <http://bgi.obs-mip.fr>

[14] <https://www.intrepid-geophysics.com>

[15] <http://www.mathworks.com>

IDENTIFICATION OF OIL DEPOSIT REFORMATION AND DEEP FEEDING ON EXTRACTED OIL COMPOSITION

Dr. Yury Turov¹

Dr. Marina Guznyaeva²

^{1,2} Surgut State University, Russia

ABSTRACT

During the operation of multilayer oil fields, there is a likelihood of the occurrence of interstratal oil flows due to the occurrence of secondary technogenic channels of migration along vertical or lateral fill-spill chains. This is due to numerous perforations of fluid-tight and fluid-insulating layers, intensive oil withdrawal, the use of intensive oil recovery technologies (hydraulic fracturing, reservoir pressure maintenance systems and the other physicochemical effects in the reservoir). Thus, the original geological structure of the oil deposit may change during its operation. Besides, for some oil deposits in the later stages of their exploitation, the oil inflows from deeper geological structures can be detected. In this paper, the detection capability of oil deposit reformation and deep feeding on extracted oil composition is shown. The geochemical composition indices are calculated based on the GC/MS analysis of the isomeric composition of paraffins and some classes of aromatic hydrocarbons in oil samples recovered from different wells. The possibility of identifying the source of oil by their values is shown. When comparing the distributions of the values of geochemical indices in different samples of oil from one field, it was found that some of the wells extract oil from one horizon, while the composition of the extracted oil from other wells is of a mixed nature. The composition of oil from one well with a long service life is significantly differ from all others and cannot be explained as the result of mixing oil from two productive horizons. The composition of this oil is highly likely influenced by deep feeding or other technogenic factors.

Keywords: *petroleum, hydrocarbon composition, geochemical indexes, interstratal flows, replenishment of stocks, crude oil mixtures*

INTRODUCTION

The initial geological structure of the deposits may change significantly in the process of exploitation of oil and gas fields, especially in the late stages of development due to numerous perforations of fluid-insulating (fluid-resistant) geological structures, as well as a result of the use of various technologies for intensifying hydrocarbon recovery.

In addition, the hypothesis of the geodynamic formation of oil and its fields which is gaining popularity suggests a high likelihood of deep recharge of already exploited fields due to ascending flows of hydrocarbon fluids [1].

These phenomena demonstrate themselves in changing the composition of the recoverable oil with an increase in the operating time of individual wells and the field as a whole.

It is well known that many in-reservoir mixing processes, biodegradation or mixing with indigenous organic matter can be detected by changing the isomeric composition of different classes of substances of recoverable oil [2], [3], [4], [5]. Multivariance of in-situ processes is a consequence of the thermodynamic nonequilibrium of the oil system [6] and in each case and in every time period requires a detailed study. Therefore, at present, there are attempts to 4D modeling of natural oil systems and oil-bearing Basin Province [7].

Detailed (thorough) geochemical support of oil and gas production processes, based on monitoring the composition of the recovered fluid can be a tool to optimize the regime of oil recovery from each well to achieve (increase) the accumulated (total) amount of extracted oil.

The aim of this work is to verify the possibility of identifying the source of the oil sample by analyzing the isomeric and homological composition taking into account the total error of the analysis results to observe changes in the composition of the recovered oil due to oil deposit reformation and deep feeding.

MATERIAL AND METHODS

We studied the hydrocarbon composition variations in oil samples and their change over time in the consistency of recovered oil during well exploitation on the territory of the Khanty-Mansiysk Autonomous Okrug (Western Siberia).

In the geological assessment of field reserves and their contouring the belonging of the oil fluid to a specific productive horizon based on the composition of the recovered oil were specified.

The isomeric composition of paraffins and several classes of aromatic hydrocarbons in oil samples obtained from seven different wells from one of the Khanty-Mansiysk Autonomous Okrug-Yugra oil fields (Western Siberia) was studied by gas chromatography / mass spectrometry (GC/MS) methods.

The complexity of the composition of crude oil necessitates its preliminary fractionation into simpler components with a quantitative assessment of the contents of the obtained fractions. In this case, seven initial crude oil samples were divided into four fractions: saturated substances, aromatic, resins and asphaltenes (**SARA** analyzes: – **S**aturates, **A**romatics, **R**esins, **A**sphaltenes) [8], [9].

The composition of saturated and aromatic fractions isolated by column adsorption chromatography in accordance with [8] was studied by full spectra GC/MS and mass-fragmentography.

Quantitative geochemical parameters (indices) were calculated from the relative isomer concentrations of saturated and aromatic substances.

RESULT AND DISCUSSIONS

More than 300 individual substances were identified in the studied samples. The total error of the results of the analysis of the isomeric composition and calculated geochemical indices was evaluated. The reproducibility of the results was 5% for the relative content of isomers and 3% for the calculated geochemical indices.

The data (information) on the isomeric composition of the studied samples were processed by the methods of cluster and factor analysis. Using techniques similar to those described in [10], [11], [12], the principal component method was able to distinguish three main groups of samples by hydrocarbon composition: 1 - oil samples from wells I and II; 2 - oil from well III; 3 - oil from well VII.

Oil from the first two wells has an almost identical composition. The composition of oil samples from wells IV, V and VI is a mixture of the first and second groups in different ratios. For the wells of the first and second groups, repeated sampling and analyzes were carried out (4 times within six months), which showed the absence of significant changes in the composition of the recovered oil for the indicated observation period. Differences in the values of geochemical indices calculated from the isomeric composition for these samples did not exceed 3% rel.

Fig. 1 is a graphical illustration of the obtained composition characteristics for the first three (I, II, III) and seventh (VII) wells. According to preliminary information received from the geological service of the oil company first three wells operating on two different productive horizons. As follows from Fig. 1 the composition characteristics of the saturated part of the oil from the wells I and II are very similar. Their diagrams in individual sections almost completely overlap; the differences in the values of geochemical indices do not exceed 3%.

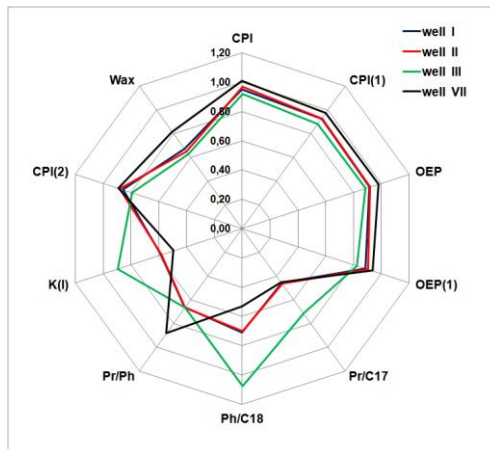


Fig. 1. Values of geochemical parameters calculated by the isomeric composition of paraffins in oil samples from different wells

CPI – carbon preference index =

$$\frac{((C25+C27+C29+C31+C33)/(C24+C26+C28+C30+C32)+ (C25+C27+C29+C31+C33)/(C26+C28+C30+C32+C34))/2}$$

CPI(1) – carbon preference index (1) = $2(C23+C25+C27+C29)/(C22+ 2(C24+C26+C28)+C30)$;

CPI(2) – carbon preference index (2) = $2(C27)/(C26 +C28)$; K(I) =
 $(Pr+Phy)/(C17+C18)$;

OEP – odd over even predominance = $(C21+6C23+C25)/4(C22+C24)$; OEP(1) –
 odd over even predominance (1) = $(C25+6C27+C29)/4(C26+C28)$

A different picture is observed for the third well (III) - the values of the parameters OEP(1), CPI(2), K(I), Pr/C17 and Phy/C18 differ significantly from the values of these characteristics calculated for oil samples from the first two wells. Differences exceed 30% for the most differentiating composition characteristics.

The maximum differences are observed for the isoprenoid coefficient K (I) (34.7%) and the ratios between the contents of pristan and heptadecane n-C17 (Pr/C17; 35.1%), as well as phytane and octadecane n-C18 (Phy/C18; 34.3%).

Composition of oil from wells VII and the values of geochemical indices calculated for it differ significantly from all others. It should be noted that this well has the longest exploitation time compared to other wells studied in this work.

Variations and differences in the isomeric composition of aromatic substances are shown in Fig. 2.

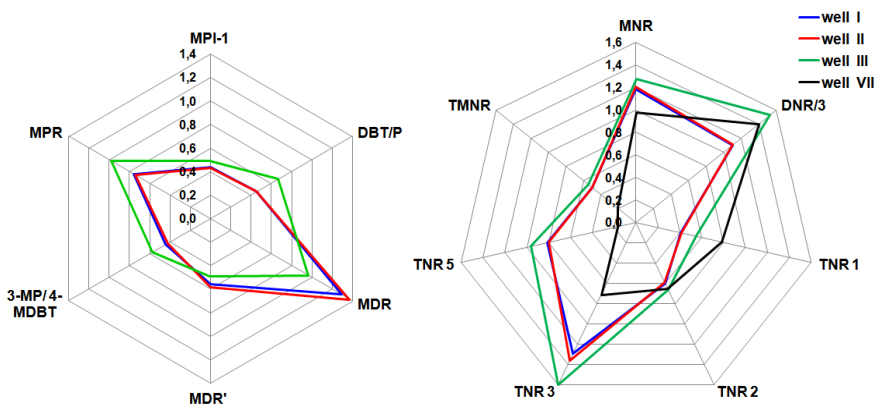


Fig. 2. The values of geochemical parameters calculated by the isomeric composition of bicyclic (right) and tricyclic (left) aromatic substances in oil samples from different wells

$MNR = 2-MN/1-MN$; $DNR = (2,6-DMN+2,7-DMN)/1,5-DMN$;

$TNR 1 = 2,3,6-TMN/(1,4,6-TMN +1,3,5-TMN)$;

$TNR 2=(1,3,7-TMN +2,3,6-TMN)/(1,3,5-TMN +1,4,6-TMN +1,3,6-TMN)$;

$TNR 3=1,3,6-TMN /1,2,5-TMN$;

$TNR = 1,3,7-TMN / (1,4,6-TMN + 1,3,5-TMN)$; $TMNR = 1,3,7-TMN / (1,3,7-TMN + 1,2,5-TMN)$;
 MN, DMN and TMN – Methylnaphthalenes, Dimethylnaphthalenes and Trimethylnaphthalenes.
 $MDR = 4-MDBT / 1-MDBT$; $MDR' = 4-MDBT / (4+1)-MDBT$; $MPR = 2-MP / 1-MP$;
 $MPI-1 = 1.5 \times (2-MP + 3-MP) / (P + 1-MP + 9-MP)$;
 P, 1-MP, 2-MP, 3-MP, 9-MP, DBT, 1-MDBT и 4-MDBT – Phenanthrene, 1-, 2- and 3-Methylphenanthrenes, Dibenzothiophene, 1- and 4-Methyldibenzothiophenes

From the above results it follows that the sources of oil can reliably differentiate and establish belonging of a sample of extracted oil to a specific reservoir based on a comparison of the relative contents of isomers of various classes of compounds and the geochemical parameters of the composition calculated from them.

In total, the composition of the recoverable oil from seven wells of one two-layer field was investigated and compared in detail. The same two productive horizons were reliably identified as sources of oil for three else wells (IV, V, VI) in accordance with the procedures for comparing the values of geochemical indices.

The oil from IV, V, VI wells and the geochemical indices calculated by their composition suggest that it has a mixed source. The values of geochemical indices are significantly different from those calculated for oil samples from each individual horizon and have intermediate values.

Most likely, the composition of recoverable oil is influenced by the presence of inter-reservoir flows, and oil composition is formed as a result of partial mixing of the oil fluid from both horizons.

The oil of the last (seventh) well is fundamentally different in composition from all previous ones. In Fig. 1 and Fig. 2 (*right*) are given geochemical parameters calculated by the isomeric composition of paraffins and alkyl naphthalenes in oil samples from well VII. This well has the longest lifetime of all investigated. And most likely, the formation of the composition of oil extracted from it is influenced by secondary processes of filling the reservoir, including replenishment from deep horizons cannot be excluded.

CONCLUSION

Reliable history reconstruction of the formation and operation of an oil field based on the results of a single sampling of the composition of recoverable oil samples is impossible. Just as it is impossible to assess the quality of a multi-part film epic and the director's talent from a single movie frame or a single episode.

Nevertheless, a detailed analysis and comparison of the composition of oil samples from different wells of the same oil field made it possible to establish the presence of interstratal oil flows, which appeared as a result of technogenic impact on the oil field in the process of hydrocarbon extraction. The detection of a well with a long service life with a dramatically different oil composition from the bulk

of the samples suggests the existence of vertical migration of hydrocarbons from deep geological structures at present in notable quantities.

However, other technogenic factors can cause a similar effect. For example, the use of physicochemical enhanced oil recovery methods of a productive reservoir to stimulate oil production. Anyways, the processes of oil deposit reformation during exploitation as a result of technogenic impact on it has been established by isomeric composition and values of geochemical indices. Regardless of the reasons that cause them.

REFERENCES

[1] Muslimov R.Kh., Plotnikova I.N., Replenishment of oil deposits from the position of a new concept of oil and gas formation, *Georesursy = Georesources*, vol. 21/issue 4, pp 40-48, 2019.

[2] van Aarssen B.G.K., Bastow T.P., Alexander R., Kagi R.I., Distributions of Methylated Naphthalenes in Crude Oils: Indicators of Maturity, Biodegradation and Mixing, *Organic Geochemistry*, vol. 30, pp 1213-1227, 1999.

[3] Nicolle G., Boibien C., ten Haven H.L., Tegelaar E., Chavagnac P., *Geochemistry: a powerful tool for reservoir monitoring*, Society of Petroleum Engineers, No. 37804, pp 395-401, 1997.

[4] Peters K.E., Magoon L.B., Bird K.J., Valin Z.C., Keller M.A., North Slope, Alaska: source rock distribution, richness, thermal maturity, and petroleum charge, *American Association of Petroleum Geologists Bulletin*, vol. 90, pp 261-292, 2006.

[5] Zumberge J.E., Russell J.A., Reid S.A., Charging of Elk Hills reservoirs as determined by oil geochemistry, *American Association of Petroleum Geologists Bulletin*, vol. 89, pp 1347-1371, 2005.

[6] Turov Yu.P., Guznyaeva M. Yu., *Oil system - structure, properties, behavior, Monograph (Study)*, Surgut State University, Surgut, Russia, 2017, 286 p.

[7] Higley D.K., 4D petroleum system model of the Mississippian System in the Anadarko Basin Province, Oklahoma, Kansas, Texas, and Colorado, U.S.A: *The Mountain Geologist*, vol. 50, pp 81- 98, 2013.

[8] Sieben V.J., Stickel A.J., Obiosa-Maife C., Rowbotham J., Memon A., Hamed N., Ratulowski J., Mostowfi F., Optical measurement of saturates, aromatics, resins, and asphaltenes in crude oil, *Energy Fuels*, vol. 31, no. 4, pp 3684-3697, 2017.

[9] Gutiérrez D., Moore R.G., Mehta S.A., Ursenbach M., Bernal A., Phase-behavior modeling of oils in terms of saturates/aromatics/resins/asphaltene fractions, *SPE Reservoir Evaluation & Engineering*, vol. 22, no. 03, pp 1-15, 2019.

[10] Peters K.E., Ramos L.S., Zumberge J.E., Valin Z.C., Bird K.J., Deconvoluting mixed crude oil in Prudhoe Bay Field, North Slope, Alaska, *Organic Geochemistry*, vol. 39, pp 623-645, 2008.

[11] Engel M.H., Imbus S.W., Zumberge J.E., Organic geochemical correlation of Oklahoma crude oils using R-and Q-mode factor analysis, *Organic geochemistry*, vol. 12, pp 157-170, 1988.

[12] Peters K.E., Ramos L.D., Zumberge J.E., Valin Z.C., Scotese C.R., Gautier D.L., Circum-Arctic petroleum systems identified using decision-tree chemometrics, *American Association of Petroleum Geologists Bulletin*, vol. 91, pp 877-913, 2007.

INDUSTRIAL TYPES OF GOLD DEPOSITS OF THE EAST KAZAKHSTAN

Dr. M. Mizernaya¹

Prof. B. Dyachkov²

Dr. A. Miroshnikova³

PhD Student A. Mizerny⁴

Dr. Z. Chernenko⁵

PhD Student S. Aitbaeva⁶

^{1, 2, 4, 5, 6} D. Serikbaev East Kazakhstan State Technical University, Ust-Kamenogorsk, Kazakhstan

³ Department of the National Center of Complex Processing of Mineral's raw materials VNIItzvetmet, Kazakhstan

ABSTRACT

The East Kazakhstan territory is the unique geologic province where a number of large-scale non-ferrous and gold deposits are concentrated [1]. Gold base metals (gold-containing) type is represented by gold-containing sulphide complex deposits. It is characterized by many large-scale commercial deposits of copper, lead and zinc where gold as well as silver, cadmium, platinum, selenium and other elements are the associate component of copper-sulphide and sulphide complex deposits [2]. There are following ore types are distinguished: gold-listvenite type occurs in the Irtysh zone (Maraliha deposit); the gold-sulphide vein-disseminated type associated with island-arc, volcanogenic-carbonate-terigenous formation C₁V₂₋₃ (Suzdalskoye, Baibura, Mirazh, Zhaima); gold-quartzite type is characterized by gold-quartzite-vein deposits in West Kalba zone (Kuludzhun, Sentash, Kazan-Chunkur and others); gold-arsenic-carbon-bearing type is presented by large, middle and small deposits of Bakyrchik's group (Bakyrchik, Bolshevik, Gluboky Log and others). Last one is formed on middle-Hercynian collision ore-bearing level (C₂-C₃) [3]. Multiple-stage concentration of gold contributed to formation of very large deposits. Gold content ranges from is 0.2 to 60 g/t, average is 8-9 g/t. Considerable part of gold is found in micro- and nanoparticles, nanotubes containing Au, Ag, Pt, Pd, W, Mo, Sn, Y, Yb, Ta and other elements [4].

Keywords: *Gold, metals, sulphide-polymetallic ores, deposits*

INTRODUCTION

In recent ten years significant progress was achieved in classification, definition and notion of different types of gold-ore deposits. Each of them has a range of specific characteristics for this type and tectonic conditions for forming. The research data on gold metallogeny of collision gold-ore deposits in Kazakhstan provide establishing of connection between structure, tectonic evolution and magmatism of the region, as well as formation of large gold deposits. [5].

A lot of authors clearly determine some metallogenic epochs on the territory of Kazakhstan. Their leading element is gold(R₃-V, €₁₋₂, O₁₋₂, O₃-S₁ D₁₋₂, D₂₋₃, C₁,

C₂₋₃, C₃-P₁, K₂ и Pg-Q). The most active from the aspect of gold ore specialization there are following three - O₃-S₁; D; C₃-P, characterized by active, magmatism and different metamorphism [6].

The leading geological and industrial types of primary gold ore deposits in Kazakhstan are: 1) gold-sulfide-quartz (plutonogenic stockwork and veined), 2) gold-sulphide (vein-impregnated), 3) gold-bearing crusts of weathering, 4) gold-adular-quartz, gold-quartz, gold-sulphide-quartz (volcanogenic), 5) gold-skarn [7].

The average gold content in Kazakhstan own gold ore deposits is 5-7 g / t. The most large-scale unique deposits are Vasilkovskoye (Akmola region) and Bakyrchik, Ridder-Sokolnoye (East Kazakhstan). Gold-bearing deposits include the following types: 1) gold-silver-pyrite-polymetallic, 2) gold-copper-porphyrific, 3) copper-pyrite and others [8].

MATERIALS AND METHODS

There were field expedition work, different type of sampling such as float sampling, litho-geochemical sampling. Samples and chips were used for making thin rock sections, polished sections. Geochemical researches were carried out in certified laboratory IRGETAS of D. Serikbaev East-Kazakhstan state technical university. There was studying of the composition of ore minerals with using optical and electronic microscopy. The study of ore minerals and gold (JSM) was carried out in separate grains and in artificial polished sections. There was also used ICP-MS for the chemical composition of ores and minerals studying.

MAIN RESULT

Gold deposits of East Kazakhstan region were formed in different geological conditions, they differ in age, material composition of ores, and immensity of mineralization. Among them there can be distinguished gold-bearing objects of various ore-formation types and gold ore deposits [9]. One of the most attractive commercial gold mining sites is the well-known base metal deposits.

Gold-copper-polymetallic (Rudny Altaic) type. This is the main geological-industrial type for East Kazakhstan, represented by gold-bearing pyrite-polymetallic deposits of Rudny Altai. It is characterized by many large industrial deposits of copper, lead and zinc, in which gold, along with silver, cadmium, platinum, selenium and other elements, is an associated component of copper-pyrite and pyrite-polymetallic deposits (Ridder-Sokolnoye, Tishinskoye, Maleevskoye, etc.) (figure 1).

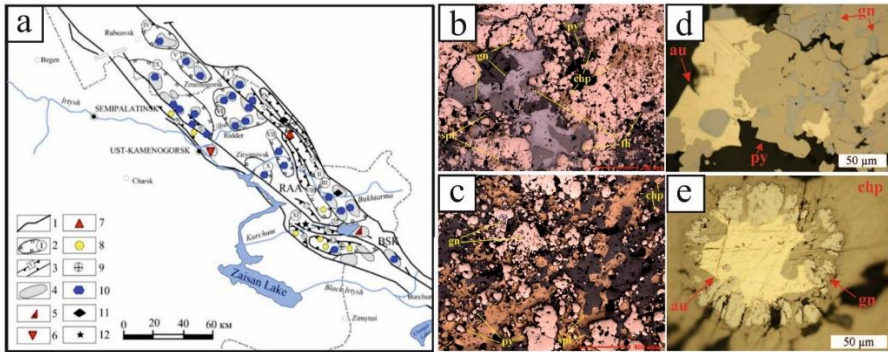


Figure 1. Rudny Altai copper-polymetallic belt 1 - boundary of metallogenic zones; 2 - ore district; 3 - ore zone; 4 - ore node; 5 - 12 - ore formations: 5 - epimagmatic; 6 - skarn; 7 - greisen-quartz-vein; 8 - quartz vein golden; 9 - gold-quartz berezitic; 10 - pyrite-polymetallic; 11 - volcanogenic-sedimentary iron-manganese; 12 - metamorphogenic (golden); a,b – mineral associations, Maleevskoye deposit; c,d - native gold in the copper-pyrite ores of Ridder-Sokolnoye deposit (G.D. Ganzhenko [10])

The deposits formed in rifting and island-arc geodynamic conditions of the Hercynian tectogenesis. They genetically relate to the group of differentiated basalt-andesite-rhyolitic formations (D1-3). Multistage of formation and multiple-deck distribution of mineralization on several stratigraphic levels are determined for a number of large deposits (Ridder-Sokolnoye, Tishinskoye, Maleyevskoye, Orlovskoye, Artemyevskoye and others). Gold is related to the main ore-forming process corresponding to formation of commercial copper-polymetallic ores. The average gold content in pyrite-polymetallic ores is 0.8-1 g / t, while developing deposits, it is extracted in passing and composes a significant part in the balance reserves of the region and in Kazakhstan as a whole [10]. Ridder-Sokolnoye deposit specially stands out. According to the total volume of gold mining it is compared with large world objects (Muruntau, Sukhoi Log, and others).

MAIN TYPES OF GOLD DEPOSITS

Gold-listvenite type. Gold deposits were formed in collision geodynamic setting and are located within the West Kalba gold ore belt and the Irtysh shear zone.

The following ore types are distinguished: gold-listvenite type occurs in the Irtysh zone (Maraliha deposit). Crystalline schist and amphibolites including serpentinite lenslike mass, dikes of diabase porphyrites and plagiogranite-porphyrites are ore-hosting. Gold-bearing ores were formed in the process of fold-thrust deformations of collision stage and is fixed in ore fold silica-listvenite zones. Ore is vein-disseminated, main ore minerals are pyrites, arsenopyrites and gold. There are also chalcocopyrite, sphalerite, galena and fahlore. Free and fine-grained gold is in pyrite, arsenopyrite and magnetic iron ore.

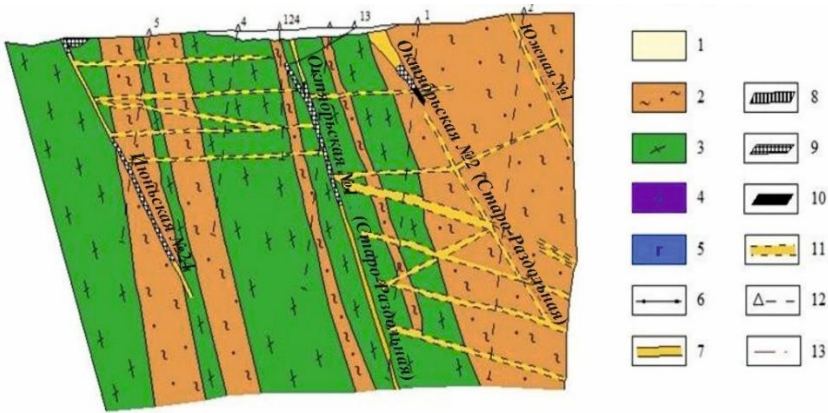


Figure 2. Geological section of the Maralikha gold deposit. 1 - loose quaternary layers, 2 - biotite - quartz-feldspar crystalline schists, undivided, 3 - amphibolites, 4 - serpentized hyperbasites, 5 - gabbro-diabases, 6 - granodiorite-porphphyry dikes; 7-11 - ore bodies with gold content (7-0-2 g/t, 8-2-4 g/t, 9-4-10 g/t, 10-10-30 g/t) and 11-expected; 12 - design boreholes; 13 - breaking disruptions.

The distribution of gold in the quartz of host rocks and quartz veins is given in the table 1. The most high-contrast contents of elements with concentration clusters (KK greater than 100) in berezites and listvenites are Au, As, and W. In quartz veins Ag, As, Au, Mo are the moderately contrasting (KK = 10-100). Low-class contents (KK less than 1) are defined for V, Ti, Zr, Mn, Cr, etc.

Table 1 - Content of gold and associated components in quartz veins of the Maralikha deposit

Sample number	Characteristic of quartz	Average content of Au, g / t	Elements of the impurity (maximum values in mass%)	Note
4327	Quartz in birch	3,9	Ag 4 g/t, As 5, Ti 0.6, Mn 0.2, Zr 0.03, Cu 0.02, V 0.01, Ni 0.008, Mo 0.0008	gold quartz
5553	Quartz in crushed birch	1,06	W 1, As 0.8, Ti 0.6, Mn 0.1, Zn 0.05, Cu 0.04, Zr 0.03, V 0.01, Mo 0.065, Ni 0.005, Sc 0.002	gold quartz
6589	Quartz in listenites	1,18	Ag 10 g/t, As 0.8, Ti 0.2, Mn 0.1, Zn 0.04, Cr 0.01, V 0.008, Mo 0.005, Ni 0.003, Pb 0.003, Cu 0.002, Sc 0.002, Co 0.0008	gold quartz
4328	Vein quartz	0,14	W 0.5, Mn 0.1, As 0.08, Ti 0.03, Ni 0.0025, Sc 0.0006	slightly gold-bearing quartz
4320	Vein quartz	0,10	Ti 0.1, Mn 0.06, Cu 0.004, Ni 0.003, Mo 0.0005	slightly gold-bearing quartz
3721	Quartz in quartz-feldspar-biotite schists	<0,01	Ti 0.1, Mn 0.025, Zr 0.005, Ni 0.003, Pb 0.003, Cu 0.0025, V 0.002, Cr 0.002, Co 0.0008, Mo 0.0006, Sc 0.0005	non-gold-bearing metamorphogenic quartz

The gold-sulphide vein-disseminated type. The gold-sulphide vein-disseminated type belongs to unconventional type of gold ore spatially associated with island-arc (Radtko 1995), volcanogenic-carbonate-terrigenous formation C_{1V2-3} (Suzdalskoye, Mirazh, Zhaima and others) [11]. Geological-genetic model of ore formation is defined as hydrothermal-metasomatic and determined by formation of gold-bearing crushed vein and jasperoids in tectonically fractured carbonate-terrigenous rocks. Ore bodies were formed as a result of minor intrusions, plagiogranite dikes and granodiorites (Kunushsky complex C₃). Main ore minerals are pyrite, arsenopyrite, and antimonite. Free gold is fine and submicroscopic (average content is 8-10 g/t). Gold-quartzite type is characterized by gold-quartzite-vein deposits widely represented in West Kalba zone (Kuludzhun, Sentash, Kazan-Chunkur and others). They are located in low carbon sediments (Aganaktinskaya suite C_{1S}). Ore is controlled by faulting and is genetically associated with minor intrusions and Kunushsky complex dikes (C₃). Ores are characterized by great variety: pyrite, arsenopyrite, gold, chalcopyrite, sphalerite, fahlores, antimonite, scheelite and others. Gold is free in polysulfide and stibial assemblages. Suzdal deposit is allocated on the flanks of the of the same name reference gold-sulfide deposit of industrial importance (Figure 3).

It type of gold mineralization occurred in volcanic-carbonate-terrigenous formations of island-arc type D_{3fm}-C_{1V2-3} (Arkalyk suite and others). The latter

during the activation of tectonic movements in the stage of the Hercynian collision underwent hydrothermal-metasomatic transformations in infolded-melange, mantled-thrust and ruptural structures, as well as in contacts with gold-bearing small intrusions and dikes of Kunushsky complex (C₃). These processes were accompanied by the addition of ore-bearing fluid flows and the formation of gold deposits and ore occurrences (Suzdal, Mirage, Baibura and others) [12]. Ore bodies are represented by discontinuous mineralized zones, bunches, veins and stockworks with impregnation of gold-bearing sulfides (mainly pyrite, arsenopyrite, less antimonite).

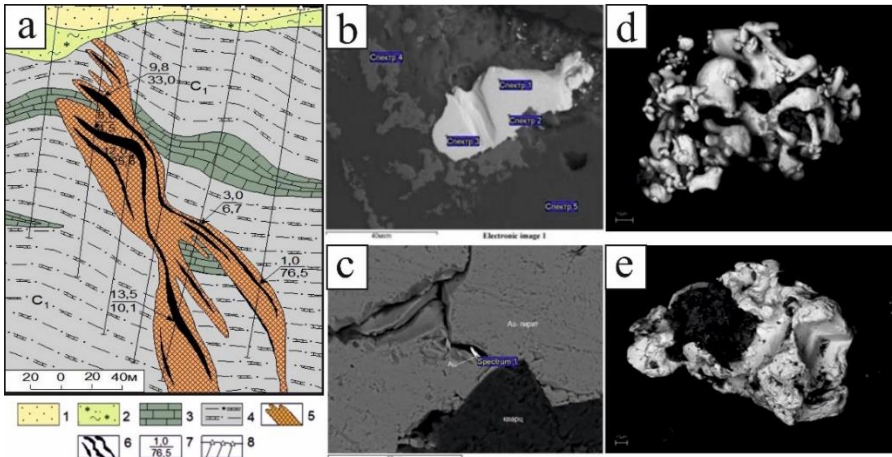


Figure 4- a - Suzdal ore field. 1 - Cenozoic loose sediments; 2 - weathering crust; 3-4 - deposits of the arkalyk formation: 3 - limestones, 4 - calcareous siltstones; 5 - gold bearing zones; 6 - ore bodies; 7 - characteristics of gold-bearing intervals: in the numerator - power in meters, in the denominator - average content of gold, g / t; 8 - wells; b,c,d,e - native gold (with admixture of Ag, Pt) in the jasperoids of Baybura deposit (Dyachkov B.,Kuzmina O.)

Gold is free, fine and submicroscopic. Its content in ores is variable, amounting to 8-10 g / t in the bedrock and weathering crusts. The main ore - hosting structure of the deposit is represented by a system of subparallel tectonic deformations in the north-eastern direction. Zones of primary gold-sulphide mineralization are crushed and strongly crumbling carbon-bearing and calcareous - carbon-bearing siltstones, limestones and sandstones containing the main ore bodies (figure 4). In the primary ores there are impregnated, veined- impregnated textures, the gold content of which is extremely random (at average value 9 g / t), gold is in a free state or in the form of finely dispersed impregnation in arsenopyrite, pyrite and quartz.

Gold-arsenic-carbon-bearing type is presented by larger deposits in terms of gold reserves (Bakyrchik, Bolshevik, Gluboky Log and others) and is formed on middle-Hercynian collision ore-bearing level (C₂-C₃). Sub-aerial grey molasses, alluvial-limnic and bog carbon-bearing black-shale lithofacies (Bukon suite (C₂₋₃)), subjected to intensive dynamic-metamorphic and hydrothermal-metasomatic

changes (zone of the Kyzylovsky deep-seated fault), and to the influence of deep seated (3-5 km) rock bodies. Multiple-stage concentration of gold contributed to formation of very large deposits (Figure 5). Gold content ranges from is 0.2 to 60 g/t, average is 8-9 g/t. Considerable part of gold is found in micro- and nanoparticles, nanotubes containing Au, Ag, Pt, Pd, W, Mo, Sn, Y, Yb, Ta and other elements[13].

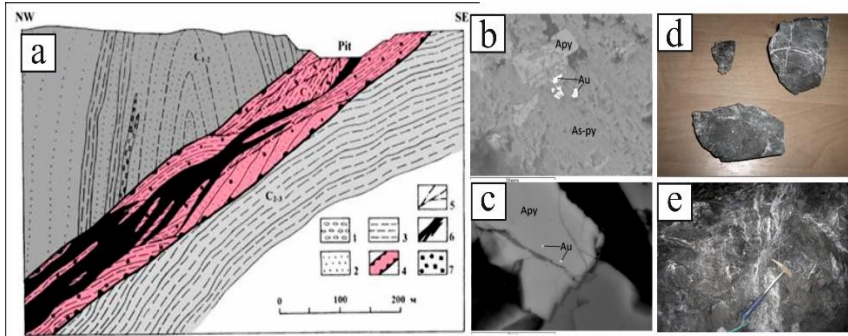


Figure 5 – a - Geological section of gold-sulfide deposit Bakyrchik through the central ore body (based on the materials of V. M. Yanovsky, Y.V. Chudikova). 1-3 carboniferous sediments: 1 - conglomerates, gravelites, 2 - sandstones, 3 - carbonaceous siltstones and shales; 4 - Kyzylovskaya zone of deep fault; 5 - faults, tectonic cracks; 6 - ore body; 7 - diffuse sulphide mineralization; b, c – gold in arsenopyrite; d, e – gold ore samples

CONCLUSION

From the modern theoretical concepts of the world geological science development, an urgent problem is the development of new scientific approaches to the analysis of the regularities in the formation of geological and ore-bearing structures in the most important mining regions of Kazakhstan with the aim to replenish the mineral and raw materials resources [14]. As a result of the analysis and generalization of geological materials of previous years and carrying out of scientific and research works on the general problem of geology and metallogeny of Great Altai, the regularities of the formation of the leading geological-industrial types of gold deposits in East Kazakhstan region have been specified. The main novelty of the results is the justification of the linear-nodal placement of gold-bearing structures and deposits. The formation of leading geological-industrial types of mineralization is connected with the collision process of Kazakhstan and Siberian lithospheric plates (C₁-C₃) [15].

On the basis of geotectonic, geophysical, geological-structural, ore-petrological and mineralogical-geochemical factors, the scientific base for the development of new forecasting technologies and searching of non-traditional apocarbonate (jasperoid) gold-sulfide mineralization and other gold ore objects has been prepared. There were defined ore-controlling role of the system of diagonal deep faults of the north-western direction (West Kalbinsky, Charsk-Gornostaevsky, and others) and the regmatic systems of latitudinal faults (Leninogorsk-Semipalatinsky and others) in the location of gold-bearing structures and objects

spatially timed to certain geochronological levels. There was studied the spatial-genetic connection of gold mineralization with small intrusions and dikes of gabbrodiorite-granodiorite-plagiogranite series of collision type (C₂₋₃-C₃) and ore-controlling role of deep mantle faults of ancient regmatic system and Hercynian activation, favourable role of the ore-hosting environment for the deposition and concentration of precious metals, the development of regional and local criteria of the new ore deposits forecast.

As a result of the carried out researches, the estimation of perspectives and gold forecast resources of the studied territory were made. The main scientific novelty and practical significance are in the justification of the definition of a new non-traditional type of gold-sulfide mineralization, which has an industrial importance, by the analogy with Suzdal deposit and the objects of Carlin trend. It is expected that the implementation of scientific and practical recommendations will contribute to the discovery of new deposits and the strengthening of the gold potential of East Kazakhstan.

ACKNOWLEDGEMENTS

This is a contribution to grant of MES of RK AP 05131489

REFERENCES

[1] Khromykh, S.V., Tsygankov, A.A., Kotler, P.D., Navozov, O.V., Kruk, N.N., Vladimirov, A.G., Travin, A.V., & Karavaeva, G.S. Late Paleozoic granitoidmagmatism of Eastern Kazakhstan and Western Transbaikalia: Plume model test. *Russian Geology and Geophysics*, 57(5), pp. 773-789, 2016.

[2] Gorzhevsky D.I., Chekvaidze V.B., Isakovich I.Z. Types of polymetallic deposits in the Rudny Altai, their origin and methods of prospecting. Moscow: Nauka. p - 197, 1977.

[3] Y.Liu, W.Li, Zh.Feng, Qu.Wen, F.Neubauer, Ch.Liang. A review of the Paleozoic tectonics in the eastern part of Central Asian Orogenic Belt // *Gondwana Research*, V - 43. - P 123-148, 2017.

[4] Mizernaya M.A, Mirosnikova A.P., Pyatkova A.P., Akilbaeva A.T. The main geological-industrial types of gold deposits in East Kazakhstan // *Naukovyi Visnyk Natsionalnoho Hirnychoho Universytetu (Ukraine)*, (5), pp. 5-10, 2019.

[5] Kuzmin M.I., Yarmolyuk V.V., Kotov A.B. Early evolution of the Earth, beginning of its geological history: how and when granitoid magma appeared. *Litosfera*, 5, pp. 653-371, 2018.

[6] Rafailovich M.S. Geology of Central Asian gold: ore evolution, metasomatic formations, explosive breccia. Monograph, Almaty, p. 423, 2013.

[7] Parilov Yu.S. Genesis of the main types of non-ferrous metals deposits in Kazakhstan (based on the results of studying fluid inclusions). - Almaty. p. 266, 2012.

[8] Mizerny, A.I, Miroshnikova, A.P, Mizernaya, M., Diachkov, B.O. Geological and structural features, magmatism and mineralization of Sekysivske and Vasylkivske Stockwork gold deposits (Kazakhstan) // *Naukovyi Visnyk Natsionalnoho Hirnychoho Universytetu (Ukraine)* (2), pp. 5-13, 2017.

[9] Han C, Xiao W, Zhao G, Su B, Sakyi PA, Ao S, Wan B, Zhang J, Zhang Z, Wang Z. Mid-Late Paleozoic metallogenesis and evolution of the Chinese Altai and East Junggai Orogenic Belt, NW China, Central Asia// *Journal of Geosciences*. pp.255-274, 2014.

[10] Ganzhenko G.D., Yudovskaya M.A., Vikenyev I.V. Gold-polymetallic mineralization of the Ridder-Sokolnoye deposit in the Rudny Altai (Eastern Kazakhstan) // *Mineralogy № 4 (1)*. pp. 8-34, 2018.

[11] Dobretsov N.L. Fundamentals of geotectonics and geodynamics: Textbook/ Novosib.state.un., Novosibirsk, p.492, 2011.

[12] The Great Altai (Geology and Metallogeny). Book 1. Geological structure. Alma-Ata: Gylym, 1998. - 229 p. Book. 2. Metallogeny. Alma-Ata: RIOVAKRK, 400 p., 2000.

[13] Bakyrchik (Geology, geochemistry and mineralization) editor Narseev V.A. Moscow: CSRGI. p.-174, 2001.

[14] Letnikov F.A. Ultradeep Fluid Systems of the Earth and Problems of Ore Genesis// *Geology of Ore Deposits V. 43, № 4*. pp. 291-307, 2001.

[15] Yarmolyuk V.V., Lykhin D.A., Kozlovsky A.M., et.al.. Composition, sources, and mechanisms of rare metal granitoids formation of Late Paleozoic East-Sayan zone of alkaline magmatism (on the example of Ulan-Tologai massif). *Petrologiya*. Vol.24, 5, 515-536, 2016.

MAPPING THE MINERAL RESOURCES DATA OF WEST BALKAN REGION INTO EXISTING EUROPEAN DATA MODEL

Mag. Katarina Hribernik¹

Jasna Šinigoj²

Dr. Duška Rokavec³

^{1, 2, 3} Geological survey of Slovenia, Slovenia

ABSTRACT

Primary and secondary mineral resources are of strategic importance for the EU. Most EU countries (including Slovenia) are already part of the pan-European Minerals Intelligence Network which provides consistent and organized data information on primary and secondary mineral resources on the European level. It was established in previous projects as EuroGeoSource, Minerals4EU, ProSUM, Mica and ORAMA. The Eastern and south Eastern European (ESEE) region represents a gap in this network, but at the same time is also identified as one of most important strategic regions for the EU with great potential for mineral supply. The large concerns are aiming to expand their business to the region, but access to relevant data interesting for the investors is still not available. There is a need for surveyed and unified mineral resources data.

In the framework of RESEERVE (EIT RM KAVA project, duration 1.4.2018-31.3.2021), national mineral resources data of six task partners from West Balkan countries (Albania, Bosnia and Herzegovina, Croatia, Serbia, Montenegro and Macedonia) were implemented and harmonized with INSPIRE directive (European directive for organizing spatial data). Since EU directives are mandatory for members only and West Balkan countries are not yet targeted (except Croatia), they are still interested in their implementation.

For that reason the main project goal is the creation of the West Balkan Mineral Register, provided by national data providers, which will represent a starting point to integrate the ESEE region into existing EU data platforms and bring it closer to common minerals market. Regional mineral data will become more accessible and relevant. The goal of the project is to anticipate the future supply and demand for minerals, particularly regarding critical minerals and therefore to contribute to the sustainable mineral supply in Europe.

Leading partner for RESEERVE project is Geological Survey of Slovenia (GeoZS), which has identified relevant data providers and examined data quantity, quality and format. GeoZS will synthesize primary and secondary raw material data into common West Balkan Mineral Register and test the harvesting of data in INSPIRE compliant European data model.

The scenarios drawn up in the project will be available through the European Geological Data Infrastructure (EGDI), which will offer easy access to existing mineral data. EGDI provides access to Pan-European and national geological

datasets and services from the Geological Survey Organizations of Europe. Through EGDI data from several European data harmonization projects are accessible. EGDI was launched in June 2016 in a Version 1 and has since then been extended to include more data sets, including mineral resources.

The article is mostly focused on workflow harmonizing the data and spreading IT knowledge of mapping the national primary and secondary minerals data to already existing European data model and developing national relational databases, that fit into European common database structure. Data harmonization was already performed through national training workshops to assist task partners in taking the first step toward INSPIRE directive implementation.

Keywords: *mineral resources, West Balkan, Geological Data Infrastructure (EGDI) Network, INSPIRE directive, data harmonization*

INTRODUCTION

In order to meet the need for mineral resources, it is essential to know the location, area quantity and availability of mineral resources. Europe, as well as its industry, increasingly depends on imports of mineral raw materials, mainly metal and industrial mineral resources, which has led the European economy to considerable instability. The security of European resources can already be compromised in the near future, as Europe is becoming increasingly dependent on external suppliers. Recently, we could have seen a significant increase in the prices of mineral raw materials, especially metal, on a global scale. Data on reserves and resources of mineral resources exists within each country, but each country collects them in their own way. Data are at different levels, from local, regional to the data of individual economic corporations that remain commercial secrecy.

As we want to reduce the dependency on the supply of raw materials from "abroad", we need to standardize the data between the individual countries at EU level. That was done by Directive of the European Parliament and of the Council on the establishment of an infrastructure for spatial information in the European Community, called the INSPIRE (INfrastructure for SPatial Information in Europe) directive, valid from 15. May 2007. It regulates the baseline for the establishment of a European infrastructure for spatial and environmental data in the Member States. Such infrastructure enables the institutions and stakeholders to share information and knowledge, to find, view and acquire standardized and harmonized geo-referenced and related data, including data on mineral resources. It integrates the best available mineral expertise and information base on the geological knowledge, in support of public policy making, industry, society, communication and education purposes at international level. [4]

At the time of the present research in the considering ESEE region there was no effective information system to support sustainable management of mineral resources, which would follow the INSPIRE directive and provide enough good and argument decisions to:

- decision makers at local level (municipalities, local communities, mayors, city councils, professional departments at ministries etc.),

- national decision makers (government, government departments, state chambers, ministries, inspectors, administrative units...),
- decision-makers at international level (Council of the EU, commissioners...).

Very important for all economics is also the knowledge of:

- the negative impacts of mining to the environment,
- recycling management and strategies,
- potential of mineral resources,
- the acquisition of trust and social consent to exploitation and
- availability of the commodities.

All these facts also apply to the countries of ESSE region; however, they have not yet had the data organized in systematic ways. Getting the good data is not easy. Even if you know where to find it, the data will probably be in a different format for each country, out-of-date and usually in non-digital form. National institutions have also their own ways of working, different dissemination, data formats and language. The RESEERVE project will bring the national minerals related geodata of the region into one virtual place through web portal, so the users can more easily get the information they need, directly onto their computer and free-of-charge. The elementary aim of the RESEERVE project is to obtain quality data and integrate it into already existing European platforms and present their data on the web portal. This will represent their starting point to follow the INSPIRE directive, obtain a strong decision-making tool for the management of mineral resources and environment protection. The expert public of the region will complement the fundamental knowledge of regional geology, mineralogy, stratigraphy, geochemistry, environmental geology, and nevertheless also of information systems. Such approach therefore will connect in an efficient way the area of organizing information systems and the geology.

METHODOLOGY, METHODS AND MATERIALS

For reaching the final harmonization of data the following methodology have been used:

Engineering of end users' requirements

First step was the analysis of end user needs. The end users are different, and they have different requirements. We can divide the users ' target groups into:

- users of databases and data providers (geological surveys, faculties, ministries...),
- other web application users (e.g. mining inspectors, students, general public, mining experts, academic circles, equipment manufacturers...),
- potential users of data (stakeholders, environmental agencies, statistical offices, other ministries, investors, mining companies...).

Qualitative and quantitative research of data

To reach this purpose, a summarized Excel table for the collection of national data on primary and secondary mineral raw materials, relevant for possible investors, was designed. The table with common attributes, using a top down approach (from general to detailed information) has been completed by all project partners. The table includes the attributers such as basic geographical and ownership information about each site, geometry, volume, technological data such status, mining methods and reserves, geological data such stratigraphy and lithology, mineral composition and rock types, stability, chemical composition, environmental impacts etc.

The recommendation, according to EU mineral demands and strategic tendencies, is to focus on metals and industrial minerals (special focus on CRM), addressed to active mines/open pits, abandoned and closed mines with reserve/resources and other potential sites, and mine/metallurgic waste sites. At the end relevant primary and secondary raw materials of the ESEE region were identified and key players from expert institutions. Quality, quantity and format of gathered data were also examined to obtain spatial data on mineral deposits and descriptive data as well.

Overview of existing EU data model and harmonizing the basic Excel table fields with INSPIRE database fields

National data of individual countries have been harmonized with the INSPIRE data model and online services for data on mineral raw materials have been established. To accomplish this end, we examined INSPIRE directive in detail, identified the fields that coincide with the directive, and adapted them accordingly to the requirements. In the first phase, we focused only on mandatory fields from the INSPIRE directive and produced extended series of Excel tables in accordance with the INSPIRE data model. In the second phase, we expanded the number of entered deposits to the minimum of 50 and started by entering extended information by filling also voidable fields.

Mapping the basic Excel table to INSPIRE customized Excel tables/ harmonization of existing data to INSPIRE-compliant data

At this stage, it was necessary to consider the specific rules required by the common data model. The data must be entered in an exact sequence, for this purpose the instructions for inserting data were also made. It is necessary to follow the provided INSPIRE code lists for interoperability with existing EGDI platform, use the specific record identifiers and correctly track the relationships between the data.

This stage of work has carried out a series of national workshops/training courses with technical support to help the partners on harmonization of existing data sets into INSPIRE compliant data and working with relational databases.

Mapping INSPIRE customized Excel tables to the Access relational database

This phase was relatively simple, since the pre-existing Excel tables have been organized in a same way as relational database and the data provider just copies the tables into it one by one. Access database is already a relational database and all the errors, made in Excel table appear, so it is also a good control of the entry itself. National workshops have also been carried out for this purpose.

At this point synthesis and creation of common primary and secondary raw materials dataset has already been established.

Mapping Access database into PostgreSQL

The following step was the migration of national Access databases to open source Solutions (PostgreSQL database, used by the project). This step was performed by GeoZS.

Harvesting national databases to the common EU database

In order to create a system with updated date, the project adopted a distributed architecture based on central harvesting database synchronized with a central database. Data harvesting is the process to automatically extract large amount of data from web services. GeoZS implemented a harvesting system to collect and validate INSPIRE compliant spatial European data of mineral resources. On a country level national provider distribute their data as A Web Feature Service (WFS), GeoZS harvesting system retrieves this data, performs data transformation and quality control and finally store validated data in the central database. [2]

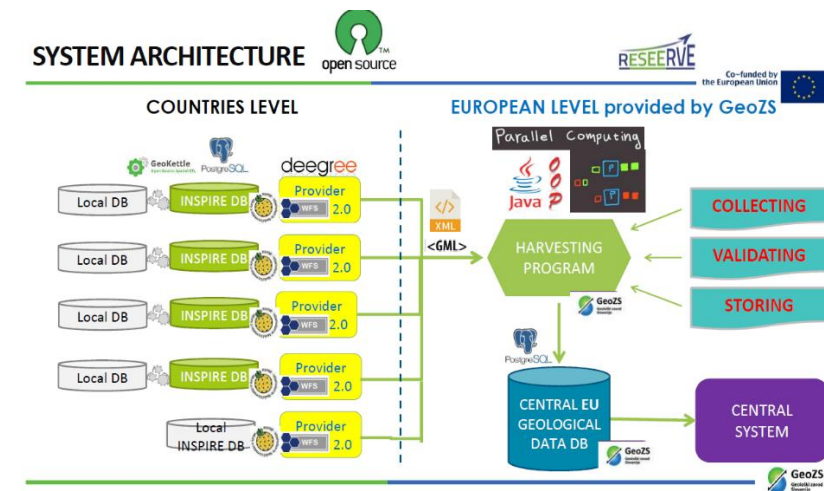


Figure 1: Architecture of harvesting system

Presentation of data on the EGDI web portal

In addition to map service displaying the mineral deposits and mines in West Balkan countries on EGDI portal, the portal also provides occurrence-specific documents related to mineral material, enabling users to make their own analyses

from a huge amount of data. It represents a new knowledge base of primary and secondary resources of the region that is interoperable with national databases. Based in this, industry can be encouraged to invest in West Balkan mineral sector. [3]

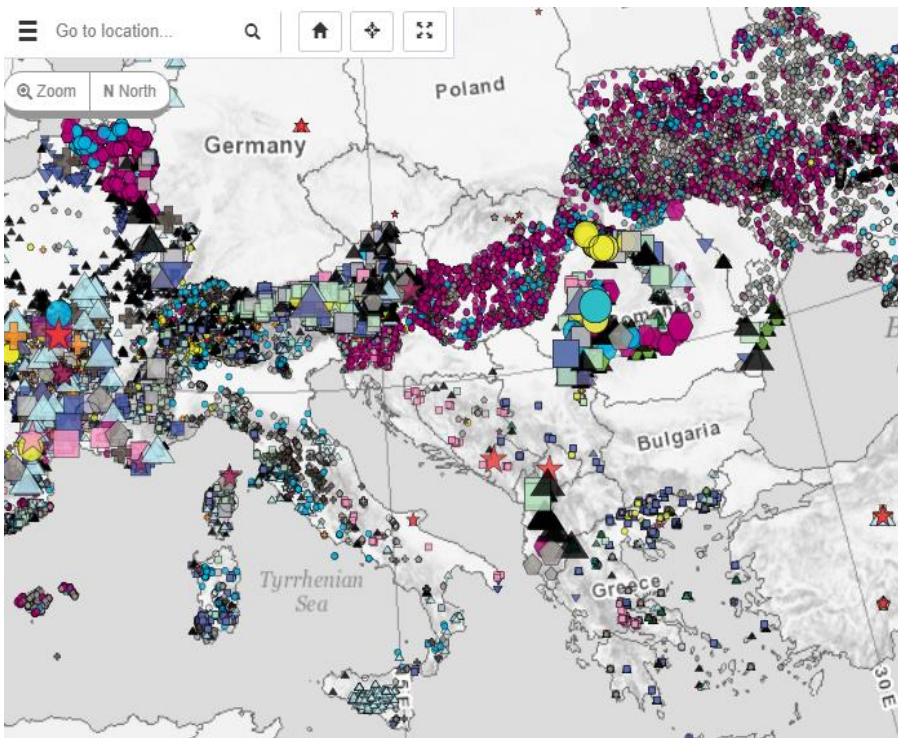


Figure 2: EGDI map viewer

RESULTS

The main result is the creation of West Balkan Mineral Register for primary and secondary mineral resources. Statistics of data collected and harmonized in first two years of project duration is following: Albania 134 primary resources altogether (41 mines) and 15 secondary mineral sites, Serbia 55 primary (43 mines) and 28 secondary resources, Croatia 183 primary (all of them are mines) and 46 secondary resources, Montenegro 50 primary (35 mines) and 4 secondary resources, Bosnia and Herzegovina altogether 134 primary (81 in Federation and 53 in Republic of Srpska) and 15 secondary resources (11 in Federation and 4 in Republic of Srpska).

All the data are already a part of EGDI accessible through a web portal (<http://www.europe-geology.eu/map-viewer/>), It provides data, tools, services and expertise to enhance sustainable development of Europe in support of public policy making, industry, society, communication and education purposes at European and national level.

Through the register existing data sources, assessment of data availability and quality has been delivered to achieve harmonization and standardization of EU mineral statistic.

The other outcomes of the project are [5]:

- investors will get the register for primary and secondary resources and list of national contacts,
- the task partners countries with increased capacity for national mineral management. Their market will become accessible,
- ensured enough flow of information on mineral resources for Europe's industry to expand their business and investments in the West Balkan Region,
- joint knowledge base from ESSE national geo-surveys, provided public data,
- increased mineral exploration activities and roadmap for the exploitation of mineral sector in the region for future implementation, updating and maintenance after the project.

CONCLUSION

Data related to raw materials, either metallic ores, industrial minerals or construction materials, of primary origin from mining and from industrial wastes certainly are available in West Balkan countries. However, they are often scattered amongst variety of institutions, including governmental institutions, agencies, universities and industries. These data are often stored in databases with their own design/architecture and vocabulary, while their merging and compilation is difficult and time consuming. Issues regarding availability, quality, organization, accessibility and sharing of data are common in all countries. Solving these problems requires access and use of interoperable data, which are now joined in West Balkan Mineral Register. The register allows to easily combine information related to primary and secondary mineral resources and to provide end-users with all the available information. Data platform represents a first step to the future effective and sustainable information system of the region. The technical solutions facilitate data update and maintenance and gives a full access to information related to the whole mineral resource's life cycle.

Joint knowledge and information from ESSE national data providers will provide publicly available data (regarding to national legislation) by generating comprehensive and useful register of primary and secondary mineral resources and increased capacity of West Balkan countries for management of mineral resources on national level. [1]

Especially the information of mine and metallurgic waste gathered throughout the project are of great importance for the region and whole Europe, because recently waste has become an important potential source of raw materials. So far waste sites have been relatively neglected due to massive primary mineral

extraction. SRM data is relatively poorly organized but created dataset of SRM contains important data for mineral extractive industry.

Extended data survey (especially regarding secondary resources) needs to be performed through follow-up projects, geographically outreaching to other ESSE countries (SVK, CZ, HUN, ROU and BGR). [5]

REFERENCES

[1] RESEERVE: Mineral potential of the Eastern and South-Eastern Europe region, <https://eitrawmaterials.eu/project/reseerve/>

[2] Minerals4EU. The EU-MKDP (Minerals Knowledge Data Platform), 2014, <https://www.slideshare.net/Minerals4EU/minerals4-eu-wp51stminceconf20141126dcassard>

[3] EGDI. About EGDI, <http://www.europe-geology.eu/about-egdi/>

[4] Directive INSPIRE. About Inspire, 2007, <https://inspire.ec.europa.eu/about-inspire/563>

[5] RESEERVE project proposal. RESEERVE: mineral potential of the ESEE region, 2017, Internal documentation of GeoZS.

ON THE REGIME OF COVID-19 EPIDEMIC IN RUSSIA AND ITS IMPACT UPON THE FUEL AND ENERGY COMPLEX, INCLUDING IN EDUCATIONAL AND SCIENTIFIC SPHERES

Dr. Svetlana Punanova¹

Dr. Mikhail Rodkin²

^{1, 2}Institute of Oil and Gas Problems of the Russian Academy of Sciences,
Moscow, Russian Federation

²Institute of Earthquake Prediction Theory and Mathematical Geophysics,
Moscow, Russian Federation

ABSTRACT

The mode of development of the COVID-19 pandemic in Russia and the impact of the epidemic on the areas of scientific research, education and functioning of the fuel and energy complex are discussed. The official statistics revealed evidence both of effectivity of the taken anti-epidemic measures in Moscow and of possible cases of incorrectness of statistical data. The social situation and the mode of development of the epidemic in Moscow and in the regions of Russia are essentially different, that reduces the effectiveness of anti-epidemic measures introduced uniformly throughout the whole country. The conditions of the pandemic and quarantine are difficult for everyone, but organizations and persons with a more modern informational character of production adapt to them more easily. In general, it can be suggested that the epidemic besides the very essential losses gives an important impulse for social-economic and political modernization of the society.

Keywords: *Regional differences in the epidemic regime in Russia, the quality of official statistics, the impact of the epidemic on scientific research, education and the fuel and energy complex*

INTRODUCTION

The economic and social impact of the COVID-19 pandemic depends on the epidemic and on the anti-epidemic measures taken. This article, following earlier publications of one of the authors [8], [9], [10], examines the regime of development of the COVID-19 epidemic in Russia, and some trends of the impact of the pandemic on education, science, and on the production process (mainly in relation to facilities related to the functioning of fuel and energy complex). Firstly, we will briefly summarize some general trends of development of epidemic in Russia and then the features of the impact of the epidemic on the society will be discussed.

Some trends in the development of the COVID-19 pandemic in Russia

In Russia, a strong difference in the development of the COVID-19 epidemic exists between megacities (primarily Moscow) and in the regions. Fig. 1 with a semi-log scale along the y-axis displays the official data on the growth of the

number of cases of infections and deaths in Moscow and in the regions of Russia. It can be seen that in Moscow, at the beginning of the epidemic, the number of cases (curve 1), and with a certain time lag, the number of deaths (curve 2), grow rapidly. Over time, the rate of growth of the epidemic decreases, and then the growth in the number of cases and deaths stabilizes at a certain (moderate) level. At the initial stage, the development of the epidemic in semi-logarithmic coordinates can be satisfactorily described by a straight line, which indicates an avalanche-like character of the first stage of development of the epidemic.

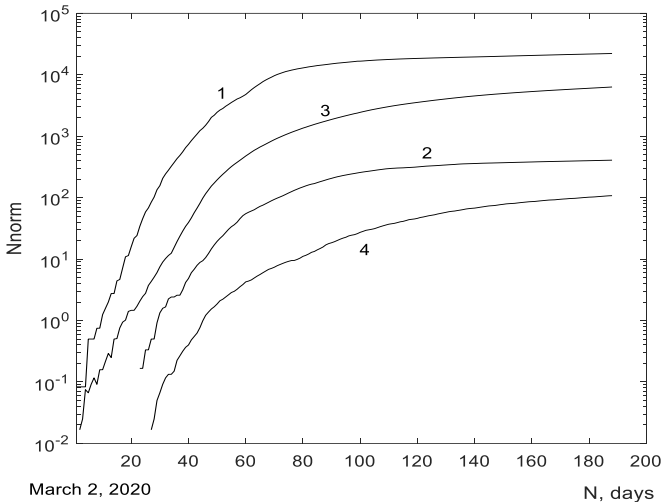


Fig. 1. Growth mode of the number of cases and deaths (N_{norm}) from COVID normalized per million population in Moscow (curves 1 and 2) and in the regions of Russia (curves 3 and 4).

A significantly different nature of the development of the epidemic is observed in the regions of Russia (outside megacities). The normalized (per million population) number of cases and deaths is much less in the regions; the growth curve of the number of cases and deaths is flatter. However, the rate of development of the epidemic in the regions decreases with time much slower. At this moment, the normalized number of victims of the epidemic in the regions is still 3-4 times less than in Moscow, but the growth rate of the number of victims in the regions is higher. It seems expectable that over time, the proportion of cases and deaths in Moscow and in the regions becomes close. Similar regional differences exist in other countries; in particular, the curves of the epidemic development in New York and in the agricultural states of the USA are qualitatively similar to the data in Fig. 1. Having this in mind, it can be suggested that cumulative losses from the COVID-19 in the countries and regions currently less affected by the epidemic can be even heavier than the ones that have taken place in big cities. See also similar discussion in https://www.un.org/development/desa/dpad/wp-content/uploads/sites/45/publication/pb_60.pdf where a similar situation is characterized as a “calm before the storm”.

For Moscow, the measures taken to limit the development of the epidemic and prevent overloading the health care system were quite effective. As noted above, the slope of the exponent has greatly decreased over time. It is essential, that these changes were uneven. Three decreases in the slope of the growth curve of the number of infected cases were mostly significant. These changes occurred on March 22, April 2 and April 18 (Fig.2). 5-7 days before this, the Moscow Mayor's Office introduced important new anti-epidemic restrictions. Starting on March 16, schooling was stopped. Starting on March 28, the work of a large number of organizations was ordered stopped, and starting on April 13, a pass system was introduced. The delay in the decrease in the growth rate of the number of cases of infections relative to the dates of the introduction of the mentioned restrictive measures in all three cases is 5-7 days, which is consistent with the data on the typical duration of the time interval from the moment of infection with COVID-19 to the onset of the disease. Analysis of the data for other countries made it possible to also identify the typical duration of severest cases, from the onset of the disease to death, that duration turned out to be about 10 days [10].

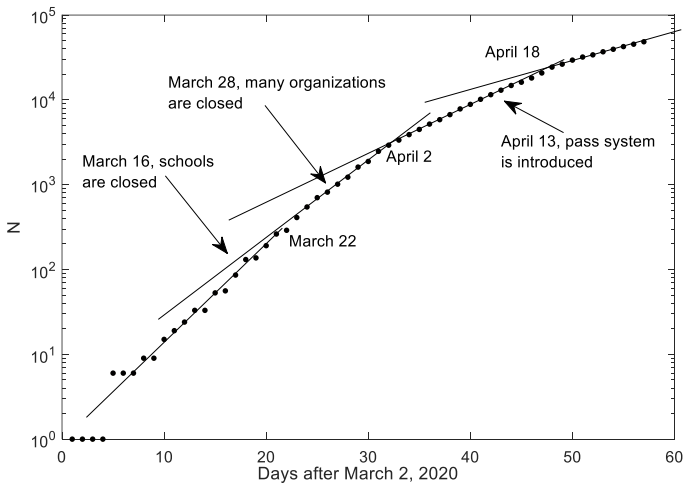


Fig. 2. *The impact of the restrictive measures taken by the City Hall on the development of the epidemic in Moscow, N – number of COVID-19 cases in Moscow, from [2], [9].*

However, not all measures taken by the Moscow City Hall were so successful. In the first day of the introduction of the passes, there were massive pass checks, causing long queues formed in the Moscow metro on the morning of April 13. Daily data on the number of infections and deaths from COVID-19 in Moscow are presented in Fig. 3. The graphs show that 6 days after the onset of the queues, there was a surge in the number of cases of the disease, and after another 10 days, a surge in the number of deaths. These maximums can be interpreted as direct consequences of queues in the metro with additional number of diseases of about 500 people and up to 30-40 deaths.

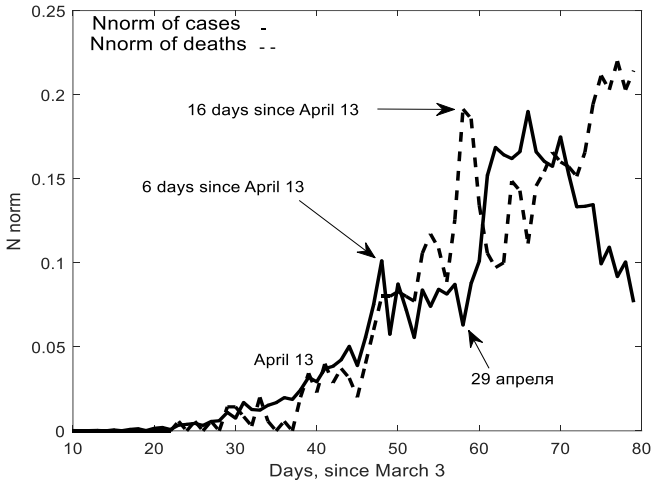


Fig. 3. Possible effect of an increase in the number of COVID-19 diseases and the deaths because of queues in the subway arising from the police checks during the first day of pass regime. Arbitrary scale is selected for the best comparison of curves.

The reasons of some features of the COVID-19 epidemic in Moscow remain unclear. Thus, for example, from April 29 up to early May, official statistics show an essential increase in the daily case numbers. However, the corresponding surge in the number of deaths was not observed. It can be assumed that this increase in the number of infections was caused by the sharp increase in the number of tests and detection of cases of latent incidence of COVID-19. However, attention is drawn also to the fact that on April 29, an order of the Ministry of Health of Russia came into force "On incentive payments to medical workers in connection with the spread of coronavirus infection" (<http://www.consultant.ru/law/hotdocs/62022.html>).

Thus, the emergence of corporate material interest of medical personnel in overestimating the number of cases of COVID-19 cannot be excluded. Note also, that some points in the official statistics appear to be dubious. For example, the mortality rate since the end of July in Moscow has remained at a quasi-constant level (Fig. 4), but with no case of the same repeating number of deaths in neighboring days, while it should take place in about a quarter of cases; this seems hardly likely from statistical reasons.

The overestimations and underestimations of the number of cases of morbidity and death from COVID-19 are closely connected also with the lack of a method for their unambiguous formalization. The difficulty in the case of the disease is associated with a possible unclearness of the clinical picture of the disease and inaccuracy of tests. In the event of a patient's death, ambiguity arises when the patient dies from other diseases, aggravated by infection with COVID-19.

Restrictive antivirus measures were often introduced in Russia uniformly throughout the whole country. The introduction of quarantine, synchronized with Moscow, often turned out to be ineffective in some regions, since quarantine was introduced at a low level of the epidemic, when the epidemic could not overload the healthcare system. The easing of quarantine, also synchronous with Moscow, was introduced frequently at the phase of a significantly greater development of the epidemic than it was at the time of the introduction of quarantine. However, the continuation of the quarantine in the regions turned out to be highly undesirable for economic reasons. Thus, the quarantine period was often inconsistent with the local mode of development of the epidemic. In this situation, quarantine restrictions are hardly effective and could be more difficult for the population than the epidemic itself.

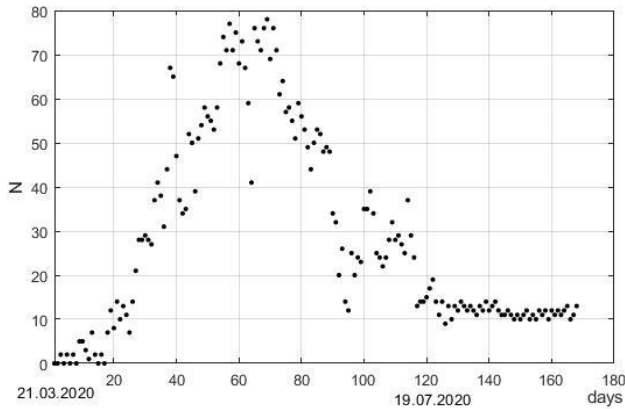


Fig. 4. Daily numbers of deaths from COVID-19 in Moscow.

The brief examination presented herein indicates that the official COVID-19 statistics in Russia reflects the rather subtle features of development of the epidemic and the implementations of anti-epidemic measures in Moscow, however, it bears features of probable falsification as well. Understanding the degree of accuracy of the official data, only sufficiently detailed, on the development of the COVID-19 epidemic is necessary for the correct understanding and use of this data.

The above is a general background in relation to further discussion of the impact of the COVID-19 epidemic and anti-epidemic measures on the social and economic situation in Russia. In this regard, we will discuss the introduction and practice of distance education at universities and research institutes, the situation with the provision of rotational work at remote oil and gas fields and questions concerning the current situation with scientific research in the field of geological sciences and environmental protection (difficulties in holding symposia and congresses, experimental and field research).

SOME ASPECTS OF THE IMPACT OF THE COVID-19 EPIDEMIC UPON SOCIETY

The impact of the COVID-19 epidemic on the oil and gas industry is two-fold. The first one concerns the fall in energy demand during the epidemic. The second one concerns the functioning of the oil and gas complex and corresponding fields of science and education, during the epidemic.

SITUATION IN THE OIL AND GAS MARKET

According to Vladimir Chuprov [1], the head of the energy program of the Russian branch of Greenpeace, the coronavirus hit hard the world oil market, which was already unstable. Reduced oil consumption in China due to that country's quarantine, reduced consumption of transport fuels which resulted in the downturn of global business activity along the chain have brought down world oil and gas prices [4]. The question arose about the financial stability of countries whose economies are overly dependent on oil production and exports. Russia is one of such countries.

Note, however, that despite the obvious vulnerability of the hydrocarbon market, the Russian leadership is still betting on a high level of oil and gas production, which requires both the discovery of new fields and further development of already exploited fields. As part of the implementation of this program, on March 5, 2020, the President of Russia signed a decree "On the Fundamentals of State Policy of the Russian Federation in the Arctic for the Period until 2035", according to which oil and gas production in the Arctic latitudes is planned to be systematically developed through government subsidies and private investment.

DISTANCE LEARNING - PROS AND CONS

In the list of anti-epidemic measures, an important role is played by the decision to introduce distance learning in schools, colleges and universities. The problems of distant learning is discussed in a number of papers (see [7], [11] as an example); main pro et contras of the distant learning are summarized in <https://www.educationtask.com/>.

Concerning the field of oil and gas education system (from Geology faculty of Moscow State University, University of Oil and Gas, Kazan University) all interviewed teachers note the difficulties with the implementation of such a learning regime. They say that distant manner of learning for students is more difficult and takes more time both for students and teachers. The following observations were obtained also: better attendance of distant lessons and increased difficulty in controlling the assimilation of study material by students. An increase in the differentiation of the quality of assimilation of the study material is also outlined. More successful and reasonably motivated students take advantage of the new opportunities of more rational use of time and choice of sources of learning. At the same time, poorly performing and poorly motivated students show worse results with a significant complication of control of their assimilation of the study material. With distance learning, hands-on and laboratory classes are especially affected, and the corresponding practical skills are not developed.

ROTATIONAL WORK AT REMOTE OIL AND GAS FIELDS

With regard to the oil and gas complex, an essential complexity is generated by the existing system of rotational servicing of many remote oil and gas fields. At the peak of the quarantine, the rotational personnel had made up the bulk of air passengers on flights to Western Siberia, Sakhalin and a number of other remote oil-producing regions. A strong decrease in the number of domestic and international passengers is the common feature typical to many countries

https://www.icao.int/sustainability/Documents/ICAO_Coronavirus_Econ_Impact.pdf

Due to the combined impact of the vacation period, cases of COVID-19 diseases, and the quarantine, significant difficulties arose in the formation of shift teams. In this situation, unpopular and tough decisions were often made. For example, due to the threat of the spread of the coronavirus infection, Gazprom Dobycha Nadym stopped the shift of personnel who worked on a rotational basis at the Yamal fields, including at the largest Bovanenkovskoye field in Western Siberia [3].

OIL AND GAS SCIENCE DURING PANDEMIC AND QUARANTINE

In the field of scientific research, the most painful difficulties center on carrying out the experimental research, fieldwork and conferences. Most of the conferences that had been planned for March 2020 and onwards were either canceled or postponed. In the cases of holding conferences online (fully or partially), the lack of familiarity with the online format by many participants, negatively affected such conferences. It is hoped, however, that such remote conferencing capabilities and skills will soon be attained.

Currently, due to the decrease in the activity of the epidemic in large cities in Russia, a few conferences have taken place recently or are planned to occur mostly offline in the near future. The following events can be mentioned:

- VIII All-Russian Meeting with International Participation "Jurassic System of Russia, Problems of Stratigraphy and Paleogeography. Syktyvkar: IG Komi Science Center UB RAS Online, September 7-10 [6];
- International Scientific and Practical Conference "On a New Paradigm for the Development of Oil and Gas Geology" dedicated to the 100th anniversary of the establishment of the Republic of Tatarstan. Kazan, September 2-4 [5];
- XI International Conference "Chemistry of Oil and Gas" dedicated to the 50th anniversary of the Institute of Petroleum Chemistry of the Siberian Branch of the Russian Academy of Sciences. Tomsk, September 28-October 2. <http://petroleum-chemistry.ru/>

The authors of this article took part in these events with reports.

The other example that can be mentioned is the Geolinks Conference, dedicated to the environmental sciences, planned to occur October 5-7, 2020 in Plovdiv, Bulgaria. www.geolinks.info. We hope, it will be held in compliance with all necessary protective measures, and with a large scientific load, and will have a great resonance. In-person communication between scientists will bring joy to the participants and colleagues after a long quarantine and forced retirement and will help to solve urgent environmental problems.

In terms of the role of science during the pandemic, it can be mentioned that dozens of Russian projects related to the study of coronavirus have received support from the Russian Foundation for Basic Research (RFBR). Already in mid-April, in the midst of the pandemic, the competition "Fundamental problems of the emergence and spread of coronavirus epidemics" was promptly organized. RFBR promptly responded to the possibility of supporting science by organizing a program of fundamental research on the pandemic problems. More than 500 applications were submitted for the RFBR competition. For the competitive selection, an expert council was formed, which included representatives from both natural science fields and humanitarian disciplines.

CONCLUSIONS

The examination of the official statistics of the COVID-19 epidemic in Russia allows both to highlight rather subtle features of the development of the epidemic (in particular, reflecting the effectiveness of the anti-epidemic measures taken), and also indicates possible cases of incorrectness of statistic data. In general, the experience of the COVID-19 pandemic in Russia provides an example of the limited effectiveness of adopting a set of measures uniformly throughout the large country. In Russia, such measures were taken under the strong influence of the situation in the capital region. However, the situation in the Moscow region is not typical of the most other regions of Russia. Thus, these measures frequently were ineffective in the regions. Moreover, they could increase social tensions.

The consequences of the pandemic are very grave for both the economy and the people. They appear to be heavier for people who are accustomed to functioning in conditions of external management and control. Internally motivated people (for example, students) who independently set tasks for themselves adapt to pandemic easier, and even find new opportunities for growth. Such people benefit from the obvious savings when the movement of people is replaced by the movement of files.

The analysis of the experience of the pandemic will undoubtedly prove to be important and required in the event of similar cataclysms in the future. Let us emphasize that a full-fledged analysis is possible only with a multidisciplinary approach, using the methodology of various fields of knowledge, both natural science and humanitarian.

ACKNOWLEDGMENTS

The manuscript was performed in the framework of the state tasks, projects No. AAAA-A19-119022890063-9 and No. AAAA-A19-119013190038-2 of the state

task of the Institute of Oil and Gas Problems of the Russian Academy of Sciences and was partially supported by the RFBR grant No. 19-05-00466.

REFERENCES

- [1] Chuprov V. Expert opinion 11.03.2020. <https://greenpeace.ru/expert-opinions/2020/03/11/koronavirus-vyjavil-strategicheskiju-oshibku-v-klimaticheskij-politike-rossii/>
- [2] Enikeev B.N. Feedback on publications: Rodkin M.V., Shikhova N.M. Mathematical modeling of the development of the COVID-19 epidemic, an attempt at forecasting. Ural Geological Journal. No. 3(135), p. 23-27. 2020. In Russian. <https://www.ural-geol-j.net/archive>.
- [3] Gazprom isolated the largest field in Yamal due to coronavirus/ Read more on RBC: <https://www.rbc.ru/business/27/03/2020/5e7db4379a7947b24a8629ff>
- [4] Ivanov K.S. On the coronavirus and the price of oil (review of the article "On the statistics of the spread of the COVID-19 virus". Ural Geological Journal. 2020, No. 2(134), p. 22-25. In Russian. <https://www.ural-geol-j.net/archive>.
- [5] Materials Int. scientific and practical conf. "About a new development paradigm Oil and Gas Geology". Kazan, Ikhlas, Russia, 584 p., 2020.
- [6] Materials VIII All-Russian meeting with international participation. "Jurassic system of Russia: problems of stratigraphy and paleogeography". Online conference. Syktyvkar: IG Komi Science Center UB RAS, 297 p., 2020.
- [7] Onyema E.M., Eucheria N.C., Obafemi F.A. et al. Impact of Coronavirus Pandemic on Education. J. Education and Practice, 11, 13, 2020, ISSN 2222-1735 (Paper) ISSN 2222-288X (Online).
- [8] Rodkin M.V., Belov S.V. On the oddities of the statistics on the coronavirus COVID-19. Use and protection of natural resources of Russia. No. 2 (162), p. 117-120, 2020. In Russian.
- [9] Rodkin M.V., Shikhova N.M. Mathematical modeling of the development of the COVID-19 epidemic, an attempt at forecasting. Ural Geological Journal. 2020, No. 3(135), p. 3-13. In Russian. <https://www.ural-geol-j.net/archive>.
- [10] Rodkin M.V., Shikhova N.M., Rukavishnikov T.A. Preliminary analysis of the dynamics and possible factors of influence of the COVID-19 pandemic. Ural Geological Journal. No. 3 (135), p. 14-22. 2020. In Russian. <https://www.ural-geol-j.net/archive>.
- [11] Tishchenko A.S. The impact of the pandemic on the education economy. Economic development of Russia. Vol. 27. No. 5. 2020. <https://cyberleninka.ru/article/n/vliyanie-pandemii-na-ekonomiku-obrazovaniya/viewer>

ORE CONCENTRATIONS OF METALS IN NAPHTHIDES OF HYPERGENESIS ZONE: ASSESSMENT AND ENVIRONMENTAL ASPECT

Dr. Svetlana Punanova

Oil and Gas Research Institute of the Russian Academy of Sciences, Moscow,
Russia

ABSTRACT

The study examines the formation of secondary-altered crude oils associated with the processes of modern or ancient hypergenesis. As a result of geological processes during intense upward movement of the earth's crust, oil undergoes physical weathering, inorganic oxidation, washing out with water, biodegradation and sulfurization, and turn into heavy oils and hard bitumen. In zones of hypergenesis, the loss of light fractions occurs and the absolute concentration of trace elements (TE) associated with resinous-asphaltene components, such as V, Ni, Co, Mo, Cr, Cu, etc. sharply increases. In addition, oils absorb elements of variable valence (V, Fe, U) from low-salinity stratal waters. As a result of experimental studies on the interaction of oils with low mineralization waters, which are characteristic of hypergenesis zones, leaching of some elements (e.g., Zn) from oils and absorption of others from contacting waters (for example, concentrations of newly-formed organometallic compounds V and Fe increased by 1.3-12 times) were found.

The author utilized the method of neutron-activation analysis to study the content of TE in oils and natural bitumens of the Volga-Ural, Timan-Pechora, Kazakhstan, Tajikistan, and etc. Ore-level concentration values were found, for example: 180-1162 ppm for V and up to 100 ppm for Ni in the oils of the Melekess depression in Tatarstan, and 940 ppm for V and 130 ppm for Ni in the oils of Kazakhstan deposits.

Classification of oils by the content of "biogenic" elements V, Ni, Fe and by physical and chemical properties revealed significant differences of hypergene-altered oils in the general cycle of genesis of naphthides. Deposits of secondarily-altered oils are found in a wide stratigraphic range in oil and gas basins of various geostructural types in traps of the combined morphology – lithologically and tectonically shielded.

During the development of oil deposits that contain high concentrations of TE, it is necessary to take into account ecological aspects. The environmental aspect is due to the fact that many metals contained in oils – V, Ni, Cd, As, Hg, U, etc. belong to highly toxic compound chemicals.

Keywords: *naphthides, environment, ecological aspects, zones of hypergenesis, trace elements*

INTRODUCTION

The formation of secondarily altered oils is due to the processes of modern or ancient retrograde diagenesis (hypergenesis). As a result of intensive upward movement, the oils get into areas of biochemical and/or chemical oxidation processes either on migration routes or in the reservoirs and are subjected to physical weathering, inorganic oxidation, leaching with waters (washout), biodegradation, and sulfurization. The accumulation zones of hypergenetic oils are confined mainly to large positive structures (arches, megaswells, swells) that have experienced intense upward movement in the final stages of their development. The most altered oils occur in zones of active water exchange at water-oil contact (WOC) and at relatively shallow depths.

In the hypergenesis zones, the processes listed above result in changes in the concentration of TE and their ratio [4], [11]. Due to the loss of light fractions, the absolute concentration of the elements V, Ni, Co, Mo, Cr, Cu, etc. associated with the resinous-asphaltenic components significantly increases in the oils. In addition, resin-asphaltene heteroatomic components of oils that contact with slightly mineralized formation waters in the hypergenesis zone are capable of absorbing variable valence elements V, Fe, and U from water.

As a result of secondary transformations of oils in the hypergenesis zone, large and giant heavy oil and natural bitumen fields have been formed in Western Canada, Eastern and Western Venezuela, the United States, Russia, and other regions [1], [2], [3], [4], [5], [6], [12], [13]. When assessing resources, these accumulations are unconventional and recognized as commercially viable with ore concentrations of metals in naphthides in many regions, and therefore, they are considered a complex raw material for the recovery of hydrocarbons and associated metals (Table 1).

Table 1. Main areas of hypergenetically altered naphthides secondarily enriched in TE

Oil and gas basin (OGB), oil and gas region, structural elements	Main deposits, age of oil and gas play	TE content in hypergenetically altered naphthides, ppm	
		V	Ni
Western Canadian OGB	Peace River, Wabasca, Athabasca; K1	168 *290	80 *120
Uintah-Paysens, Utah, Rocky Mountains OGB	Asphalt Ridge, WhiteRocks; P-T, J2, K1-Upper Paleogene	110	30
Eastern Venezuela (Orinoco) OGB	Oficina, Temblador, Cerro Negro; K, Oligocene-Pliocene	182 *470	72 *90
Western Venezuela (Maracaibo) OGB	West Mara, Mara, Bochakero; K, Paleogene-Neogene	216-1000 *935-1250	96 *110- 150
Lena-Tunguska OGB, Lena-Aldan, Olenek arch	Olenek; PR2, J3	124 *3640	53.6 *640
South Mangyshlak OGB, Buzachinskii arch	Northern Buzachi, Karajanbas; J2, K1	70-384	50-164
Surkhan-Vakhsh OGB, Afghan-Tajik depression	Uchkizyl, Haudag, Koshkar; Paleocene, Bukhara formation	570	170

Timan-Pechora OGB, Ukh-ta-Izhma swell, Varandei-Adzvininskaya structure	Ust'-Voiskoe, Izhma, Usa, Yarega; D, C-P	253	100
Volga-Urals OGB, South Tatar arch, Melekes depress	Nurlatskoe, Ashalchinskoe, Sugushlinskoe; C1, P1, P2	900 *1200	100 *340

* V and Ni content in natural bitumens.

RESULTS AND DISCUSSION

Our generalization is based on the author's data on TE composition of naphthides from the Volga-Ural and Timan-Pechora OGB as well as the Buzachi arch (Kazakhstan) and Afghan-Tajik depression (Tajikistan). In addition, we processed a great body of factual material on oils and solid bitumens from petroleum basins of Russia, the United States, Canada, Brazil, and Venezuela. The productive sediments from the upper sedimentary sequences of the Tatarstan and Ul'yanov district often contain heavy (0.902-0.984 g/cm³), high in sulfur (3.5-4.6%), viscous oils with high contents of resinous-asphaltic components. The contents of TE reach high values (in ppm): V (180-1162), Fe (131), Ni (up to 124), Cu (38), Mn (12), Pb (8.0), Zn (6.0), Ti (4.0), Cr (0.7), and Ge (0.7). Average TE data on oils of Tatarstan [8] are shown in Table 2.

Table 2. Average characteristics of TE composition of oils of the Volga-Ural OGB [8]

Region	Tectonic element	Age	Content in oil			V/ Ni	Influence of Hypergenesis
			V, ppm	Ni, ppm	S, %		
Tatarstan	Melekes Basin	C ₁₋₂	500.2	82	3.8	6.1	++
		D ₃	147	34	2.6	4.3	-
	South Tatar arch	C ₁₋₂	250	57	4.7	4.4	+
		D ₃	70	34	1.6	2.1	-

* *Hypergenesis processes: the dash denotes that the processes were not manifested; plus, manifested; two pluses, strongly manifested*

The oils from Devonian, Carboniferous, and Permian sediments of the South Tatar and Bashkir arches and Bira saddle presumably belong to the vanadium type initially enriched in TE and likely unaffected by hypergenesis. The oils in Carboniferous sediments of the Tatar arch bear clear evidence of hypergene transformations, which manifested themselves in the Melekes depression [8]. The highest V and Ni contents, correlated with elevated sulfur content, were found in oils from Lower Carboniferous reservoirs in the eastern flank of the Melekes basin, for instance, at the Stepnoozerskoe (870 and 74 ppm, respectively) and Nurlatskoe (658 and 93 ppm) fields. The bituminous sequences of Tatarstan are most studied on the western slope of the South Tatar arch and the eastern flank of the Melekes depression. Accumulations of bitumens are mainly situated at depths up to 400 m in the Permian sediments. Maximal average concentrations of V and Ni were found in bitumens from lower Permian deposits (V = 910 ppm, Ni = 177 ppm) [7].

Hypergenesis leads to a sharp increase of TE in vein asphaltites relative to asphalts and solid bitumens, i.e., in the series of their genetic transformations from oils to solid bitumens (Table 3). As noted by Yakutseni [13], naphthides also differ in Au and Re contents. Asphaltites are considerably enriched in these metals.

Table 3. Variations of trace elements (ppm) in heavy oils and natural bitumens of the Ural-Volga area [13]

Element	Heavy oils	Maltha, asphaltenes	Asphaltites, veined
V	200-1400	230-2000	2350-4800
Ni	100-195	100-190	520-708
Mo	2.2-15	-	22
U	-	5.9	-

Oils of the Buzachi Arch (Kazakhstan) are ascribed to the hypergene-altered type, based on all of their features. Regardless of their localization, they are heavy (0.920-0.940 g/cm³), highly resinous (18-30%), sulfurous (up to 2%), highly viscous (up to 500 mPa/s), highly cyclic oils with low solidification temperature (20-27°C), and are undersaturated with gas under stratal conditions. These parameters increase from the arch part to the outlines. The oils are enriched in TE. The studied oil composition, namely of Fe, V, Ni, Cr, Cu, Mn elements, of the Northern Buzachi and Karazhanbas fields is shown in Table 4 [11].

Table 4. Trace element composition of oils from the Buzachi petroleum area [11]

Deposit	Age	Depth, m	Density, g/cm ³	Content of trace elements, ppm						V/Ni
				Fe	V	Ni	Cr	Cu	Mn	
Northern Buzachi	J ₂	470	0.940	660	240	29	3.8	2.2	1.3	8.3
Karazhanbas	K ₁	267	0.930	1300	190	50	8.5	0.3	0.5	3.8
Karazhanbas	J ₂	370	0.920	450	70	45	2.4	0.8	0.1	1.5

Oils of Paleogene sequences of the Afghan-Tajik depression are genetically related to the carbonate sequence of the Paleocene Bukhara Beds of the Surkhandar'ya and Vakhsh synclinerium zones and the southern part of the Kafirnigan anticlinal zone. They are characterized as heavy (density of 0.970 g/cm³), viscous, resinous-asphaltene (sum of resins and asphaltenes is 43.2%), and sulfuric (S = 5.2%) oils subjected to intense and long-term impact of hypergenesis factors [11]. These oils have elevated concentrations of V, Ni, Cu, Fe, Co, and other elements. Intense manifestation of hypergenesis processes leads to their sequential transformation into maltha and asphaltenes (Surkhandar'ya zone).

Figure 1 demonstrates distribution of ten metals in hypergenesis altered oils and their ash from the Afghan-Tajik depression as compared to the TE distribution in clay rocks, and in unaltered oils from the same region.

TE are arranged in order of increasing content in clays. Oils and especially oil ashes of the Afghan-Tajik depression are enriched in V (1000 times), Ni and Cu (100 times), Co (10 times), and Cr (5 times) with respect to the average contents.

The approved criteria of oil hypergenesis include not only increase in the concentrations of TE in naphthides, but also changes in their ratios, for instance, Zn/Co and V/Ni. The comparison of oils from the Devonian terrigenous sequence of the Timan and Izhma-Pechora depression from the deepest strata position (Dzh'er deposit) toward their exposure on the surface (Yarega field) revealed systematic decrease of Zn/Co ratio from 15.5 to 1.2 with intensification of hypergenesis. Lowered Zn/Co ratios occur because Zn gets flushed into the water. Similarly, Zn/Co ratio in Brazil oils changes from 8.2 to 0.8 during supergenesis [2].

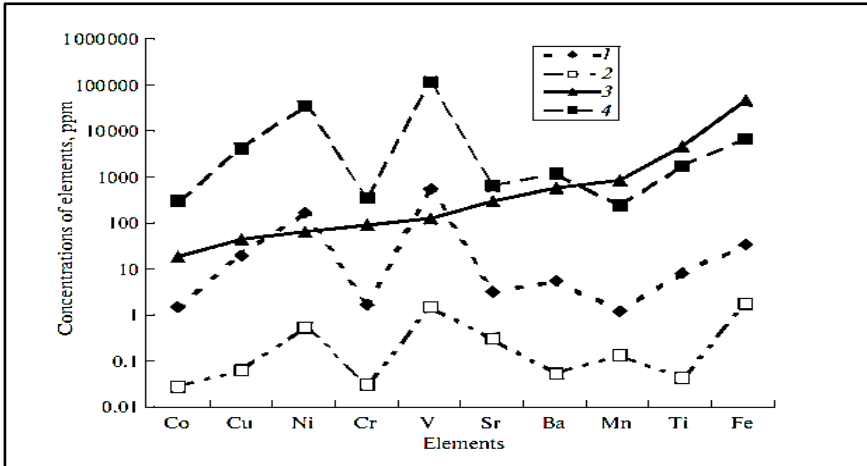


Fig. 1. Content of TE in oils from fields of the Afghan-Tajik basin, which were subjected (1) or not (2) to the hypergenesis, as well as in clays (3) and ash of hypergenesis transformed oils (4)

The study of TE composition of oils in the WOC zone, in particular, variations of Zn/Co and V/Ni ratios in oils depending on sampling position relative to the WOC zone, was carried out at the multibed Western Tebuk field of the Timan-Pechora OGB. Oils taken from the WOC zone have lowered Zn/Co ratios (5.6), while samples from boreholes located at a significant distance from it (>300 m) and at the top of the reservoir have the higher ratios (up to 23.7). Oils in the WOC zone are also distinguished by a high Fe content and increased V/Ni ratios (up to 14.5) (Table 5). Similar conclusions were obtained when studying the oil of the Piltun-Astokhskoye and Odoptu-Sea deposits of Northern Sakhalin [9].

Table 5. Change in hydrocarbon and ME indicators in the oils of the Western Tebuk field depending on the position of the oil extraction point relative to the WOC [11]

Oil sampling interval position regarding WOC	Zn/Co	V/Ni	$\frac{iC_{19}+iC_{20}}{nC_{17}+nC_{18}}$	$\frac{iC_{19}+iC_{20}}{\Sigma (iC_{14}-iC_{18})}$
Top of the reservoir	23.7	3.0	0.8	1.5
Located far from WOC (> 300 m)	20.7	2.7	0.8	1.1
Located close to the zone WOC (< 300 m)	10.0	4.4	2.2	2.1
From zone of WOC	5.6	14.5	3.9	3.3

Analytical data on hydrocarbon composition of oils from the Western Tebuk field confirm biodegradation in the WOC zone [11]. Experimental studies of oil interaction with low salinity waters as exemplifying the bottom waters of the oil field showed that concentrations of most elements remain unchanged in oils. It was established that Zn is rinsed from oils at the WOC, which results in the decrease of Zn/Co ratio. In addition, it was experimentally proved that when oils are in contact with water, the water becomes enriched in resins and asphaltenes. In the WOC zone, the latter are potentially sorption components and capable of sorbing V, and partly Fe from water. This also explains an increase of these elements in oils and the considerable growth of V/Ni ratio in the WOC zone.

Ascending movements in regional and local petroleum basins and lateral migration of oils in reservoirs, open to the hydrogeological discharge zone, facilitate entrance of oil into hypergenesis zones, thus triggering mechanisms of TE accumulation in them [4-6]. The main driving force of these phenomena is geodynamic activity of the OGB. Table 6 shows the amplitudes of the uplifting of sedimentary cover of the OGB in the Cenozoic [11].

Table 6. The scale of sediment uplifts in the OGB at the inverse stage of their development in the Cenozoic

Oil and gas basin	Maximum amplitude of uplift, in m
Western Canadian	2000
Eastern Venezuelan	1800
Uinta Piceance, United States (Rocky Mountains)	1500
Tunguska, Eastern Siberia	1000
Volga-Ural (Tatar arch)	300-400
Timan-Pechora	200-300

CONCLUSION

Typification of oils by content of the “biogenic” elements V, Ni, Fe and physicochemical properties revealed significant differences of supergene altered oils in a general cycle of naphthidogenesis. They were distinguished by us as an independent group and ascribed to naphthides secondarily enriched in TE, thus

sharply differing from primarily enriched oils [10]. These are vanadium ($V > Ni > Fe$) or ferroan ($Fe > V > Ni$) types of oils with the genetic criterion $V/Ni > 1$ (Fig. 2). The foundation of the classification was based on the analysis of the scientific literature and studies covering the wide range of deposits around the world. Deposits of secondarily altered oils are found in a wide stratigraphic range (Upper Proterozoic-Neogene) in oil and gas basins of various geostructural types in traps of the combined type – lithologically and tectonically shielded.

The contents of V and Ni in oils of many deposits exceed, respectively, more than 100 and 50 ppm. They also have elevated concentrations of Mo, Cu, Zn, Re, and other elements (from 0.1 to 4 ppm). The oils are biodegraded, heavy (average density 0.954 g/cm^3), resinous (sum of resins and asphaltenes average 29%), sulfurous (average 4.2%), and highly viscous. The reservoirs of this type are frequently situated at shallow depths ($< 2.0 \text{ km}$) in platform areas, but also occur in the mobile zones, rift, aulacogens, marginal troughs, and intermountain depressions.

Of great importance is the connection of the oil composition with the predicted trap. It can be argued that it is precisely the oils of the hypergenesis zone that are often confined to traps of complex combined structure – lithologically and stratigraphically limited, to traps of erosive incisions, and to traps with tectonic restriction. With geological inversions and the restructuring of structural plans in the hypergenesis zone along tectonic faults that limit the trap along the channels that arise during this, potentially toxic elements of heavy oils and solid bitumen can penetrate into the environment. This process causes tremendous damage to our nature.

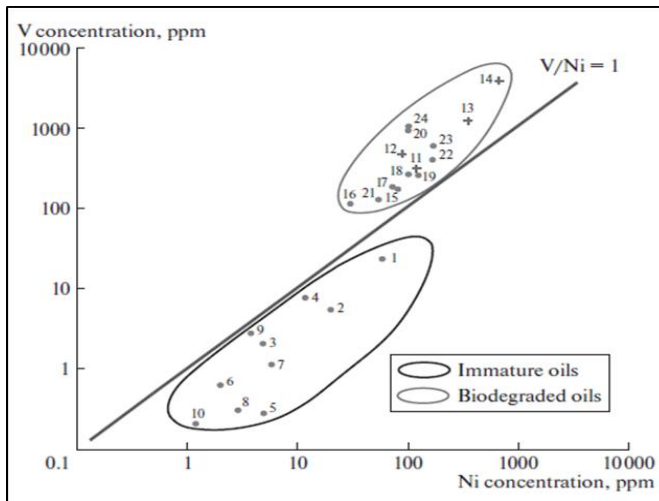


Fig. 2. Concentrations and V/Ni ratios in immature and hypergene oils and natural bitumens in various regions

Legend

Zone of immature oils:

1 – California; 2 – Belarus; 3 – Sakhalin; 4 – Japan; 5 – Azerbaijan; 6 – Georgia; 7 – Ciscaucasia; 8 – China; 9 – Western Siberia (Cenoman); 10 – New Zealand.

Zone of Hypergenesis (biodegraded) naphthides:

Bitumens: 1 – Western Canada; 12 – Venezuela Orinoco; 13 – Volga-Ural; 14 – Lena-Tunguska; **Oils:** 15 – Western Canada; 16 – Rocky Mountain Basin; 17 – Venezuela Orinoco; 18 – Timan-Pechora; 19 – Volga-Ural D-C, 20 – Volga-Ural P; 21 – Lena-Tunguska; 22 – Mangyshlak, 23 – Afghan-Tajik Basin; 24 – Venezuela.

During the development of oil deposits that contain high concentrations of TE, it is necessary to take into account the technological (e.g., deterioration of well equipment), industrial (e.g., extraction of valuable metals, such as V, U, Ge, and Mo from raw naphthides), and ecological aspects. The environmental aspect is due to the fact that many metals contained in oils – V, Ni, Cd, As, Hg, U, etc. – belong to highly toxic compounds. Once they enter the atmosphere, hydrosphere, and get on the earth's surface, they have a negative effect on plants and living organisms. In particular, vanadium belongs to the first class of environmentally hazardous chemicals.

ACKNOWLEDGEMENTS

This work was written as part of a state assignment on the topic of “Development of the Scientific and Methodological Foundations of the Search for Large Accumulations of Hydrocarbons in Nonstructural Traps of a Combined Type within the Platform Oil and Gas Basins.”

REFERENCES

- [1] Akinlua A., Ajayi T.R., Adeleke B.B. Organic and inorganic geochemistry of northwestern Niger delta oils. *Geochem. J.* Vol. 41, pp. 27-281, 2007.
- [2] Duyck C., Miekeley N., Fonseca T., Szatmari P., Neto S. Trace element distributions in biodegraded crude oils and fractions from the Potiguar Basin, Brazil. *G. Braz. Chem. Coc.* Vol. 19(5), pp. 978-986, 2008.
- [3] Escobara M., Márquez G., Azuajed V., Da Silvad A., Toccoe R. Use of biomarkers, porphyrins, and trace elements to assess the origin, maturity, biodegradation, and migration of Alturitas oils in Venezuela. *Fuel.* № 7, pp. 186-196, 2012.
- [4] Galarraga F., Reategui K., Martínez A., Martínez M., Llamas J.F., Márquez G. V/Ni ratio as a parameter in palaeoenvironmental characterization of nonmature medium-crude oils from several Latin American basins. *Journal of Petroleum Science and Engineering.* Vol. 61. № 4, pp. 9-14, 2008.

[5] Goldberg I.S. Naftometallogenetic provinces of the world and the genesis of ore concentrations in heavy oils and bitumen. *Geology of oil and gas*. No. 3, pp. 2-7, 1990.

[6] Gribkov V.V. One of the possible natural processes of oil enrichment with vanadium. *Oil and gas geology. Theory and practice*. 2007. Vol. 2. <http://www.ngtp.ru/rub/10/010.pdf>.

[7] Kayukova G.P., Petrov S.M., Uspenskii B.V. Properties of Permian Heavy Oils and Bitumens of Tatarstan in Natural and Anthropogenic Processes. GEOS, 2015, Moscow, 343 p. [in Russian].

[8] Mukhametshin R.Z., Punanova S.A. Composition of natural bitumens from the Ural-Volga region. *Solid Fuel Chemistry*, vol. 48, pp. 58-70, 2014.

[9] Popovich T. A. Assessment of Biodegradation of Sakhalin and Shelf Oils: Genesis of Oil and Gas. GEOS, Moscow, 2003, p. 260. [in Russian].

[10] Punanova S. Trace Elements in Naphtides in Oil and Gas Basins. *Doklady Earth Sciences*. Vol. 488, part 2, pp. 1207-1210. © Pleiades Publishing, Ltd. 2019.

[11] Punanova S.A. Supergene Transformed Naphthides: Peculiarities of Trace Element Composition. *Geochemistry International*. Vol. 52, No. 1, pp. 57-67. © Pleiades Publishing, 2014.

[12] Sukhanov A.A., Yakutseni V.P., Petrova Yu.E. Assessment of the prospects for the industrial development of the metal-bearing potential of oils and possible ways of its implementation. *Oil and Gas Geology. Theory and practice*. T. 7. No. 4. 2012. <http://www.ngtp.ru>.

[13] Yakutseni S.P. Occurrence of Hydrocarbons Enriched in Heavy Trace Elements: Environmental Risk Assessment. Nedra, St. Petersburg, 2005. [in Russian], 372 p.

POTENTIALLY TOXIC CHEMICAL ELEMENTS OF SHALE PLAYS – ECOLOGICAL THREAT TO THE ENVIRONMENT

Dr. Svetlana Punanova

Oil and Gas Research Institute of the Russian Academy of Sciences, Russia

ABSTRACT

This research considered the content of trace elements (TE), including potentially toxic elements (PTE) in shale plays and deposits in various regions of the world. Their comparative analysis was carried out and the highest concentrations of PTE in the shales of some regions were revealed. The author notes that the destruction of organometallic compounds occurs during the development of shale hydrocarbon (HC) using horizontal drilling with hydraulic fracturing – injecting large volumes of chemicals while increasing the temperature. During such destruction processes, PTE can escape into the environment: into groundwater, soil layers, and other objects of economic use, and also deteriorate well equipment. In connection with the noted environmental hazards present during the development of shale HC, this paper proposes to monitor the content of TE in both shale rocks as well as in extracted shale oil in order to mitigate the risks of their release into the environment. In addition, developers and scientists should consider the losses of industrially significant volumes of valuable metals that occur due to the lack of cost-effective technologies for their capture and extraction from naphthides.

Keywords: shale plays, trace elements, potentially toxic elements, environment, ecological threats

INTRODUCTION

With a fairly detailed coverage in the domestic and foreign literature of all the pros and cons of shale horizontal drilling projects, and in particular the negative environmental consequences of hydraulic fracturing, the problem associated with the high content of metals and non-metals in shales and oils is practically not considered. A significant number of them belong to the category of PTE, dangerous to the environment [3], [6].

The development of oil shale deposits, primarily in the United States, has completely refocused the international oil market in recent years. With the start of the shale revolution in 2010, American producers have become one of the key suppliers of raw materials in the world, having increased production by 10% to 9.3 million barrels per day since mid-2016, which is close to the levels of Saudi Arabia and Russia (<http://rusjev.net/2017/05/30/sanktsii-zadushili-slantsevuyu-neft-v-rf/>). Great success was achieved with the use of horizontal and/or cluster drilling. Shale formations are located mainly in the sedimentary basins as platform (Perm, Michigan, Illinois, etc.), and intra-fold (Green River, Winta, Paradox, etc.) types [3], [6].

The negative impact of this technology causes enormous harm to the environment. This facet is well known and frequently noted by many practitioners and scientists. In recent times the controversy over the environmental consequences of shale gas recovery and its role in the future of world energy has not only not abated, but has inflamed with renewed vigor (Fig. 1).

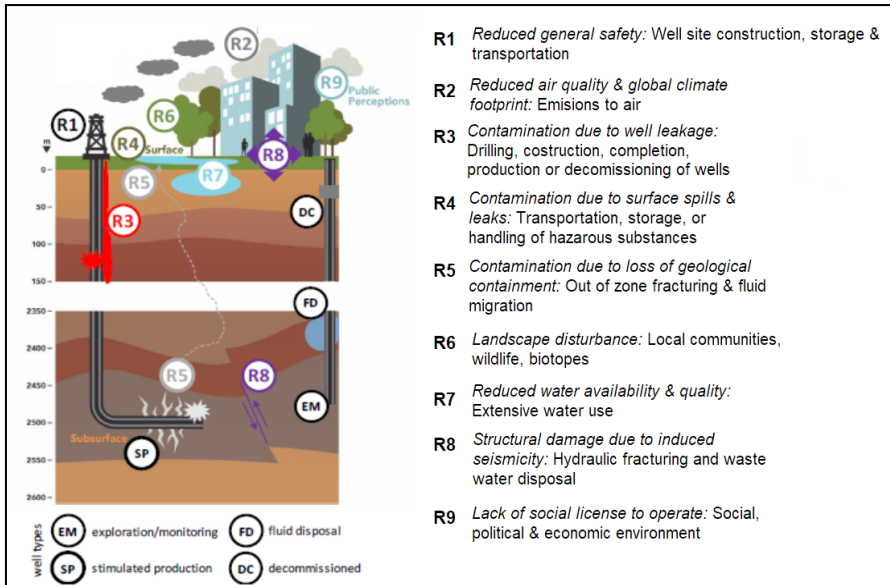


Fig. 1. Shale operation and its environmental impact [11]

In Europe shale gas/oil exploration and development is presently only permitted in 7 countries. This low level of support mostly stems from concerns related to the use of hydro fracturing and its environmental impact. Countries with a possible shale hydrocarbon resource but with no present exploration activities include: Austria, Belgium, Bulgaria, Croatia, Czech Republic, France, Ireland, Italy, Portugal, and Sweden [2].

While the country lacks a shale-specific investment regime, Bulgaria's conventional oil and gas production terms remain attractive. Production licenses extend for 35 years, with royalties ranging from 2.5% to 30% on a sliding scale, with a 10% corporate income tax. The Economy and Energy Minister has suggested that Bulgaria's shale gas resources could be in the range of 0.3 to 1.0 Tm³ but no supporting study has been released. The Shale Gas Research Group, a newly formed consortium of Sofia University and Bulgaria's Institutes of Geology and Organic Chemistry, is conducting long-term studies of organic-rich shale deposits in Bulgaria [2]. In the sedimentary successions of the Moesian Platform in Bulgaria, four intervals dominated by organic-rich dark shale have been identified: Silurian – Lower Devonian (?) shales; Lower Carboniferous shales – Trigoraska and Konarska plays; Lower Jurassic shale sediments – Ozirovo Formation (Bucorovo & Dolnilucovit Mbs); Middle Jurassic shales – Etopole Formation (Stefanets Mb). From the estimated 4 targets for shale gas only the Lower Carboniferous shales (in

the western zone) and both Jurassic shale intervals may present a moderate interest [2]. The main target in the Moesian Platform is the Jurassic Etropole Shale, considered the main petroleum source rock in northwest Bulgaria. In particular, its organic-rich lower portion, the Stefanetz Member, contains thick, carbonate-rich (40-50%) black shale with interbeds of marl and limestone. It was deposited in a marine environment and seems similar to the Upper Jurassic Haynesville Shale. TOC ranges from 1.0% to 4.6%, with Type II kerogen predominating. The Etropole Shale generally ranges from 2.5 to >5 km deep and is over-pressured in much of the region, with an elevated pressure gradient of 0.78 psi/ft. Thermal maturity falls in the oil window in the north, increasing to wet and dry gas in the south near the Balkan thrust belt (Ro 1.0% to 1.5%) [3].

With a fairly detailed coverage of all the advantages and disadvantages of horizontal drilling of shale plays, and in particular the negative environmental consequences of hydraulic fracturing, the problem of the TE composition of both shales and shale oil is practically not addressed. However, when developing and extracting oil and gas resources of shale formations, it is necessary to take into account the large concentrations of metals and nonmetals in the formations.

RESULTS AND DISCUSSION

About 15-20% of raw materials produced by HC already contain in their composition toxic TE in quantities exceeding their safe level, and the volumes of its production increase with the years. Hg, Cd, As, etc. are the most migratory-mobile and volatile of them. Among the strongly chemically bound in complex organometallic compounds in HC include V, Ni, Co, Cr, Cu, Zn, and other biologically inert elements in oil and natural bitumen. However, they are actively dangerous in the microdispersed state after anthropogenic impact on raw materials, especially at high-temperature (>450oC). Actinides, regardless of the bond strength with molecular structures of HC, are considered actively dangerous in any state. Therefore, the content of such highly toxic and volatile elements as Cd, Hg, As, Se, Mo, etc. should be assessed at the preliminary stages of the development of any HC deposits, including shale deposits [7], [9].

Thermal effects on the reservoir, increases in pressure, and injections of chemical reagents during hydraulic fracturing with large numbers of perforations over long horizontal sections can lead to the release of organoelemental compounds and possibly volatile metals into the environment. Thus, it is known that thermochemical methods, such as in-situ combustion during the development of vanadienous naphthide reserves, are not acceptable given the significant losses of metals in the reservoir and also because of the possible entry of V and Ni into the overlying aquifers used for water supply of the population. Similar results have already been recorded in sections of in-situ combustion of the Karazhanbas field, from the analysis of reservoir water samples of wells in this section. The possibility of mass transfer of ore and organic material by pore waters, pressed from clay rocks with a high organic matter (OM) content under conditions of geodynamic loads, is confirmed by experimental studies on the compaction of oil shales (kukersites) and the separation of pore waters significantly enriched by TE [1].

Let us consider and estimate in greater detail the content of TE in black and combustible shales. Shales are rocks of mixed lithologic composition, consist of aleuritic and pelitic fractions, and contain schistose and a high content of OM. The permeability of shales, as a rule, is below 1 mD, with the minimum being 0.01-0.001 mD.

The calculated concentration coefficients (for the whole mass of Qi and for the mineral matter, the ash QiA), representing the ratio of elemental content in shales to its Clarke (K) in clays, allow us to evaluate the processes of their concentration in shales [9]. Table 1 shows typomorphic elements (according to [4], these are the elements for which $Q_i > K$) in the shales of different regions (according to analytical data [5], etc.).

Table 1. Typomorphic elements of caustobioliths

Caustobiolites	Typomorphic TE*	
	On a dry weight basis $Q_i > 1.4$	On a mineral matter basis (on the ashes) $Q_{iA} > 2.0$
Coal	Au, Se, Hg, Re, Ge, As	Au, Se, Hg, Re, Ge , As, W, Mo, Be , (B, Pb), U, Ag, Gd
Combustible shale	Se, Hg, (Re, Cs), (Ce, Sc, Nb)	Se, Hg, (Re, Cs), Ce , Sc , Nb , Hf , B, Zn, (W, Ge)
Black shale	Re, Se, (Ag, Mo), Hg, (Cs, As, Au, U)	Re, Se, (Ag, Mo), Hg, (Cs, As, Au, U), (Zn, W, V), Ge
Oil	–	Hg, Mo, Se, V , Au, Ni , Ag, Cs, Zn, As, Co , U, Cu , Ga , Cr , Rb

* Highlighted in bold are the TE that are typomorphic only for one type of caustobiolyte. The TE are shown in ascending order of Q_i and Q_{iA} .

Detailed averaged data for 36 TE given in Table 2 confirm the increased concentration of TE in shales (the content of many ore elements is higher than 100 ppm).

Table 2. Distribution of averaged TE content in mineral matter of shale

An object	Concentration of TE in shales (by decades), ppm						
	< 0.01	0.01–0.1	0.1–1.0	1.0–10	10–100	100–1000	>1000
Black shale	Au		Hg, Re, Ag	Ge, W, Be, U, Hf, Th, Sn, Cs, Se	Sc, Nb, Co, Ga, Pb, Y, Mo, As, La, Li, Cu, Ce, B, Rb, Ni, Cr	Zr, Sr, Zn, V, Mn, Ba	Ti
Combustible shale	Re, Au	Ag	Hg	Ge, Mo, W, Be, U, Hf, Th, Sn, Cs	As, Se, Sc, Nb, Co, Ga, Pb, Y, La, Cu, Li, Ni, Ce, Cr, Zn	Rb, Zr, B, V, Sr, Mn, Ba	Ti

In Figure 2, using the Periodic Table of D.I. Mendeleev, the author presents a comparative average characteristic of the concentration of TE in on a mineral matter

shale relative to Clarkes clay rocks. Four gradations of a statistical assessment are allocated. An analysis of these data emphasizes the wide diversity of the composition of TEs in shale plays. The group of elements enriching shale includes rock elements, iron groups, metallic, rare, metalloid, and radioactive.

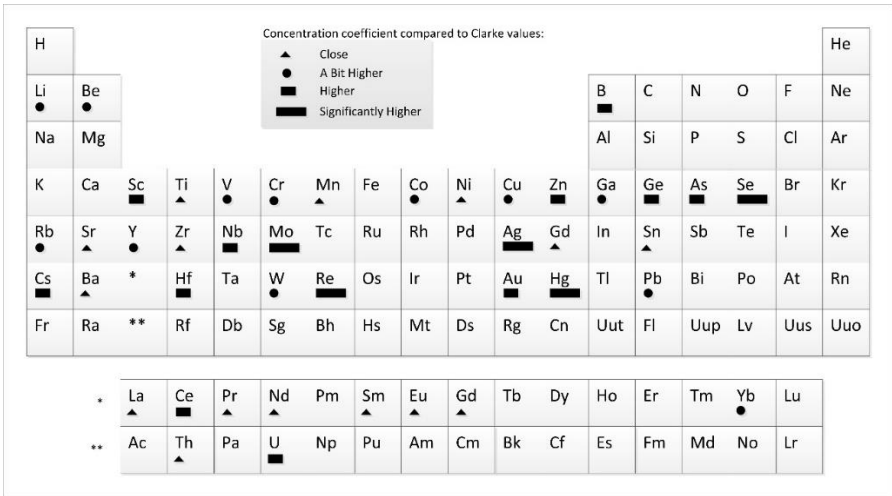


Fig. 2. Concentrations of elements in shales relative to Clarkes

Legend: Close ($Q_{IA}=0.6-1.4$); A Bit Higher ($Q_{IA}=1.4-2$); Higher ($Q_{IA}=2-5$); Significantly Higher ($Q_{IA}>5$)

The maximum enrichment values are characteristic of elements that are highly mobile in the Earth's crust (Hg, Se, Mo, As, Re, Ag, Sc, Ce, etc.). The enrichment values in some cases turn out to be similar to the concentrations of elements in ore deposits, which makes it possible to use shale conjunctly, i.e. as a potential source of a number of ore elements.

Different concentrations of elements in shales of various basins of the world are shown in Figure 3.

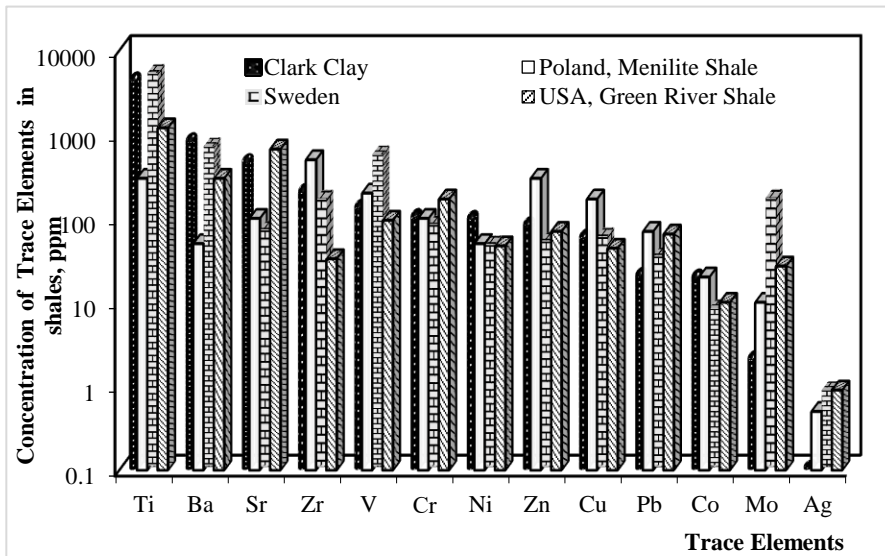


Fig. 3. Distribution of TE in shale of different regions (to analytical data [5], [3], [12]).

The contents of the following ore elements are higher than Clarkes of in shales: in menilite shales of the Polish Carpathians – Zr, Zn, Cu, Ag, Mo, V; in shale formations of Green River (USA) – Sr, Cr, Pb, Mo, Ag; Sweden’s Cambrian dictionemic shales – V, Pb, Mo, Ti, Ag. Analysis of the contents of a large group of TE in shale of the Barnett Formation (USA) also indicates high concentrations of a number of PTE in them: V, Ni, Rb, Fe, Ti. Data on high TE concentrations in the Bazhenov Formation of Western Siberia are also given (in ppm): Au (0.035–0.02), Pt (0.013–0.005), Ni (336.7, which is higher than the values for ordinary clay rocks by a factor of 5.3), Mo (264.5, higher by a factor of 9), Co (30.3, higher by a factor of 2.6), U (66.5), Th (5.0), and K (0.81). It should be kept in mind that the content of elements in the OM shale can be even higher. So, for example, in the Domanic deposits of the Volga-Ural bitumoids, the content of V reaches (ppm) – 1400-1700, and Ni – 1200 [9].

As can be seen from the above material, not all shales are equally rich in PTE. A comparison of TE concentrations in slates of different ages showed that it is impossible to reveal a clear correlation with the age of shale-bearing formations. This is due to the influence of other factors, namely: the facies type of deposits, the geostructural position of the shale basin, and sources of ablation. The maximum TE content of shale is often confined to platform formations (Domenic bituminous rocks of the Russian Platform, Bazhenov Formation of Western Siberia). However, some clay-shale formations of geosynclinal regions can also be enriched in TE (the Baisunsky deposit of Uzbekistan and Suzak shales of Tajikistan). This confinement of increased TE concentrations in caustobioliths is related to the fact that, in these

basins or their parts, favorable opportunities were created for both syngenetic (with maximum manifestation of transport, resource, barrier, environment-forming, and other functions of living matter and OM) and epigenetic (temperature, hydrothermal, and geodynamic) accumulations of TE in the studied caustobioliths.

Data on the correlation between the TE composition of clays, coals, and oil shales with the chemical composition of the continental crust are presented in Table 3.

Table 3. The relationship of the ME composition of caustobioliths with the chemical composition of a number of geo-reservoirs.

Clays and caustobioliths	Continental crust			Biota			
	upper	middle	lower	plants		animals	
				marine	terrestrial	marine	terrestrial
Clay	*0.90 /41	0.85/40	0.83/41	0.77 /28	0.72/29	0.53/23	0.46/28
Coal	0.84 /41	0.76/40	0.78/41	0.78 /28	0.71/29	0.48/23	0.50/28
Black shale	0.82/41	0.84 /40	0.80/41	0.78 /28	0.75/29	0.57/23	0.56/28
Comb. shale	0.84 /35	0.76/34	0.79/35	0.76 /28	0.74/29	0.54/23	0.55/28
Oil (average)	0.60/37	0.58/36	0.63 /37	0.61 /26	0.58/29	0.59/24	0.54/28

** The value of the correlation coefficient / the number of used values of the logarithms of element concentration; the maximum values in a row are marked in bold*

Calculations of the correlation coefficients (r) between the logarithms of the average TE contents [8] show a closer relationship between the TE composition of clays, coals, oil shales (obviously upper crustal formations), and the TE composition of the upper continental crust ($r = 0.84$ - 0.90) compared to the TE composition of the lower continental crust ($r = 0.79$ - 0.83). The TE composition of black shales has a more notable relationship with the TE composition of the middle crust ($r = 0.84$). The formation and reformation of black shales takes place at great depths (unlike the formation of oil shales) and over a longer period of geological time. Therefore, the effect of deep penetrations with a set of so-called deep TEs is more likely. In contrast, the TE content in oils is more closely correlated with the TE composition of the lower continental crust ($r = 0.63$) compared with the upper ($r = 0.60$) and middle (0.58) ones. Moreover, the correlations obtained for the average TE of the oil composition with the crust composition turn out to be significantly lower than the correlations for clays, coals, and shales, which indicates the greater complexity and possible polygenicity of the formation of its TE composition. High correlation dependencies are revealed between TE compositions of caustobioliths and biota of various origin. The maximum figures (up to 0.78) are characteristic of the relationship between the TE composition of caustobioliths and the TE composition of marine plants. The correlation results indicate that deep components play an important role in the genesis of HC.

CONCLUSION

This research considered the content of TE, including PTE (V, Ni, Mo, Co, Cd, As, Hg, Cr, U, etc.) in shale plays and deposits in various regions of the world (Breznikskoye, Pirinskoye, Borovdolskoye, Radomirskoye in Bulgaria; Barnett Formations, Green River in USA; Meniliths in Ukraine and Poland; Bazhenites in Western Siberia; Domanikits in Volgo-Ural region of Russia; Narke in Sweden). Some of those concentrations significantly exceeded Clarke contents. For example, Bulgaria shales are very rich in Mo and U. Uranium content can reach values from 28.5 to 50 ppm. The correlation of TE content between shales (combustible and black) and the upper continental crust was found to be higher than between shales and the lower continental crust. Hence, the author concludes that the TE composition of shale rocks has received greater contribution from the matrix of the OM of sedimentary rocks than from the deep zones of the earth's crust. About 15–20% of the extracted HC contain PTE in the amounts that exceed their safe levels, and the production volumes continue to increase over the years. The most migratory and volatile of them are Hg, Cd, and As. V, Ni, Co, Cr, Cu, Zn are strongly chemically bonded in complex organometallic compounds in HC but toxic in the micro-dispersed state after technogenic impact on the HC. Actinides, regardless of bond strength with the molecular structures of HC, are actively dangerous in any state.

Thus, the development of shale formations via horizontal drilling, with the use of hydraulic fracturing in order to improve economic indicators, remains a priority worldwide. However, with all the aforementioned advantages in the development of shale deposits by this method, it is necessary to take into account the adverse environmental effects of the high concentrations of PTE (V, Ni, Mo, Zn, U, Hg, As, etc.) in shales and oils due to their possible release into the environment. In the development of an integrated technology for the processing of shale with the recovery of gas, oil, and metals, additional studies are required for evaluating the trace element composition of both shale deposits and their naphthide components in order to avoid negative environmental consequences.

ACKNOWLEDGEMENTS

This work was carried out as part of a state assignment on the topic “Development of the scientific and methodological basements of the search for large hydrocarbon accumulations in non-structural traps of the combined type within platform oil and gas basins”.

REFERENCES

[1] Abramova O.P., Abukova L.A. Clay sediments of sedimentary basins are generators of naphthydo- and ore-forming fluids. Black shales: geology, lithology, geochemistry, significance for the oil and gas complex, prospects for using as an alternative hydrocarbon raw material: Proc. All-Russian Sci. and Pract. Conf. Yakutsk: Akhsaan. 2015, pp. 9-11.

[2] Anthonsen K.L., Schovsbo S., Britze P., Overview of the current status and development of shale gas and shale oil in Europe. Report T3b of the EUOGA study (EU Unconventional Oil and Gas Assessment) commissioned by JRC-IET to GEUS. September 2016, 133 p

[3] Johnson R.C., Birdwell J.E., Mercier T.J., Brownfield M.E. Geology of Tight Oil and Potential Tight Oil Reservoirs in the Lower Part of the Green River Formation, Uinta, Piceance, and Greater Green River Basins, Utah, Colorado, and Wyoming. Scientific Investigations Report 2016. Geological Survey, Reston, Virginia: 2016, U.S. 75 p.

[4] Ketris M.P., Yudovich Ya.E. Estimations of Clarkes for carbonaceous biolithes: World averages for trace element contents in black shales and coals. *Int. J. Coal. Geol.*, vol. 78, № 2, pp.135-148, 2009.

[5] Kler V.R., Nenakhova F.Ya., Saprykin F.Ya. et al. Metallogeny and geochemistry of coal-bearing and shale-bearing strata of the USSR. Regularities of concentration of elements and methods of their study. Moscow: Nauka Publ. 1988, 256 p.

[6] Nemeč R. Thriving in a Major U.S. Shale Play the Bakken Unpacked. *Pipeline and Gas Journal*. November, pp. 56-60, 2016.

[7] Parviainen A., Loukola-Ruskeeniemi K. Environmental impact of mineralized black shales. *Earth-Science Reviews*, 192, pp. 65-90, 2019.

[8] Punanova S.A., Rodkin M.V. Comparison of the contribution of differently depth geological processes in the formation of a trace elements characteristic of caustobiolithes. *Georesursy = Georesources*, 21(3), pp. 14-24, 2019.

[9] Punanova S.A., Shpirt M.Ya. Ecological Consequences of the Development of Shale Formations Containing Toxic Elements. *Solid Fuel Chemistry*, 2018, vol. 52, No. 6, pp. 396–405, 2018.

[10] Technically Recoverable Shale Oil and Shale Gas Resources: Other Eastern Europe. *Independent Statistics & Analysis*. U.S. Department of Energy. Washington, DC, September, 2015.

[11] ter Heege J. How Sweet is European Shale? A Story about the Uncertain Potential, Problematic Recovery and Public Concerns of Shale. *Gas Development in Europe*. Search and Discovery Article #70381, 2019.

[12] Voronin D.O., Panova E. G. () Chemical weathering of lower paleozoic black shales of South Sweden. *Journal of Mining Institute*, vol. 230, pp. 116-122, 2018.

THE CONSOLIDATION OF SOFT CLAY FOUNDATION GROUND USING GEOSYNTHETICS COMBINED WITH THE ELECTRO-OSMOSIS PROCESS

Eng. Florin Sebastian Mustăţea ¹

Dr. Eng. Raluca Ioana Nicolae ²

^{1,2} SC Geostud SRL, Romania

ABSTRACT

In the last decade, the construction of communication routes has intensified in Romania. As a result, many case studies related to the presence of saturated clayey soils in the foundation ground have emerged. In order to speed up the execution of highways and railways in a safely manner, the designers use different methods of improving soft clays in terms of compressibility.

The present study aims to evaluate the efficiency of an electrical current used for the vertical dewatering of a soft clay subgrade, through simple physical models. The experimental study is being performed on a laboratory scale model by using electrodes and geosynthetics for drainage, along with the vacuum technique.

The vertical drainage capacity during the electro-osmotic dewatering process, combined with preloading, drainage, vacuum and heat induction is being evaluated.

The integrated effect of these methods on the consolidation process will be analyzed for the final conclusions.

Keywords: *electro-osmosis, geosynthetics, drainage, soft clay*

INTRODUCTION

In engineering practice, a common problem is the high compressibility of the reduced consistency clay soils, having values of the IC consistency index <0.5 , according to the technical norms in force. In this context, the problem of reducing the compaction of soft clay deposits arises, because of the settling process under the loads induced by the engineering constructions. Another problem complementary to the one mentioned above is the shortening of the time period in which the settlements registered as a result of the consolidation process reach the values admitted from the point of view of the deformation limit state, as a limit state of the normal exploitation, according to the Romanian norms.

As a result, we started a series of experiments focused on the following objectives:

- study of the electro-osmosis effect on the speed of the consolidation process and implicitly, on the values of the main compressibility parameters;
- analysis of the integrated effect of other measures already known and applied in other countries, which, together with the electro-osmosis,

will lead to the reduction of the time required to complete the primary consolidation; In this way, the aim is indirectly to reduce the period of realization of the railways and road embankments and respectively, to improve the soil in order to execute the direct foundations for different types of constructions.

THEORETICAL ELEMENTS

Terzaghi's theory of consolidation

The main assumptions on which this theory is based and implicitly, the laboratory model, are the following:

- the clay is saturated;
- water and clay particles are incompressible;
- Darcy's law is valid in any horizontal section within the saturated clay layer, the total and effective unitary efforts remaining constant in value;
- during the variation of the Δ_n soil porosity, corresponding to the variation of the effective unitary effort $\Delta\sigma'$, the permeability coefficient k and the volumetric compressibility coefficient m_v have constant values;
- the clay within the model is laterally confined;
- the water circulation within the clay layer occurs only in a vertical direction.

Based on the above assumptions, the time variation of pore water pressure within the soft clay layer is generated by the following differential equation:

$$\partial u \partial z = c_v \nabla^2 u \partial z^2 \quad (1)$$

, where: c_v = consolidation coefficient; it is determined in the laboratory by compression testing – consolidation [m^2/s]; m_v = volumetric compressibility coefficient [m^2/kN].

$$c_v = k m_v w \quad (2)$$

$$m_v = \Delta V V \Delta p = \Delta H H \Delta p \quad (3)$$

In the classical theory of consolidation [1], the evolution of consolidation is expressed by the U_v degree of consolidation, which is determined by the following relation:

$$U_v = S_t S_f \quad (4)$$

, where S_t [m] is the settlement at the t time, and S_f [m] is the settlement recorded at the end of the consolidation process, which can be calculated with the following relation:

$$S_t = \Delta n \cdot H = m_v \cdot H \cdot p \quad (5)$$

The time required to consume the primary consolidation is determined by the following relation:

$$t = T_v H^2 c_v \quad (6)$$

, where T_v is the time factor that varies with the values of the degree of U_v consolidation.

After the completion of the primary consolidation process, the settlement continues under the p pressure during the secondary consolidation process. However, this settlement, compared to the settlement from the primary consolidation, is negligible.

The electro-osmosis effect on the consolidation process

In the case of normally consolidated clayey-silty deposits, with low concentrations of electrolytes in the pore water, electro-osmosis is a process by which the depth consolidation can be accelerated, a procedure not very well known and/or applied in our country(Fig. 1).

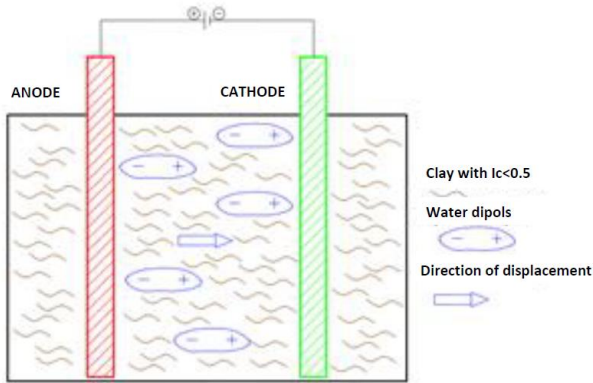


Figure 1. Principle diagram of the electro-osmotic process

If we consider only the hydraulic consolidation, then the flow filtered horizontally according to Darcy's law is:

$$Q_h = K_{hi} h \cdot A \quad [m^3/s] \quad (7)$$

, where K_h = the permeability coefficient in a horizontal direction [m/s]; i_h = hydraulic gradient; A = the area crossed in front of the moving water (m^2).

The Q_h flow can also be calculated with the following relation [2]:

$$Q_h = K_i \cdot I \quad [m^3/s] \quad (8)$$

, where K_i is the flow rate corresponding to the electric current unit between the electrodes ($m^3/s/A$), and I is the current intensity between the electrodes (A).

The flow of water removed from the volume of cohesive saturated soil between the electrodes decreases with time, as the consolidation process unfolds. The reduction of the water pressure from the Δu pores in the area of the anode, compared

to that of the cathode area, leads to the start of the filtration process from the cathode to the anode, as a result of the hydraulic gradient that appeared.

Through the measurements made within the laboratory model described in the next chapter, the main specific parameters of the electro-osmosis will be highlighted.

EXPERIMENTAL METHODS

Materials used and their properties

The soil sample used in the experiments consisted of clay-46%, silt-38% and sand-16%.

The sample was grinded, homogenized and mixed with water until a humidity of 46.94% was obtained. The soil sample was then introduced in a plastic container of 27x18x12 cm.

The electrodes used (the anode and the cathode) consisted of two carbon iron bars (OB 37), which were inserted into the ground on the median line of the sample, at a distance of 17 cm, resulting in a voltage gradient of 1.03 V / cm. The power source consisted of a auto rectifier, with power supply at 220 V / 50 Hz, the resulting voltage being 12 V / direct current.

Within the experiments carried out, a series of improvised drains, covered in Polypropylene of 270 g / m² and 1.6 mm thickness, were introduced into the soil sample (in the cathode area), to facilitate the drainage process and to accelerate the consolidation..

Experimental model

Variant 1- the phenomenon of electro-osmosis (simple) – Fig. 2

To limit moisture loss during the experiment, the plastic container was covered and the circuit was maintained for 72 hours.



a)



b)

Figure 2. Experimental model: a) installation of electrodes and connection to the power source; b) installation of drainage covered in geotextile

Variant 2- the phenomenon of electro-osmosis with preload (Fig. 3a)

For the second variant of the experiment, we chose to perform the phenomenon of electro-osmosis together with the preload. Around the anode we put a preload of 3144 g to speed up the consolidation process.

Variant 3- the phenomenon of electro-osmosis and lime columns (Fig. 3b)

In this experiment we chose to combine the phenomenon of electro-osmosis with the execution of columns of non-hydrated lime. As a result, we used the same material as in versions 1 and 2, with an initial humidity of 59.38%. We made a grid of 16 columns, which we filled with non-hydrated lime. This, by releasing heat, reduces soil moisture.



Figure 3. Experimental assembly a) for variant 2; b) for variant 3 - filling columns with lime in the experimental model

Variant 4 - increasing the efficiency of electro-osmosis by vacuum (Fig. 4)

The vacuum consolidation method has become one of the techniques used worldwide for acceleration dewatering and improvement of soft foundation ground. The suction represents the maximum pressure difference generated by the vacuum pump.



Figure 4. Experimental assembly for vacuuming

EXPERIMENTAL RESULTS AND INTERPRETATIVE GRAPHICS

Variant 1- he phenomenon of electroosmosis (simple)

After about 15 minutes from the beginning of the experiment, the effects of the electro-osmosis phenomenon were visible, forming hydrogen bubbles around the cathode. After almost 2 hours, the process of electroosmosis began to take place, this being observed by the fact that the water migrated from the anode to the cathode, forming a film of water near the cathode (Fig. 5a). During the experiment we introduced at different points a thermometer to measure the temperature variation from anode to cathode (Fig. 5b). The temperature around the anode was 22.3°C, and around the cathode 24.3°C (Fig. 6).



Figure 5. Experimental model: a) the film of water formed around the cathode; b) temperature measurement in the soil sample

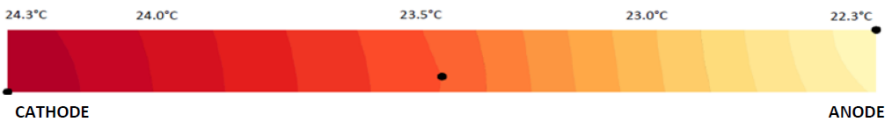


Figure 6. Temperature variation between anode and cathode, measured at the base of the sample

Following the results we can state the following (Fig. 7):

- the humidity difference between anode and cathode is 13.71%;
- the difference of humidity at the anode against the initial humidity is 9.13%;
- at the cathode, the humidity increased by 4.58% compared to the initial humidity.

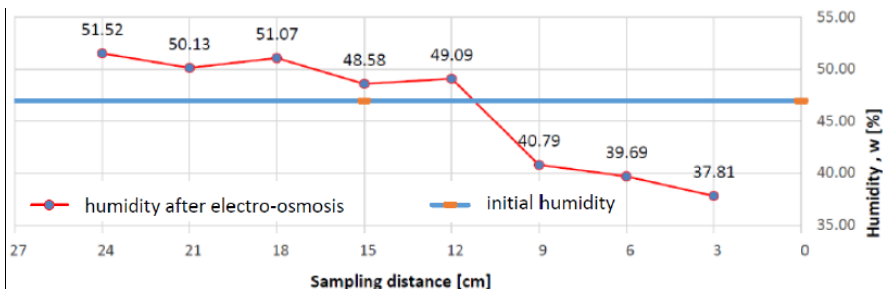


Figure 7. Variation of moisture in the sample

In order to be able to observe the improvement of the foundation ground by the phenomenon of electro-osmosis, we also performed “vane test” tests. We obtained an initial cohesion value of 0.5 kPa and a value of 5.1 kPa following the consolidation process. Also, following the experiment, the anode oxidation was observed, losing 0.36 g, which represents about 0.49% of the initial mass.

Variant 2- the phenomenon of electroosmosis with preload

We followed the same steps as in variant 1 with only one difference, namely, the initial humidity of the material was 80.21%. Following the results we can state the following (Fig. 8):

- the humidity difference between anode and cathode is 56.99%;
- the difference of humidity at the anode against the initial humidity is 40.58%;
- at the cathode the humidity increased by 16.41% compared to the initial humidity.

Comparing the results obtained in both cases, we can say that the results obtained in case 2 are more favorable. Water drainage around the anode is performed faster, accelerating the consolidation process.

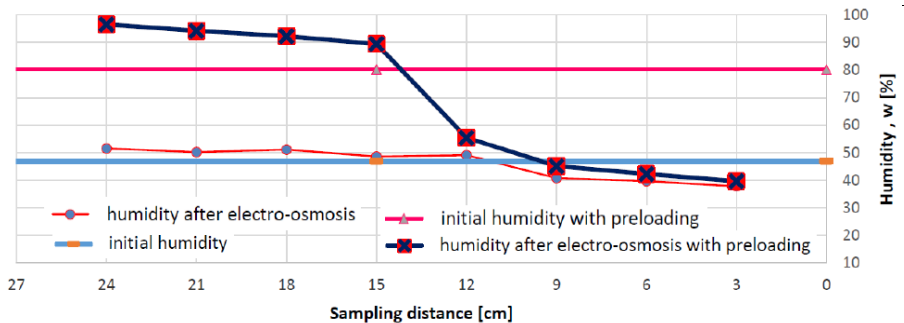


Figure 8. Variation of moisture in the sample

Variant 3- the phenomenon of electro-osmosis and lime columns (Fig. 9)

Around the anode, the humidity in the columns was very close to the initial humidity of the sample, respectively 59.24%, and in the cathode area, it was 87.26%. In this variant, compared to the two above, the humidity obtained in the 8 measurement points did not exceed the value of the initial humidity, so the lime brings an increase of the bearing capacity. Following the results we can state the following:

- the difference of humidity between anode and cathode is 10.40%;
- the difference of humidity at the anode against the initial humidity is 17.03%;
- at the cathode, the humidity decreased by 6.62% compared to the initial humidity, in the case of the two variants above, the result being an increase in humidity.

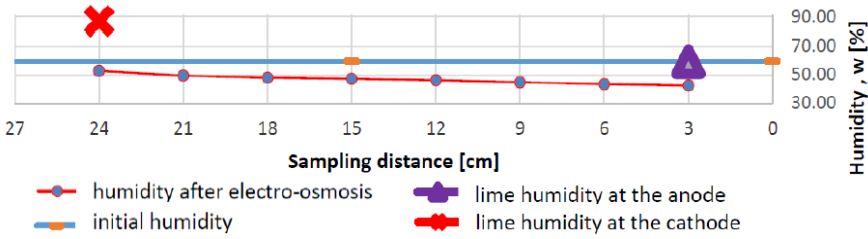


Figure 9. The effect of quicklime on the variation of moisture in the sample

Variant 4- increasing the efficiency of electro-osmosis by vacuum

Due to the suction effect on the surface of the soft clay layer and the cancellation of the atmospheric pressure, the drainage of the clay water in a vertical direction was hastened. As a result, the flow of water that is eliminated by electro-osmosis increases considerably. According to previous research [3], the reduction of the humidity for the 17 cm distance between the anode and the cathode, corresponding to the experimental model, is 6%. Figure 10 shows how the moisture in the clay layer varies through this process in the form of a parabolic curve with the maximum value in the vertical direction of the vacuum point. It is important to note that the effect of the vacuuming process is felt in the first stages of an experiment, which helps to release the free water from the land mass. The elimination of bound water content from the land can be done further by applying electro-osmosis.

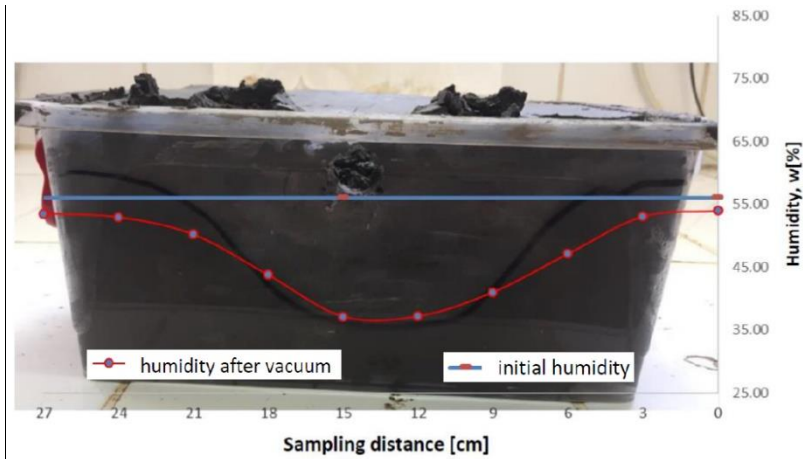


Figure 10. Humidity variation in the sample superimposed over the experimental model

CONCLUSION

According to the conclusions of several researches in order to increase the efficiency of the electro-osmotic process, other processes such as vacuuming and lime use can be used complementarily. In the first case, the major effect consists in the faster elimination of the water resulting from dehydration by producing a

section (negative pressure), which will cancel the atmospheric pressure. In the second case, by the chemical reaction accompanying the hydration of the lime with heat release, the moisture in the clay volume decreases and it acts positively on the mechanical properties of the clay (compressibility and shear resistance). During the research on the efficiency of the electro-osmotic process, we also considered these aspects. The granulometric composition of saturated cohesive soil mainly influences the effect of electro-osmosis. Thus, if the clay fraction component is large (over 50%), the effect is smaller than in the case of silty clays, the initial osmotic pressures being lower. Therefore, according to the model, the efficiency of the electro-osmotic process can be effected by the simultaneous use of the preload with positive or negative pressure (vacuuming) and, respectively, the treatment of the land with lime. According to the graph in figure 11, the positive contribution of the combination of the effect of the electro-osmosis with other processes from at least two more important aspects is evident:

- increasing the flow of water eliminated/consumed by the exogenous chemical reaction typical of lime hydration;
- increasing the shear strength of saturated, soft clay.

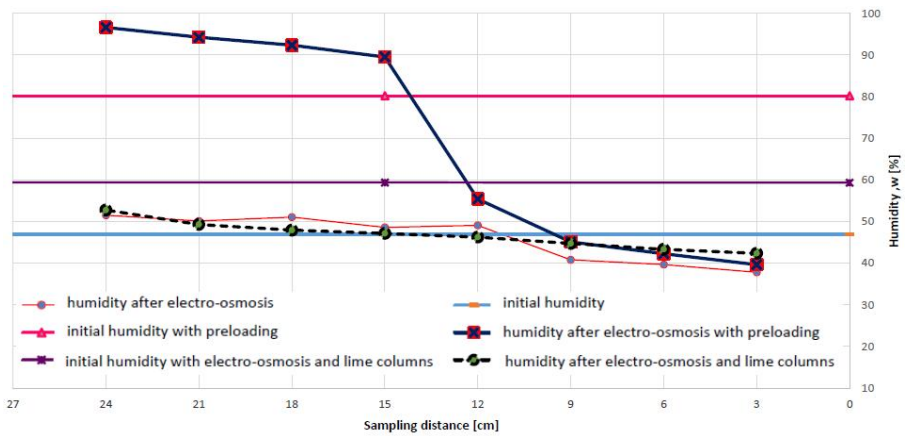


Figure 11. Moisture variation in the sample in the analyzed cases

REFERENCES

[1] Terzaghi K., Structure and volume of voids of soils, in „Erdbaumechnik auf bodenphysikalischer Grundlage”, Deuticke, Wien; Translated by A. Casagrande in From Theory to Practice in Soil Mechanics, New York, John Wiley and Sons, 1925;

[2] Zamfirescu Fl., Comşa R., Matei L., Clay rocks in engineering practice (in Romanian), Editura Tehnică, 399 pag., 1985;

[3] Shen Y., Qiu C., Li Y., You Y., Performance of Conductive Plastic Vertical Drainage Board Under Vacuum Preloading Combined with Electro-osmotic

Consolidation, In: Bian X., Chen Y., Ye X. (eds), Environmental Vibrations and Transportation Geodynamics. ISEV 2016. Springer, Singapore, 2018.

THE VARIATION OF TEMPERATURE OF DIFFERENT OIL RESERVOIR DENSITIES EXPLOITED BY THERMAL METHODS

PhD Student Eng. Ionescu (Goidescu) Nicoleta Mihaela ¹

Prof. Dr. Eng. Vasiliu Viorel Eugen ²

Prof. Eng. Onutu Ion ³

^{1, 2, 3} University of Oil and Gas Ploiesti, Romania

ABSTRACT

Enhanced oil recovery (E.O.R) is oil recovery by the injection of materials not normally present in the reservoir. Thermal methods such as the steam injection process are the best heavy oil recovery methods. Improvement of mobility ratio in the reservoir and economic recovery from heavy oil reservoirs depend mainly on reduction of heavy oil viscosity. For a steam injection process should consider the heat and mass transfer.

Heavy oil reservoirs contain a considerable amount of hydrocarbon resources of the world. Meanwhile, further demand for oil resources in the world reduction of natural production from oil reservoirs, and finally price of oil in recent years have attracted notices to production methods from heavy and extra heavy oil reservoirs. High viscosity and great amounts of asphaltene in these hydrocarbons make difficulties in extraction, transportation, and process of heavy oil.

In Romania, there have been numerous theoretical and laboratory researches, as well as site experiments on the application of secondary recovery methods, Romanian specialists having a wide experience in this field

Keywords: *Thermal, thermodynamic, viscous, mobility, conductivity*

INTRODUCTION

Steam injection is the most effective method for viscosity reduction of heavy oil.[1] Meanwhile, modeling of steam injection wells for continuous estimation of pressure and temperature as a function of depth and time is crucial for well design, planning of steam injection projects and data gathering for reservoir management. Once the steam is injected into the good design, both pressure and temperature of the injected steam and accordingly the densities of water and steam phases will change. These changes are due to heat exchange between steam and cold formation surrounding the well, the friction between steam and the inner tubing surface and variation of hydrostatic pressure along the depth. More importantly, the quality of injected steam will drop due to heat loss from the wellbore system towards the cold formation. Multiphase nature of flow inside the wellbore, complex heat transfer mechanisms between the wellbore and the surrounding medium make the entire system intricately coupled and extremely difficult to solve.[2], [3].

Thermal energy is transferred to the thermodynamic agents (gas, hot water, steam – by injection of hot fluids) and transported by surface pipes, injection wells and then –through the reservoir (by steam injection and underground combustion).The transformation provide necessary energy for transporting the oil from the reservoir to the surface .The effect of heat on heavy and viscous oil is very important and there is no exploitation technology to rival with thermal methods. The use of thermal recovery permits: 1. Primary exploitation of heavy and/or viscous oil 2.bituminous sand exploitation.3.secondary or tertiary recovery of oil from energy exhausted reservoirs.

During exploitation by steam injection or underground combustion appear physical and chemical modifications including changes in the thermal conductivity. The thermal conductivity of an oil reservoir can be estimated by computations, using idealized models, or by expressing this property as a function of other properties of the reservoirs: density, porosity, permeability.[4], [5]

To measure the thermal conductivity of an oil reservoirs in its initial stage are available in literature [6], [7], [8]

This paper presents results of experimental studies regarding the estimation of the thermal conductivity in the following conditions :

- Sample composed of rock and fluids, combustioned in laboratory
- Sample of fluids taken directly from the oil fields from Romania

METHODS

The laboratory experiments used installations from the laboratories of Oil and Gas University Ploiesti and samples fluids and rocks from Romania fields situated in different areas.

Depending on the density of the crude oil , a classification of the crude oil was made and can be seen in table 1.

Table 1 Oil classifications

	Relative density		Oil viscosity in res condition
	Density at 15°	API (15°)	mPa*s
Slight oil	<0.870	>31.1	-
Medium oil	0.870...0.920	31.1-22.3	-
Heavy oil	>0,920	<22.3	<10000
Bitumen	>1	<10	-
Tar sands	-	-	> 10000

The flow properties are better described by the viscosity. As such some crude oil may be heavier , but have a lower viscosity than the light ones.

For the experiments have been used 4 samples of oil from different oil fields with properties presented in table2.

Table 2 Characteristics of the fields

Field	Reservoirs		Rock properties			Oil properties	
	Thickness	Depth	Permeability	Porosity	Oil Sat	Density	Viscozity
	m	m	mD	%	%	Kgf/dm3	mPa*s
A	10	<1500	120	22	66	0.8	10
B	15	1100	130	20	65	0.85	6.4
C	20	1300	110	23	70	0.91	70
D	25	1000	145	25	68	0.98	> 2000

In order to carry out the experiments, a combustion mini-cell was constructed, made of steel with two hermetically sealed caps .It was filled with two types of sands : one with porosity 23% and bituminous sand. Bitumen, dense, highly viscous petroleum based hydrocarbon that is found in deposits such as oil sands and pitch lakes.[9], [10]

Bitumen is defined by the U.S Geological Survey as an extra-heavy oil with an API gravity less than 10° and a viscosity greater than 10000 centipoise. At the temperatures normally encountered in natural deposits , bitumen will not flow ; in order to be moved through a pipe , it must be heated and, in some cases diluted with a lighter oil.It owes its density and viscosity to its chemical composition-mainly large hydrocarbon molecules known as asphaltenes and resins, which are present in lighter oils but are highly concentrated in bitumen.

METHODOLOGY

The experiments were conducted in 4 different days for different densities of the oil and follow the same procedures for every experiment following the safety rules to avoid possible accidents.

For better understanding of experiments was necessary to review the specific literature from Romania about graphs represent the variability of temperature, time and densities for different oils .[11]

Have been decided to built in the end of the experiments, a ternary diagram which will displays the three variable used: time, temperature and densities.

These diagrams were built using specific AutoCAD(CAD) software which is a computer aided design that architects, engineers and construction professionals rely on to create precise 2D and 3D drawings.Draft and edit 2D geometry and 3D models with solids, surfaces and mesh objects.[12]

The figure 1 shows a scheme of the installation design and made by the author.

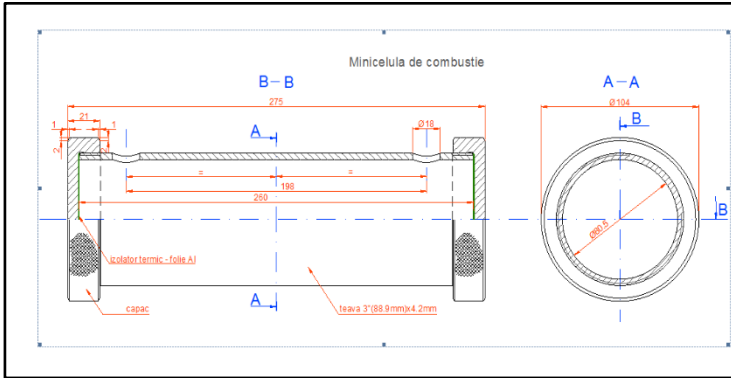


Figure 1 The installation for preparing the sand combustion

As was specified before, the author organized 4 experiments (because of the 4 oil densities).The experiments follow the same steps presented below:

1. The .mini-cell was filled with about 500 gr of sand (porosity 23%)
- 2.Sand was saturated with oil of different density (every experiment with specific density)
3. The cell fixed on a support, added 2 stone thermometers left and write (Figure 2)
4. On the right side a heat source was applied and starting to read the temperature T1(right) and T2 (left).Than recorded into a table.
5. For each experiment was constructed a ternary diagram with the variable T1, T2, time elapsed between two temperature reading.



Figure 2 : Oil samples, Mini-Combustion cell , 2 stone thermometers

The ambient temperature was every day 24 °C.Experiments were continuously monitored to register the temperature till 200 °C.(Figure 3)

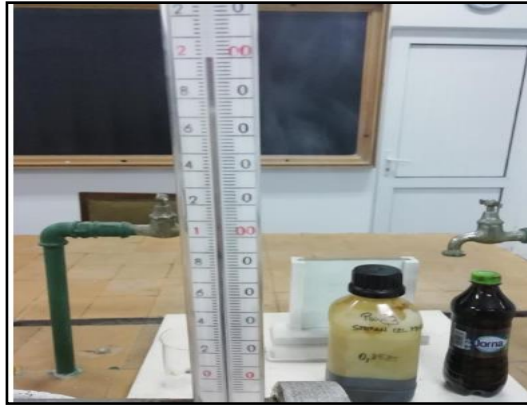


Figure 3: Maximum of temperature 200 °C

When reaching the temperature of 100 °C was observed that the oil started to boil for a short time and was supposed is because of water presence in the sand.

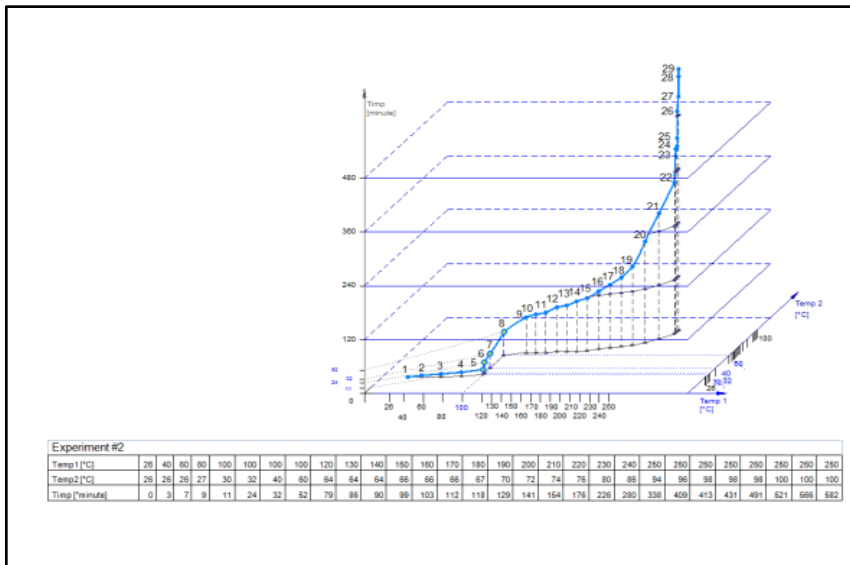
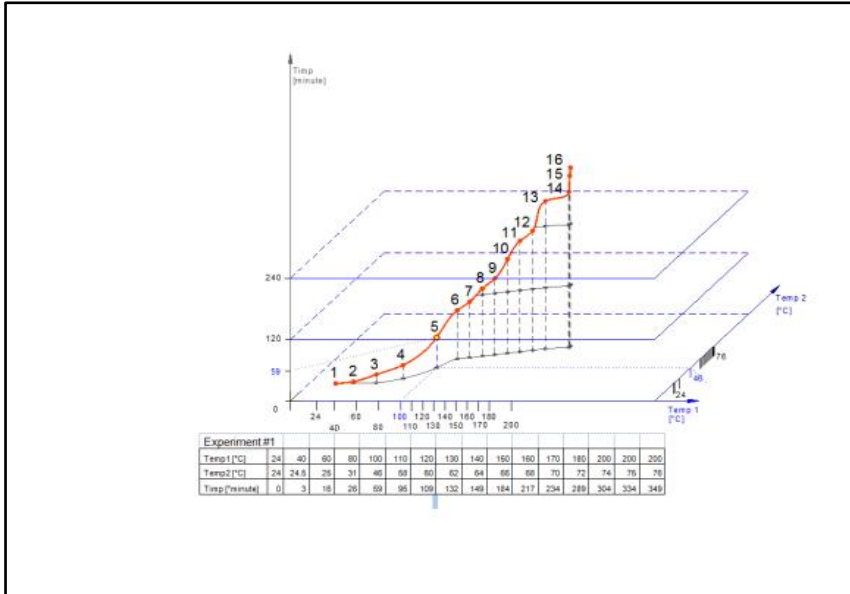
Another observation common to all 4 experiments was that around 180 °C appeared a strong smell of burnt hydrocarbons.

RESULTS

These experiments aimed to assimilate more clearly the notion of thermal conductivity, which is a characteristic property of each body, which can be determined experimentally or can be calculated with different formula. It has been found that heat transport can occur:

Electronic-the electrons move from the high temperature areas to the low ones , tranfering with them the termal energy

The heat transfer is dependent of oil density (experiments 1- 4), sand porosity and the variation in time can be seen on the graphs.



Graphic variation of temperatures -Experiments 1,2

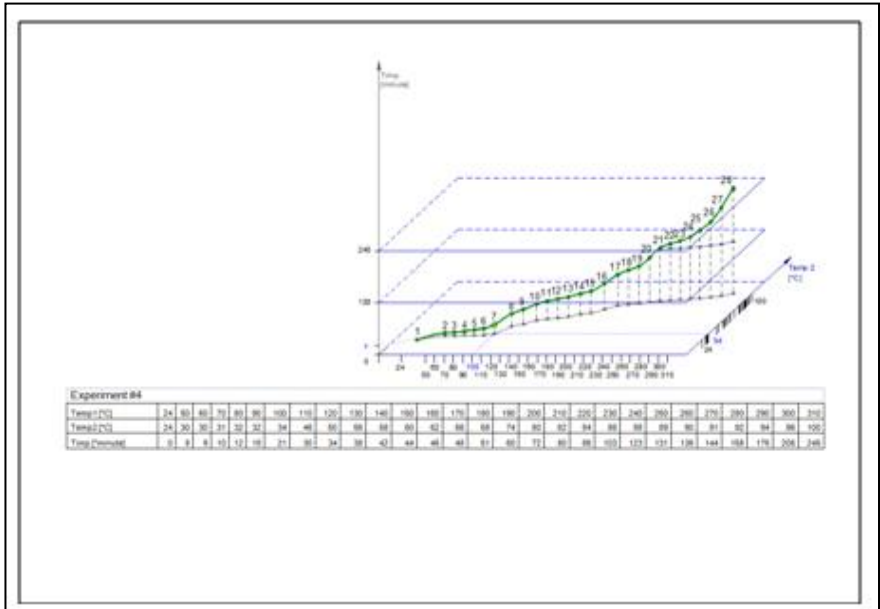
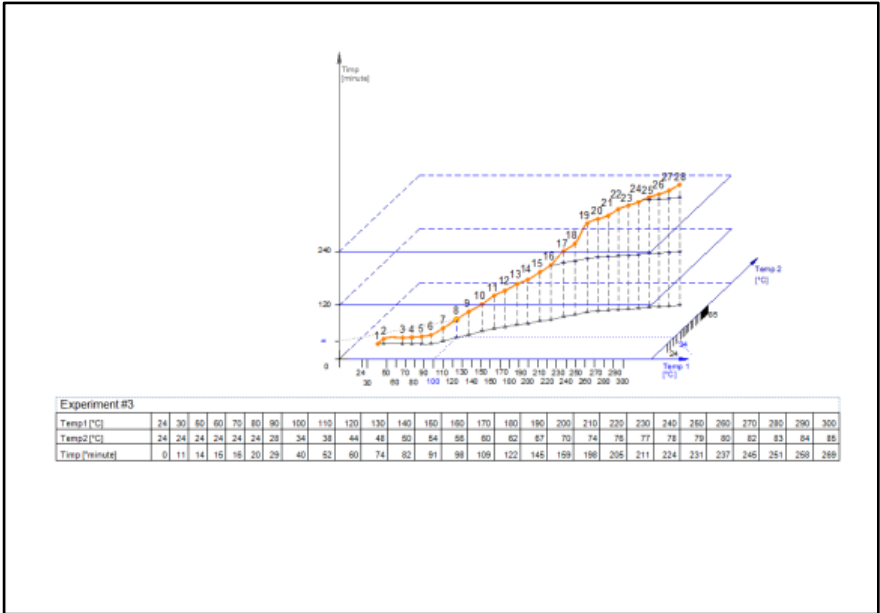


Figure 5 – Graphic variation of temperatures -Experiments 3,4

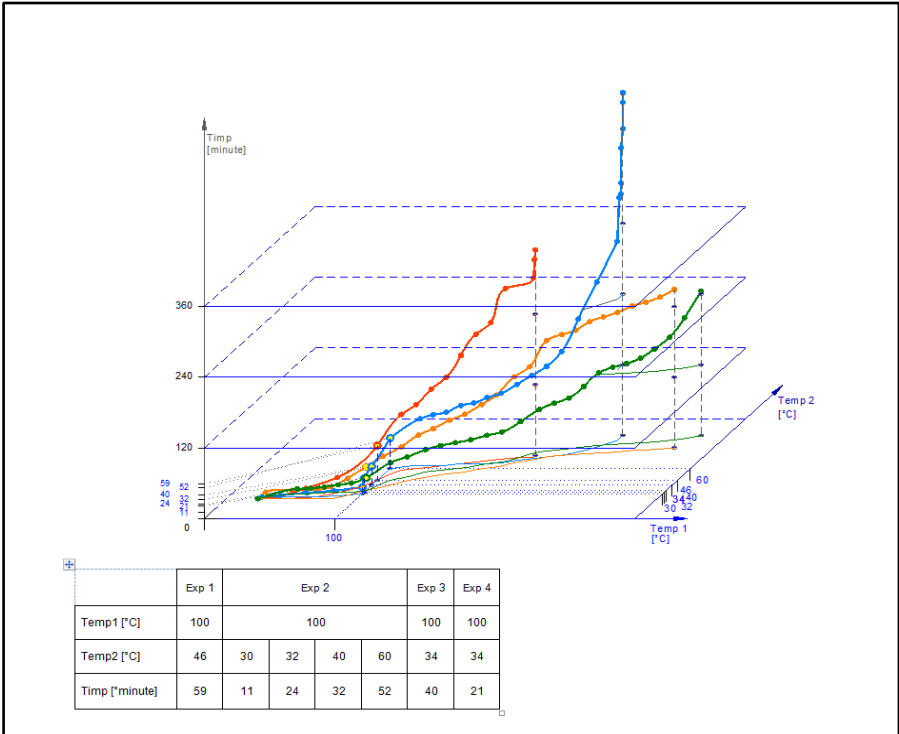


Figure 6 Graphic variation of temperatures – Experiments 1-4

It is known that the thermal conductivity varies with the nature of the body, with its state of aggregation, with the humidity of the body, with the nature and concentration of impurities contained in the body, with the porosity.

Thermal conductivity is a characteristic property of the environment, analogous to electrical permittivity, molecular diffusion or electrical conductivity. Solids and fluids that make up a hydrocarbon deposit represent a porous medium saturated with fluids. In a permanent thermal conduction regime, a porous medium saturated with fluids can be assimilated to a continuous equivalent medium for which the thermal conductivity is defined as a tensor. This depends of the conductivity of each phase.

CONCLUSION

Information technology in the oil and gas complex can be widely used at all stages, namely oil and gas exploration, extraction, transportation and processing.

Improvement of production in heavy oil reservoirs depends on reducing oil viscosity, and understanding better the heat transfer. The technologies of construction of „intelligent” injection and production wells are the most important tasks in actual fields from Romania. In the future, special attention should be paid to the development of special mature fields from Romania to ensure the automation of basic processes in the design and technological control over exploratory drilling.

The task of cost reduction in production, transportation and processing of hydrocarbons provides an opportunity to analyse the thermal methods and to apply the best method.

The role of experiments were to visualise the variation of heat transfer inside a mini-combustion cell. Have been used 4 different samples of crude oil of different densities: low, medium, high values. (500ml for every sample).The cell was completed with quartzite sand and after saturated in every experiment with different oil density.

However, during experiments the author used a heat source trying to achieved

300 °C. During experiments the author considered an idealized oil field with parallel heat transfer, porosity of sand 20% and different oil density. The effect of pressure was not take in consideration. In thermal processes the heat transfer from the hot agent to the environment is done by conduction , convection or radiation.

Building these diagrams based on temperature control, heat transfer and different oil type will be more easier to apply the thermal methods.

Romania is classified as a mature hydrocarbon province, but still the most important producer in the South-Eastern European countries. Significant oil potential is present in oil fields and the Enhanced Oil Recovery methods will represent new concept for increasing production. There are ongoing effort to redevelop mature oil fields, currently used steam injection, in-situ combustion, hot water injection, polymer injection.

ACKNOWLEDGEMENTS

The author thanks OMV Petrom Romania and National Mineral Agency for borrowing crude oil samples.

REFERENCES

- [1] Larry W. Lake, Enhanced Oil Recovery, pp.53-10, Ed.2019
- [2] Abrams A., The influence of fluid viscosity, Interfacial Tension and Flow Velocity on Residual Oil saturation Left by Watreflood, Society of Petroleum Engineers Journal, 5 (1975), 437-447.
- [3] Buckley S.E., Leverett M.C., Mechanism of fluid Displacement in Sands transactions American Institute of M and Metalurgical Engineers, 146 (1942), 107-116
- [4] Caudle B.H, fundamentals of Reservoir Engineering, Part II, dallas: Society of Petroleum Engineers
- [5] Anand, J.Somerton, Gomma E.- Predicting thermal conductivities of formations from other known properties, SPEJ, Oct 1973
- [6] Beck A.E , An improved method of computing the termal conductivity of fluid filled sedimentary rocks, Geophysics, vol 41, nr1, February 1976

[7] Cretu I., Beca C., Babskow Al., Ingineria zăcămintelor de hidrocarburi, vol 1, 1981

[8] Cristescu T., Osnea Al., Marcu N. Aspecte privind calculul fluxului termic disipat la injectia aburului intr-un zacamant de petrol, Revista termotehnica, nr.1 , anul II, Bucuresti 1994

[9] Cristescu T. Consideratii energetic privind extractia titeiului prin metode termice, National Conference News and Perspectives in drilling and extraction, Ploiesti ,1994

[10] Branoiu Ghe., Frunzescu D., Nistor I, Ionescu (Goidescu) Nicoleta Mihaela, On some mineralogical characteristics of the reservoir rocks in the Moreni field (Carpathian Foredeep Romania)

[11] Ionescu (Goidescu) N., The role of 3D seismic interpretation for building structural model-Case study in the Muntenia oil field (Romania)

[12] Autodesk Autocad LT, 2018 for WINDOWS



Section

SOIL SCIENCE

Plant and soil science

Soil management

Soil Biology

GRAFTED TOMATOES – ECOLOGICAL ALTERNATIVE FOR CHEMICAL DISINFECTION OF SOIL

PhD. Student eng. Dorin Sora ¹

PhD. eng. Mădălina Doltu ²

^{1,2} Research and Development Institute for Processing and Marketing of the Horticultural Products – Horting, Romania

ABSTRACT

This study aimed to identification of an ecological alternative for the chemical disinfection of soil in the greenhouses from Romania. Tomato (*Solanum lycopersicum* L.) is one of the most popular vegetable crops in the world. The carbohydrate, vitamins, salts of important mineral elements and organic acids content of tomato fruits is very important. Tomato crops are very sensitive to climatic vagaries, so fluctuation in climatic parameters at any phase of growth can affect the yield and the fruit quality. Grafting on *Solanaceae* is a method which has improved and spread quickly during the past years, a similar approach to crop rotation, a practice meant to increase productivity, resistance or tolerance to biotic and abiotic stress factors and at increasing fruit quality. The research was conducted in a glass greenhouse of the Horting Institute, Bucharest, Romania. The biological material used was a Romanian tomato hybrid (Siriana F1), a Dutch tomato hybrid (Abellus F1) and four rootstocks, a Dutch tomato hybrid (Emperador F1) and three Romanian tomato cultivars (L₅₄₂, L₅₄₃ and L₅₄₄) obtained from the Research and Development Station for Vegetable Growing, Buzău, Romania. The rootstocks have had resistance to biotic stress factors (soil diseases and pests) and the chemical disinfection of soil has was eliminated. The result of this research are presented in this paper.

Keywords: *Fusarium*, *grafted plants*, *Meloidogyne*, *resistance*, *Solanum lycopersicum*

INTRODUCTION

Methyl bromide is a broad-spectrum soil fumigant. Mixtures of these two fumigants, methyl bromide and cloropicrin, work synergistically in controlling a wide range of plant pathogens and pests, including fungi, nematodes, insects, mites, rodents, weeds, and some bacteria. Methyl bromide was listed in 1993 by the Parties of the Montreal Protocol as an ozone-depleting compound. According to the Montreal Protocol, the import and manufacture of methyl bromide in the United States of America (USA) and other developed countries will be banned by 2005, after stepwise reductions in 1999, 2001 and 2003. Currently, there is a need for environmentally sound and economically feasible alternatives [1].

In Romania the use of methyl bromide in soil treatments for plant protection (fumigation applications) is banned from 2002 January 1st and the use of methyl bromide in storage applications is banned from 2005 January 1st (Gov Ordinance no. 89/1999, approved by Law no. 159/2000, art. 9) [4].

Farmers often use perilous chemicals to overcome the loss due to disease and pests. Though Various other environment friendly methods like using resistant varieties or cultivars produced by conventional method of breeding or by using biotechnological tools are also available but they are too much time consuming and require a huge input on research and trials on and off field [10].

Grafting on *Solanaceae* is a similar approach to crop rotation [3].

It is a practice meant to increase productivity, a method which has improved and spread quickly during the past years. This method of tomato vegetative multiplication is aimed at producing plants with higher resistance or tolerance to soil diseases (*Fusarium* and *Verticillium*) and pests (nematodes).

Grafting is a promising tool to enhance plant performance of *Solanaceae* under growth conditions in which the fruiting vegetables are exposed to salinity, water stress, alkalinity, heavy metals contamination, and excessive amounts of trace elements. Several effective rootstocks are already in practical use, or used in breeding programs. Augmentation of this knowledge may help to select and breed appropriate rootstocks which improve the adaptability of fruit vegetable crops to salinity, water stress, alkalinity, heavy metals contamination, and trace element toxicity [6].

Research focus currently relies on combinations of environmentally friendly approaches among which is grafting for pathogen management. Grafting has potential to provide resistance to multiple soilborne pathogens, for example, nematodes, after a susceptible plant (scion) is united with resistant rootstocks. Sources of resistant rootstocks include species from the same family or closely related species, hybrids, and weeds. Farmers select rootstocks with desirable genetic properties, for example, resistance to nematodes, flooding, salinity, extreme temperatures, and increased yield production. Tomato are the most grafted plants in the Solanaceous family [8].

The method is based on the contact between a crop variety (scion) and a wild variety (rootstock), the last one possessing a robust root system, a high resistance to the soil pests and diseases; the result of the grafting process is the increase of the resistance against soil diseases such as *Fusarium* spp., *Verticillium* ssp. and nematodes [5].

Commercial susceptible varieties grafted on rootstocks resistant to soilborne pathogens is one technique used as an alternative method to methyl bromide [Bogoescu, 2007, 4].

The most common rootstocks used for commercial tomato grafting are hybrids (F1) or inter-specific hybrids, which have been specifically bred for resistance against pathogens and other diseases such as nematodes, *Verticillium* wilt, and *Fusarium* wilt. Hybrids are produced by crossing selected tomato varieties with other wild *Solanum* species with the genetic ability to offer resistance to specific diseases and pathogen infection. In Europe, tomato hybrids are used as rootstocks compared to other *Solanum* spp., because of their high level of genetic improvements. There are other plants that share the same family with tomato (*Solanum torvum*, *S. aethiopicum*, and *S. macrocarpon*); these can serve as

rootstocks for their tolerance to *Fusarium* wilt and root knot nematode infestation [8].

Tomato are very popular crops in Romania, but its are very sensitive to climatic vagaries, so fluctuation in climatic parameters at any phase of growth can affect the yield. The tomato grafting is useful in Romania. Sensivity to diseases and pest has imposes introduction grafting onto resistant rootstocks. The rootstocks have a big resistance to *Meloidogyne* spp. and *Fusarium* spp. attack, compared to the ungrafted tomatoes.

This study regarding grafting of some tomatoes is important to highlight some resistances to biotic stress factors. The researches in the tomato grafting domain began at Horting Institute, Bucharest, Romania in 2002 and have continued up to now.

MATERIALS AND METHODS

The experience was carried out in a glass greenhouse on soil without chemical or thermal disinfection from Research and Development Institute for Processing and Marketing of the Horticultural Products – Horting, Bucharest, Romania.

The biological material used was a Romanian tomato hybrid (Siriana F1), a Dutch tomato hybrid (Abellus F1) and four rootstocks, a Dutch tomato hybrid (Emperor F1) and three Romanian tomato cultivars (L₅₄₂, L₅₄₃ and L₅₄₄) obtained from the Research and Development Station for Vegetable Growing, Buzău, Romania.

This research was implemented in a randomized complete block design with two grafting combinations and the ungrafted control for each cultivar used. 30 plants were used in 3 replications of 10 plants each for every combination and control, in the following experimental scheme (variants):

- V1–Siriana×Emperor;
- V2–Siriana×L₅₄₂;
- V3–Siriana×L₅₄₃;
- V4–Siriana×L₅₄₄;
- V5–Siriana, control (ungrafted);
- V6–Abellus×Emperor;
- V7–Abellus×L₅₄₂;
- V8–Abellus×L₅₄₃;
- V9–Abellus×L₅₄₄;
- V10–Abellus, control (ungrafted).

Siriana F1 is a creation from the germplasm bank of Research and Development Station for Vegetable Growing, Buzău, Romania and is tested as grafted and ungrafted plants cultivated in greenhouses at Horting Institute.

It has great vigor, spherical shaped and slightly flattened fruit, red in color, with an up to 150 g in weight, the height of 5 cm, diameter of 6.5 cm and 4-5 seminal lodges. The plant is early (110-115 days), indeterminate and well adapted to field conditions and protected areas.

Abellus F1 (the seed source is the Rijk Zwaan company in the Netherlands) is a Dutch hybrid, very frequently cultivated in Romania and tested as grafted and ungrafted plants cultivated in greenhouses at Horting Institute Bucharest.

It has great vigor, spherical shaped and slightly flattened fruit, red in color, with up to 150-180 g in weight. The plant has indeterminate growth, with early maturation and well adapted to field, greenhouse and solarium conditions.

Emperador F1 (the seed source is the Rijk Zwaan company in the Netherlands) is a very vigorous tomato rootstock which impacts the grafted plant with a harmonious growth. This rootstocks is very resistant to the attack of the nematodes and to *Fusarium* sp., *Verticillium* sp. and *Tomato Mosaic Virus*, recommended for protected areas and field.

L₅₄₂, L₅₄₃ and L₅₄₄ are three tomato genotypes obtained by amelioration works performed by some horticultural researchers from VDRS Buzău and tested in experimental fields in the Horting Institute, Bucharest for homologation as rootstocks for tomato grafting.

The efficiency of the tomato grafting method was assessed by severity of attack induced by *Fusarium oxysporum* f. sp. *lycopersici*, severity of root galls induced by *Meloidogyne incognita*, a 0–5 scale (0 = no galls; 1 = 1–5 galls), after Di Vito [7].

The index descriptors were used:

0 = no galls;

1 = slight infection, not widespread galls, presence of 1-5 galls located only on few roots;

2 = slight infection, widespread galls, presence of no more than 20 galls well spread on root system;

3 = infection with widespread galls, more than 20 galls evident and well spread on root system;

4 = strong infection, root system cut down and deformed due to the presence of big galls on the main roots;

5 = very strong infection, root system cut down and totally deformed due to the presence of big galls, absence capillary roots.

The root index (0–5) was calculated as follows:

Σ nematode index of all plants / Number of plants

For pathogens determined there were calculated the frequency, intensity and level of pest attack:

- $F\% = N \times 100 / N_t$
where: N – no. attacked plants, N_t – total plants
- $I(\%) = \sum(i \times f) / n$
where: i - % index, f – no. of attacked plants, n = total number of plants
- $GA\% = F\% \times I\% / 100$

RESULTS AND DISCUSSION

In comparative analysis, the recorded results are presented as average / variant on combinations of rootstock x scion, for grafted plants, comparative with the average result of the ungrafted plants (Table 1).

Table 1. Incidence of soil pathogens and pests in tomato plots

Variants	GA%	
	<i>F. oxysporum</i>	<i>M. incognita</i>
V1	0,04	0,05
V2	0,02	0,06
V3	0,03	0,07
V4	0,05	0,08
V5 (control)	1,5	1,10
V6	0,01	0,04
V7	0,02	0,06
V8	0,02	0,07
V9	0,04	0,07
V10 (control)	1,1	0,5
Average		
grafted	0,03	0,06
ungrafted	1,3	0,8

The grafting influence on the resistance of tomatoes to soil-borne pathogens and nematodes at identified species of *F. oxysporum* f.sp. *lycopersici* and *M. incognita*: the grafted plants showed resistance to attack of *F. oxysporum* (0,03%) and *M. incognita* (0,06%) comparing with ungrafted tomato plants where the level of *F. oxysporum* attack was 1,3% and the level of *M. incognita* attack was 0,08%.

When plants were challenged with *Meloidogyne*, all rootstocks tested showed a significantly lower number of galls and egg masses in comparison to the control. Information on the response of nematode-resistant tomato rootstocks to root-knot nematode species and populations is still limited to few studies that show increased variability in terms of nematode infectivity and reproduction among the rootstocks. For instance, the resistant rootstock Big Power displayed high resistance in soils naturally infested with *M. javanica* and *M. incognita*. In the same study, Maxifort and Beaufort showed partial resistance to the Southern root-knot nematode compared to non- and self-grafted controls. The effect of growing resistant tomato rootstocks aiming at nematode suppression and tomato yield increase in nematode infested fields could vary depending on the tomato rootstocks and the *Meloidogyne* populations present in an area, thus limiting their resistance value as an efficient nematode management tool [9].

Nematode reproduction on resistant tomato cultivars was similar or higher than on resistant rootstocks for all tested *Meloidogyne* isolates in the short period experiment, but not in the long period experiment. The response of tomato cultivars and rootstocks to *Meloidogyne* isolates varies depending on the isolates of *Meloidogyne* or the length of the growing period [2].

Grafting used for a long time ago to increase resistance to biotic stresses of vegetatively propagated plants. The primary purpose of grafting vegetables worldwide has been to provide resistance to soil borne diseases (corky root, fusarium wilt, verticillium wilt, bacterial wilt) and nematodes; these are some of the biotic stress cause, damages in vegetable production and especially in continuous cropping in greenhouses [11].

CONCLUSION

The use grafted tomatoes, the grafting combinations (scions x rootstocks) researched in the Horting Institute, may be recommended for the vegetable crops in Romania. Development of grafted tomato that are resistant to *Fusarium* spp. and *Meloidogyne* spp. can be done more quickly than breeding.

These rootstocks (Emperor, L₅₄₂, L₅₄₃ and L₅₄₄) are used in Romania for conventional and ecological crops; its have had good results by grafting with some scions (Siriana and Abellus).

Sensitivity to diseases and pest has imposes introduction grafting onto these resistant rootstocks to some biotic stress factors (*F. oxysporum* f. sp. *lycopersici* and *M. incognita*) for tomato crops cultivated in protected spaces on the soil without chemical or thermal disinfection because in Romania the use of methyl bromide in soil treatments for plant protection is banned.

Based on the above mentioned results, it can be said that the rootstocks played a important role in plant resistance to soil disease and pest.

The results showed that tomato grafting on the suitable rootstock has positive effects on the crops compared to the ungrafted tomatoes.

The researches regarding tomato grafting at Horting Institute are in evolving for the development of the vegetable crops in Romania.

REFERENCES

[1] Ajwa H., Klose S., Nelson S., Minuto A., Gullino, M., Lamberti F., Lopez A., Jose M., Alternatives to Methyl bromide in Strawberry Production in the United States of America and the Mediterranean Region, *Phytopathologia Mediterranea*, vol. 42, pp 220-244, 2003;

[2] Aydinlı G., Mennan S., Resistance Response of Tomato Cultivars and Rootstocks Carrying the Mi-1.2 Gene to Isolates of *Meloidogyne arenaria*, *M. incognita*, and *M. javanica* at Two Different Growing Periods, *Korean journal of horticultural science and technology*, vol. 37, pp 509-519, 2019;

[3] Blestos F.A., Olympos C.M., Rootstocks and grafting of tomatoes, peppers and eggplants for soil-borne disease resistance, improved yield and quality, *The European Journal of Plant Science and Biotechnology*, vol. 2(1), pp 62-73, 2008;

[4] Bogoescu M., Doltu M., Iliescu L., Tănasa N., Phase-out methyl bromide in Romania horticulture – consecutive at preservative actions of the ozon layer, *Bulletin USAMV, Horticulture Cluj-Napoca, Romania*, vol. 64, 2007;

- [5] Bogoescu M., Doltu M., Sora D., Mohora A., Iordache B., Results on establishing the technology for obtaining the watermelons grafted seedlings, Bulletin UASVM, Horticulture Cluj-Napoca, vol. 66(1), pp 397-403, 2009;
- [6] Colla G., Fiorillo A., Cardarelli M., Roupshael Y., Grafting to improve abiotic stress tolerance of fruit vegetables, Acta Horticulturae, vol. 1041, pp 119-126, 2014;
- [7] Di Vito M., Lamberti F., Carella A., La resistenza del pomodoro nei confronti dei nematodi galligeni: prospettive e possibilità, Rivista di Agronomia, vol. 13, pp 313-22, 1979;
- [8] Nyaku S.T., Amissah N., Grafting: An Effective Strategy for Nematode Management in Tomato Genotypes, Advances in Tomato Breeding and Production, 2018;
- [9] Rumbos C.I., Khah E.M., Sabir N., Response of local and commercial tomato cultivars and rootstocks to *Meloidogyne javanica* infestation, Australian Journal of Crop Science, vol. 5(11), pp 1388-1395; 2011
- [10] Sen A., Chatterjee R., Bhaisare P., Subba S., Grafting as an Alternate Tool for Biotic and Abiotic Tolerance with Improved Growth and Production of Solanaceous Vegetables: Challenges and Scopes in India, International Journal of Current Microbiology and Applied Sciences, vol. 7, pp 12-135, 2018;
- [11] Yassin H., Hussen S., Reiview on Role of Grafting on Yield and Quality of Selected Fruit Vegetables, Global Journal of Science Frontier Research D: Agriculture and Veterinary, vol. 15(1), 2015.

THE APPLICATION AND VALIDATION OF PHYSICALLY-BASED EROSION AND EMPIRICAL MODEL IN CENTRAL POLAND

Ing. Zuzana Némětová ¹

Ing. Adam Krajewski, PhD. ²

Prof. dr hab. Kazimierz Banasik, PhD. ³

Prof. Ing. Silvia Kohnová, PhD. ⁴

^{1,4} Slovak University of Technology, Bratislava, Slovakia

^{2,3} Warsaw University of Life Sciences – SGGW, Warsaw, Poland

ABSTRACT

The general problem of an appropriate erosion modelling can be seen in a lack of available data and in the validation and verification of the methodologies applied. The article includes two significant and challenging topics, i.e. the evaluation of the sediment amounts in a catchment and the validation of the methodologies used. The importance of the sediment estimation can be found not only in the modelling and prediction fields but also in the terms of engineering practice. The significance of erosion model validation lies in the confidence in the model itself and in the detection of its applicability and relevance. In this study, results obtained from the physically-based EROSION-3D model was compared with the sediment yield of a small agricultural catchment in central Poland. The estimation of sediment yield from the agricultural catchment has been conducted using the empirical method (USLE) coupled with a sediment delivery ratio (USLE-SDR) and verified by reservoir measurement. Firstly, the application of a physically-based EROSION-3D model has been done based on a continuous rainfall series for the selected period and afterwards the results have been compared with the sediment yield obtained by the empirical methods in order to test a model's performance. The results of the paper point to the comparison of the results obtained by two different approaches, i.e. the physically-based and empirical methods together with the validation of the methods through the acoustic depth measurements.

Keywords: *erosion modelling, physically-based model, sediment estimation, rainfall events, empirical model*

INTRODUCTION

Among the different soil degradation processes, the water erosion represents the most serious position and about 55% of the eroded land is caused by soil water erosion [1]. The growing and critical global problem of soil degradation represent the natural process, but it is strongly accelerated by inappropriate human activities and is directly linked to climate change. The research of a connection between climate change and soil erosion have been started since the 1940s [2] Leopold, 1951). However, the consequences of climate change include direct and indirect impacts. The direct effects include changes in rainfall characteristics, i.e. rainfall amount [3], [4], rainfall intensity [5] and temporal and spatial distribution of rainfall

patterns [6]. In reverse, the indirect impacts are linked to the rising temperature and warming climate which affects soil erosion through changes in vegetation cover and soil moisture [4]. Due to climate change, the number of intensive rainfall events is expected to increase in the future [7], [8], [9]. The role of such events directly impacts soil erosion rate and maybe worse under a changing climate. Based on the facts mentioned above, the understanding of soil erosion processes and developing assessment methods have an important meaning in the sense of soil protection as a fundamental source to ensure basics human needs, i.e. to provide food.

The importance of soil erosion prediction together with the sediment yields prognosis from the small catchments lies in the requirement to provide relevant information for engineering hydrology and for environmental modelling and forecast. The estimation of sediment yields can be conducted using a variety of methods but choosing a suitable method is still a very complex and intricate issue. Many models suffer from a different kind of problems (overestimation, the uncertainty of the models, lack of input data) because the modelling of a natural system is always restricted by many factors, such as spatial and temporal scales, spatial heterogeneity, and very unstable input data [10].

In the contribution, the amount of sediments have been calculated for a small lowland agricultural catchment using physically-based Erosion-3D model and using the empirical Universal Soil Loss Equation together with a sediment delivery ratio (USLE-SDR) and the modelled results were confronted with the amount of sediment deposited in a reservoir at the catchment outlet.

MATERIALS AND METHODS

Physically-based EROSION-3D model

The physically-based EROSION-3D model represents event based method which can be applied for calculating the amount of surface runoff generation, the amount of soil loss, sediments, the volume and concentration of eroded sediments and deposition processes on agriculture land produced by intensive rainstorms [11]. The model has been developed since 1995 by Michael von Werner at the Department of Geography at the Free University of Berlin and consists of two main submodels, i.e., the infiltration and the erosion model. The erosion submodel describes the soil erosion processes in three steps, i.e., the detachment of soil particles from the impact of raindrops and their transport and deposition. The submodel includes the processes of rainfall infiltration, the generation of surface runoff, the detachment of soil particles involved by the kinetic energy of raindrops and surface runoff. The infiltration submodel uses the Green-Ampt approach to define the process of infiltration and considers the soil as a rigid and homogeneous soil matrix (vertical changes in the physical soil properties, dynamic processes or changes in soil structure due to biological activity are not considered).

As mentioned previously the EROSION-3D model has been predominantly established as an event based model but thanks to the long-term simulation submodel are possible to perform long-term simulations. In the contribution the long-term simulation is based on a continuous rainfall series consists of a series of

single rainfall events that occur within the period evaluated. Each rainfall event requires its own soil data set whose parameters account for the individual soil conditions and the stages of crop growth as of that date.

Study area

The Zagożdżonka catchment (Figure 1) represents a small lowland agricultural catchment, situated in central Poland, about 100 km south of the capital city Warsaw. The watershed area up to the Płachty gauging station is 82.4 km². The whole catchment is characteristic by topography specific for this part of Poland with the minimum altitude 148 m a. s. l. and the maximum altitude 185 m a. s. l. The mean annual temperature is about 8°C and the mean annual relative humidity is about 79-81%, which indicates low spatial distribution. The mean annual precipitation in the catchment ranges from 414 mm to 941 mm (1963-2015). Nowadays, the main part of the catchment area is formed by forest (about 60% of total area) and arable land (about 25%), and the rest of catchment area belongs to the pastures (Figure 1B) and Figure 3 [12]. Hydrological research in the upper part of the Zagożdżonka River has been conducted by the Warsaw University of Life Sciences since the 1960s. All measurements are done according to the standard methodology recommended by the Polish Institute of Meteorology and Water Management-National Research Institute.

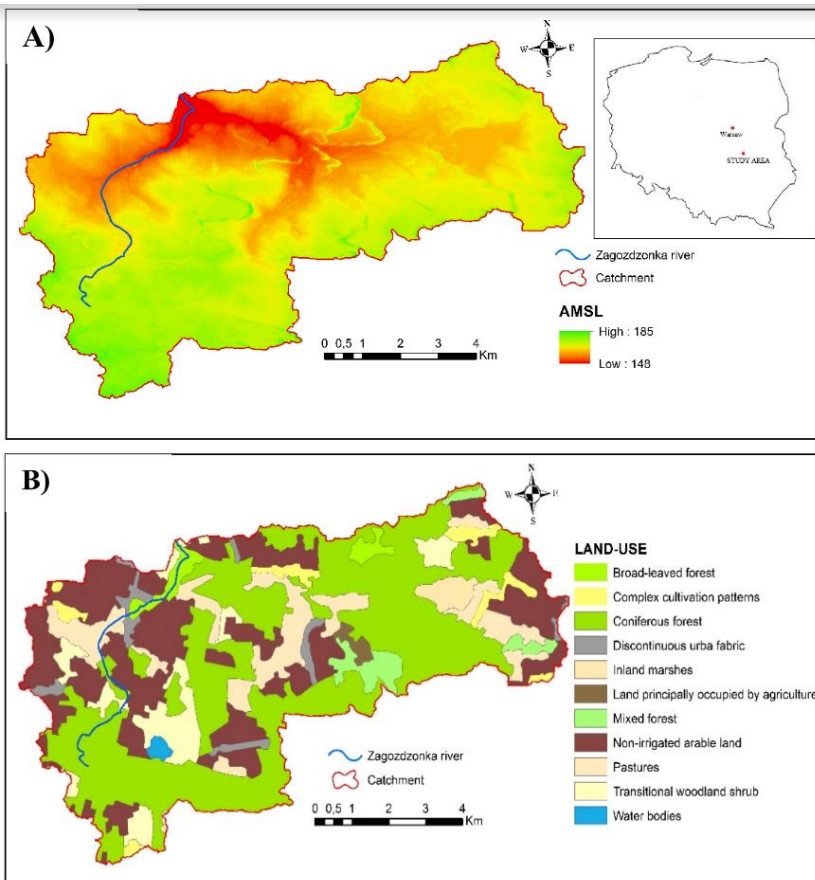


Figure 1. The characteristics of the Zagożdżonka catchment study area: A) Relief and location in Poland; B) Land use characteristics of the study area (Corine Land cover, 2018).

Input data

Physically-based Erosion-3D model

The physically-based Erosion-3D model requires three input data, i.e. terrain characteristics in the form of a square grid (digital elevation model), rainfall characteristics (duration and intensity) and soil input data (eight soil characteristics). The rainfall events (a ten-minute step) were recorded at the Plachty gauge station during the period selected (III.2013-X.2014). The model's runs were conducted for the rainfall events, which have been occurred during the years 2013 and 2014. The characteristics of the rainfall events with the dates of occurrence are introduced on Figure 2. The soil input parameters were set according to the dates of individual rainfall events.

Empirical model USLE-SDR

Amount of sediments estimated by empirical equation USLE together with the sediment delivery ratio SDR was conducted using the formula [15]:

$$Y_r = \text{SDR} \cdot E \cdot AE \quad (1)$$

where:

- Y_r annual sediment yield from the catchment of reservoir ($\text{Mg} \cdot \text{year}^{-1}$),
- SDR sediment delivery ratio (-)
- E annual soil loss per unit area ($\text{Mg ha}^{-1} \cdot \text{year}^{-1}$)
- AE the active area of the catchment (ha)

The proper application of USLE requires to determine regionally sensible parameter, e.g. the rainfall and runoff erosivity R which had been done for Polish condition in the studies [13] and [14].

Reservoir Staw Gorny

The Staw Górny Reservoir within the Zagożdżonka catchment was built in 1976 with the area of 14 ha and the original volume of 252 000 m^3 . Because the construction of the reservoir has caused sediment deposition within the reservoir as well as in the area above the reservoir, the estimation of sedimentation intensity and reservoir surveys are crucial for a different reason and are considered as the most reliable technique established for sedimentation intensity determination. The first survey was done during the period 1979-1980 using the range line method, and then in the years 1991, 2003 and the last survey was conducted in 2009 [15]. The survey reservoir undertaken in 2003 and 2009 were done using a survey vessel equipped with a hydrographic system comprising an echo-sounder unit and a Global Positioning System (GPS) receiver.

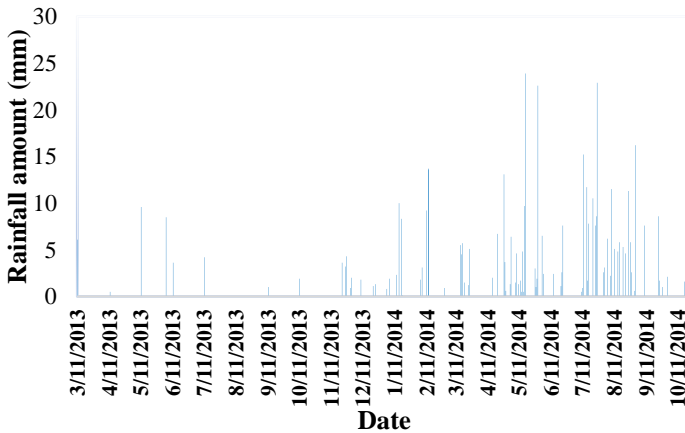


Figure 2. Total rainfall amounts and date of occurrence of rainfall events during the two time periods: (a) March 2013 - December 2013; January 2014 - October 2014

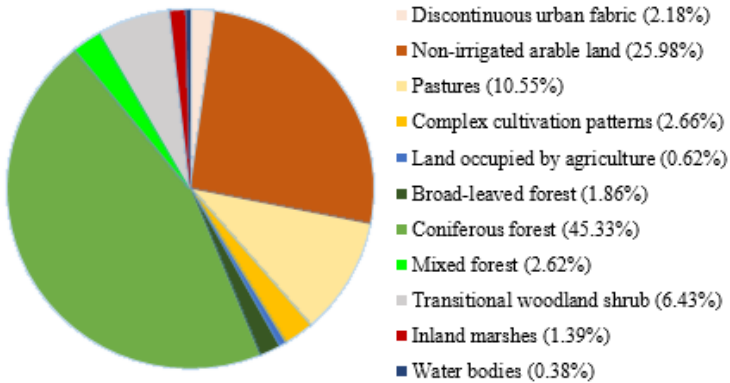


Figure 3. *Percentual representation of landscape elements in the investigation territory*

RESULTS AND DISCUSSION

The article deals with the estimation of sediments amount by the physically-based EROSION-3D model and empirical model USLE together with a sediment delivery ratio (USLE-SDR) and with the confrontation of results modelled with the sediment amount deposited in a reservoir at the catchment outlet. According to the reservoir survey average annual volume of sediment deposits is 1080 m³. It must be noted that the total sediment input to the reservoir consists of bed load and suspended load as well while the sediment amounts calculated by physically-based EROSION-3D model consider only suspended sediments. When compared the EROSION-3D model and empirical model USLE-SDR the results show, the empirical model USLE-SDR are more close to the measured amount of annual deposition than the Erosion-3D model (Table 1). Based on the results, it is clear that the Erosion-3D model represents a more appropriate and satisfactory approach to determine the spatial localization of places endangered by water erosion (Fig. 4). The intensity of the erosion is higher in the second period evaluated (Fig. 4B) since the period has been richer in rainfall amount that the first period, which made the soil more vulnerable to the erosion processes (Fig. 4B).

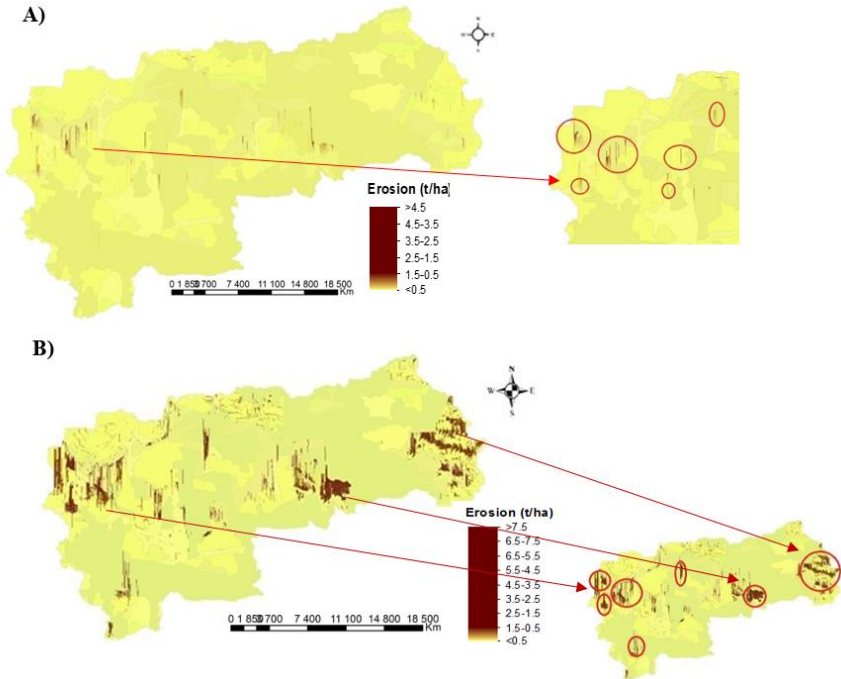


Figure 4. Results obtained from the physically-based EROSION-3D model (calculated for a period evaluated): A) March 2013 - December 2013; B) January 2014 - October 2014

Table 1. Comparison between the measured data and modelled data of the sediment volume

METHOD FOR THE DETERMINATION OF SEDIMENTS	SEDIMENT VOLUME (m ³)
USLE-SDR	708
RESERVOIR (total amount of sediments)	1080
EROSION-3D model (Period A)	508
EROSION-3D model (Period B)	678

CONCLUSION

The physically-based EROSION-3D model was applied to simulate the erosion processes and to simulate the amount of sediments in the catchment located in central Poland. The model helps to identify the most sensitive erosion and deposition zones within a catchment (Fig. 4). The calculations were performed using long-term simulations and were done for two periods selected; (March 2013 - December 2013; January 2014 - October 2014). The difference can be found in the total number of rainfall events because the second period (I. 2014-X.2014) was richer in the rainfall amount than the first period (III. 2013-XII. 2013), which made the soil more vulnerable to the erosion process. In reverse, the second period

resulted in higher values of the erosion process as reflected in Figure 4.B). In the case of predicted (modelled) and measured sediment volume in the Zagożdżonka catchment, the physically-based Erosion-3D model calculated a lower amount of sediments for both period evaluated (March 2013 - December 2013 and January 2014 - October 2014) (Tab. 1.) in comparison with the empirical model USLE-SDR and with the observed sediments amounts as well. It is important to mention that results obtained from USLE represent averaged suspended sediment load and the reservoir deposits cover annual volume of suspended load together with the bed load. The possible errors in the predicted amount of sediments estimated by the Erosion-3D model are associated with the model parameters, especially in the case of soil moisture which is highly variable before each rainfall event. The parameters of the EROSION-3D model were chosen from the Parameter Catalogue for EROSION-3D, which contains their tabularized values by the type of soil, land use and the specific crop and its growth phase in different months within the year. This inaccuracy has to be improved for further work with the model to provide high-level results. At the end can be concluded, the Erosion-3D model reflects a useful tool for identification of areas prone to erosion processes.

ACKNOWLEDGEMENTS

The investigation has been conducted during STSM of first author at Warsaw University of Life Sciences – SGGW in October 2019 as part COST Action CA16209 ‘Land4Flood’.

REFERENCES

- [1] Bridges E.M., Oldeman L.R., Global assessment of human-induced soil degradation. *Arid Soil Research and Rehabilitation*, vol. 13/issue 4, pp 319–325, 1999.
- [2] Leopold L.B., Rainfall frequency: an aspect of climatic variation, *Eos. Transactions, American Geophysical union, United States*, vol. 32/issue 3, pp 347–357, 1951.
- [3] Bangash R.F., Passuello A., Sanchez-Canales M., Terrado M., López A., Elorza F.J., Ziv G., Acuña V., Schuhmacher M., Ecosystem services in Mediterranean river basin: climate change impact on water provisioning and erosion control, *Science of the Total Environment, Spain*, pp 458–460, 2013.
- [4] Nearing M.A., Pruski F.F., O’Neal M.R., Expected climate change impacts on soil erosion rates: a review, *Journal of Soil and Water Conservation, United States*, vol. 59/issue 1, pp 43–50, 2004.
- [5] Tang J.L., Cheng X.Q., Zhu B., Gao M.R. Wang T., Zhang X.F., Zhao P., You X., Rainfall and tillage impacts on soil erosion of sloping cropland with subtropical monsoon climate — a case study in hilly purple soil area, *Journal of Mountain Science, China*, vol. 12/issue 1, pp 134–144, 2015.
- [6] Maeda E.E., Pellikka P.K.E., Siljander M., Clark B.J.F., Potential impacts of agricultural expansion and climate change on soil erosion in the Eastern Arc

Mountains of Kenya, *Geomorphology, Kenya*, vol. 123/issue 3-4, pp 279–289, 2010.

[7] Hlavčová K., Kohnová S., Borga M., Horvát O., Šťastný P., Pekárová P., Majerčáková O., Danáčová Z., Post-event analysis and flash flood hydrology in Slovakia. *Journal of Hydrology and Hydromechanics, Slovakia*, vol. 64/issue 4, pp 304–315, 2016.

[8] Michael A., Anwendung des physikalisch begründeten Erosionsprognosemodells EROSION 2D/3D—Empirische Ansätze zur Ableitung der Modellparameter, Dissertation Thesis, Freiberg, Germany, pp 191, 2000.

[9] Dolák L., Řezníčková L., Dobrovolný P., Štěpánek P., Zahradníček P., Extreme precipitation totals under present and future climatic conditions according to regional climate models, *Climate change adaptation pathways from molecules to society*, Brno, Czech Republic, Chapter 3, pp 27–37. 2017.

[10] Jakeman A.J., Green T.R., Beavis S.G., Zhang L., Dietrich C.R., Crapper P.F., Modelling upland and instream erosion, sediment and phosphorus transport in a large catchment, *Hydrological Processes*, vol. 13/issue 5, pp 745-752, 1999.

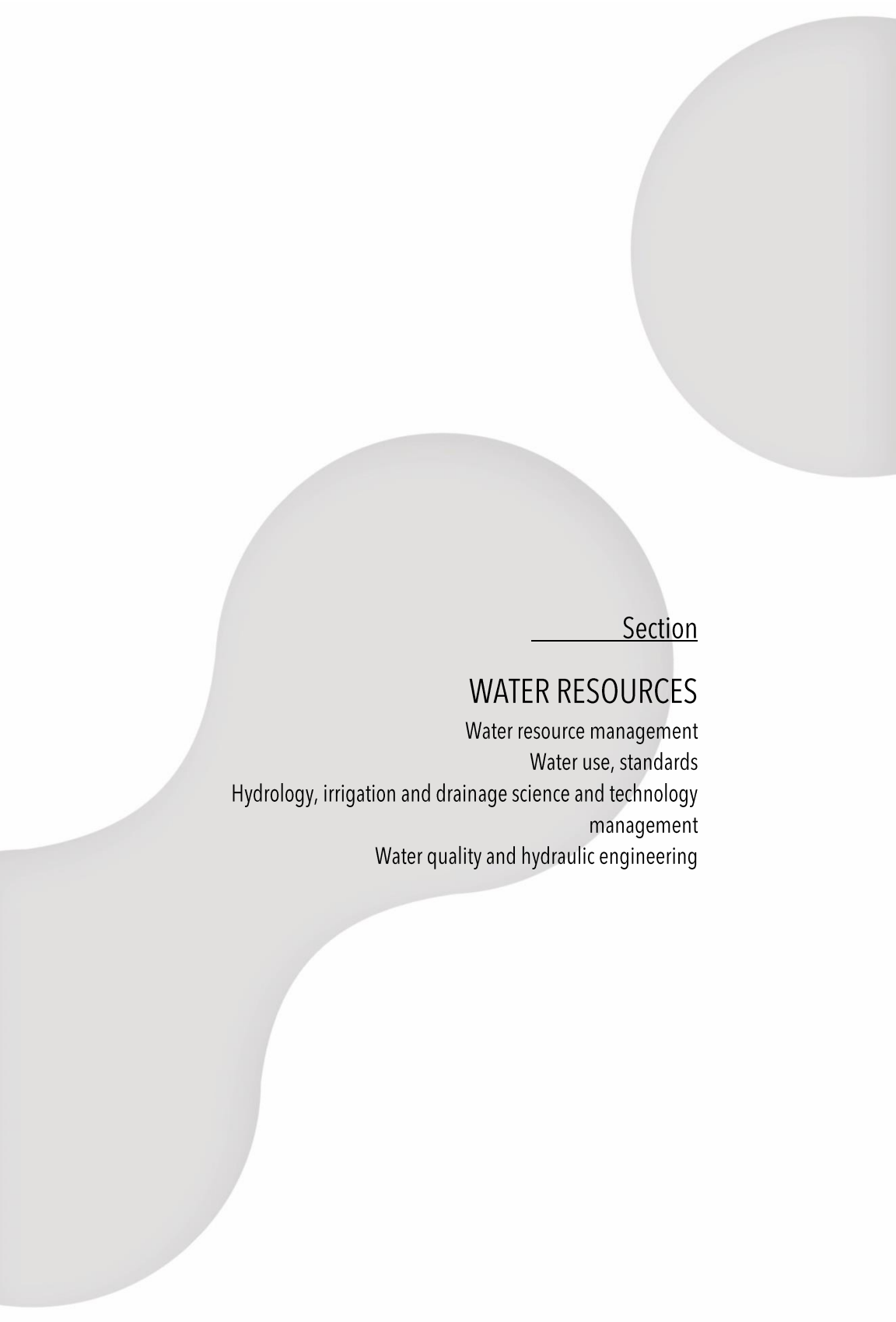
[11] Werner M. Erosion-3D Version 3.0 User manual – Samples, GeoGnostics Software, Germany, Berlin, 2003, 34 p;

[12] Krajewski A., Sikorska-Senoner A., Ranzi R., Banasik K., Long-term changes of hydrological variables in a small lowland watershed in Central Poland, *Water, Poland*, vol 11/issue 3, 2019.

[13] Banasik K., Gorski D., Evaluation of rainfall erosivity for East Poland, *Runoff and Sediment Yield Modelling, Proceedings of the International Symposium, Poland*, pp 129-134, 1993.

[14] Banasik K., Gorski D., Mitchell J., Rainfall erosivity for East and Central Poland, *Soil Erosion Research For the 21st Century, Proceedings, Germany*, pp 279-282, 2001.

[15] Banasik K., Górski D., Popek Z., Hejduk L., Estimating the annual sediment yield of a small agricultural catchment in central Poland, *IAHS-AISH Publication, Poland*, pp 356, 2012.



Section

WATER RESOURCES

Water resource management

Water use, standards

Hydrology, irrigation and drainage science and technology
management

Water quality and hydraulic engineering

COMPARING VALIDATION RESULTS OF 1D VERSUS 2D MATHEMATICAL MODEL FOR BUNA RIVER

PhD. Stud. Elona Abazi¹

Assoc. Prof. Dr. Sotirag Pandazi²

Assoc. Prof. Dr. Miriam Ndini³

¹ Institute of Geosciences, Energy, Water, and Environment/Polytechnic University of Tirana, Albania

² ELBA Consulting Engineers Ltd –Company, Tirana, Albania

³ EPOKA University, Tirana, Albania

ABSTRACT

Mathematical models are a valuable tool to study different water-related problems. 1Dimensional and 2Dimensional mathematical models are widely used in river engineering studies. 1D and 2D mathematical models are set up for Buna River using SOBEK software developed from Deltares Institute, the Netherlands. Buna River is part of the water system of Shkodra Lake, Drini and Buna River. This water system is the largest in Albania, and receives significant amounts of annual precipitation ranging from 1600 mm to 4000 mm. This water system discharges all its waters into the Adriatic Sea through Buna River bed, which has a total length of around 44 km. Around 1.5 km from flowing out of Shkodra Lake, Buna River joins Drini River, and then meanders in a low land area before discharging into the sea.

Validation is a very important step in the process of building a mathematical model for a water system. Validation of 1D and 2D mathematical models for Buna River is done by using the hourly water level data from on-line stations for an event. The results of both models are evaluated based on graphical comparison and statistical tests such as: Root Mean Square Error, Mean Absolute Error, and Correlation Coefficient. The 1D mathematical model shows a better performance for the flow inside the river banks (bankfull discharge) due to a more accurate representation of the river bathymetry.

Keywords: *Buna River, 1D and 2D mathematical models, validation, water level*

INTRODUCTION

The water system of Shkodra Lake, Drini and Buna River, which is the largest in Albania, collects the waters from a total surface of 19580 km². The drainage area of this water system is extended in different countries such as: Albania, Montenegro, Kosovo, and North Macedonia. Drini River with its branches Kiri and Gjadri has a total drainage area of 14400 km². Shkodra Lake has a total drainage area of 5180 km² [1]. All the waters of this water system are discharged into the Adriatic Sea through Buna River bed. Total length of Buna River is 44 km. After 1.5 km away from its source out of Shkodra Lake, Buna River has a junction with Drini River. Figure 1 shows the location of the study area, which is situated in the northwestern part of Albania.

River engineering studies are carried out by 1Dimensional and 2Dimensional mathematical models. 1D models consider that the hydraulic variables (velocity and depth) change mainly in the direction of the flow. 2D models consider the horizontal velocity components in two dimensions (V_x and V_y). Other types of models are coupled 1D/2D models, where river flow is modeled in 1D and floodplain flow is modeled in 2D. This modeling technique is very effective, because gives accurate results while reducing the calculation time.



Figure. 1: Location of the study area (Source: Google Physical)

An important step in the process of building a mathematical model is validation. After the mathematical model is calibrated, should be validated in order to be reliable to be used in the future for various scenarios.

MATERIAL AND METHODS

The water system of Shkodra Lake, Drini and Buna River it is modeled using the SOBEK software. This software is provided in the framework of IPA Cross Border Albania-Montenegro project. SOBEK software is developed by the Deltares Institute in Delft, the Netherlands. SOBEK is an integrated software package for river, urban and rural management [2]. This software is designed to perform one-dimensional hydraulic calculations for a full network of natural or constructed channels, and also 2Dimensional hydraulic calculations on two-dimensional (2D) horizontal grids [2]. This software offers the opportunity of using the coupling 1D/2D modeling technique. The philosophy of 1D/2D coupling in SOBEK is based on the fact that the width of the river channel is small compared to the size of the

2D grid cell [3]. This can be applicable for relatively small rivers with a large floodplain. Buna River is a wide river, with cross sections which varies from 300 m to 600 m. For this reason, the coupling 1D/2D modeling technique is not appropriate. The water system of Shkodra Lake, Drini and Buna River it is modeled in 1D and fully 2D using the SOBEK software.

Mathematical model equations

To model the flow SOBEK software solves the full Saint-Venant equations. These equations are derived from the principle of conservation of mass (equation 1) and the principle of conservation of momentum in X and Y direction (equations 2 and 3). The Saint-Venant equations solved in SOBEK software [2] are given as follow:

$$\frac{\partial \zeta}{\partial t} + \frac{\partial(uh)}{\partial x} + \frac{\partial(vh)}{\partial y} = 0 \quad (1)$$

$$\frac{\partial u}{\partial t} + u \frac{\partial u}{\partial x} + v \frac{\partial u}{\partial y} + g \frac{\partial \zeta}{\partial x} + g \frac{u|\bar{u}|}{c^2 h} = 0 \quad (2)$$

$$\frac{\partial u}{\partial t} + u \frac{\partial u}{\partial x} + v \frac{\partial u}{\partial y} + g \frac{\partial \zeta}{\partial x} + g \frac{u|\bar{u}|}{c^2 h} = 0 \quad (3)$$

where: ζ water level above plane of reference [m]

h total water depth $h = \zeta + d$ [m]

d depth below plane of reference [m]

C Chézy Coefficient [\sqrt{m} /s]

u, v velocity in x and y - direction [m/s]

$|\bar{u}|$ velocity magnitude $|\bar{u}| = \sqrt{u^2 + v^2}$ [m/s]

The Saint-Venant equations are solved in SOBEK software by the Delft numeric scheme. This numerical scheme developed by Stelling, is a finite difference numerical technique based on the rectangular staggered grid [4]. In 1D modeling technique, the equation of conservation of mass and momentum in x direction (along the river channel) are solved. In 2D modeling technique, the equation of conservation of mass and momentum in x and y direction are solved.

Setting up the 1Dimensional mathematical model for the study area

The 1D mathematical model using SOBEK software was set up based on the digital terrain model developed from the topographic survey made in the study area during the period 2005-2006, from the Albanian Academy of Sciences and the Academy of Sciences and Arts of Montenegro [5]. The topographic survey was carried out for a large number of cross sections in Buna River and lower part of Drini River. The mathematical model built in SOBEK software for the water system of Shkodra Lake, Drini and Buna River is presented in figure 2. An important step in the process of setting up a 1D mathematical model is entering the cross section data. For this reason, it is very important to have a large number of cross sections to describe the geometry of the river system. The quality of the mathematical model depends on the accuracy of the terrain data. For the study area were used around

400 cross sections in total. Cross sections were measured at intervals of around 100 m from each–other, which gives a good representation of river bathymetry. Some of the cross sections are used to describe the bathymetry of Buna River mouth in Montenegro and Albania, and some cross sections in the downstream part of Drini River (1 km before joining Buna River). Another important element, which describes the river cross sections, is the roughness coefficient. For the river cross sections in SOBEK, which are Y-Z profiles, are used different roughness coefficients for main channel and overbank area. Figure 3 represents Manning’s roughness coefficient n for a given cross section in the 1D mathematical model in SOBEK software.

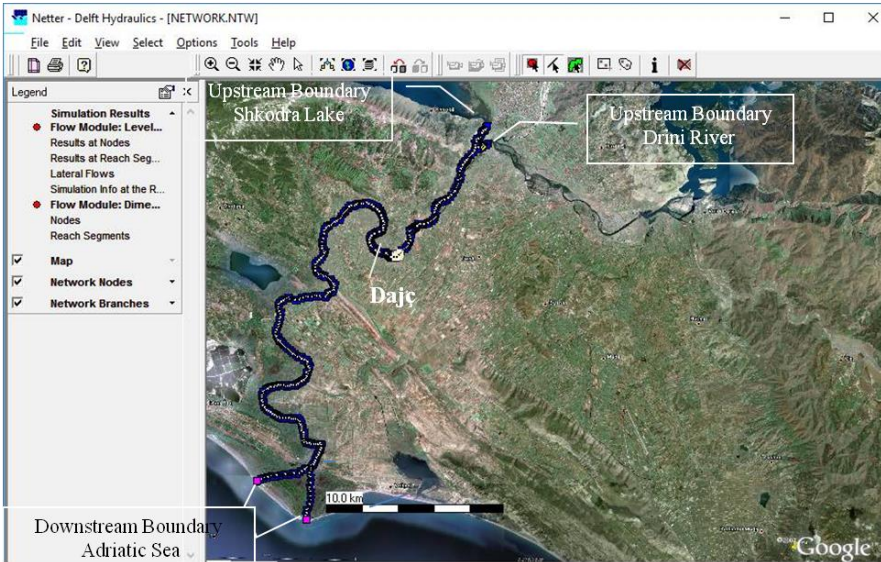


Figure 2. The 1D mathematical model built in SOBEK software for the study area

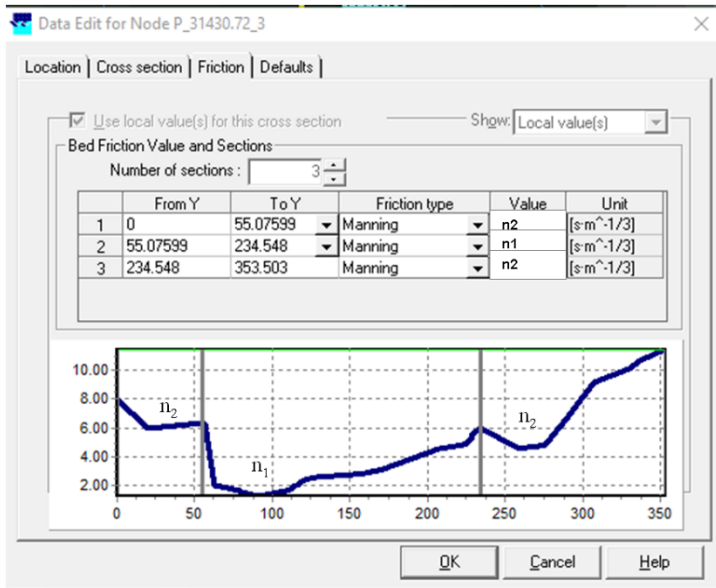


Figure 3. Representation of roughness coefficient for the 1D model built in SOBEK

Roughness coefficient values for the main channel (n_1) and for the overbank area (n_2) are given preliminary values based on tables and figures compiled by Ven Te Chow [6]. During the calibration process different values of Manning roughness coefficient n_1 and n_2 were tested. Manning roughness coefficient n_1 and n_2 , which give the best match between the measured values and model outputs were accepted.

Setting up the 2Dimensional mathematical model for the study area

The digital terrain model (DTM) is an important component of the 2Dimensional mathematical model. The quality of the mathematical model depends on the accuracy of the DTM for the study area. The DTM includes the topography of the river bed and topography of the floodplain. The DTM of river bed and overbank area was generated based on topographic survey carried out in the study area in 2005-2006, in the framework of a joint project between Albania and Montenegro [5]. The DTM for the floodplain was generated based on the digitalization of about 43 topographic maps on scale 1:10 000 covering the study region [7]. The topography of the study area is represented in SOBEK software by a rectangular 2D grid with grid cell size $\Delta x = \Delta y$. To have a good representation of the topography of the main channel and overbank area, the grid cell size of $\Delta x = \Delta y = 15$ m was chosen. The 2D mathematical model built in SOBEK software for the study area is presented in figure 4. Another important element of the 2D model for the study area is the 2D grid of roughness coefficient. This grid consists on the values of roughness coefficient for Buna River and lower part of Drini River, and values of roughness coefficient for the floodplain area. The roughness coefficient for the floodplain area was evaluated based on CORINE Land Cover 2012 database. Roughness coefficient values (Manning coefficient) for the cells in

the main channel (n_1), and for the cells in the overbank area (n_2) were given preliminary values based on literature recommendation [6]. After the calibration process, the roughness coefficient values (n_1) and (n_2), which give the best match between the measured values and model outputs were accepted.

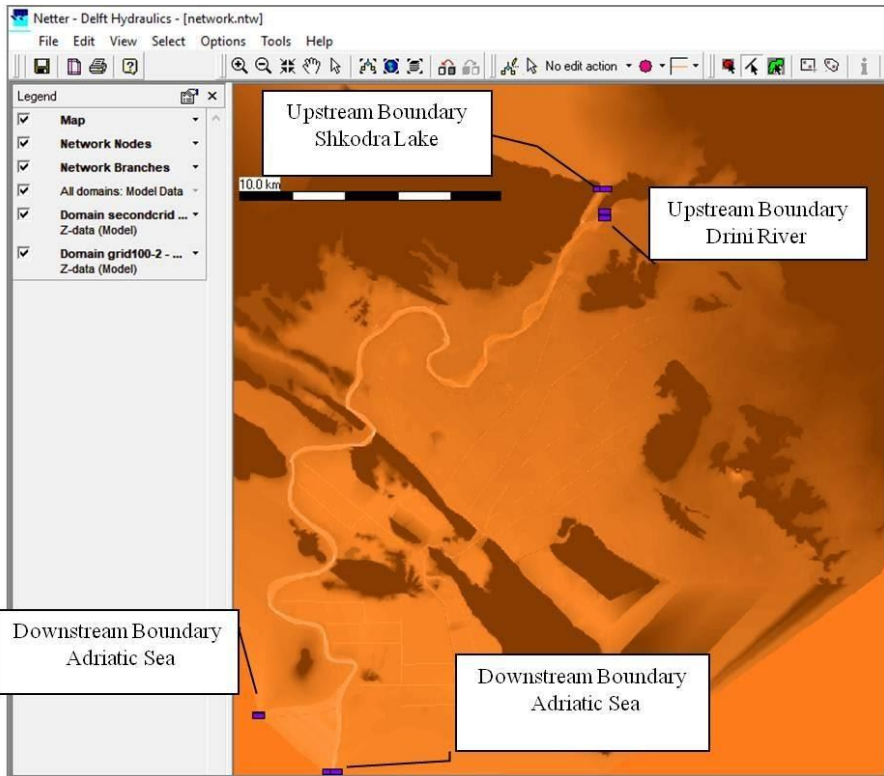


Figure. 4: View of 2D mathematical model built in SOBEK software for the study area

RESULTS AND DISCUSSION

Model validation is an important step in the process of modelling of a water system. According to ASME [8], validation is the process of determining the degree to which a model is an accurate representation of the real world from the perspective of the intended uses of the model. During the validation process, the predictive capability of the mathematical model is evaluated. After the mathematical model is calibrated, it is then validated for a new set of measured data different from the ones used in the calibration process. The purpose of calibration process is to match the model results with field measurements by changing different model parameters, while the purpose of validation is to test the calibrated values of the model parameters.

The 1D and 2D mathematical models for the study area are validated based on hourly water level measurements from the online automatic stations of Dajç

(Buna River), Buna Bridge (Buna River), and Bahçellëk Bridge (Drini River) shown in figure 2. The inflow hydrograph at Buna Bridge takes into account the flow coming out of Shkodra Lake into the Buna River. Whereas the inflow hydrograph at Bahçellëk Bridge takes into account the flow coming into Buna River from Drini River. The inflow hydrographs at Buna Bridge and Bahçellëk Bridge are used as upstream boundary conditions, whereas as downstream boundary condition it is used the hydrograph of Adriatic Sea water level at Buna River mouth in Albanian and Montenegro. The discharge hydrographs at Buna Bridge and Bahçellëk Bridge station are calculated based on stage–discharge relationship created from discharge measurements done in these stations for the period 1992–2001, and 2010 [9].

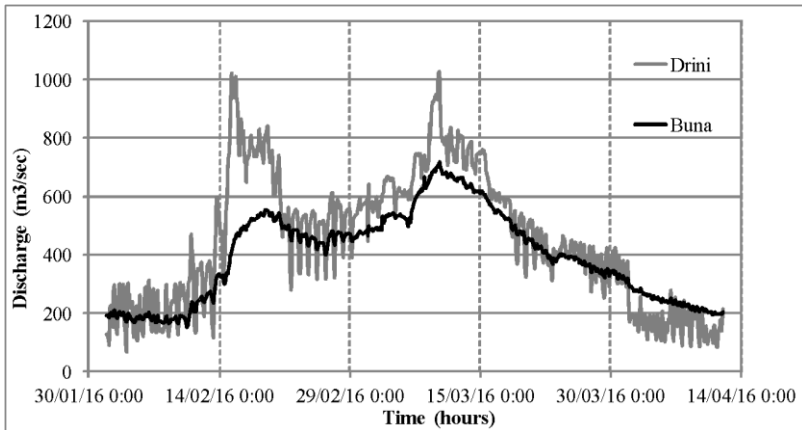


Figure. 5 The inflow hydrographs at Buna and Drini River for the validation period

Performance analyses of 1D versus 2D mathematical model

According to Silgram and Schoumans [10], the accuracy of the mathematical model is defined as the degree to which the predicted values of the model are close to the corresponding measured values. Mathematical model performance is evaluated based on graphical comparison of simulated values against measured data and statistical test. Statistical tests used to evaluate the performance of 1D and 2D mathematical models for the study area are: Root Mean Square Error (RMSE), Mean Absolute Error (MAE), and Correlation Coefficient (R). The validation period is from 01-02-2016 until 11-04-2016. This period is chosen because the river flow goes from low to high flow. Missing and inconsistent data from hourly water levels from the online stations are corrected. In figure 6 are presented hourly water level results from the 1D and 2D mathematical model versus measurements from the on-line station in Dajç for the period of validation.

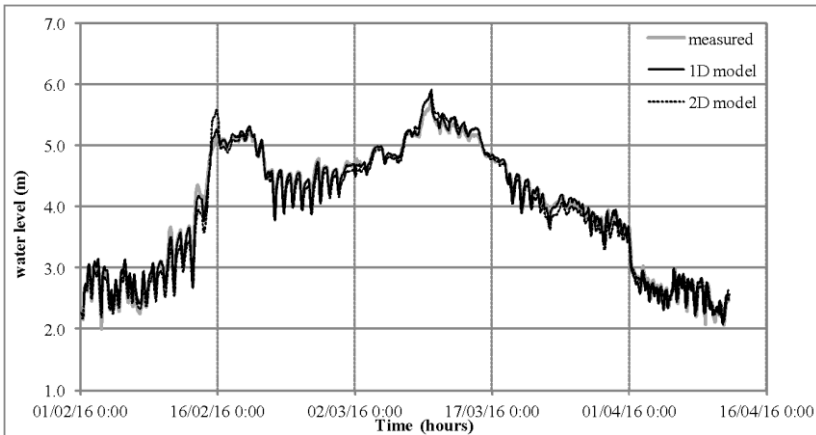


Figure 6. Measured versus simulated water levels from the 1D and 2D model for the validation period

Based on graphical comparisons there is generally strong agreement between measured and simulated water levels at Dajç station from the 1D and 2D models. The discrepancies between the measured and simulated water levels from the 1D and 2D models generally are within ± 15 cm, which is an acceptable value. The 1D and 2D model results appear to match the time of the peak, but slightly overestimate the peak flood levels (especially in the second peak). From the graphical comparison, the water level predicted from the 1D model are much closer to measured level in comparison with the water levels predicted from the 2D model.

The performance of the 1D and 2D mathematical model is analysed based also on statistical tests. For the 1D model the values of statistical tests are as follow: RMSE=11.6 cm, MAE=9.4 cm, R=0.95. For the 2D model the values of statistical tests are as follow: RMSE =13.1 cm, MAE=10.1 cm, R=0.94. The results of the statistical tests indicate that the 1D model performs better than the 2D model having smaller values of RMSE and MAE and a slightly higher Correlation Coefficient value than the 2D model.

As a final remark, the 1D model for the study area performs better than the 2D model for the validation period based on graphical comparison and statistical tests.

CONCLUSIONS

Buna River is part of the water system of Shkodra Lake, Drini and Buna River, which is the largest in Albania. This water system was studied through the 1D and fully 2D mathematical modeled built in SOBEK software. The 1D mathematical model represents the River Buna and lower part of Drini River bathymetry with around 400 cross sections spaced at a distance of 100 m from each other. The 2D model uses a rectangular grid, with cell size of 15 m. This value is chosen because it gives a good representation of the river bathymetry and the irregular floodplain area. Smaller grid cell sizes will make the 2D model more accurate, but will increase the total number of grid cells. This will lead to the increase of the computation time

and will face software limitations for the total number of cells that can handle during the simulation.

Graphical comparison between measured water levels and computed from 1D and 2D model for the validation period shows an acceptable difference value. The timing of the two flow peaks are predicted well from both models, but the peak water levels are slightly higher than measured water levels, especially for the 2D model. Regarding the statistical tests, the 1D and 2D model have quite satisfactory errors values.

Validation results indicate that 1D model performs better than the 2D model based on graphical comparison and statistical tests. This fact makes the 1D model more suitable to model the flow up to bankfull discharge. The 1D model performs better than the 2D model saving also computational time, due to a more accurate representation of the river bathymetry with river cross sections. Rectangular 2D grids have problems in representing complex geometric river shapes. In contrary, 2D curvilinear grids follow the river channel and can capture well the river bathymetry. The curvilinear grid, which is currently been implemented from Deltares Institute will improve the flow representation in the fully 2D model.

REFERENCES

- [1] Institute of Hydro-Meteorology of Albania, Academy of Science of Albania, Hydrology of Albania, Albania, 1984.
- [2] Deltares, SOBEK User Manual, Version 2.13, <https://www.deltares.nl/>, Delft.The Netherlands, 2013.
- [3] Verwey A, Latest Developments in Floodplain Modelling-1D/2Dintegration, Proceedings of 6th Conference on Hydraulics in Civil Engineering, The State of Hydraulics, Australia, pp 13-24, 2001.
- [4] Stelling G.S., Duinmeijer S.P.A., A staggered conservative scheme for every Froude number in rapidly varied shallow water flows, International Journal For Numerical Methods in Fluids, vol. 43, pp 1329-1354, 2003.
- [5] ASA & AASM, Topo-geodetic measurements of Buna River, Academy of Sciences of Albania Academy of Sciences and Arts of Montenegro, 2006.
- [6] Chow V.T., Open Channel Hydraulics, McGraw-Hill Book Co, NY, USA, 1959.
- [7] Pandazi S, Abazi E, Regulation of the hydraulic regime of the water system of Shkodra Lake, Buna, and Drini Rivers, Project of National Agency of Research and Innovation, INEUM, 2011.
- [8] ASME (The American Society of Mechanical Engineers), Guide for Verification and Validation in Computational Solid Mechanics, 2006.
- [9] GIZ, German Federal Enterprise for International Cooperation, Climate Change Adaptation in Transboundary Flood Risk Management, Western Balkans, 2018.

[10] Silgram M., Schoumans O.F., 2003, Modeling approaches: Model parameterization, calibration and performance assessment methods in the EUROHARP project, EUROHARP report 8, NIVA report SNO 4740, Oslo, 2004.

FACTOR ANALYSIS OF GEOGRAPHIC COORDINATES AT POINTS OF THE CHANNEL OF A SMALL RIVER ON SPACE IMAGES

Dr. Sc., Prof. Peter Matveevich Mazurkin ¹

Yana Oltgovna Georgieva ²

^{1,2} Volga State University of Technology, Yoshkar-Ola, Russia

ABSTRACT

The purpose of the article is the analysis of asymmetric wavelets in binary relations between three coordinates at 290 characteristic points from the source to the mouth of the small river Irovka. The hypsometric characteristic is the most important property of the relief. The Irovka River belongs to a low level, at the mouth it is 89 m high, and at the source it is 148 m above sea level. Modeling of binary relations with latitude, longitude, and height has shown that local latitude receives the greatest quantum certainty. In this case, all paired regularities received a correlation coefficient of more than 0.95. Such a high adequacy of wave patterns shows that geomorphology can go over to the wave multiple fractal representation of the relief. The Irovka River is characterized by a small anthropogenic impact, therefore, the relief over a length of 69 km has the natural character of the oscillatory adaptation of a small river to the surface of the Vyatka Uval from its eastern side. This allows us to proceed to the analysis of the four tributaries of the small river Irovka, as well as to model the relief of the entire catchment basin of 917 km². The greatest adequacy with a correlation coefficient of 0.9976 was obtained by the influence of latitude on longitude, that is, the geographical location of the relief of the river channel with respect to the geomorphology of the Vyatka Uval. In second place with a correlation of 0.9967 was the influence of the height of the points of the channel of the small river on local longitude and it is also mainly determined by the relief of the Vyatka Uval. In third place was the effect of latitude on height with a correlation coefficient of 0.9859. And in last sixth place is the inverse effect of altitude on local latitude in the North-South direction.

Keywords: *river, channel, latitude, longitude, altitude*

INTRODUCTION

One of the possible ways of analyzing the Earth's remote sensing is to use the approaches of mathematical landscape morphology — the direction of landscape science, which studies the quantitative laws of building mosaics formed on the earth's surface and develops methods for their mathematical analysis [1].

The article [2] gives a brief overview of the experience of using harmonic analysis for morphometric characteristics of the relief. Up to 10 harmonics with constant period and amplitude of oscillation were obtained. The Fourier transform can be used for the classification and zoning of the earth's surface according to its

harmonic characteristics that determine the specifics of the topographic division of the site.

In recent years, interest in ecology has noticeably increased, and attention to small rivers has increased. Small rivers are the most vulnerable link in river systems, which is associated with their low water content and low erosion-transporting ability. Hence the special sensitivity of small riverbeds to anthropogenic impacts: the construction of earthen dams, bridges, local water intake and discharge of untreated (usually) wastewater, deforestation and plowing of watersheds. Any of these actions causes irreversible changes in the small river system until its death [3].

The fractal distribution of rivers by length in a river network has certain advantages over other morphometric indicators that are used to describe river networks. The fractal approach significantly increases the possibility of a quantitative description of river and erosion-channel networks [4].

Using satellite images, we measured coordinates (latitude, longitude, altitude) [5] according to methodological recommendations [6]. The characteristic points from the source to the mouth were selected on the line of the small river rod by changes in the longitudinal profile of at least 10-150 at the channel of the small river. Then, according to the measurement results, a coordinate table is compiled to identify patterns according to the method [7].

The goal is the analysis of asymmetric wavelets in binary relations between three coordinates at 290 characteristic points from the source to the mouth of the small river Irovka.

MATERIALS AND METHODS

Table 1 shows the results of measurements of three coordinates in the form of a fragment.

Table 1. Characteristic coordinates points of the channel of the river Irovka

The hypsometric characteristic is one of the most important properties of the relief. By elevation of the land surface above sea level, a low-lying (absolute height from 0 to 200 m) relief is distinguished [8].

The Irovka River has a height of 89 m at the mouth, and 148 m at the source (Fig. 1).

Point rank	Latitude α , minute	Longitude β , minute	Height h , m
0	0	17.39	59
1	0.02	17.50	52
2	0.19	17.62	48
...
287	23.84	2.019	4
288	23.87	2.035	2
289	23.89	2.017	0

According to the hypsometric picture in Figure 1, Irovka flows inside a rectangle 23.89 minutes long (local latitude) and 18.89 minutes wide (local longitude). Sudden changes in the channel curvature in terms of 290 characteristic points gave several wave equations. Next, consider binary relations.

Oscillations (wavelet signals) are written by the wave formula [7] of the form

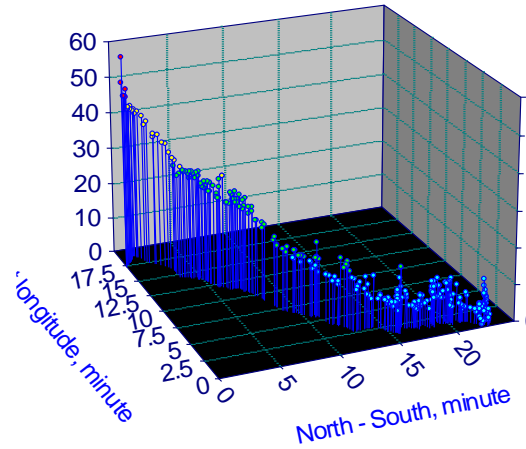


Fig. 1. Spatial hypsometry of the river

$$y_i = A_i \cos(\pi x / p_i - a_{8i}), \quad A_i = a_{1i} x^{a_{2i}} \exp(-a_{3i} x^{a_{4i}}), \quad p_i = a_{5i} + a_{6i} x^{a_{7i}}, \quad (1)$$

where y - is the indicator (dependent factor), i - is the number of the component of the model (1), m - is the number of terms in (1), x - is the explanatory variable (influencing factor), a_1 - a_8 - are the parameters (1) that take values during structural-parametric identification in CurveExpert-1.40, A_i - the amplitude (half) of the wavelet (axis y), p_i - the half-wave period (axis x).

According to the formula (1) with two **fundamental physical constants** ℓ (the number of Neper or the number of time) and \mathcal{T} (the number of Archimedes or the number of space), a **quantized wavelet signal** is formed from within the studied phenomenon and/or process. The concept of wavelet signal allows us to abstract from the physical meaning of many statistical series of measurements and consider their additive decomposition into components in the form of a sum of individual wavelets.

A signal is a material carrier of information. And we understand information as **a measure of interaction**. The signal can be generated, but its reception is not required. A signal can be any physical process or part of it. It turns out that the change in the set of unknown signals has long been known, for example, through the series of meteorological measurements. However, there are still no statistical models as the dynamics of weather parameters.

At the information technology level, the 23rd Hilbert problem (development of methods of variational calculus) was solved by us [7].

At the same time, **the variation of functions** is reduced to the conscious selection of stable laws and the construction of adequate stable laws on their basis. We adhere to the concept of Descartes on the need to apply an algebraic equation

of General form (1) directly as a finite mathematical solution of unknown differential or integral equations.

RESULTS AND DISCUSSION

After identifying the general model (1) from three coordinates in table 2, six binary relations were obtained.

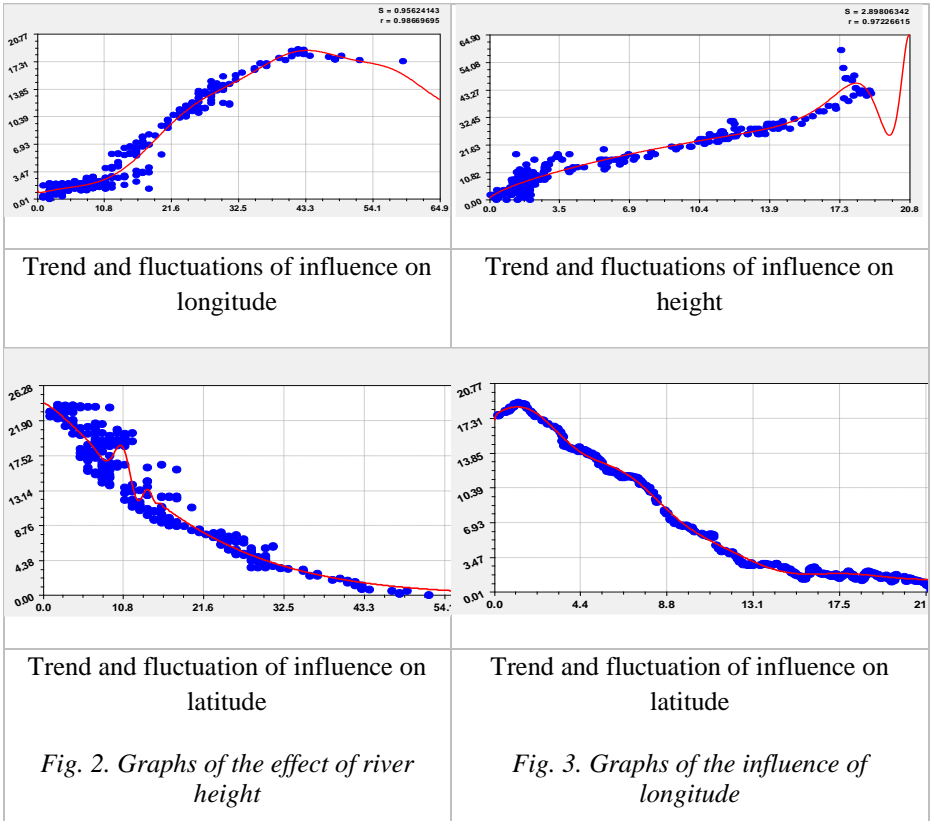
Table 2. Model parameters for binary relations of the coordinates of the Irovka River

Number <i>i</i>	Wavelet								Coef. corr. <i>r</i>
	$y_i = a_{1i} x^{a_{2i}} \exp(-a_{3i} x^{a_{4i}}) \cos(\pi x / (a_{5i} + a_{6i} x^{a_{7i}}) - a_{8i})$								
	Amplitude (half) of oscillations			Half oscillation			Shift		
	a_{1i}	a_{2i}	a_{3i}	a_{4i}	a_{5i}	a_{6i}	a_{7i}	a_{8i}	
The effect of altitude from the mouth to the source of the river on the longitude									
1	0.036510	1.84872	0.0001525	2.25378	0	0	0	0	0.9967
2	2.17901	0	0.060421	0.28602	10.34394	-0.0034879	1.50771	1.02204	
The effect of altitude from the mouth to the source of the river on the latitude North-South									
1	24.11765	0	0.021872	1.28116	0	0	0	0	0.9693
2	-4.1157e-2	33.7806	3.19877	1	10.11218	-0.14566	1.41996	-3.8745	
The effect of longitude from the left point of the channel on the height from the mouth									
1	4.58566	0.73085	0	0	0	0	0	0	0.9723
2	2.03445	0	-1.7537e-5	3.90439	42.76414	-1.60613	1/03524	-1.2629	
The effect of longitude from the left point of the channel on the North-South latitude									
1	22.87329	0	0:0022749	2.42253	0	0	0	0	0.9724
2	-9.48597	3.81920	2.13995	0.64925	0	0	0	0	
3	3.10268e8	6.37127	19.73370	0.25275	0.41871	0.019294	1.94415	0.14850	
The influence of latitude North-South from source to mouth on the height from the mouth									
1	58.96563	0	0.11761	0.85812	0	0	0	0	0.9859
2	-1.71136e6	0.70048	12.14870	0.057545	0	0	0	0	
3	1.4690e-34	38.8795	1.67667	1.03588	83.45225	-4.18801	0.91671	-2.7359	
The effect of North-South latitude from source to mouth on longitude from the left point									
1	19.08116	0	0.039811	1.32388	0	0	0	0	0.9976
2	-1.6119e-6	26.2539	14.89933	0.49461	0	0	0	0	
3	-2.09089	0	0.82090	0.40884	2.36913	0.0028086	1.55183	-0.3599	

The greatest adequacy with a correlation coefficient of 0.9976 was obtained by the influence of latitude on longitude. In second place with correlation 0.9967 was the influence of the height of the points of the channel of the small river on local longitude, and it is mainly determined by the relief of the Vyatka Uval. In third place was the influence of latitude on height with a correlation coefficient of 0.9859.

And in last sixth place is the inverse effect of altitude on local latitude in the North-South direction. All two-three-membered models have the strongest adequacy, that is, the correlation coefficient is more than 0.95.

The influence of altitude from the mouth to the source of the river and longitude from the left point of the channel. Figures 2 and 3 show graphs of the influence of altitude and longitude for the models from table 2.



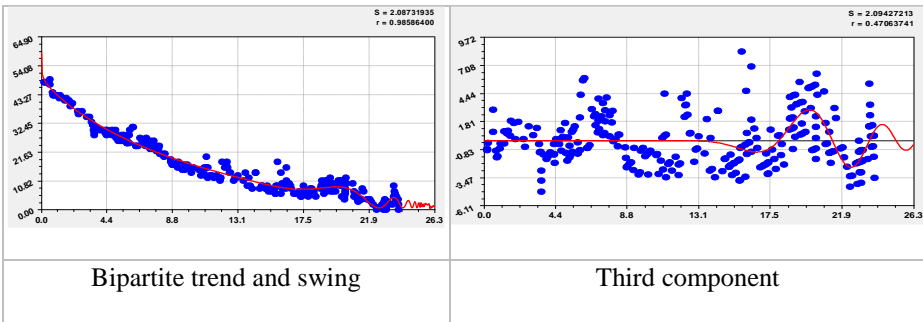
High adequacy allows us to conclude that the coordinates of the small river bed have common properties. One of them is the continuity of the water flow.

The impact of North-South latitude from source to mouth. Latitude affects the other two parameters (altitude and longitude) fractally (Table 3 includes 11 members, Table 4 - 13 wavelets). This fractality is determined by the multiple structure of the components (1).

Table 3. The influence of North-South latitude from source to estuary of the height of the Irovka River

Number <i>i</i>	Wavelet								Coef. corr. <i>r</i>
	$y_i = a_{1i} x^{a_{2i}} \exp(-a_{3i} x^{a_{4i}}) \cos(\pi x / (a_{5i} + a_{6i} x^{a_{7i}}) - a_{8i})$								
	Amplitude (half) of the oscillation				Half oscillation			Shift	
	a_{1i}	a_{2i}	a_{3i}	a_{4i}	a_{5i}	a_{6i}	a_{7i}	a_{8i}	
1	58.96563	0	0.11761	0.85812	0	0	0	0	0.9859
2	-1.71136e6	0.70048	12.14870	0.057545	0	0	0	0	
3	1.46900e-34	38.87949	1.67667	1.03588	83.45225	-4.18801	0.91671	-2.7359	
4	0.156044	3.10878	0.486002	1	2.82186	1.2071e-4	2.76209	1.22940	0.3909
5	2.89862e-15	20.01880	1.28894	1.01392	0.071542	0.0097915	1.07050	13.4560	0.3601
6	5.09823e-99	116.0002	2.35448	1.33230	0.077773	0	0	4.71515	0.2785
7	5.26586e-6	4.85253	0.153153	0.990526	0.106066	0	0	1.39946	0.1704
8	2.71862e-81	0	4.18864	1	0.113739	2.66500	0	0	0.1474
9	5.20858e-23	35.73529	3.03928	1.01566	4.04816	0.0655608	1.23614	-3.8501	0.1035
10	0.0921386	1.56575	0.172271	1	0.524478	4.53850	0	0	0.1791
11	0.896703	2.36906	0.877726	0.901428	0.771798	0	0	2.92625	0.1891

The adequacy of the influence of latitude can reach a correlation coefficient of 1. And this fact shows that the influence of local latitude has a high degree of certainty of quantization by wave equations (Fig. 4-7). This is called full factor analysis.



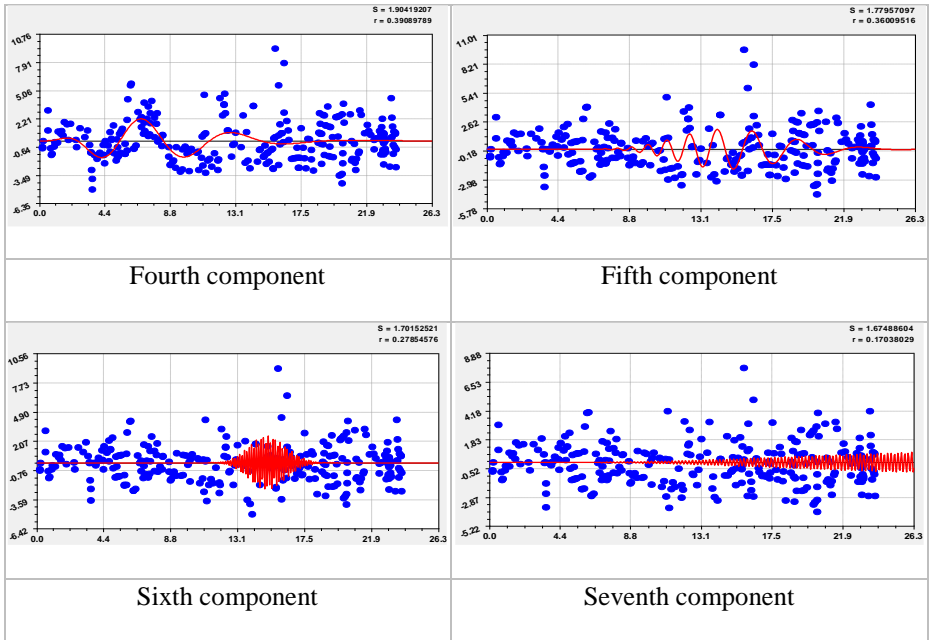


Fig. 4. Graphs of the effect of North-South latitude from source to mouth on the height of the Irovka River

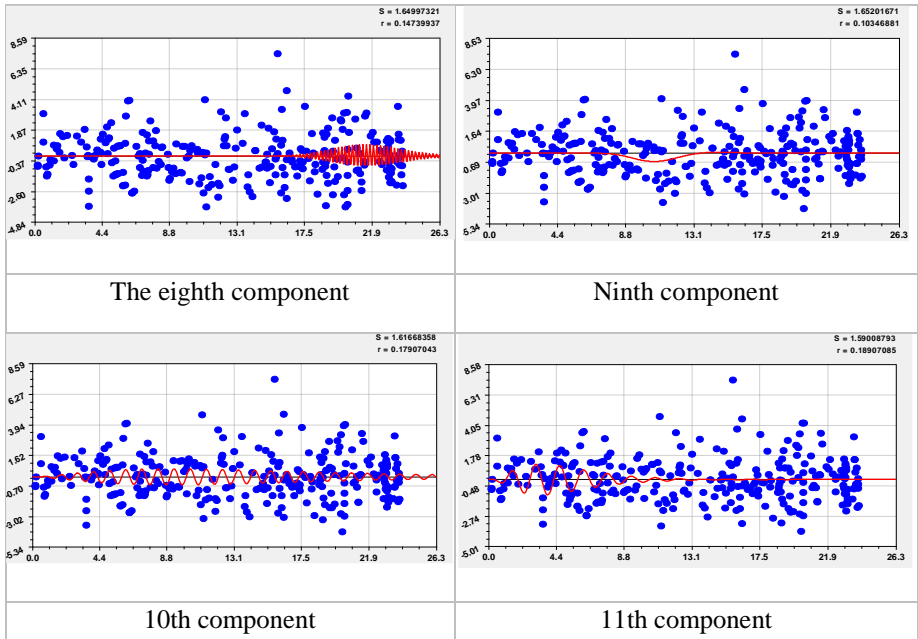
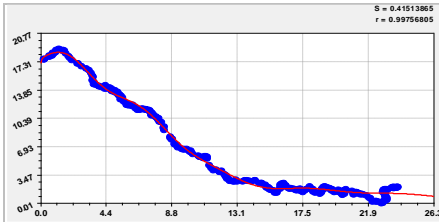


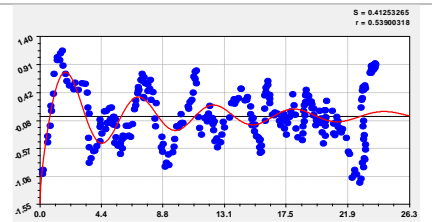
Fig. 5. Graphs of the influence of the North-South latitude on the height from the mouth to the source of the Irovka River

Table 4. The effect of North-South latitude from source to mouth on the longitude of the Irovka River

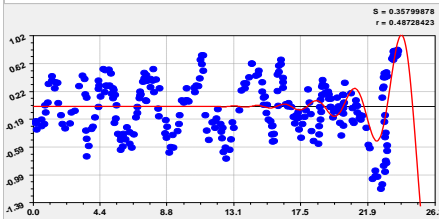
Number <i>i</i>	Wavelet								Coef. corr. <i>r</i>		
	$y_i = a_{1i}x^{a_{2i}} \exp(-a_{3i}x^{a_{4i}}) \cos(\pi x / (a_{5i} + a_{6i}x^{a_{7i}}) - a_{8i})$				Amplitude (half) of oscillations			Half oscillation		Shift	
	a_{1i}	a_{2i}	a_{3i}	a_{4i}	a_{5i}	a_{6i}	a_{7i}	a_{8i}			
1	19.08116	0	0.039811	1.32388	0	0	0	0	0.9976		
2	-1.6119e-6	26.2539	14.89933	0.49461	0	0	0	0			
3	-2.09089	0	0.82090	0.40884	2.36913	0.0028086	1.55183	-0.35993			
4	1.95823e-5	0	0.448432	1.00282	0.0820466	0.0119878	1.00090	5.45636	0.4873		
5	0.0168527	3.08551	0.378919	1.00055	1.58592	6.8921e-5	2.25901	2.74470	0.5584		
6	4.51507e-6	4.65846	0.0012670	2.65421	0.156256	0.232502	0.21971	12.0842	0.3172		
7	0.0074286 4	0	2.07429	0.127857	-0.033421	1.99360	0.07957	6.22674	0.3006		
8	1.14486e-8	7.88750	0.253085	1.12234	5.64354	1.01837	0	0	0.2100		
9	1.59713e-7	5.97718	0.379652	0.825954	0.857850	0	0	6.11295	0.2035		
10	1.28249	0.78853	1.19686	0.595343	0.772734	0.0263791	0.91301	1.77834	0.3538		
11	1.7925e-13	11.7651	0.564683	0.905328	0.375291	0	0	2.47176	0.1360		
12	0.0264789	1.10650	0.119784	0	0.497133	0	0	1.05946	0.2198		
13	1.31795e-8	11.2761	2.044278	0.735657	0.594690	0	0	0.97851	0.0465		



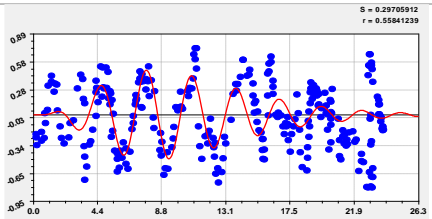
Bipartite trend and swing



Third component



Fourth component



Fifth component

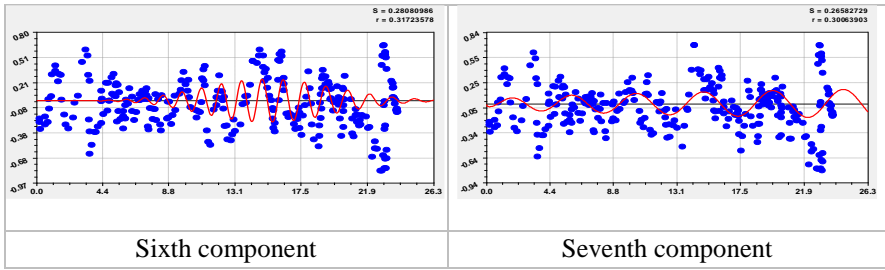


Fig. 6. Graphs of the influence of North-South latitude on longitude from the left point of the channel of the Irovka River

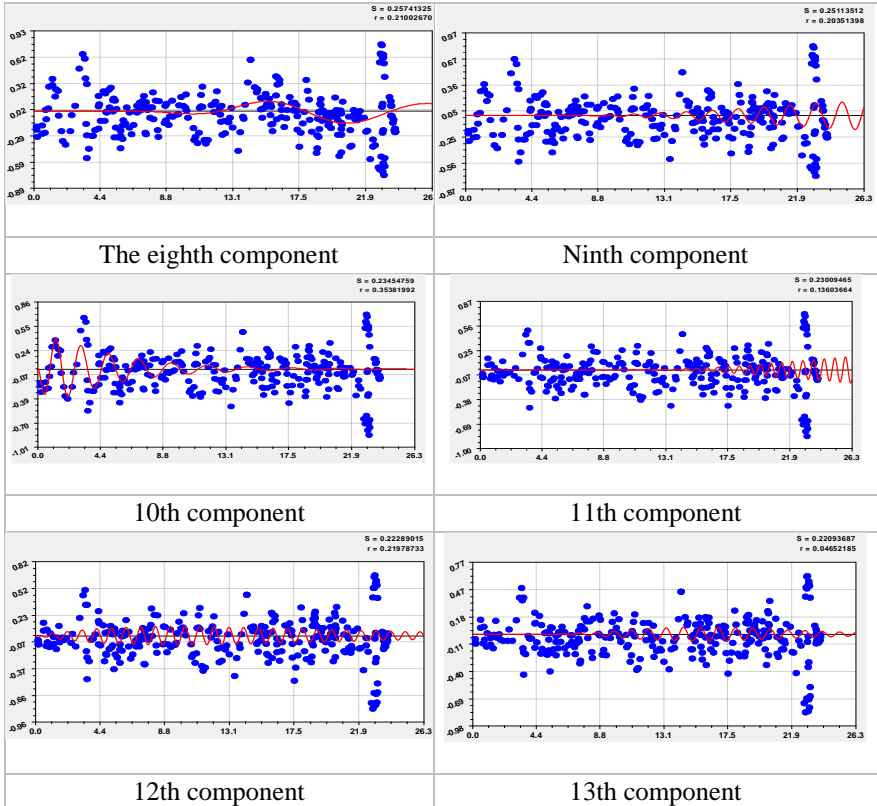


Fig. 7. Graphs of the influence of North-South latitude on longitude from the left point of the channel of the Irovka River

Thus, of the three coordinates for 290 characteristic points of the channel of the small river Irovka, the largest level of non-multiple fractality has the set of 13 wavelets of the influence of the local North-South latitude on the local longitude. A comparison of rank distributions showed that model (1) for latitude received 25 members, for longitude 18 and for a height of 12 members.

CONCLUSION

The hypsometric characteristic is the most important property of the relief. The Irovka River belongs to the low level, at the mouth it is 89 m high, and at the source it is 148 m above sea level. The article shows the possibility of obtaining patterns of hypsometry.

Modeling of binary relations between the three coordinates (latitude, longitude, and height) of the characteristic points of the Irovka river showed that the local latitude receives the greatest quantum certainty. In this case, all paired regularities received a correlation coefficient of more than 0.95. Such a high adequacy of wave patterns shows that geomorphology can go over to multiple fractal representation of the relief. The Irovka River is characterized by a small anthropogenic impact, therefore, the relief over a length of 69 km has the natural character of the oscillatory adaptation of a small river to the surface of the Vyatka Uval from its eastern side. This allows us to proceed to the analysis of the four tributaries of the small river Irovka.

The greatest adequacy with a correlation coefficient of 0.9976 was obtained by the influence of latitude on longitude, that is, the geographical location of the relief of the river channel relative to the geomorphology of the land on the eastern side of the Vyatka Uval. In second place with a correlation of 0.9967 was the influence of the height of the points of the channel of the small river on local longitude, and it is also mainly determined by the relief of the Vyatka Uval. In third place was the influence of latitude on height with a correlation coefficient of 0.9859. And in last sixth place is the inverse effect of altitude on local latitude in the North-South direction.

REFERENCES

- [1] Sadkov S.A. Morphological structure of plains subject to ground Subsidence on the basis of mathematical morphology of landscapes approach // *Geomorphology RAS*. 2019;(1);48-58. doi: 10.31857/S0435-42812019148-58.
- [2] Kharchenko S.V. Application of harmonic analysis for the quantitative description of earth surface topography // *Geomorphology RAS*. 2017;(2):14-24. doi: 10.15356/0435-4281-2017-2-14-24.
- [3] Azizov Z.K. The structure of the valleys of small rivers of the Ulyanovsk region: dis. ... cand. geo sciences. Kazan: KSU, 2000.177 s. URL: <https://www.dissercat.com/content/stroenie-dolin-malykh-rek-ulyanovskogo-predvolzhya> (Accessed October 10, 2019).
- [4] Sidorchuk A.Y. Fractal geometry of the river network // *Geomorphology RAS*. 2014;(1):3-14.doi: 10.15356/0435-4281-2014-1-3-14.
- [5] Mazurkin P.M., Georgieva Y.O. Measurement of coordinates by satellite imagery along the bed of the small river Irovka in the Republic of Mari El // *Successes in modern science*. 2019.No 12 (part 2). S. 294-300; URL: <http://www.natural-sciences.ru/en/article/view?id=37304> (date of treatment: 01.24.2020).

[6] Maps of heights, slopes. URL: <http://votetovid.ru/#56.201192,48.95536,17z,51v30l> (date of treatment 02.10.2019).

[7] Mazurkin P.M. Wavelet Analysis Statistical Data. *Advances in Sciences and Humanities*. Vol. 1.No. 2. 2015. pp. 30-44. doi: 10.11648/j.ash.20150102.11.

[8] Levers G.I. *Geomorphology*. Textbook for academic undergraduate. M.: Yurayt, 2018.396 p

HYDROLOGICAL MODELLING AND ESTIMATION OF THE SEDIMENTS ACCUMULATION IN BOVILLA RESERVOIR

PhD Student Klodian Zaimi ¹

Assoc. Prof. Fatos Hoxhaj ²

^{1,2} Institute of GeoSciences, Energy, Water and Environment, Albania

ABSTRACT

Bovilla reservoir is the main source of water supply for around 1 million inhabitants in Tirana, the capital of Albania. The reservoir was created in 1998 from Bovilla Dam and belongs to the upper part of the Terkuza River catchment. The dam previously was planned in a smaller size for irrigation purposes. Intense erosion due to large deforestations followed by increasing nutrient run-off from cultivated land is a challenge for the Bovilla Dam management authority because it is influencing the water quality in daily use and decreasing the dam lifespan in long term. Zall Bastari stream transports high amounts of solid materials. Other streams show also a strong torrential character, after rainfall events the water level suddenly rises which leads to massive erosion. Daily meteorological parameters and 30 meters Digital Terrain Model is used together with Land Cover Map in the HEC-HSM hydrological model which is designed to simulate the complete hydrologic processes of watershed systems, including the erosion and sediment transport. The lack of water level and discharge data made impossible the calibration of the hydrological model. The creation of a new data series for the daily discharges was crucial for further analyzes of the sediment transport and accumulation into the reservoir. Bovilla basin has been divided into many sub-basins in order to better calculate the inflow at the reservoir. The lack of previous bathymetric data caused the usage of alternative ways to calculate total accumulated sediment into the reservoir instead of the classical way in lifespan analysis. The characteristics of the sediment in the sub-basins and in the riverbed have been defined through gradation curves got from some available data. Sediment yield has been evaluated based on the conditions of the previous 21 years, from the construction of the dam in 1996 to nowadays. The old storage curve has been interpolated to be compared with the one defined after the survey specifically done in 2017. The analysis was very important to understand the way how are accumulated sediment into the reservoir but also their distribution through the reservoir bed.

Keywords: *hydrological model, sediments, land-use, catchment, reservoir*

INTRODUCTION

The Bovilla reservoir is one of the largest hydro-technical constructions in Albania, built to deliver sufficient drinking water to the capital Tirana. The catchment area is mountainous and belongs to the upper part of the Terkuza River. The dam is made from conglomerate rocks and gravel. The dam is 91 m high and 130 m long. Construction work originally began in 1988 but stopped with the

collapse of the communist political system. In October 1993, work was resumed thanks to the support of the Italian government. After the end of construction in 1996, the lake took until 1998 to fill and begin to serve its purpose. The volume of the reservoir is about $80 \times 10^6 \text{ m}^3$ at the normal level, quoted at 318 m a.s.l., on a surface of about 4.6 km^2 . The original maximal depth was 53 m, the difference between the quotes of 265 m to 318 m a.s.l. (normal water level) found near the dam, now reduced to about 45 m due to the sediments brought in by the Terkuza River. The residence time of the water is about one year. The volume of the body of the dam is $650\,000 \text{ m}^3$. The average annual inflow of water in the reservoir is $105 \times 10^6 \text{ m}^3$ [1]. The catchment is part of the Terkuza River and is divided between two municipalities, Zall Bastari (Tirana) and Culli (Kruja). The Bovilla catchment belongs to the sub-hilly Mediterranean Climate, where two climate sub-zones are distinguished, hilly Mediterranean (up to 700-800 m a.s.l.) and pre-mountainous Mediterranean (in higher altitudes). The catchment is characterized by heavy precipitations mainly during the end of winter and end of autumn [2]. In the hilly zone, the rainfall dominates, distributed in two peaks, autumn, and winter, while the mountainous peaks are often covered with snow during the winter. The catchment is split into a diverse hydrographic network consisting of many brooks, torrents, and tributaries of the Terkuza River. Bovilla catchment has some springs with a moderate or small flow and some small irrigation reservoirs. The main torrents originate from the Zall Bastari and Zall Mneri villages. The length of the main tributary is about 12 km. The average slope of the river is around 5.7% in the valley and around 10% in the mountains.

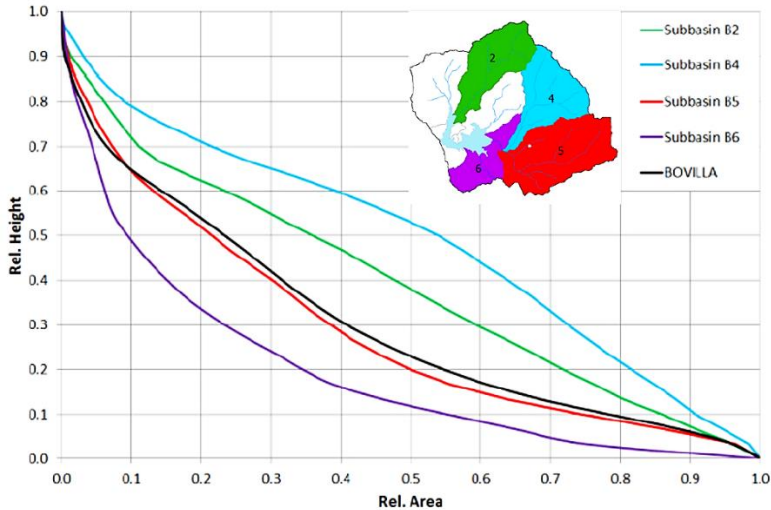


Figure 1 – Hypsometric curves of some sub-basins: sub-basins n.5 and 6 (red, violet) are in the old age, sub-basins 2 and 4 (green, blue) are in the maturity age.

Figure one shows the hypsometric curve of the Bovilla basin: it can be observed that the basin can be considered in the maturity stage according to Scheidegger's definition [3]. Analyzing more in detail the different sub-basins, some of them present a different stage, in particular, the hypsometric curves of the sub-basins

show that the younger is still in their maturity age. The geologic formations in the watershed belong mainly to Flysch, but only the formations in the higher parts seem to be more resistant to erosion. The lower part is hilly, built up of Flysch cliffs, frequent with eroded slopes, especially around the Mneri village. This group of rocks belongs to highly productive karst aquifers and moderately productive fissured (or fissured and porous) aquifers. Intense erosion due to large deforestation followed by increasing nutrient run-off from cultivated land has led to eutrophication of the aquatic system. Additionally, the river Terkuza is continuously filled with gravel, which is subsequently deposited in the Bovilla reservoir. Moreover, keeping the reservoir in a natural state will prevent costly water treatment measures and guarantee Tirana town access to the drinking water of high quality. Zall Bastari stream transports high amounts of solid materials. Other brooks show also a strong torrential character, after stormy rainfall events the water level suddenly rises which leads to massive erosion. Erosion, logging, desertification, and intense rainfall have amplified such clayey torrents, erosion spots, and landslides. Due to the lack of artificial sedimentation trapping, the eroded solid material is deposited in the lake resulting in a sedimentation rate of approximately 1 to 1.3 meters per year [4].

MATERIALS AND METHODS

Land use maps for Bovilla watershed has been collected from two different sources. In order to validate the high coverage CORINE map, it has been collected from the Ministry of Tourism and Environment (MTE) the detailed 2017 map for the Bovilla watershed. In CORINE map Land Use is classified in 44 classes of which only 12 used in the study area, in MTE map it's classified in 19 classes over the study area. The classes in 8 macro-classes, with a good correspondence between the two sources. This useful information has then been used in the Hydrological Model to define sediment delivery.

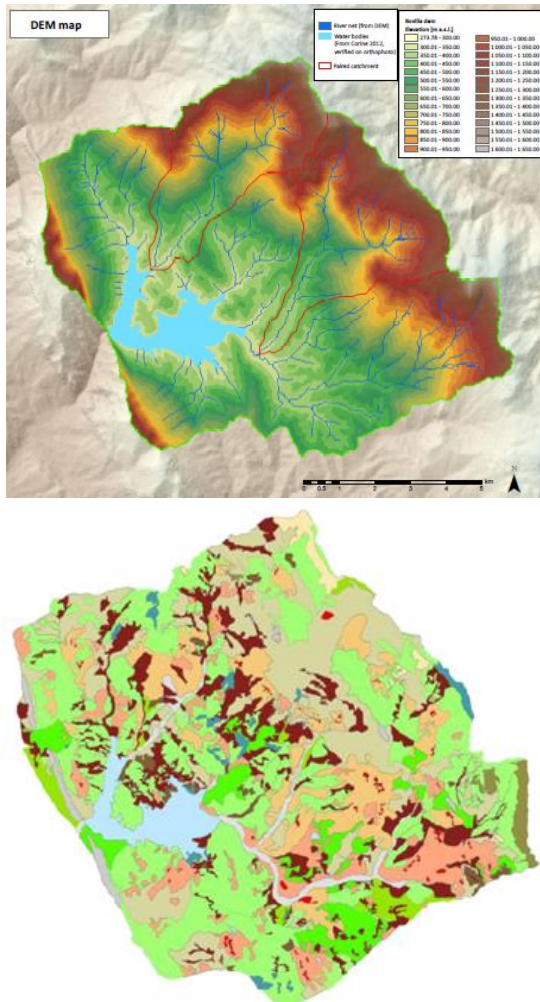


Figure 2 – Bovilla watershed Topography from (SRTM) and Land Cover maps from EU Copernicus Programme database.

Below is shown a list of data collected and used for the study:

- Digital Terrain Model 30 m cells by Shuttle Radar Topography Mission (SRTM);
- Land Cover Maps from CORINE 2000, 2006, and 2012 (44 classes);
- Land Cover Map for Bovilla watershed 2017 by the MTE;
- River networks from EU-Hydro Drainage Database EEA39;
- River watersheds from EU-Hydro River network dataset derived from EU-DEM;
- Meteorological data from 2002 to 2011, daily precipitation, daily minimal and maximal temperature.

The topographical surveys as part of this study are a complementary part, which contains the extension of the lake's basin above the water elevation up to dams' crest elevation to complete the reservoirs water volume curves. The purpose of bathymetric surveys for Bovilla reservoir have been performed to investigate on:

- The scale of sedimentation volumes accumulated during the time of operation since the first impounding of the reservoir;
- Quantify the progress of the sedimentations on the Bovilla reservoir;
- Evaluate the current lifespan of the reservoir through the HEC-HMS hydrological model;

The data collected have been analysed for their utility for this study, their completeness in terms of data series, spatial coverage and their consistency. Concerning meteorological data, some stations are available close to Bovilla but meteorological stations inside the basin would be more constructive. Using meteorological data from outside the basin, bring some limitations to the analysis. It would be important and useful to establish new monitoring points within the target watersheds to have better local data in particular for water level and discharge gauge for Bovilla reservoir and precipitation and temperature for Bovilla watershed. For the study was not possible to have some other data about river topography (i.e. river section) and siltation even if the data collected has been very useful for the calibration of the HEC-HMS hydrological model. Meteorological data cover an adequate period (10 years) for the purpose of the hydrologic modeling and the time series is quite complete (at least 95% for temperature data and more than 98% for precipitation data).

The hydrological model provides the results for each hydrologic element, i.e. outflow, liquid water at the soil surface, snow water equivalent, melt rate, soil storage, excess precipitation, precipitation losses, direct runoff, sediment load, etc. The software chosen for this kind of analysis, as stated in the Inception Report, is the open-source HEC-HMS of the US Army Corps of Engineers (USACE), which is designed to simulate the complete hydrologic processes of dendritic watershed systems, including the erosion and sediment transport. The Hydrologic Modeling System (HEC-HMS) is one of the most widely used simulation tools developed by the U. S. Army Corps of Engineers Hydrologic Engineering Center (HEC) and is designed to simulate the rainfall-runoff processes. A soil moisture accounting (SMA) algorithm has been used to evaluate the performance of the HEC-HMS model for many river basins. The software includes many traditional hydrologic analysis procedures such as event infiltration, unit hydrographs, and hydrologic routing. HEC-HMS also includes procedures necessary for continuous simulation including evapotranspiration, snowmelt, and soil moisture accounting.

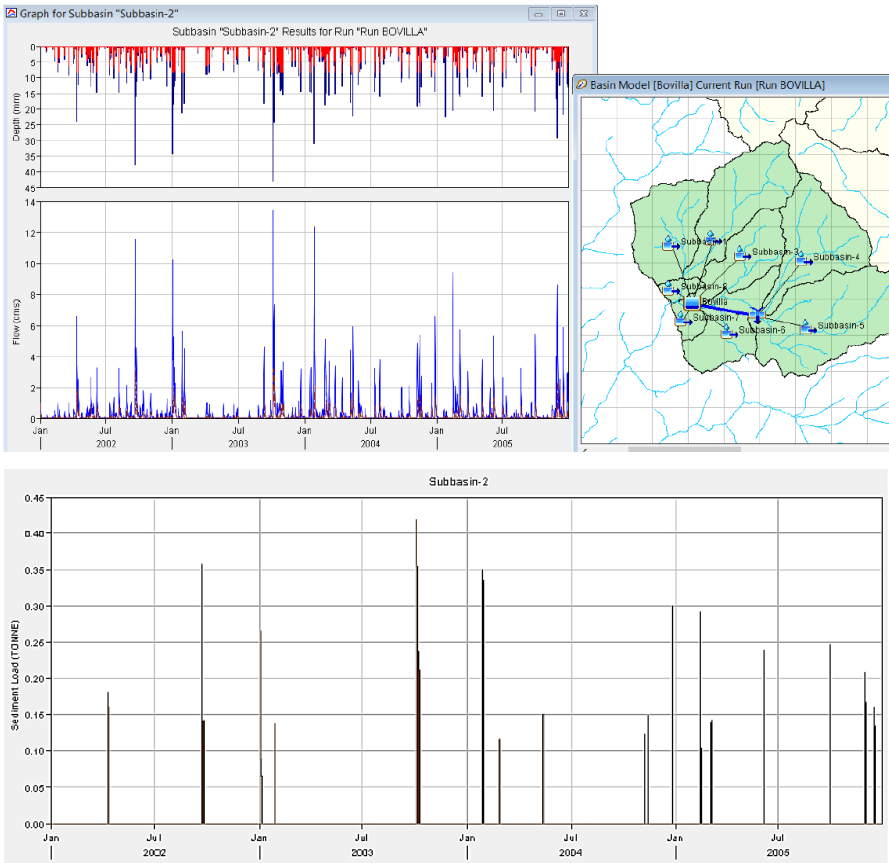


Figure 3 – Calculated precipitation loss (in red), outflow (in blue) and sediment load (in brown) for sub-basin 2 in the period 2002-2005.

Advanced capabilities are also provided for gridded runoff simulation using the linear quasi-distributed runoff transform (ModClark). Supplemental analysis tools are provided for model optimization, forecasting streamflow, depth-area reduction, assessing model uncertainty, erosion and sediment transport, and water quality [5].

The lack of water level and discharge data precludes the calibration of the model. So, the model has been implemented literature parameters except for the morphological ones (time lag, slopes, etc). Figure 3 shows an example of the calculated precipitation loss (in red), outflow (in blue) and sediment load (in brown) for sub-basin 2 in the period 2002-2005.

RESULTS AND DISCUSSION

The simulated annual water balance with the Hydrologic Modeling System (HEC-HMS) shows a runoff coefficient (direct runoff/precipitation volume) equal to 0.51. Figure 4 shows the simulated inflow in the period 2002-2010 and the annual inflow volume to Bovilla reservoir: the average simulated annual inflow volume is 80 Mm³.

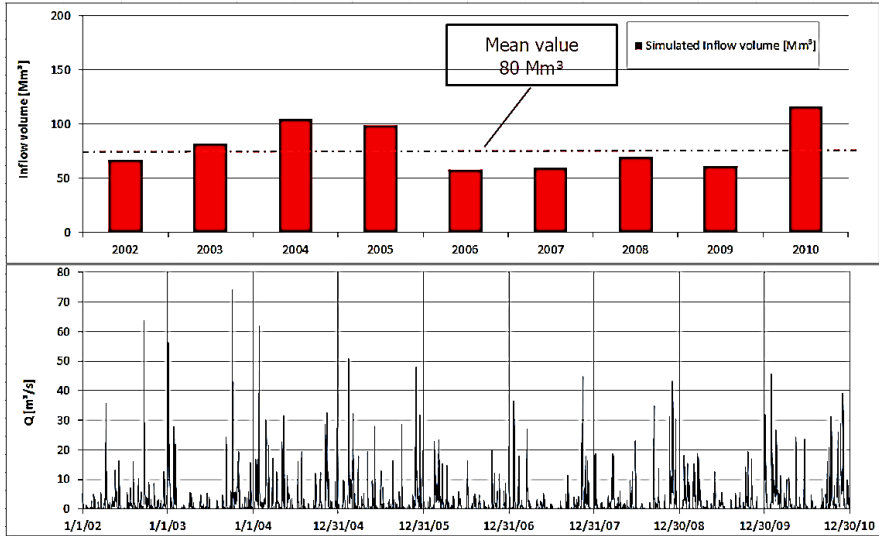


Figure 4 – Top: annual inflow volume to Bovilla reservoir; bottom: simulated inflow to Bovilla in the period 2002-2010.

Previous topographic measurements of the area at the moment of Bovilla dam construction are not available. The only available data was the water capacity of the reservoir and its storage curve. The lack of previous topographic data caused the usage of alternative ways to calculate total deposited sediment into the reservoir instead of the classical way. 1996 storage curve has been interpolated to be compared with the one defined after the survey specifically done in 2017 (Figure 5).

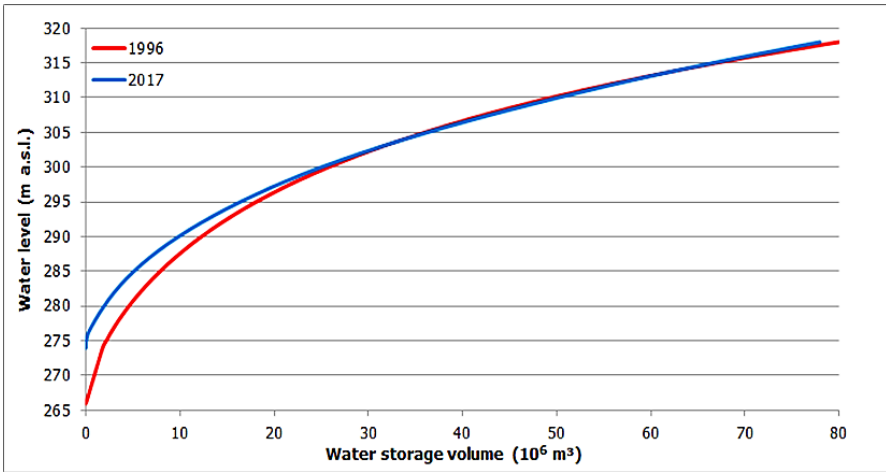


Figure 5 – Comparison between 1996 and 2017 storage curves of the Bovilla reservoir.

The dead storage, below 275 m a.s.l., has been completely filled with sediments. Total storage volume, from 1996 to 2017, it has reduced about 2 million m^3 from 80 to 78 million m^3 . Most of it is due to the filled dead storage; the operational storage volume has not significantly varied until now, but evolution on topography is clear. The lower part of the reservoir, below 285 m a.s.l., shows a clear trend to sediment deposition due to, in the authors' opinion, the low flow speed that permits the compaction of the sediment trapped over there. Even the higher part of the reservoir, above 310 m a.s.l., shows a trend to sediment deposition. In the upstream area of the reservoir, especially near the tributary, sediments are with bigger fraction and cannot be re-transported downstream. In the middle part of the reservoir, major affected by a variation on the water level that doesn't permit consolidation of sediment, it has been noticed a trend to erosion.

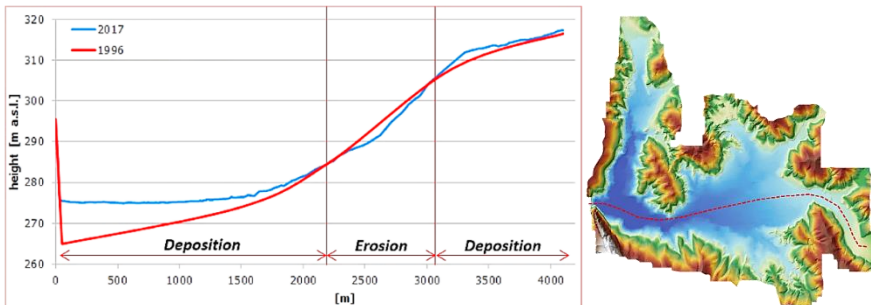


Figure 6 – Comparison between 1996 and 2017 bed-lines of the Bovilla reservoir.

Knowing the total quantity of deposited sediment into the reservoir is not enough. Distribution of these sediments through the reservoir bed is also very important. For this purpose, from the 2017 survey data were extracted a long profile of the reservoir near the middle of the water mirror (blue line in Figure 6) to be

compared with the one of 1996 obtained from interpretation and elaboration of available data. The above qualitative consideration must be confirmed when more detailed information about the area topography would be available. Sediment yield has been evaluated based on the condition in the previous 21 years, from the construction of the dam in 1996 to now. As below, the sediment volume during reservoir life has been evaluated in 2 million m³, which originated from a watershed of 95.5 km². The HEC-HMS hydrological model has been used with the (MUSLE) parameters (Universal Soil Loss Equation), based on precipitation intensity changed the formulation to calculate erosion from surface runoff instead of precipitation, and it reproduces the average value of the total sediment transport. The model works transporting the sediment that reaches the reservoirs during main hydrological events. The average annual quantity of the reservoir siltation (effective annual sediment yield) is evaluated in 95723 m³/y and the specific average annual quantity of the reservoir siltation (specific sediment yield) is evaluated 1002 m³/y, km². Considering an average bulk density of bottom sediment of 1.25 t/m³, the specific average annual quantity of the reservoir siltation is evaluated in 1253 t/y, km². Because of the trapping efficiency of the reservoir of 94%, as above evaluated, the total specific average annual sediment inflow is defined in 1333 t/y, km². Total specific average annual sediment inflow measured for Bovilla (1333 t/y, km²) is consistent with other studies done previously from Albanian institutions in relation to erosion processes in Albanian rivers.

CONCLUSION

Bovilla reservoir capacity is very important for the water supply system of the capital of Albania. In the absence of flow measured data, the parameters' values of the hydrological model were assigned based on acceptable data ranges from the manual, literature, and based on the experience. Only some type of heavy precipitation events can cause surface erosion. Definition of the threshold can be used to set the lower limit for runoff events that cause erosion. The lack of water level and discharge data precludes the calibration of the model. The lack of previous topographic data caused the usage of alternative ways to calculate total deposited sediment into the reservoir. The dead storage, below 275 m a.s.l., has been filled with sediments and the total storage volume, from 1996 to 2017, it has reduced about 2 million m³ from 80 to 78 million m³. Total specific average annual sediment inflow calculated for Bovilla (1333 t/y, km²) is consistent with the estimation done from the Albanian literature for sediment transport in Erzen and Ishem rivers [6]. More river sections, together with many grain-size analyses along the rivers, would be useful to describe the river morphology, the sediment transport capacity, and availability. For better evaluation, Geological and Hydrogeological surveys are needed to take into account the underground water processes. It is very important and useful to establish new monitoring hydrometeorological network in the Bovilla watershed for better local data for precipitation and discharge inflow in Bovilla reservoir.

REFERENCES

- [1] Anonymous, Impianti Hidroteknik i Bovillës / Impianto Idrotecnico di Bovilla, Ministria e Ndërtimit dhe Turizmit, Tirana, 1996, pp 1-24.
- [2] Kabo M., Gjeografia fizike e Shqipërisë, Akademia e Shkencave e RPS të Shqipërisë, Qendra e Studimeve Gjeografike, Albania, 1990.
- [3] Scheidegger A.E., Systematic geomorphology, Wien and New York Springer, 1987.
- [4] Miho A., Shuka L., Çullaj A., Bachofen R., Environmental Analyses of Bovilla Watershed, Limnological Study, Tirana, Albania, Julvin 2, 2009.
- [5] USACE 2000, HEC-HMS hydrologic modeling system user's manual, Hydrologic Engineering Center, Davis, CA, USA, 2000.
- [6] Instituti Hidrometeorologjik, Hidrologjia e Shqipërisë, Akademia e Shkencave e RPS të Shqipërisë, Albania, 1985.

INTEGRAL ASSESSMENT OF ANTHROPOGENIC PRESSURE ON WATER BODIES IN THE LAKE BAIKAL BASIN

Dr. Irina Ulzetueva ¹

Prof. Bair Gomboev ²

Dr. Daba Zhamyanov ³

Dr. Valentin Batomunkuev ⁴

Mr. Zorikto Banzaraktsaev ⁵

^{1, 2, 3, 4, 5} Baikal Institute of Nature Management SB RAS, Russia

² Buryat State University, Russia

ABSTRACT

The integrated assessment of the ecological state of the main rivers of the lake Baikal basin - Verkhnyaya Angara, Tyya, Barguzin, Selenga, Snezhnaya, Bolshaya Rechka, Khilok, Chikoy is based on the assessment of the variability of the basin system under the influence of two groups of indicators: 1) Direct (immediate) impact - the volume of water intake and wastewater discharge, water use and sequential water supply. Assessment of the impact on the state of the above-listed rivers basins from wastewater was performed using the algorithm proposed by A. Korolev et al. (2007). 2) Indirect (mediate) impact - indicators of areal and linear-network impacts on the catchment area. Based on the calculation of the integral anthropogenic pressure on the territory of the above-listed river basins, only the Selenga river experiences an “average” anthropogenic load. On the territory of most river basins, the anthropogenic load is “lowered” and “low”.

Keywords: *water assessment, Lake Baikal basin, anthropogenic pressure / load, water quality, wastewater*

INTRODUCTION

The integrated assessment of the ecological state of the main rivers - Verkhnyaya Angara, Tyya, Barguzin, Selenga, Snezhnaya, Bolshaya Rechka, Khilok, Chikoy is based on the assessment of the variability of the basin system under the influence of two groups of indicators:

Direct (immediate) impact - the volume of water intake and wastewater discharge, water use for drinking, industrial, agricultural and other needs, the water consumption of industries, the volume of reverse and sequential water supply.

Indirect (mediate) impact - indicators of areal and linear-network impacts on the catchment area: population size and density, agricultural land structure, industrial and agricultural production in value and kind, volumes of pesticides used in agriculture and the amount of agricultural technology used, length of shipping ways, timing of navigation, cargo volume and others.

METHOD AND METHODOLOGY

Approaches to assessment of the direct effects parameters

Analysis parameters direct impact is made on the basis of information on the use of water facilities industries.

The intensity of the load is determined based on the volumes of abstraction and discharge of water:

- high -> 100 million m³ / year
- average - 11-100 million m³ / year
- low - 1-10 million m³ / year
- very low - <1 million m³ / year
- insignificant or absent - 0 m³ / year.

Assessment of the load from wastewater on water bodies of the state of the river basins Verkhnyaya Angara, Tyya, Barguzin, Selenga, Snezhnaya, Bolshaya Rechka, Khilok, Chikoy was performed using the algorithm proposed by Korolev A.A., Rosenberg G.S., Gelashvili D.B. et al. [1]. To quantify the degree of water bodies pollution as a result of wastewater discharge, the authors propose the calculation of the load factor by wastewater on streams within the river basin.

The load factor by wastewater is defined as a ratio of the volume of wastewater discharged into water bodies of the water-resource region to the average annual water flow within the boundaries of this region:

$$k=qW, (1)$$

where k is the load factor;

q - the total volume of wastewater discharged into the water bodies of the water-resource region, mln. m³/year;

W - is the average annual water flow in within of the water-resource region, mln. m³/year.

Below is a diagnostic table for assessing the load from wastewater on water (table 1).

Table 1. Diagnostic table for assessing the load from wastewater on water bodies (WB).

Category of water body according to the degree of load by wastewater	The load factor of wastewater at WB	
	value	load characteristic
I	0.00-0.20	very weak
II	0.20-0.37	weak
III	0.37-0.63	moderate
IV	0.63-0.80	significant
V	0.80-1.00	big
VI	>1	very big

An important characteristic of the ecological state of water bodies is a water quality. Assessment of the water quality of water bodies that are sources for centralized drinking water supply is carried out as part of the system of social and

hygienic monitoring carried out by the territorial departments of the Federal Service for Supervision of Consumer Rights Protection and Human Welfare [2], [3], [4]. As an indicative hygienic indicator characterizing the condition and quality of water of water sources, the proportion of water samples of water sources that do not meet hygienic standards for sanitary-chemical and microbiological indicators is used.

The assessment of the water bodies quality by hygienic indicators was carried out on the basis of data from the State reports on the sanitary-epidemiological situation in the Republic of Buryatia, Irkutsk Region and Trans-Baikal Territory.

Approaches to assessment of the indirect effects parameters

To assess the intensity of anthropogenic load, indicators of indirect (including area) impact are important. The following parameters were used as a basic (main):

- the population density of the territory (person/km²), characterizing the demographic load on the catchment area;
- the density of industrial production (the volume of industrial production in the region in thousand rubles per 1 km²) indirectly determines the load from industrial production on the catchment area;
- plowing of the territory (the ratio of the area of arable land to the total area of the basin of the rivers in question, in %), indicates the intensity of use of the territory for agriculture;
- the livestock load (the number of livestock cattle per 1 km²) determines the intensity of the use of the territory of river basins for the development of livestock.

The plowing of the territory and livestock loading together determine the agricultural load on the territory of the river basins.

For each of the indicators, a conventional scale from 8 steps was adopted (table 2), which was based on the gradation of the main regional indicators of anthropogenic load developed by the Institute for Water and Environmental problems SB RAS as applied to the conditions of Siberian regions [5].

The used indicators are grouped by type of anthropogenic impacts: demographic, industrial and agricultural. The average value of each is estimated as the average level of the corresponding anthropogenic load in the basin of the rivers under consideration. The agricultural load is obtained as the arithmetic average of the scores of the intensity of agricultural (plowing) and livestock loads.

Table 2. The scale of the main indicators of anthropogenic load.

Indicator	Load intensity (points)							
	1	2	3	4	5	6	7	8
	Insignificant	very low	low	reduced	average	increased	high	very high
Population density, people/km ²	0.0	≤ 0.1	0.2-1.0	1.1-5.0	5.1-10.0	10.1-25.0	25.1-50.0	> 50.0
Density industrial production, thousand rubles/km ²	0.0	≤ 10.0	10.1-100.0	100.1-1000.0	1000.1-3000.0	3000.1-4000.0	4000.1-5000.0	> 5000
Ploughness, %	0.0	≤ 0.1	0.2-1.0	1.1-5.0	5.1-15.0	15.1-40.0	40.1-60.0	> 60.0
Livestock load, conditional heads/ km ²	0.0	≤ 0.1	0.2-1.0	1.1-2.0	2.1-3.0	3.1-6.0	6.1-10.0	> 10.0

The total anthropogenic load is defined as the average arithmetic mean value of the points of demographic, industrial and agricultural loads.

RESULTS AND ITS DISCUSSION

The analysis of the direct (immediate) impact factors on water bodies, in the form of natural water intake and wastewater discharges, showed that water bodies of the most economically developed area located along the river Selenga, including Lake Goose are experiencing a relatively high anthropogenic load.

Table 3. Intensity of anthropogenic pressure on water bodies as a result of natural water intake and wastewater discharge (indicators for 2013 year)

Water-resource region code	Natural water intake		Sewage discharge	
	Volume of water intake, million m ³	intensity	volume of water disposal, million m ³	intensity
V. Angara			40.409	average
Tyya			0.860	Very low
Barguzin	4.770	low	1.144	low
Selenga	471.062	high	445.840	high
Snezhnaya			0.0715	Very low
Bolshaya Rechka			0.118	Very low
Khilok	27.430	average		average
Chikoy	3.278	low		

Very low anthropogenic pressure is experienced by water bodies of the rivers Tyya, Snezhnaya, Bolshaya Rechka, Chikoy. Water bodies of other river basins experience medium and low anthropogenic pressure.

The discharge of insufficiently treated or contaminated wastewater is one of the most important reasons for the deterioration of the ecological state of water bodies. Depending on the quantity and quality of wastewater, the assimilating

ability of watercourses and reservoirs, the level of wastewater loading on water bodies is formed, which largely determines their current environmental status.

The anthropogenic load of wastewater on water bodies of river basins is assessed as “very weak”, which is explained by the incommensurability of the volume of water flow and the volume of wastewater discharged. All water bodies are assigned to category I according to the degree of loading by sewage (table 4).

Table 4. Parameters of anthropogenic load by the total volume of wastewater at the water-resources regions of the Selenga river basin.

Water body	The average annual runoff, W, mln. m ³ /year	Wastewater discharge, q, mln. m ³ /year	Load factor q / W	Load characteristic
V. Angara	8450	40.409	0.005	very weak
Tyya	1265	0.860	0.0007	very weak
Barguzin	2240	1.144	0.0005	very weak
Selenga	28729.3	445.840	0.016	very weak
Snezhnaya	193.6	0.0715	0.0003	very weak
Boshaya Rechka	135.6	0.118	0.001	very weak
Chickoy	8452	0.61	0.0001	very weak
Khilok	3106	9.78	0.0031	very weak

Analysis of the parameters of indirect effects.

Industrial load. An integral indicator of industrial load on the area of river basins Verkhnyaya Angara, Tyya, Barguzin, Selenga, Snezhnaya, Bolshaya Rechka, Khilok, Chikoy be an indication of the density of industrial production, defined as the volume produced in the area of industrial production in thousand rubles per 1 km².

In accordance with the methodology “System of indicators of socio-economic development of a constituent entity of the Russian Federation (RF)” approved by the head of the Federal State Statistic Service of the RF (Rosstat) on March 23, 2006, the volume of industrial production in the region in monetary terms determines the indicator “Goods of own production shipped, work and services completed on our own for a full range of manufacturers on clean activities of sections C, D, E of OKVED”. Data on the cost of goods shipped, work and services performed by city districts and municipal districts of the Verkhnyaya Angara, Tyya, Barguzin, Selenga, Snezhnaya, Bolshaya Rechka, Khilok, Chikoy are provided by the territorial authorities of the Rosstat: Irkutskstat, Buryatstat and Zabakalkraistat.

Industrial load. The density of industrial productivity in the Republic of Buryatia is 221.3 thousand rubles/km², respectively, “reduced”. The intensity of the load is 4 points. In the river basins of Verkhnyaya Angara and Tyya, the industrial production density was 26.011 thousand rubles/km², in the Barguzin river basin -

31.91 thous. rubles/km², in the basins of other rivers it is characterized as low and very low.

Agricultural load is defined as an integral indicator of agricultural and livestock loads. An indicator of the agricultural load is the plowing of the territory, livestock - the number of conditional heads of cattle (cattle) per 1 km².

Agricultural load. The structure of agricultural land use in river basins is formed by two main types of activity - animal husbandry and crop production.

Livestock is the main branch of agriculture. Crop production is mainly an auxiliary industry providing livestock feed. Most of the agricultural products are accounting for livestock.

The territory of river basins, as a whole, is characterized by a low agricultural load. "Average" agricultural load in the Khilok and Barguzin river basins. In the rest of the basin, the agricultural load is "reduced" (table 5). Livestock load in the river basin Selenga changes from "lowered" to "low".

In the Upper Angara and Tyya river basins, agricultural development is constrained by harsh climatic conditions. The main livestock sector in the region is dairy cattle breeding, which is relatively less unprofitable in comparison with other sectors of agriculture. The main livestock population is concentrated in personal subsidiary plots of citizens (86 %). A significant amount of agricultural products is produced in personal subsidiary plots of the population.

Table 5. Agricultural load intensity in river basins.

Water body	Plowing			Livestock load		
	%	intensity		conv. heads / km ²	intensity	
		characteristic	points		characteristic	points
V. Angara	0,69	Low	2	0.44	Low	2
Tyya	0,07	low	2	0.4	Low	2
Barguzin	9.9	average	5	0.7	Low	2
Selenga	4.5	lowered	4	3.1	Increased	4
Snezhnaya	0	insignificant	1	3.9	Increased	4
Boshaya Rechka	0	insignificant	1	3.9	increased	4
Chickoy	1.8	lowered	4	0.9	low	3
Khilok	5.5	average	5	1.4	lowered	4

The demographic load in the river basins within the boundaries of the constituent entities of the RF is unevenly distributed. The pattern of resettlement has a distinct ribbon character; settlements are concentrated in the valleys of the Selenga river and its tributaries Uda, Khilok, Chickoy, Dzhida, as well as along the Trans-Siberian Railway, Baikal-Amur Mainline Railway (BAM) and the southern railway to Mongolia.

Within the Selenga river basin, the bulk of the population of Buryatia is concentrated (almost 9/10). The average population density in the basin is 6 people/km². In the “Buryat” part of the basin, this indicator is 8.7 people/km² and almost five times higher than the same indicator in the Trans-Baikal Territory (1.8 people/km²). The most densely populated is the central part of the basin, including the territories of Ivolginsky, Kyakhtinsky, Zaigraevsky, Mukhorshibirsky, Selenginsky, Tarbagataisky, Kabansky, Bichursky, Pribaikalsky districts of Buryatia. In the territory, which occupies about 30 % of the basin, 77 % of its population is concentrated. East and west, population density is declining. Significantly lower than the average population density in Zakamensky and Dzhidinsky districts is 2-4 people/km², the lowest population density (1-1.5 people/km²) in the north-eastern regions of Buryatia (Eravinsky, Khorinsky), as well as areas of Trans Baikal Territory with relatively less favorable conditions and low transport accessibility.

The settlement frame in the Buryat part of the Selenga river basin is formed by 4 cities, 7 urban-type settlements and 404 rural settlements. More than 3/5 of the population (483.8 thousand people) live in urban settlements.

The average demographic load is experienced the Selenga river basin. The demographic load on the territory of most of the water-resource region is reduced (table 6).

Table 6. The intensity of the demographic load in river basins

Water-resource region code	Population density, people / km ²	Load intensity characteristic	Load intensity, points
V. Angara	0.6	low	3
Tyya	4.9	Lowered	4
Barguzin	1.8	lowered	4
Selenga	8.7	average	5
Snezhnaya	0.13	Low	3
Boshaya Rechka	4.9	lowered	4
Chickoy	1.5	lowered	4
Khilok	1,5	lowered	4

CONCLUSION

Integral anthropogenic load on the territory of the river basins

Among the river basins, only the Selenga experiences an “average” anthropogenic load. On the territory of most river basins, the anthropogenic load is “lowered” and “low” (table 7).

Table 7. Integral anthropogenic load on the river basins.

Water-resource region code	Load intensity, points				
	demographic	industrial	agricultural	livestock	anthropogenic
V. Angara	3	3	2	2	4
Tyya	4	3	2	2	2
Barguzin	4	3	5	2	3
Selenga	5	4	4	4	5
Snezhnaya	3	2	1	4	2
Boshaya Rechka	4	2	1	4	2
Chickoy	4	3	4	3	4
Khilok	4	3	5	4	

ACKNOWLEDGEMENTS

The work was carried out within the framework of the state assignment of BINM SB RAS.

REFERENCES

[1] Korolev A.A., Rosenberg G.S., Gelashvili D.B. et al. Ecological zoning of the Volga basin according to the degree of wastewater loading based on the basin principle (by the example of the Upper Volga), Bulletin of the Samara Scientific Center of the Russian Academy of Sciences /Russia, 2007, T. 9, № 1, pp 265-269;

[2] State report "On the state of the sanitary-epidemiological well-being of the population in the Irkutsk region" for 2008-2012. [Electronic resource]. - Access mode: <http://38.rospotrebnadzor.ru/396>;

[3] State report "On the state of the sanitary-epidemiological well-being of the population in the Republic of Buryatia" for 2008-2012. [Electronic resource]. - Access mode: <http://03.rospotrebnadzor.ru/documents/>;

[4] GOST 2761-84. Sources of centralized drinking water supply;

[5] Rybkina I.D., Stoyashcheva N.V., Assessment of anthropogenic load on the catchment area of the Upper and Middle Ob, World of science, culture, education, Russia, 2010, № 6, Part 2, pp. 295-299.

PROCESSING AND QUALITATIVE VISUALIZATION IN PSEUDO-TRUE COLOURS OF LONG-TERM SERIES OF SATELLITE DATA

Lyudmila Shagarova ¹

Mira Muratova ²

Aray Yermenbay ³

^{1, 2, 3} Satbayev University, Ahmetsafin Institute of Hydrogeology and Environmental Geoscience, Kazakhstan

ABSTRACT

Free access to moderate resolution remote sensing data enable worldwide users for their studies of many key geophysical parameters of the Earth's system, solving various tasks on regular monitoring of natural phenomena, including tasks on ecological space monitoring. This requires multilevel processing of satellite data. The processing results are given for the Aral Sea. This endorheic salt lake is located in Central Asia on the border of Kazakhstan and Uzbekistan. Aral was chosen as an example not by chance as because before shallowing, it was the fourth-largest lake in the world. During the process of drying, the lake was divided into three parts. Currently, the eastern part of the lake has completely disappeared. To the Aral Sea is happening a real ecological disaster. A long-term series of satellite data are needed to monitor the dynamics of changes.

The active operation of remote sensing satellites usually exceeds their estimated lifetime. For example, spacecrafts "Terra" and "Aqua", launched in 1999 and 2002, respectively, have an estimated lifetime of sensor MODIS as 6 years, but they are still used in the NASA EOS program aimed at Earth exploration. With the aging sensors has been a degradation of its optics equipment which affects the quality of the data in some channels. It limits the simple creation of a color image in TRUE colors by put the bands spectral range of visible radiation to corresponding layers RGB-composite. The article describes the technology of making quality images by digital operations with MODIS channels. It eliminates such a problem as "banding" of the image and creates new synthesized bands. The results of processing are demonstrated using annual Terra/MODIS data for the autumn period from 2000 to 2019.

Besides, taking into account that a water body has been chosen as the object of monitoring, the article presents the options of water surface detection based on spectral indices - indices calculated in mathematical operations with different spectral ranges (channels) of remote sensing data related to certain parameters. Thematic processing in Geomatica software is shown on Landsat-8 images: the sample profile of index image is demonstrated. Taking into account that the survey area exceeds the size of the standard Landsat scene, a mosaic image was made for complete coverage of the region.

In 2021 a partnership between NASA and the U.S. Geological Survey was scheduled to launch the next spacecraft of Landsat mission which started in 1972. Thus, the repeat images will create conditions for studying the dynamics of changes in the objects under research.

Keywords: *Aral Sea, space images, Landsat, MODIS, monitoring*

INTRODUCTION

The Aral Sea is a lake in Central Asia on the border of Kazakhstan and Uzbekistan (its northern part is in Kazakhstan). The lake is located on Turan plain at the eastern Ustyurt plateau. Until 1960, the area of Aral water surface was 66.1 thousand km², length – 428 km, width – 2,354 km, basin area – 690 thousand km², water volume – 1,075 km³ [1].

The water of the Aral Sea basin is formed mainly by large rivers – Amudarya and Syrdarya, that originate from Tajikistan and Kyrgyzstan.

Water use in Central Asia facilitated the increase of irrecoverable water intake, including from rivers feeding Aral. Their estuaries lost their water regulating capacity which affected the sea level. Precipitation in the form of rain and snow give the Aral Sea much less water than is lost while evaporating from its surface. As a result, Aral water volume reduces, and the salinity degree increases. With the water level falling, the groundwater level also reduced in Aral which accelerated the process of the region desertification. Cropped out sea bottom is covered with salts that are spread by the wind throughout the basin territory and adjacent areas.

A long-term series of satellite data are needed to monitor the dynamics of changes.

METHODS AND METHODOLOGY

Monitoring of the Aral Sea shallowing was performed with the use of archive images with moderate spatial resolution: Terra/MODIS, refining of subject information – based on data of Landsat/OLI [2], [3].

MODIS (Moderate Resolution Imaging Spectroradiometer) is one of key tools onboard of American satellites Terra and Aqua. 36 MODIS spectral zones cover the range with wavelength from 0.4 to 14.4 μm. Observations in red and infrared electromagnetic wavelength ranges are done with a resolution of 250 m, in five zones of visible and near infrared range with a resolution of 500 m, and others – 1 km. Data is freely available.

Landsat is the most long-lasting project studying the planet Earth with the help of satellite images. The first satellite of Landsat mission was launched in 1972, currently, Landsat-7 and Landsat-8 operate on orbit. Surveys of the earth surface are performed in modes: VNIR (Visible and Near Infrared), SWIR (Shortwave Infrared), PAN (panchromatic) and TIR (thermal). Landsat multispectral data spatial resolution is 30 m, in the panchromatic channel – 15 m. Starting from 2009, all satellite images of Landsat program are freely available.

The active operation of remote sensing satellites usually exceeds their estimated lifetime. For example, spacecrafts “Terra” and “Aqua”, launched in 1999 and 2002, respectively, have an estimated lifetime of sensor MODIS as 6 years, but they are still used in the NASA EOS program aimed at Earth exploration [4]. With the aging sensors has been a degradation of its optics equipment which affects the quality of the data in some channels.

Another example – functioning spacecrafts Landsat-7 and Landsat-8 were placed in orbit in 1999 and 2013 respectively, their design life according to documentation was 7 and 5 years. In 2003, there was a failure in the operation device ETM+ (Enhanced Thematic Mapper Plus) of Landsat-7. Such failure was caused by the scan line corrector. The observations are continued but in the mode of SLC-off scan line corrector turned off.

Despite sensors aging, the processing of long-term sequence of single-type satellite data requires also their quality visualization. Figure 1 shows fragments of Terra/MODIS space images for the autumn period from 2000 to 2019, illustrating changes of borders of the Aral Sea for 20 years, in the composition center – state-of-the-art of Aral by data for 2019. By Figure 1, it is possible to state that the eastern part of Aral “disappeared” for the first time in 2014, the situation repeated in 2019. The stability of the situation with Small Aral is conditioned by 17 km Kokaral dam built in 2003-2005 from the Kokaral peninsula to Syrdarya estuary. The dam has a flow-control valve to regulate the reservoir level [5].

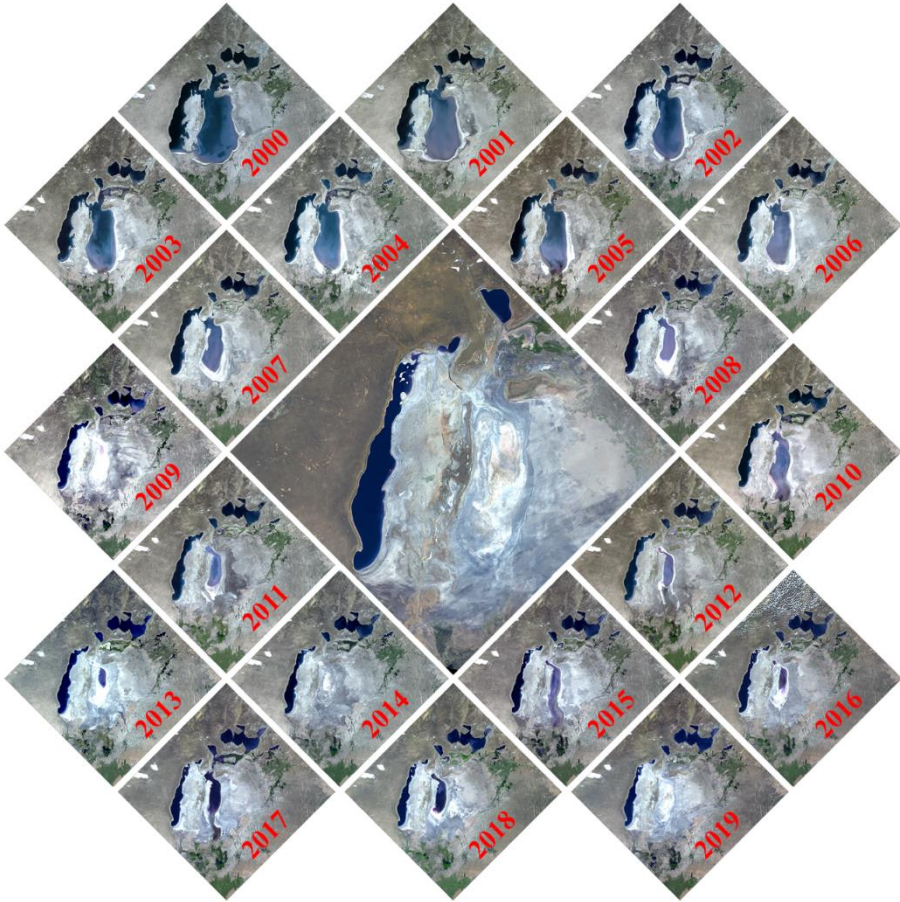


Figure 1 – Aral Sea shallowing dynamics

To obtain such a composition, the following actions were performed.

Terra/MODIS baseline data characterized by cloudless nadir location of the area under study, downloaded in the volume of 6.02 Gb in “raw” format PDS (MOD00F by EOS range of products), scene identifiers are given in Table 1.

Table 1 – List of TERRA/MODIS Identifiers

№	Identifier	Date	Time UTC
	MOD00F.A2000252.0710.20062340336.001.PDS	08.09.2000	07:10
2.	MOD00F.A2001256.0650.20062930852.001.PDS	01.09.2001	06:50
3.	MOD00F.A2002250.0650.20070080507.001.PDS	07.09.2002	06:50
4.	MOD00F.A2003249.0715.20063580602.001.PDS	03.09.2003	07:15
5.	MOD00F.A2004268.0715.20070262232.001.PDS	24.09.2004	07:15
6.	MOD00F.A2005261.0720.20062270027.001.PDS	18.09.2005	07:20
7.	MOD00F.A2006245.0650.20062461222.001.PDS	02.09.2006	06:50
8.	MOD00F.A2007248.0650.20072480720.001.PDS	05.09.2007	06:50
9.	MOD00F.A2008247.0715.20082470837.001.PDS	03.09.2008	07:15
10.	MOD00F.A2009265.0715.20092650945.001.PDS	22.09.2009	07:15
11.	MOD00F.A2010247.0655.20102470705.001.PDS	04.09.2010	06:55
12.	MOD00F.A2011246.0720.20112460709.001.PDS	03.09.2011	07:20
13.	MOD00F.A2012256.0725.20122560718.001.PDS	12.09.2012	07:25
14.	MOD00F.A2013289.0645.20132890707.001.PDS	13.10.2013	06:45
15.	MOD00F.A2014247.0715.20142470712.001.PDS	04.09.2014	07:15
16.	MOD00F.A2015266.0715.20152661009.001.PDS	23.09.2015	07:15
17.	MOD00F.A2016248.0655.20162480654.001.PDS	04.09.2016	06:55
18.	MOD00F.A2017250.0655.20172500655.001.PDS	07.09.2017	06:55
19.	MOD00F.A2018246.0650.20182460721.001.PDS	03.09.2018	06:50
20.	MOD00F.A2019263.0700.20192630653.001.PDS	20.09.2019	07:00

Files of Level 0 were converted into standardized within the frameworks of EOS products of Level1A and 1B. Processing included operations of data reformatting, its gridding and calibration.

At the initial stage, files of Level 0 were unpacked into data of Level 1A of HDF format (MOD01 by EOS range). MOD01 includes detectors' data array, and also service onboard information and metadata added to file during processing. MODIS Level1A data file gridding was carried out as the result of filling in fields of Level1A file describing the geographical position. Thus, geolocation file was formed (MOD03 product by EOS range) with arrays of latitude and longitude, survey geometrical parameters such as scan angles, Sun position and some other parameters.

Input data for MODIS calibration is data of Level 1A and geolocation (i.e. MOD01 and MOD03 files simultaneously). As a result of calibration process, standard product was created (MOD02 by EOS range) in HDF format. Each type of output files has its own standard identifier in accordance with channels special resolution: MOD02QKM (QKM/quarter kilometer), MOD02HKM (HKM/half kilometer), MOD021KM (1KM/1 kilometer). To create pseudo-true colours, files MOD02QKM and MOD02HKM were used (table 2).

Table 2 – MODIS spectral bands

MOD02	Spectral channel	Band width (mkm)	Spatial resolution (m)
MOD02QKM	channel 1 - Red	0.620-0.670	250
MOD02KM	channel 2 - Near Infrared, NIR	0.841-0.876	250
MOD02HKM	channel 3 - Blue	0.459-0.479	500
MOD02HKM	channel 4 - Green	0.545-0.565	500

A color image in pseudo-true colors is usually created by substitution channels with respective spectral range into RGB-composite. Pursuant to Table 2, for MODIS data such a composite looks like a combination of channels 1-4-3. And the resulting special resolution is contributed by two channels with resolution of 500 m, and only one channel with resolution of 250 m. Consequently, the resulting image will have resolution of 500 m. Taking into account that on later images, with regard to survey instruments ageing factor, there appeared interferences on individual channels, this is reflected by strips on images. This problem and an option for its solving is illustrated on figure 2.

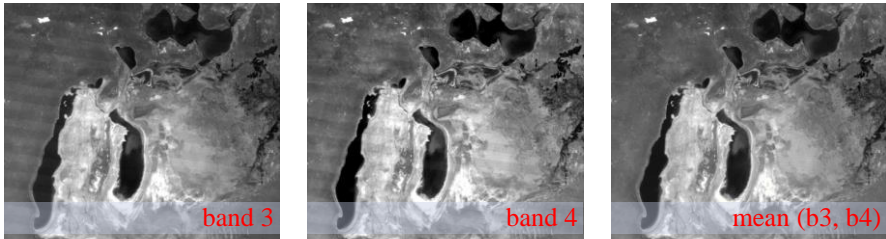


Figure 2 – View of Green and Blue MODIS channel

To achieve quality image, spectral conversion of digital data is necessary; formulas for new data synthesizing are given in Table 3. A new synthesized image nevertheless can be successfully presented with 250 m resolution since major part of baseline data in this case has resolution of 250 m.

Table 3 – RGB-composite options

R-G-B	True Colours	Pseudo-True Colours
RED	Band1	Band1
GREEN	Band4	(band2+3*SyntGreen)/4
BLUE	Band3	-0.1*band2+0.01*band1+0.7*band3+band42 as SyntGreen

RESULTS

Figure 3 presents resulting images of both options.

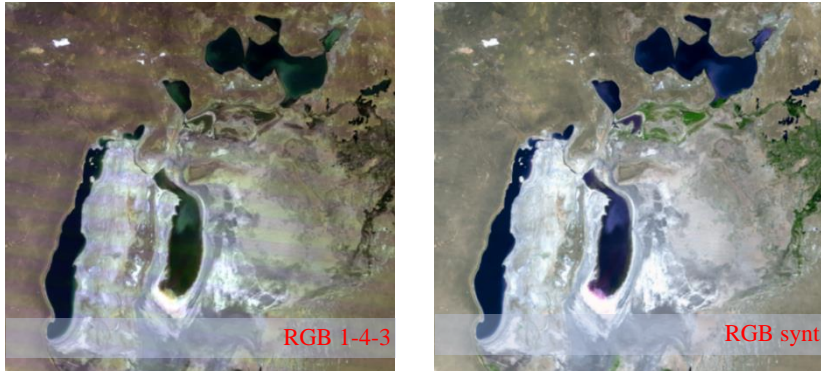


Figure 3 – Resulting images of both options

Scientists are exploring the state, trends and future of water resources development in the Central Asia [6]. Aral experiences water table level and area fluctuations. According to remote sensing data for 1975 – 2013, Aral water table area reduced by 82% [7].

Water table area is calculated as the result of subject index processing of space images. Spectral satellite information allows calculation of the following

- - vegetation index (formula 1) characterizing peculiarities of vegetation cover based on the knowledge that the most expressed peculiarity of plants range is the minimum in red spectral range and maximum in infrared

$$NDVI = \frac{NIR - RED}{NIR + RED} \quad (1)$$

- - water index (formula 2) based on the knowledge that the most expressed feature of water range is minimum in infrared range and maximum in green range.

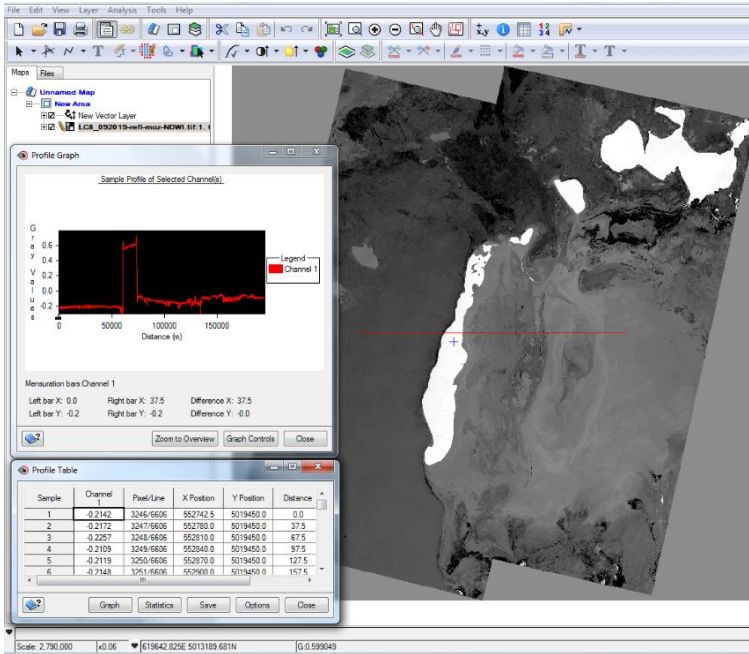
$$NDWI = \frac{GREEN - NIR}{GREEN + NIR} \quad (2)$$

Both indexes give identical results, unambiguously allowing finding a water body. Figure 4 demonstrate a profile of index images. Subject processing performed with Geomatica software.

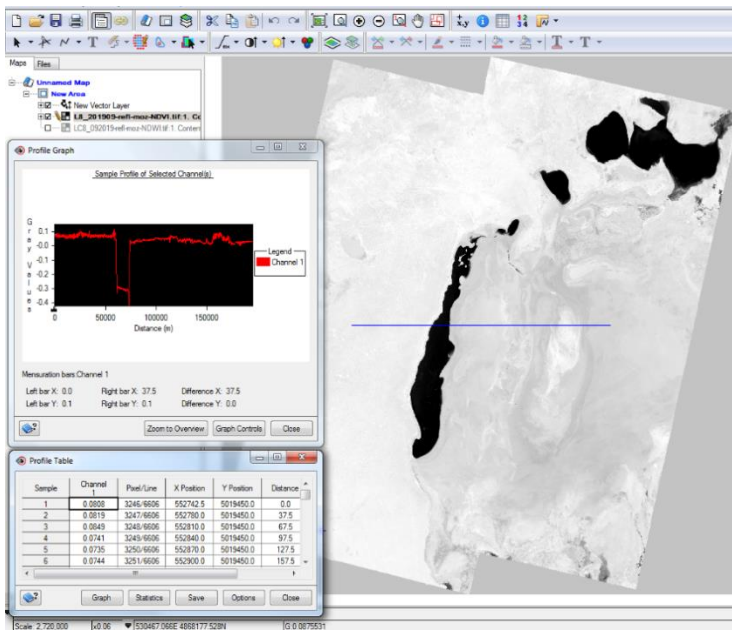
Taking into account that the study area exceeds the size of Landsat standard scene, their mosaic was made for full coverage of the Aral region, identifiers of Landsat-8 scenes used for this example are given in Table 4.

Table 4 – List of Landsat-8 identifiers

Date	Path	Row	Identifier
12.09.2019	161	28	LC08_L1TP_161028_20190912_20190917_01_T1.tar
12.09.2019	161	29	LC08_L1TP_161029_20190912_20190917_01_T1.tar
19.09.2019	162	28	LC08_L1TP_162028_20190919_20190926_01_T1.tar
19.09.2019	162	29	LC08_L1TP_162029_20190919_20190926_01_T1.tar



a)



b)

Figure 4 – Spectral index for Landsat-8 19.09.2019, 12.09.2019: a) NDWI, b) NDVI

CONCLUSION

Described technology permit to get quality images by digital operations with MODIS channels. It eliminate a “banding” problem of the image as a result of create new synthesized bands. Result – the qualitative visualization in pseudo-true colours of long-term series of satellite data.

Water detection performed on opposite spectral indices NDWI and NDVI. These numerical indicators derived from optical satellite images as mathematical operations with spectral ranges of remote sensing data. Thematic processing completed in Geomatica software.

Thus, thematic maps built on the basis of satellite images allow tracking the process of the Aral Sea shallowing – present-day ecological disaster. The repeat images will create conditions for studying the dynamics of changes in the objects under research.

REFERENCES

- [1] V.A.Smolyar, B.V.Burov, V.V.Veselov, T.T.Makhmutov, D.A. Kasymbekov Water resources of Kazakhstan. Almaty: SIC «ФЫЛЫМ», 595 p., 2002.
- [2] Peng, FF; Wang, L; Zou, SY; Luo, J; Gong, SS; Li, XR. Content-based search of earth observation data archives using open-access multitemporal land cover and terrain products. International journal of applied Earth Observation and Geoinformation, 81, Pp. 13-26, 2019, doi.org/10.1016/j.jag.2019.05.006
- [3] Cretaux, J. & Bergé-Nguyen, Muriel. Aral Sea Hydrology from Satellite Remote Sensing, 2014, doi.org/10.1007/978-3-642-02356-9_11.
- [4] Xiaoxiong Xiong, Emily Aldoretta, Amit Angal, Tiejun Chang, Xu Geng, Dan Link, Vincent Salomonson, Kevin Twedt, Aisheng Wu Terra MODIS: 20 years of on-orbit calibration and performance. Proc. SPIE 11127, Earth Observing Systems XXIV, 1112714, 9 September 2019, doi.org/10.1117/12.2531933.
- [5] Water resources of Kazakhstan in the new millennium, UNDP, Kazakhstan, №UNDPKAZ 07, Almaty, 2004, 132 p
- [6] Abror Gafurov, Vadim Yapiyev, Mohamed Ahmed, Jay Sagin, Ali Torabi Haghghi, Aigul Akylbekova and Bjørn Kløve Groundwater resources // Aral Sea Basin. Water for Sustainable Development in Central Asia, Edited by Stefanos Xenarios, Dietrich Schmidt-Vogt, Manzoor Qadir, Barbara Janusz-Pawletta, Iskandar Abdullaev. The Taylor & Francis Group (United Kingdom), 2019 – P 320.
- [7] L. Shagarova, M. Muratova, O. Skakova. Long-term monitoring of the Aral Sea by remote sensing data // 14th International Multidisciplinary Scientific GeoConference SGEM 2014, Conference Proceedings, June 19-25, 2014, Book 3, Vol. 2, 631-636 pp. doi.org/10.5593/SGEM2014/B32/S15.0

PROSPECTS OF WATER SUPPLY WITH FRESH GROUNDWATER UNDER ANTHROPOGENIC IMPACT CONDITIONS

Aray Yermenbay¹

PhD Lyudmila Shagarova²

Dr. Prof. Malis Absametov³

PhD Sergey Osipov⁴

^{1, 2, 3, 4} Satbayev University, Ahmetsafin Institute of Hydrogeology and Environmental Geoscience, Kazakhstan

ABSTRACT

The role of water resources at the present stage of human development becomes more and more significant every year and, actually, just the availability of water resources of required quality limits the further production force growth, city enlargement and the improvement of living standards and industry and agriculture development.

The water supply deficit reduction and the water supply level increase are some of the priority national objectives, which are also related to the international obligations of the Republic of Kazakhstan.

The prospects for fresh groundwater supply under anthropogenic impact conditions are given in the article for the water-stressed region as exemplified by Nur-Sultan city.

Currently, the centralized water supply of Nur-Sultan city is provided by supplying water from the Vyacheslav Water Reservoir on the Esil River, which under the existing population size, does not satisfy completely the city's water demand.

The problem of utility and drinking water supply in the capital becomes more acute due to the growth population and its economic activity and, increased impact on natural components and geosystems.

As a result of consolidation and analysis of the information on the anthropogenic impact as the most significant factor of change in the groundwater formation conditions, the article shows it's the negative impact on the fresh groundwater resource quantity and quality. It is noted that the main groundwater pollutants in the research area are the sewage ponds, domestic and industrial waste deposits of Nur-Sultan city, as well as the livestock breeding complexes, filtration fields and ash-disposal areas. According to the monitoring results, the areas of groundwater pollution have been identified in the zone of individual deposit influence.

Various methods of geophysical and geochemical surveys, as well as the Earth remote sensing methods are used to identify large pollution areolas and prospective areas for groundwater exploration.

The results of the integrated use of modern methods are shown, which increases the prospecting and exploration work efficiency. The specified prospects for fresh groundwater supply are especially relevant for water-stressed regions.

Keywords: *Groundwater, Hydrogeology, Water supply, Anthropogenic impact, Remote sensing data*

INTRODUCTION

Reducing the deficit of water resources and water supply level increase are among the priority objectives of the state-related inter alia to the international commitments of the Republic of Kazakhstan. In recent years, the problem of utility and drinking water supply to the capital of the Republic of Kazakhstan – Nur-Sultan city is becoming more and more critical. At present, centralized water supply to Nur-Sultan city is ensured by a supply of water from Astana water-storage reservoir on the Esilriver, which with the existing population does not fully cover present-day needs of Nur-Sultan city in water.

In 2010, to satisfy the capital's need in drinking water, the Ministry of Industry and New Technologies carried out exploration works and completed the reevaluation of usable groundwater resources in Atbasarskoye, Atbasar-Priishymkoye, Nurinskoye and Rozhdestvenskoye deposits. In the long term (until 2040), to cover possible drinkable water deficit, it is necessary to envisage discovering of promising areas and sites in the territory of Akmola region, exploring groundwater on them and engaging additional groundwater resources within the explored territory with account to conditions of groundwater distribution and formation, rock water abundance, well output, water salinity within limits of aquifers and aquifer systems.

The issue of water supply to population, use of reserves and resources of good quality groundwater for supplying water to population centers is becoming exceptionally important due to growing year in year out water supply deficit with the account to human impacts and demographic factors. So, space-planes shown on Figure 1 are indicative of rapid growth of Kazakhstan capital – Nur-Sultan city, which is accompanied by the growing men-induced load upon the environment.

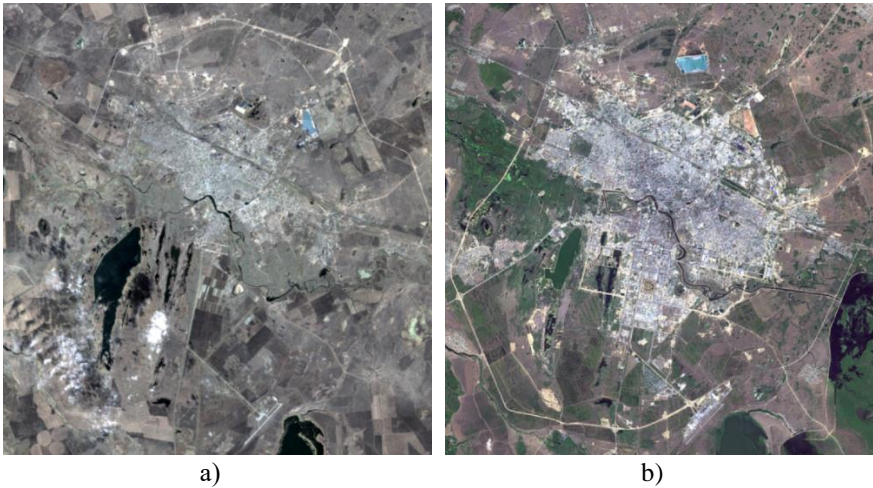


Figure 1- Landsat image of city a) 2001 year, b) 2019 year

METHODS AND METHODOLOGY

Methods of geophysical and geochemical surveys, as well as the remote sensing method, are used to discover perspective areas to search for groundwater and large pollution areas [1], [2].

Extensive statistical, archived, published and library material of previously conducted geological, hydrogeological and geological-geophysical surveys in the territory of Akmola region was collected, processed and consolidated in the process of surveys, where, due to environmental and man-made factors, hydrogeological conditions significantly changed, change in aquifers and aquifer systems hydrogeological parameters occurred. As a result, corrections were made and groundwater deposits design hydrogeological parameters were adjusted with account to ecological changes in the natural environment and impact of human economic activity (anthropogenic loads) upon groundwater runoff.

To calculate operation capabilities of key aquifer systems and water-bearing horizons, extracts of their hydrogeological parameters were made (water abundance data, design and actual flow rates and decreases of groundwater bedding and piezometric level, water dynamic level fluctuations, water loss (gravitation and resilient), design distribution areas, thickness, duration of design life cycle, lithic characteristics etc.).

RESULTS AND DISCUSSION

Based on materials collected, preliminary collation of data of groundwater chemical composition was carried out, key regularities of chemical composition of groundwater in the first from the surface aquifer were established. Hydrochemical zoning is closely linked with hydrodynamic regularity, since the development and intensity of various hydrochemical processes occurring in groundwater are regulated by water flow dynamics and water exchange activity.

Main source of utility and drinking water supply and process water supply to the city of Nur-Sultan is the surface water of rivers and lakes located close to population centers.

Fresh groundwater is confined mainly to valleys of large rivers of the region – Esil and Nura, as well as to valleys of temporary streams and sites of ancient buried valleys. Formation of salinity and chemical composition of valley alluvial deposit interstitial water is predetermined by floodwater and precipitation chemical composition conditioning their main feed.

Interpretation of remote sensing data was performed to explore groundwater resources in valleys of rivers of Esil and Nura, and also on sites for groundwater artificial replenishment for water-supply to Nur-Sultan [3]. Cloudless fragments of satellite images Landsat-8 for 2013 - 2016 were processed. To increase their information value, spectral transformations of source space images were carried out. To create a uniform coverage of the territory under study (figure 2), tiled data Landsat-8 for August 30, 2016, May 19, 2016, September 30, 2015, August 25, 2016 was made.

To reach the set hydrogeological objectives based on remote sensing data, composite images 7-4-2 and 5-6-4 were also used as well as normalized differential water index NDVI which is calculated as dependency of difference and sum of waves absorption indexes in green (0.53-0.59 μm) and near infrared spectral range (0.85-0.88 μm) of OLI sensor Landsat-8 satellite.

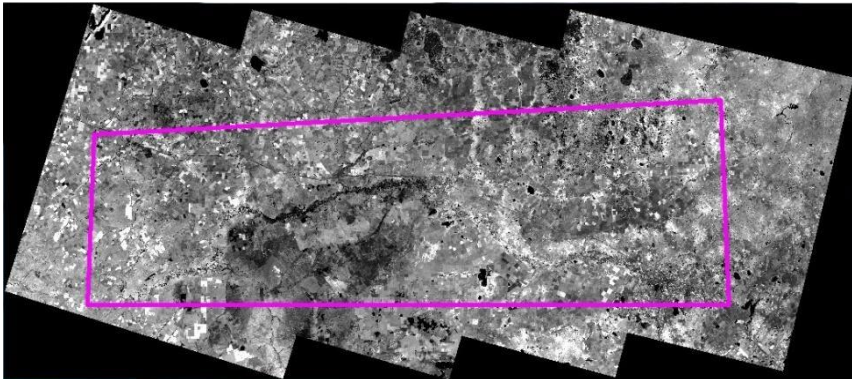


*Figure 2 - Tiled data Landsat-8, Channel 6 - SWIR1 (560-1660 nm),
testing site №6 Akmola region*

Taking into account that lineaments may indicate rock fracturing, Lineament Extraction procedure was applied. Calculations of small linear elements of distribution and orientation were made based on the texture of medium infrared channel SWIR-1 spectral range 1.56-1.66 μm . Display of the above deformation on satellite images is explained by the fact that the processes occurring at different lithosphere depth levels impact the super strata and predetermine peculiarities of day surface geology. On the terrain, lineaments are displayed by regularly aligned areas formed by straight-line boundaries or rectified sites of image texture. To exclude areas with contours representing evident linear sections from the

interpretation process, postprocessing of derived lineaments was carried out by linear objects editing.

As a result, lineaments density maps were made [4]. Figure 3 present a fragment of lineaments density map in the territory under study and diagrams of their directivity as an example.

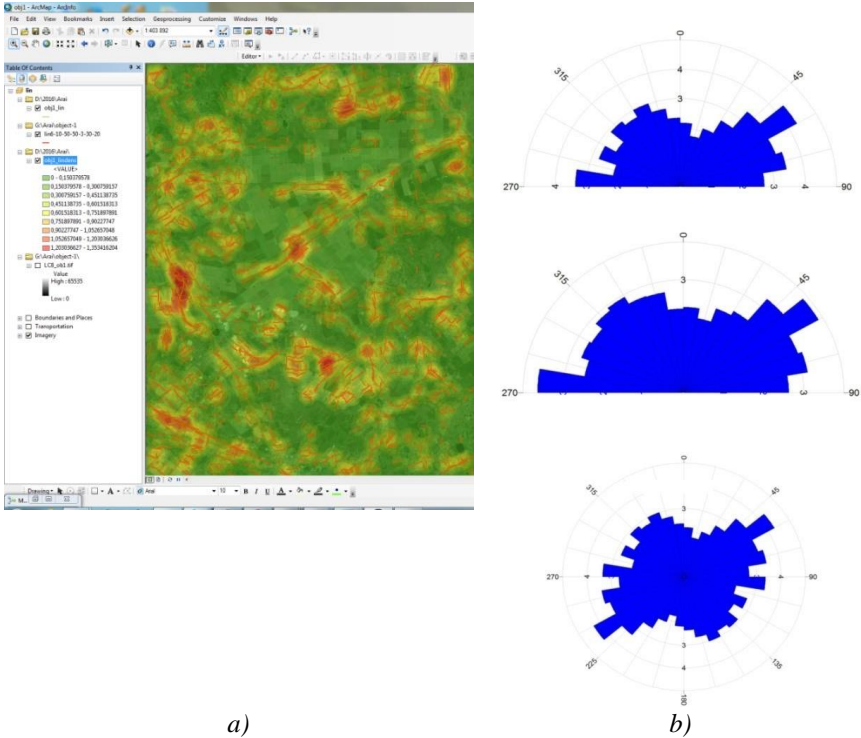


Figure 3 Lineaments map

a) Lineaments density map, b) Diagram of rock fracture direction in space images interpretation

Works results were used to confirm the prospectivity of areas discovered based on data of the Earth remote sensing, as well as sites for groundwater artificial replenishment for drinking water supply in Nur-Sultan.

The issue of utility and drinking water supply to the capital of the Republic of Kazakhstan – Nur-Sultan city is becoming more and more acute due to growing population, official statistics [5], [6] is given on Diagram (figure 4).

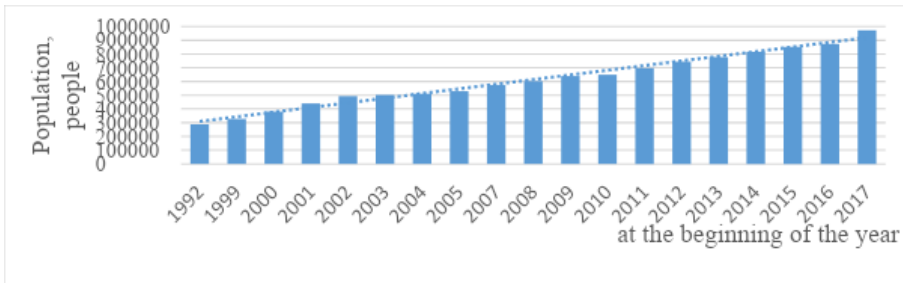


Figure 4 – Population of Nur-Sultan city (Astana)

At present, centralized water supply to Astana city is ensured by water supply from Astana (Vyacheslavskoye) water-storage reservoir on the Esilriver, it is the main source of water supply to Nur-Sultan. The volume of water in the water-storage reservoir is 291.91 mln m³, which is 60.6% of the design volume 410.9 mln m³. Water is supplied to Nur-Sultan in the volume of 210 thousand m³/daily [7]. Almost all the water volume is taken to satisfy consumers' needs. The share of groundwater in the overall balance of utility and drinking water consumption of the city is less than 1 %.

The current and potential need of Nur-Sultan in quality drinking water was defined based on the materials of Kazgiprovodkhoz and data from akimat. The current need of Nur-Sultan – 210 thousand m³/daily; the potential need of the city – 439.2 thousand m³/daily.

Thus, taking into account growing population and anthropogenic load, Astana water-storage reservoir does not fully satisfy the present need of Nur-Sultan in water.

Despite worsening of surface water quality, akimat of Nur-Sultan developed a short-term plan of finding an acceptable solution to improve water supply to the city at account of surface water of the Nura river (Nura-Esil channel) and Irtysh – Karaganda channel (water conduit from K.Satpaev channel to the Esil river), and also Seletinskoye water-storage reservoir. The available capacity of groundwater is not taken into account.

Use of almost single source of water to supply a country capital with population of almost one million people bears the risk of occurrence of hazards of normal water supply failure of both men-made nature, as well as risks related to water intake structure contamination.

To mitigate risks, it is necessary to engage alternative sources of water-supply, in particular groundwater poorly used in this region. From the point of view of security, groundwater has a number of advantages over surface sources of water supply. They are much better protected from contamination ingress into water, has as a rule much better sanitary condition and organoleptic indicators, allow performing distributed intake throughout the area of aquifer distribution.

For utility and drinking water supply to Nur-Sultan, four groundwater deposits were explored previously: Tselinogradskoye, Akmolinskoye, Rozhdestvenskoye and Nurinskoye. These deposits are confined to river valleys alluvial formations,

their reserves are replenished by surface water. Worsening of environmental situation in river valleys in the course of intensifying economic activity results in pollution of surface water of rivers Nura, Esil, Koluton, to the valleys of which the explored groundwater deposits are confined. Surface water pollutants ingress aquifers. Mode of river valley groundwater feeding has a seasonal periodicity. Within spring snow melting and high water, water level in rivers increases and surface water actively feed the groundwater, at that moment, salinity of surface water decreases as well as pollutants concentration due to dilution with relatively low-polluted melt water. In low-water season, reverse process occurs: river valley groundwater is discharged into river bed ensuring land runoff.

The most perspective proven deposits with approved groundwater reserves were selected to be engaged as sources of water supply to Nur-Sultan (Table1).

Table 1 – List of deposits recommended for drinking water supply to Nur-Sultan

Deposit name	Useful resources, thousand m ³ /daily	Water salinity, g/l	Distance from Astana, km
I-stage			
Zhabaiskoye	16.6	0.5	243
Atbasarskoye	21.2	0.2-1.0	220
Arbasar-Priishymskoye	65.0	0.5-1.2	230
Nurinskoye	48.0	0.3-0.8	68
Rozhdestvenskoye (Nizhneromanovskiy site)	19.5	1.0	36
Rozhdestvenskoye (Verhneromanovskiy site)	22.0	1.0	36
Tamsorskoye	24.1	0.1-2.9	196
Chaglinskoye-2	17.3	0.1	276
Total	233.7		
II-stage			
Nizhne-Kievskoye	37.0	1.0	94
Kievskoye	18.9	1.0	113
Molodetskoye	116.8	up to 3.0	158
Kotyorskoye	105.0	0.4-0.8	187
Zhartasskoye	103.3	0.4-0.6;0.3-1.2	200
Headwater	228.9	0.9-1.5	186
Tailwater	26.9	0.5-1.2	159
Total	636.8		
III-stage			
Pavlodarskoye-Priirtyshye	2669	0.2-0.4;1.5-2.0	430
Priirtyshskoye	498.2	1.0-1.3	485
Total	3167.2		

At the first stage, it is suggested to use deposits located within Akmola region only, at the second stage – engagement of deposits located in the territory of neighboring Karaganda region and at the third stage –engagement of deposits located in the territory of Pavlodar region where reserves of high-quality fresh confined groundwater allow ensuring water supply to the capital for period of up to 2050 and further.

The above deposits comply with the existing sanitary regulations and norms: water is fresh, salinity – below 1 g/l, quality is satisfactory. Their approved useful resources vary from 16.6 to 2969.0 thousand m³/daily.

Based on the results of monitoring, groundwater pollution sites were found in the area of influence of individual deposits. Moreover, multiple unowned wells that are not closed even with covers are the hazardous sources of groundwater contamination. Analysis of contamination showed that large sources of contamination in Nur-Sultan are treatment facilities of large, waste water storage facilities, domestic and industrial waste disposal sites, as well as animal production units, absorption fields and ash dumps [8]. Due to the above-stated, it is necessary to construct intake structures on the explored deposits.

Based on the results of works performed, it is possible to make a conclusion about the possibility of staged transition of Nur-Sultan city water supply to the use of groundwater.

CONCLUSION

It is necessary to use surface and groundwater for utility and drinking water supply to population of Nur-Sultan. Poor use of groundwater reserves explored for this purpose observed.

Current and potential need of Nur-Sultan in quality drinking water identified.

It is recommended to introduce staged use of groundwater deposits to ensure drinking water supply to Nur-Sultan with account to preliminary analysis of hydrogeological conditions, water quality, volume of groundwater explored and approved commercial reserves.

Use data of the Earth remote sensing in finding promising areas for forecasting of new perspective zones for initiation of exploration.

Increase of groundwater exploration effectiveness will allow improvement of quality drinking water reserves supply to population in Nur-Sultan and reduce the growing deficit of water resources.

REFERENCES

[1] Absametov M.K., Osipov S.V., Livinsky Yu.N., Murtazin E.Zh., Yermenbay A.M. Identification of prospective areas and assessment of underground water resources in water-deficient areas of North and Central Kazakhstan for water supply of populated items (Monograph), Almaty, 2017, 271 p.

[2] Osipov S.V., Livinsky Yu.N., Yermenbay A.M. Influence of anthropogenic environmental changes on the groundwater formation in Kazakhstan // Conference Proceedings of XIX International Multidisciplinary Scientific GeoConference SGEM 2019: Conference Proceedings: Informatics, Geoinformatics and Remote Sensing, Issue 2.2, Section: Hydrogeology, Engineering Geology and Geotechnics, Volume 19, Albena, 2019, pp. 337-342. DOI 10.5593/sgem 2019/2.2

[3] Schauvenerdt R.A. Remote sensing. Models and methods of image processing. - M.: Technosphere, 2010, 582 p.

[4] Shagarova L.V., Murtazin E.Zh. On the main stages of processing optical-electronic data of remote sensing data for constructing lineaments for the solution of hydrogeological problems // Reports of the XIII International Scientific and Practical Conference New Ideas in Earth Sciences, April 5-7, 2017. T.2. - M.: MGRI-RGGRU, 2017, pp.230-231.

[5] Regional Statistical Yearbook of Kazakhstan / Goskomstat of the Republic of Kazakhstan, Alma-Ata, 1992, 569 p.

[6] Demographic Yearbook of Kazakhstan / Statistical Digests of the Agency of the Republic of Kazakhstan on Statistics, Astana.

[7] Site of Astana Su Arnasy State-run Utility Company: <https://astanasu.kz>

[8] Sanitation-and-epidemiological requirements to water sources, utility and drinking water supply, places of cultural and general water use and safety of water bodies / Approved by order of the Minister of National Economy of the Republic of Kazakhstan 16.03.2015 No. 209.

WATER TREATMENT RESULTING FROM THE EXPLOITATION OF GAS DEPOSIT - CASE STUDY

Eng. PhD. Student Carmen- Matilda Marinescu (Badica) ¹

Eng. PhD. Student Marius- Nicolae Badica ²

Assoc. Prof. Dr. Silvian Suditu ³

Assoc. Prof. Dr. Monica Emanuela Stoica ⁴

^{1, 3, 4} Oil and Gaz University of Ploiesti, Ploiesti, Romania

² University of Petrosani, Petrosani, Romania

ABSTRACT

The water produced is the water brought to the surface through the oil and gas wells. It is made of natural deposit water, mixed with the hydrocarbons in the deposit. Due to the fact that more and more deposits are reaching maturity, the volume of water produced increases over time, so its disposal is now mandatory and conditions the continuation of gas production. Separation of the impurity gases is carried out within the group of probes, by means of installations called liquid separators. They are mounted on the path of each pipe of the well's supply, and their maintenance is equal to the duration of the probe's production time. The mounting of the separators for the adduction wells is usually done inside the well group, so that they can be controlled and exploited according to some rigorously designed schemes. This study presents the separation of the gases from the water using the separators with F.S. filter type.

***Keywords:** deposit, separators, filter, gas, water injection*

INTRODUCTION

The exploitation of natural gas is most often associated with the "exploitation", independent of our will, of the reservoir water, condensate or other mechanical impurities. Separation and retention of liquid and solid impurities resulting from or resulting from condensation due to lower temperatures in the extraction pipes, is the most important function of the surface technological installation, at a natural gas extraction well. Due to technological interests, it is necessary to perform a 3-step separation of the gas from the other impurities. Of all the impurities, the reservoir water raises the most delicate problems.

PRODUCED WATER

The water produced is the water brought to the surface through the oil and gas wells. It is made of natural deposit water, mixed with the hydrocarbons in the deposit. Because more and more deposits are reaching maturity, the volume of water produced increases over time, so its disposal is now mandatory and conditions the continuation of gas production.

The produced waters are usually salt solutions, having a high content of substances. In figure 1. the range of possible components of the produced water is

presented. In general, the produced waters are very complex, there are numerous methods of treating them. In some cases, the separation of the water from the crude oil can be easily achieved by simple gravitational separation. In this situation, the quality of the separate production water has almost the same values as the water quality needed for the injection. However, there are deposits for which the fluids produced can contain stable emulsions, H₂S, fine solid particles in suspension and sand. In these situations, treating it to obtain sufficiently pure / clean water to be injected back into the layer can be a real challenge. Taking into account the main impurities found in the production water, the treatment process will focus on the separation of the oil / water emulsion and the removal of the suspended solids and crude oil. [1]

In addition, various chemical treatment methods may be needed to ensure corrosion control, crust formation and bacterial activity.

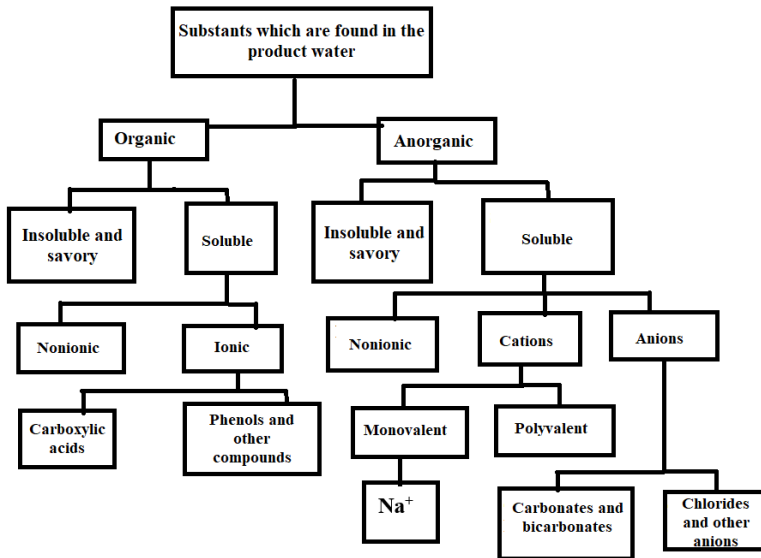


Fig.1. Possible constituents of the water produced.

WATER TREATMENT: METHODS AND METHODOLOGY

The properties of the deposit formation determine the quality of the water needed for the long-term success of the injection process. In this sense, the water source usually requires special treatment. The use of this treatment is mainly determined by the quality of the raw water available and the quality of the water needed. Each source of water, for example water from aquifer, seawater or production water, requires special treatments. This analysis will focus on the water produced from the gas fields, as this is the most widely used source of water for injection, requiring also underground drainage.

Methods

Separation of the impurity gases is carried out within the group of probes, by means of installations called liquid separators. They are mounted on the path of each pipe of the well's supply, and their maintenance is equal to the duration of the probe's production time.

The mounting of the separators for the adduction wells is usually done inside the well group, so that they can be controlled and exploited according to some rigorously designed schemes.

The operating principle of liquid separators is based on the use of centrifugal force (centrifugal separators with filter type F.S.- fig. 2 a, b, c), or gravitational (gravitational separators - fig. 3.a and b). Gravitational separators are the most numerous and functionally support the separation of water by depositing it at the bottom of the separator. [2], [3]



Fig. 2. a F.S type natural gas separator filter

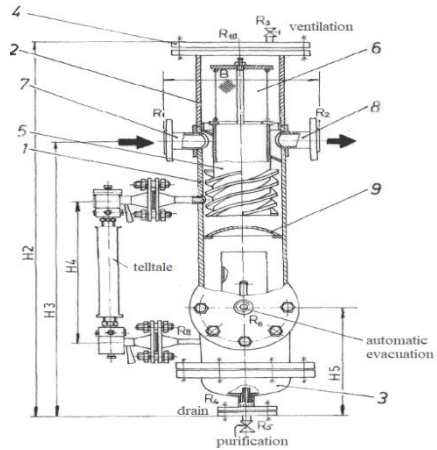


Fig. 2. b -F.S.- with automatic evacuation

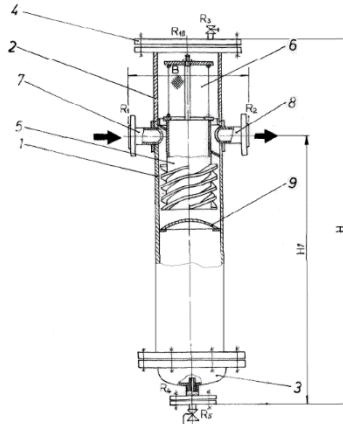


Fig. 2. c - F.S. - without automatic evacuation and without level indicator

F.S. type filter components:

1. the body of the separator;
2. the filter body;
3. blind flange provided with drain and purge connection;
4. blind flange provided with vent connection;
5. separator tube;
6. filter cartridge;
7. Inlet connection provided with flange;
8. outlet connection provided with flange;
9. deflector.

Methodology

The operating principle of the filter type F.S.

- the gas enters the separator body through the inlet connection;
 - a centrifugal motion is printed here;
 - due to the centrifugal and gravitational forces, the solid and liquid particles are mostly separated in the separator tube;
 - the gas then hits the deflector, changing its direction by 180 °, then passing through the filter cartridge to the outlet through the filter body;
 - the filter cartridge will hold the rest of the solid and liquid particles.
- [4], [5]

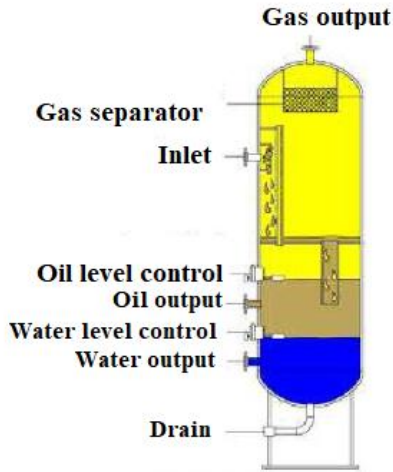


Fig. 3. a Schematic of the three-phase vertical gravity separator

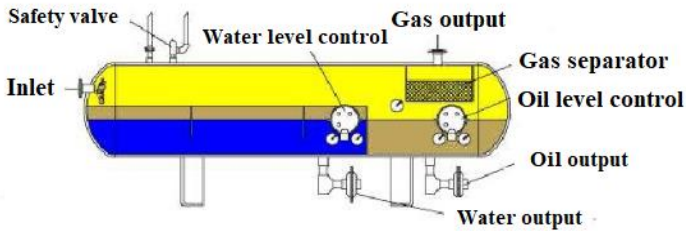


Fig. 3. b Schematic of the three-phase horizontal gravity separator (SOT).

The horizontal gravity separator is used in gas processing plants to separate impurities from natural gas. The separator can also be used to separate the liquid phases from the extraction gas fields.

WATER TREATMENT RESULTING IN THE EXPLOITATION OF OMEGA GAS DEPOSIT - CASE STUDY

For the groundwater, the analyzes that are carried out consider the degree of pollution with liquid or gaseous petroleum products. The natural state of the groundwater is influenced by the characteristics of the rock layers and the subsoils they cross. In some situations, there are strong interactions between naturally occurring compounds in groundwater and compounds from various sources of pollution.

In general, the status of groundwater is characterized by the size of the following parameters:

- content of petroleum products;
- temporary and permanent hardness;

- pH;
- suspensions;
- dissolved gases;
- anion content;
- radioactivity;
- electrical conductivity;
- corrosiveness;
- microbiological content;
- organoleptic characteristics.

The assessment of the results obtained from the analyzes carried out on the samples taken from the reservoir waters must take into account the degree of precision of the methods and the analysis equipment used. [1], [5]

The water resulting from the exploitation of the OMEGA gas deposit is analyzed and the resulting values are passed in the analysis bulletin represented in table 1.

RESULTS

Table 1. The result of the analysis for the water resulting from the exploitation of the OMEGA deposit

Nr. Crt.	Determination	Measured value	U. M.	Method of determination
1	pH	6,1	PH units	SR ISO 10523-2012
2	Chloride	105469,12	mg/l	SR ISO 9297/ 2001
3	Calcium	4288,56	mg/l	SR ISO 6058- 2008
4	Magnezium	1288,96	mg/l	SR ISO 6059- 2008
5	Total alkalinity	854	mg HCO ₃ /l	SR EN ISO 9963/1-2002
6	Total materials in suspension	213	mg/l	STAS 6953- 1981
7	Salinity	173,80	gNaCl/l	Laboratory analysis
8	Salinity	17,38	% NaCl	Laboratory analysis

The analysis data contains the following data: [5]

1. **Beneficiary: Gas extraction company**
2. **Sample identification data:**

Sample type: Reservoir water;
 Sample code: L1;
 Sampling point: OMEGA deposit;
 Sample collection: Laboratory;
 Date of receipt: 12.06.2017;
 Date of sampling: 12.06.2017;
 Measuring conditions pH: 25 ° C;
 Water density: 1.110 g / cmc.

3. Performer: Analyst X

The used equipment to measure water salinity is a laboratory conductometer for EC / TDS / Salinity with ATC-HI 2300 (Fig. 4). It is a device for measuring electrical conductivity, salinity and temperature.

The meter uses a 4-ring potentiometric conductivity probe with platinum sensors. By using four-ring probes, it is possible to measure very low or very high conductivity levels without having to change the probes.

The HI2300 also offers three options for temperature compensation, as well as an adjustable temperature coefficient. It can be connected to the computer via USB, facilitating the transfer of measured data.

This apparatus is designed for choosing the appropriate conductivity and can be easily changed in salinity mode to measure from 0.0 to 400.0‰ NaCl.

For calibration the apparatus will be made using the standard HI7037 100‰ NaCl solution.



Fig. 4 - Laboratory conductometer for EC / TDS / Salinity with ATC - HI 2300. [5], [6]

Before transporting crude oil and gas for processing, they are treated on site by removing sand and water. If the oil and gas are extracted together, their separation takes place.

The scheme for separating water, oil and gas is presented in figure 5.

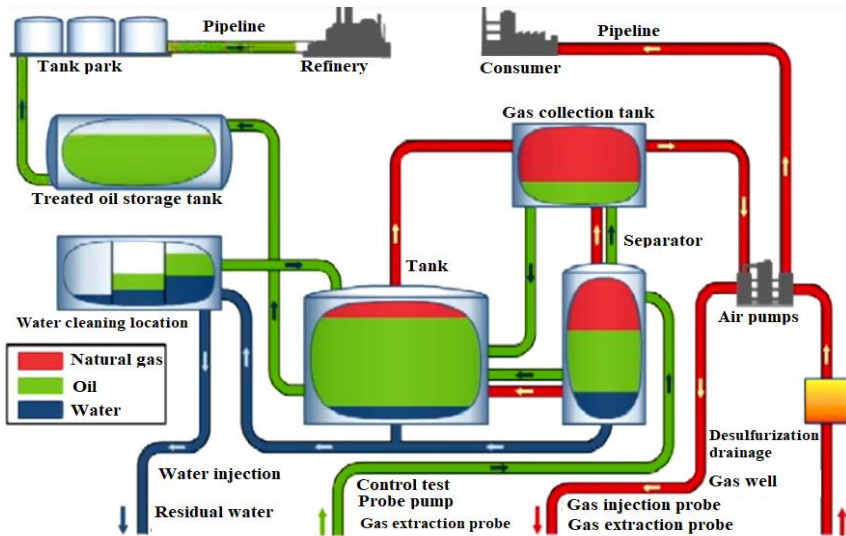


Fig. 5. Scheme for the separation of water, oil and gas [5]

METHODOLOGY

The probe fluid enters the separator body through the inlet connection and meets the deflector (1). Due to the impact, an initial separation of the liquid from the gas occurs and atomization of the fluid flow leading to a faster separation of the droplets. The liquid is directed to the accumulation area, and the large droplets carried by the gas flow immediately begin to fall due to the gravitational force, the phenomenon being favored also by the sudden decrease of the speed as the passage section increases. The gas, which has low density, and the small droplets will float in the upper area of the vessel, while the liquid phases will accumulate at the lower part of it. There is a natural separation between water and liquid hydrocarbons, because water has a higher density than that of hydrocarbons. A separation plate (7) delimits the area of accumulation of water from that of hydrocarbons. The plate (7) has adjustable height, in this way it is possible to adapt the operation of the three-phase separator to very different concentrations of the phases present in the well fluid. Further, the fluid passes through the coalescer plates (3) which are intended to facilitate the fusion of the droplets of liquid for their gravitational separation. To reduce the tendency of foaming of the liquid phase, the separator is provided with a soothing plate (4). Before leaving the vessel, the gas passes through the tank (5) which will filter out the small droplets remaining in the stream. The gas pressure is kept constant by means of a pneumatic pressure regulator. Water and liquid hydrocarbons are discharged through specially provided fittings. Their purging is done with the help of pneumatic control valves, controlled by pneumatic level controllers. Liquid levels can be observed using visual magnetic level indicators. After the phases are separated and leave the separator vessel, their measurement is followed. [5], [7]

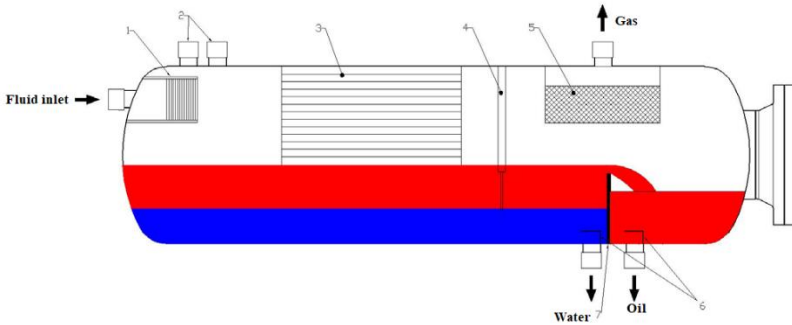


Fig. 6 - Three-phase separator vessel 1 - deflector; 2 - safety valve connections; 3 - coalescer plates; 4 - calming plate; 5 - demister; 6 - flow stabilizers; 7 - separation plate.

CONCLUSION

1. The quality of the injection water is the first step in choosing the treatment equipment.
2. The quality parameters of the water injection must be selected in the design of the reservoir engineering in correlation with the type of injection (above or below the fracture pressure) and the properties of the deposit.
3. The treated water is not stable (the content of suspended particles and their size increases over time), either due to precipitation of iron hydroxide, calcium carbonate, iron sulphide or bacterial activity.
4. Following the separation action next to the water from the gas, some hydrocarbons that are in liquid form are also separated, which must be recovered and directed to the fractionation plants.
5. After receiving and interpreting the results of the analyzes, it is determined whether the water treatment or its injection will be carried out in the layer.
6. Investigations for water treatment involve high costs, approved equipment and authorized personnel. Research results can also be used in similar cases.

REFERENCES

- [1] Hand out Water Management Course, Petrom, October 2015;
- [2] Stefanescu, D-P., "Practica extractiei gazelor naturale", vol. I, Editura Universitatii "L. Blaga", Sibiu, 1998;
- [3] Stefanescu, D-P., "Practica extractiei gazelor naturale", vol. II, Editura Universitatii "L. Blaga", Sibiu, 1998;
- [4] KIRJAVAINEN, V., -Fundamental concepts in flotation, Helsinki University of Technology, Mechanical Process Technology and Recycling, 2001;

[5] Carmen-Matilda (Badica) Marinescu - “ Cercetări privind tratarea apei rezultate în urma exploatării unui zăcământ de hidrocarburi, în scopul stabilirii metodelor de reintroducere a acesteia în circuitul natural ” RCS 3, Ploiesti, 2019;

[6] <https://hannainst.ro/hi2300-ec-tds-salinitate-metru-de-laborator.html> ;

[7] http://www.totalgaz.ro/uploads/datasheet/CT-STG-655-testare-sonde_EN.pdf .

WAVELET ANALYSIS OF HEIGHT AT POINTS OF THE CHANNEL OF A SMALL RIVER FROM THE MOUTH ON SPACE IMAGES

Dr. Sc., Prof. Peter Matveevich Mazurkin ¹

Yana Oltgovna Georgieva ²

^{1,2} Volga State University of Technology, Yoshkar-Ola, Russia

ABSTRACT

The purpose of the article is to analyze asymmetric wavelets of changing the coordinate - the local elevation of the Irovka river channel, as well as the influence of local latitude and longitude on it of 290 characteristic points along the river channel from source to mouth. After identifying the general wavelet equation, 12 terms were obtained in the form of asymmetric wavelets with variable amplitude and oscillation period. The first three members gave a correlation coefficient of 0.9993, which is slightly less than for latitude 0.9999, but more than for longitude 0.9991. As a result, all three coordinates have the strongest factorial relation with an adequacy of more than 0.999. All 12 wavelets distribute 95.52% of the points of the channel with a model error of up to 5%. The first term of the error distribution formula at 290 points of the river bed is the Laplace (Mandelbrot, Zipf-Perl, Pareto) law of exponential decline, and the second equation shows the stress excitation of the number of errors according to the biotechnical law. The comparison showed that 25 fractal terms were obtained for latitude, 18 for longitude, and 12 wavelets for altitude. As a result, height as a factor also shows high certainty in the quantization of wave equations. A zero rank in the fractal distribution of 12 wavelets receives an arithmetic mean value. The standard deviation decreases from 12.219 for the arithmetic mean to 1.489, that is, 8.2 times, for the first term. After the 12th wavelet, according to the tri-sigma rule, a spread of 0.3 m is formed, which is much less than the actual measurement error of 0.5 m for height from satellite images.

Keywords: river, satellite image, height, wavelets

INTRODUCTION

Images transmitted by Earth remote sensing satellites (ERS) are used in many sectors - agriculture, geological and hydrological research, forestry, environmental protection, territorial planning, educational, reconnaissance and other purposes. Remote sensing space systems allow for a short time to obtain the necessary data from large areas (including hard-to-reach and hazardous areas).[1].

To date, there is no single reasonable choice of the type of function. With the development of the slope, the washing and deposition rate of the material at different points of the profile should change. This determines the self-development of slope systems due to feedback, when the slope-dependent diffusion coefficient is responsible for the profile shape itself [2].

Mathematical and geomorphological modeling of erosion landscapes using a geoinformation medium and high-resolution satellite imagery makes it possible to identify the main characteristics of landscapes in real time and use them as the basis for theoretical and experimental studies of ecological and geomorphological processes. Thus, we get a modern tool for studying the processes that determine the state and degree of development of landscapes [3].

The longitudinal profile of the channel flow always has a series of steps or, rather, gentle undulating bends that do not cause a continuity gap like rapids and waterfalls. Graduation as an indispensable feature of channel flows was noted by most researchers [4]. But wave equations have not yet been obtained.

The goal is the analysis of asymmetric wavelets of height distributions from source to mouth at 290 characteristic points and the influence of the latitude and longitude of the small river Irovka.

MATERIALS AND METHODS

From satellite images, coordinates (latitude, longitude, altitude) were measured according to the recommendations [5].

On the rod line of a small river, characteristic points are selected from the source to the mouth according to sharp changes in the longitudinal profile of the small river, for example, when the channel turns in any direction in terms of more than 10-15°. Based on the measurement results, a data table is compiled for modeling by identifying stable patterns [6]. Table 1 shows the coordinates measurements and their comparison with the models: ε_{12} - residues after the 12th component (1); Δ - relative error.

Table 1. Rank distributions of the height of the characteristic points of the channel of the Irovka River

Point rank	Rank R_h	Latitude α , minute	Longitude β , minute	Height h , M	Estimated values from rank		
					h , M	ε_{12} , M	Δ , %
0	0	0	17.39	59	59.1	0.123212	0.21
1	1	0.02	17.50	52	52.0	-0.0367244	-0.07
2	3	0.19	17.62	48	48.0	0.0170352	0.04
3	3	0.2	17.67	48	48.0	0.0170352	0.04
4	3	0.27	17.64	48	48.0	0.0170352	0.04
...
286	247	23.83	1.970	4	4.0	-0.00580508	-0.15
287	247	23.84	2.019	4	4.0	-0.00580508	-0.15
288	269	23.87	2.035	2	2.1	0.0747201	3.74
289	286	23.89	2.017	0	-0.4	-0.422514	$-\infty$

The hypsometric characteristic is one of the most important properties of the relief. By the degree of elevation of the land surface above sea level, a low-lying (absolute height from 0 to 200 m) relief is distinguished [7]. The Irovka River belongs to the low level, at the mouth it is 89 m high, and at the source the height reaches 148 m above the Baltic Sea [8], [9].

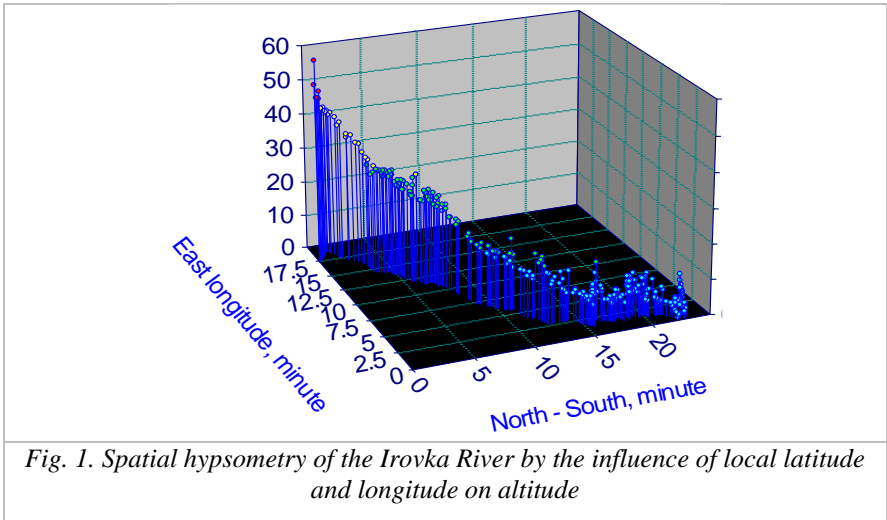
RESULTS AND DISCUSSION

Figure 1 shows a spatial hypsometric curve along 290 characteristic points of change in local height from the mouth to the source of the river, depending on local latitude and longitude.

The model is obtained on the basis of the condition that at first one-factor models are identified, and then they are placed to increase the correlation coefficient as a measure of the adequacy of the revealed patterns.

Oscillations (wavelet signals) are written by the wave formula [4] of the form

$$y_i = A_i \cos(\pi x / p_i - a_{8i}), \quad A_i = a_{1i} x^{a_{2i}} \exp(-a_{3i} x^{a_{4i}}), \quad p_i = a_{5i} + a_{6i} x^{a_{7i}}, \quad (1)$$



where y - is the indicator (dependent factor), i - is the number of the component of the model (1), m - is the number of terms in the general model (1), x - is the explanatory variable (influencing factor), $a_1 - a_8$ - are the parameters of the model (1) that take different numerical values in the process of structural-parametric identification in the software environment CurveExpert-1.40, A_i - the amplitude (half) of the wavelet (axis y), p_i - the half-cycle of the oscillation (axis x).

Table 2 shows the values of parameters (1) for two terms of the influence of local longitude on altitude, and the residuals of the second term as an influencing variable are the values of local latitude from the data in Table 1. Figure 2 shows graphs of two factors.

Table 2. The effect of longitude and latitude from source to mouth on the height

Factor and number i	Wavelet								Coef. corr. r	
	$y_i = a_{1i}x^{a_{2i}} \exp(-a_{3i}x^{a_{4i}}) \cos(\pi x / (a_{5i} + a_{6i}x^{a_{7i}}) - a_{8i})$				Amplitude (half) of the oscillation			Half oscillation		Shift
	a_{1i}	a_{2i}	a_{3i}	a_{4i}	a_{5i}	a_{6i}	a_{7i}	a_{8i}		
β_1	4.58566	0.73085	0	0	0	0	0	0	0.9723	
β_2	2.03445	0	-1.7537e-5	3.90439	42.7641	1.60613	1.03524	-1.26285		
α_1	2.30115	0	-0.026287	1	2.86126	0.019765	1	0.007428	0.6761	
α_2	5.5514e-13	165.938	10.02393	1	0.03908	0.019846	1	2.21030		
α_3	1.54657	0	0	0	2.28105	0.001715	1	-0.77225		

According to the hypsometric picture in Figure 1, the small Irovka River flows in a rectangle 23.89 minutes long (local latitude North-South) and 18.89 minutes wide (local longitude). Sharp changes in the channel curvature in terms of 290 characteristic points gave wave equations according to table 2.

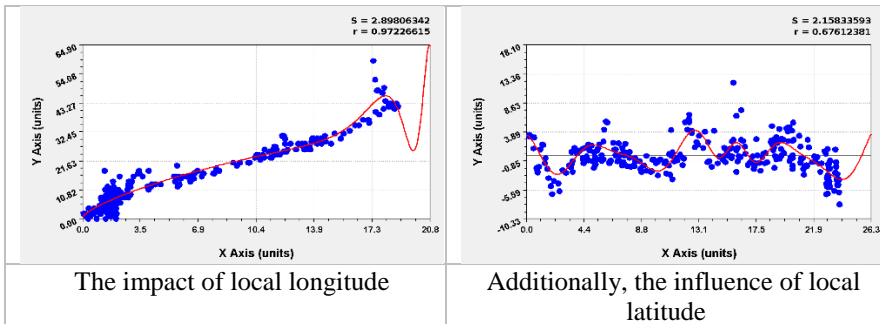


Fig. 2. The influence of longitude and latitude from source to mouth on the height of the channel of the Irovka River

The first equation for the influence of longitude shows that as east longitude increases, the height of the river increases according to the exponential law. It can be seen from the picture in Figure 1 that the increase in altitude occurs from a shorter longitude (closer to the mouth) to a greater longitude (closer to the source). In this case, the second wave equation shows that the amplitude increases according to the exponential law of growth, and the half-period of the oscillation increases from 42.76 ranks at minimum longitude.

Additionally, the influence of latitude on height by the third term occurs according to the law of exponential growth from source to mouth. Therefore, a decrease in altitude occurs mainly due to a decrease in local longitude. This third term from Table 2 is the law of Laplace (in mathematics), Mandelbrot (in physics), Zipf-Perl (in biology) and Pareto (in econometrics). The law $a_{4i} = 1$. After identifying the general model (1), 12 wavelets of rank distribution of local height were obtained (Table 3, Figs. 3-5).

Table 3. Parameters of wavelets of rank distribution of the local height of the Irovka

Number <i>i</i>	Вейвлет								Coef. corr. <i>r</i>
	$y_i = a_{1i}x^{a_{2i}} \exp(-a_{3i}x^{a_{4i}}) \cos(\pi x / (a_{5i} + a_{6i}x^{a_{7i}}) - a_{8i})$								
	Amplitude (half) of the oscillation				Half oscillation			Shift	
	a_{1i}	a_{2i}	a_{3i}	a_{4i}	a_{5i}	a_{6i}	a_{7i}	a_{8i}	
1	58.87679	0	0.0008808	1.09926	0	0	0	0	0.9993
2	-6.38434	0.48652	0.070117	0.46505	0	0	0	0	
3	3.47327	0.84367	1.36494	0.26690	4.78474	0.51777	0.78599	5.06935	
4	0.458135	0.692074	0.459628	0.418576	5.06960	0.168685	0.838476	8.53040	0.7594
5	9.3361e-7	4.10453	0.0650157	1	3.73444	0.0408429	0.489883	0.194488	0.3095
6	0.394701	1.23562	0.447487	0.682474	3.12365	0.551263	0	0	0.4576
7	0.781908	1.36008	0.256209	1.03850	3.16303	0.0119643	2.26069	2.1713	0.4440
8	3.1833e-11	6.49697	0.0664222	1	10.78055	0.0254631	0.996656	1.18507	0.6270
9	6726.89934	2.21488	14.79868	0.099782	4.67037	0.0082493	1.19103	-1.11802	0.4141
10	5.0896e-9	4.247939	0.0018925	1.53230	1.47780	0	0	0.257972	0.3900
11	5.2799e-12	21.44634	2.22290	1	0.832376	0	0	3.50578	0.2969
12	3.2771e-47	2941689	0.214460	1.07043	1.05525	0	0	2.34453	0.5136

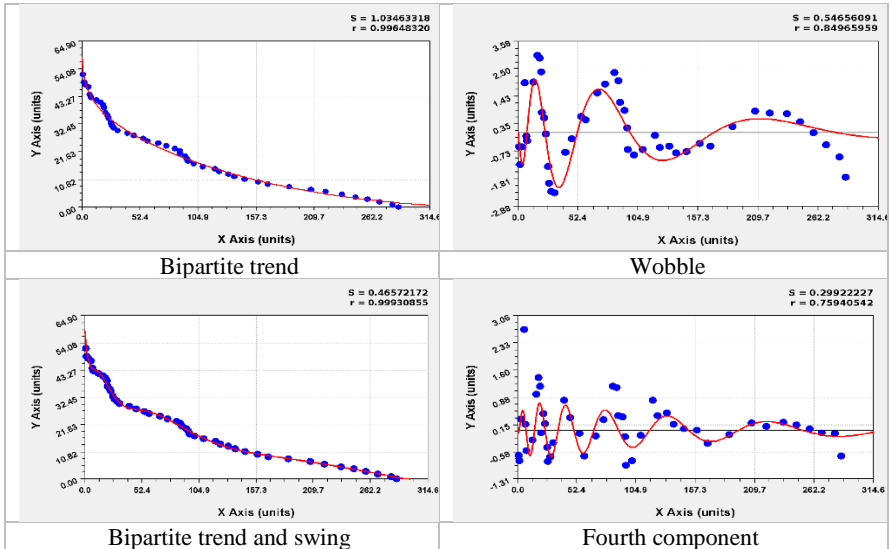


Fig. 3. Graphs of the trend and two fluctuations in the rank distribution of the height

The first three wavelets gave a correlation coefficient of 0.9993 for the capabilities of the CurveExpert-1.40 software environment. The first term is the Laplace or Mandelbrot law [4] modified by us under condition 1, and it shows an exponential decrease in the average height of two banks from source to mouth. The second term shows a decrease in height according to the biotechnical law [4] approximately to the middle of the length of the river. Approximately the first two terms form a trend in the change in the line of the water surface of a small river

(Fig. 3). The remaining 10 waves (Fig. 4 and Fig. 5) show, due to the positive sign, the oscillatory adaptation of the relief to an increase in height. The first two vibrations show the relief from the source.

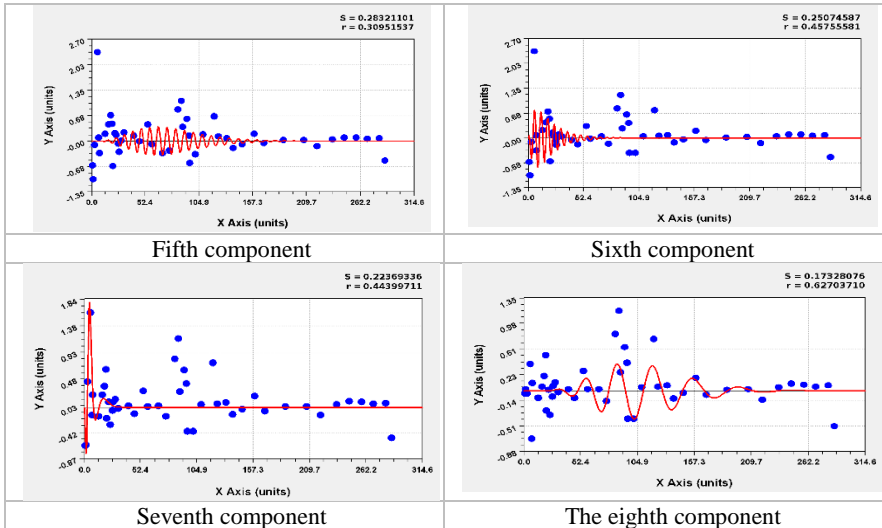


Fig. 4. Graphs of models of the rank distribution of the height of the Irovka River

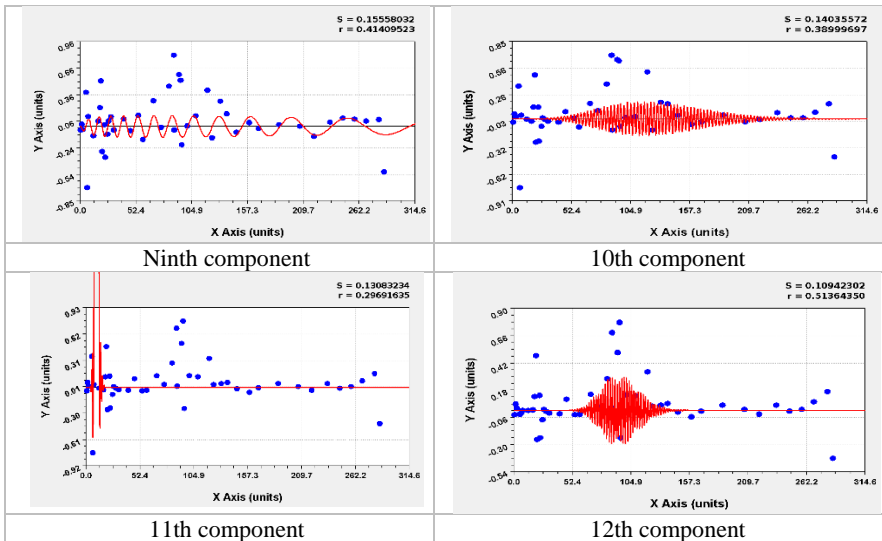


Fig. 5. Graphs of the latest models of the rank distribution of the height of the Irovka

The remaining eight members show a local change in the height of the river topography. Thus, the height along the small river changes, like latitude and longitude, in a wave-like fashion, which, of course, is affected by fluctuating distances in plan and in height between the characteristic points along the rod of the small river Irovka.

Figures 4 and 5 show several short wavelets at characteristic points. In addition, members 6, 7, and 11 show strong relief fluctuations in the upper reaches of a small river. With a decrease in the water content at the source in summer, the canal is now drying up.

Further identification of model (1) is difficult, so we stop the process of identifying patterns. The residuals are less than the measurement error of ± 0.5 m (Fig. 6).

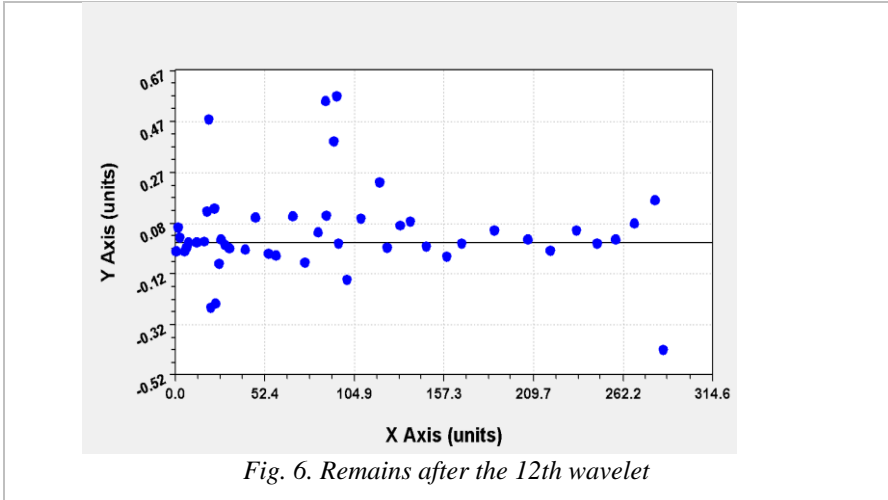


Fig. 6. Remains after the 12th wavelet

Four points (with ranks 252, 263, 266 and 289) due $h = 0$ to gave an infinite error.

At 0.1 intervals, the error was distributed as follows (modulo): at zero, 9 pcs. (3.10%); 0 - 0.1% 46 pcs. (15.86%); 0.1 - 0.2% 59 pcs. (20.34%); 0.2 - 0.3% 11 pcs. (3.79%); 0.3 - 0.4% 29 pcs. (10%); 0.4 - 0.5% 7 pcs. (2.41%) etc. At large intervals: 0 - 1.0% of all points 203 pcs. (70%); from 0 to 5% 277 points, which is equal to 95.52% of 290 characteristic points. We accept the norm of measurement and modeling errors of 5%, then the remaining $290 - 277 = 13$ points of the longitudinal channel profile require separate consideration.

Figure 7 shows a graph of the distribution of the model error by the formula

$$n = 9.00800 \exp(-2.47276\Delta_{0,1}) + 84.75096\Delta_{0,1}^{0.20200} \exp(-2.54418\Delta_{0,1}) . \quad (2)$$

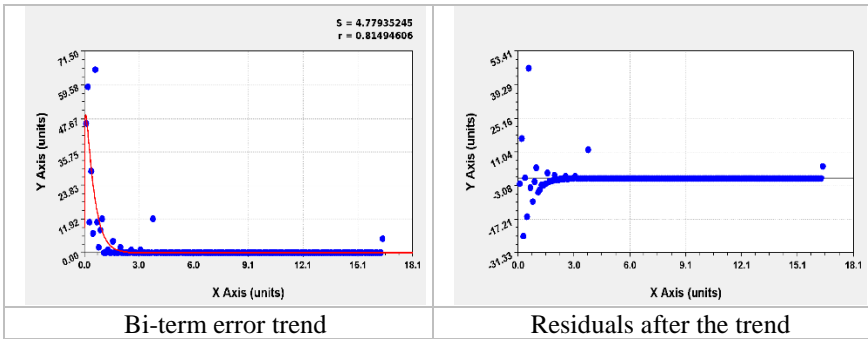


Fig. 7. Graphs of the distribution of the error in modeling the height of the Irovka River

The first term (2) is the Laplace law of exponential decay, and the second equation shows the stress excitation [4] of the number of errors. The comparison showed that model (1) for latitude received 25 members, for longitude 18 and for a height of 12 members.

Table 4 gives the wavelet ranks and the calculated values of the actual distribution of the standard deviation.

Table 4. Dynamics S, m

Wavelet rank i	Standard deviation S
0	12.219
1	1.489
2	1.035
3	0.466
4	0.299
5	0.283
6	0.251
7	0.224
8	0.173
9	0.156
10	0.140
11	0.131
12	0.109

In the upper right corner of the graphs, the figures show the mean square deviation (standard deviation) S .

Zero rank gets the equation $y=a$ of arithmetic mean value. The first rank has the first member in table 3.

The standard deviation decreases from 12.219 for the arithmetic mean equation to 1.489, that is, 8.2 times. After the 12th wavelet, a three-fold deviation forms 0.3 m, which is much less than the actual measurement error of ± 0.5 m.

After identifying the model (1), the formula (Fig. 8) is obtained

$$S = 12.21824 \exp(-2.51054i) + 1.68900i^{2.35427} \exp(-1.18462i) \quad (3)$$

The first term of equation (3) is again the law of Laplace (in mathematics), Mandelbrot (in physics), Zipf-Perl (in biology) Pareto (in econometrics) and therefore shows the multiple fractal distribution of all 12 wavelets. Then the Mandelbrot fractals become special cases.

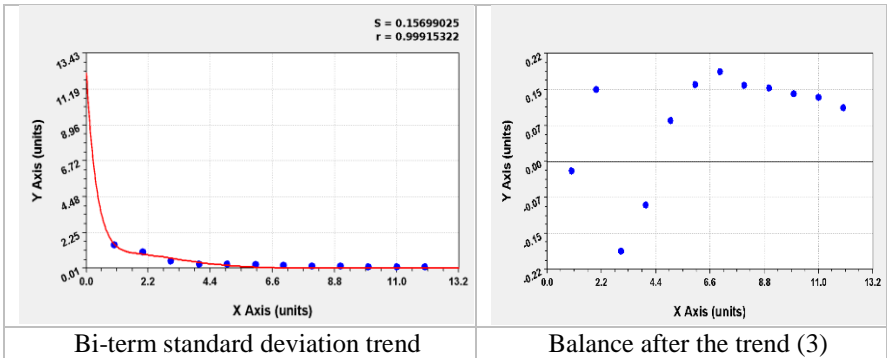


Fig. 8. Distribution graphs of the standard deviation of height from the wavelet rank

It can be seen from the residuals in Fig. 8 that the asymmetric wavelet will become the third term in formula (3). This proves that quantization of the relief height by fractals can have not only multiple values, but even occurs according to wave equations.

CONCLUSION

Modeling the distributions of the height reduced to a small river made it possible to obtain 12 wavelets with a distribution of 95.52% of the points with a modeling error of up to 5%. The first term in the formula for the distribution of errors at 290 points of the river bed is the Laplace law of exponential decline, and the second equation shows the stress excitation [4] of the number of errors. The comparison showed that model (1) for latitude received 25 members, for longitude 18 and for a height of 12 members.

The first three members of the height model gave a correlation coefficient of 0.9993, an adequacy level of more than 0.9 or the strongest link. The remaining 9 members increase the level of adequacy to almost 1. As a result, height as a factor shows certainty in quantization.

The zero rank in the fractal distribution receives the equation $y = a$ of the arithmetic mean value. The standard deviation decreases from 12.219 for the arithmetic mean equation to 1.489, that is, 8.2 times. After the 12th wavelet, a three-

fold deviation (the tri-sigma rule) forms 0.3 m, which is much less than the actual measurement error of 0.5 m for the height from satellite images.

REFERENCES

[1] Sadkov S.A. Morphological structure of plains subject to ground Subsidence on the basis of mathematical morphology of landscapes approach // *Geomorphology RAS*. 2019;(1);48-58. doi: 10.31857/S0435-42812019148-58.

[2] Salugin A.N., Kulik A.V. Mathematical modeling of the development of the long profile of ad eluvialslope // *Geomorphology RAS*. 2019;(1);59-65. doi: 10.31857/S0435-42812019159-65.

[3] Rulev A.S., Yuferev V.G. Mathematical and geomorphological modeling of the erosion landscapes // *Geomorphology RAS*. 2016;(3):36-45. doi: 10.15356/0435-4281-2016-3-36-45.

[4] Makkaveev N.I. River bed and erosion in its basin. M.: Publishing House of the Academy of Sciences of the USSR, 1955. 346 p.

[5] Maps of heights, slopes. URL: <http://votetovid.ru/#56.201192,48.95536,17z,51v301> (date of treatment 02.10.2019).

[6] Mazurkin P.M. Wavelet Analysis Statistical Data. *Advances in Sciences and Humanities*. Vol. 1.No. 2. 2015. pp. 30-44. doi: 10.11648/j.ash.20150102.11.

[7] Levers G.I. *Geomorphology. Textbook for academic undergraduate*. M.: Yurayt, 2018. 396 p.

[8] Georgieva Ya.O., Mazurkin P.M. Changing the curvature of the channel of the small river Irovka from satellite imagery // *SCI-ARTICLE.RU*. URL: <http://sci-article.ru/stat.php?I=1574276162> (Access date 11/16/2019).

[9] Mazurkin P.M., Georgieva Y.O. Measurement of coordinates by satellite imagery along the bed of the small river Irovka in the Republic of Mari El // *Successes in modern science*. 2019.No 12 (part 2). S. 294-300; URL: <http://www.natural-sciences.ru/en/article/view?id=37304> (date of treatment: 01.24.2020).

